MULTIPHYSICS MODELLING AND MITIGATION OF AGEING IN ASPHALT PAVEMENTS

EMAN LAFTA SALMIN OMAIREY

Doctor of Philosophy

ASTON UNIVERSITY

March 2021

ASTON UNIVERSITY

Multiphysics Modelling and Mitigation of Ageing in Asphalt Pavements

EMAN LAFTA SALMIN OMAIREY

Doctor of Philosophy

2021

Thesis Summary

Bitumen binders oxidise with air and cause ageing deterioration of asphalt pavements in the form of hardening, cracking and an overall decline in the mechanical performance. The degree of oxidative ageing is governed by many coupled internal and external physics and variables, making it difficult to predict. Mathematical models were established to represent the multiple physics that contribute to oxidative ageing of asphalt pavements. By coupling them together, these models can simultaneously simulate heat transfer, oxygen diffusion and oxidation kinetics to predict the oxidative ageing of asphalt pavements. The challenge lies in the non-linearity and circular dependency of these physics, making them difficult to solve and converge in numerical applications.

The current study establishes a partial differential equation (PDE) based Finite Element (FE) modelling framework to solve these multiple physics using a weak form method. The framework is validated using field measurements of within-pavement temperatures and oxidative ageing products. A laboratory-based experimental investigation is conducted to select anti-ageing compounds (AACs) to mitigate oxidative ageing of bitumen binders effectively. Thin-film oven ageing and Fourier transform infrared spectroscopy (FTIR) tests are used primarily to select potential AACs. Detailed rheological and chemical tests are followed to detect any effects of these AACs on the long-term ageing performance of bitumen binders.

Results indicate that the weak-form PDE-based model can effectively address the circular dependency among ageing-related Multiphysics. The model can reliably predict hourly profiles of temperature, oxygen pressure and oxidation products growth along the pavement depth, in different climate zones and for extended periods of field ageing. The air void content and distribution play a vital role in limiting oxidative ageing. Dense asphalt pavements with a low air voids content (<5%) experience little to no ageing, whereas asphalt pavements with air void content of 5-9% experience a growing oxidative ageing rate with an increasing air void content. Pavements with high air voids (> 9%) will have a full access to oxygen from the atmosphere, thus the average carbonyl content is high and uniform across asphalt pavement depth with no clear ageing gradient. A normalised carbonyl index (NCI) was proposed to quantify the oxidative ageing of bitumen modified by AACs. The activation energy of oxidation is found to be a suitable parameter to evaluate and assort the effectiveness of different AACs. Bitumen samples modified with 12% (1 furfural: 5 Irganox 1076), 15% Irganox 1076 and 3.5% (3 DLTDP: 4 furfural) demonstrated the best anti-ageing behaviour by retarding carbonyl content growth and decreasing the fatigue damage among selected AACs without sacrificing the stiffness of binder. The study represents a step forward in the understanding of long-term behaviour of asphalt pavements.

Keywords: Bitumen, Oxygen Diffusion, Heat Transfer, Anti-ageing Compounds, Field Ageing.

Acknowledgements

This PhD study would not have been possible without the unwavering support, enormous efforts, and continuous encouragement of my supervisor, Dr Yuqing Zhang. I am incredibly grateful to him for sharing his invaluable scientific knowledge and clear vision that guided me throughout this study. Dr Zhang has supported my research and professional development in every way possible. His attitude toward research always astonished me. I am incredibly thankful and privileged for having him as my supervisor in this exciting PhD journey.

I would also like to express my sincere thanks to my associate supervisor, Prof Sahar Al-Malaika, for her invaluable support and technical advice, especially in testing anti-ageing materials. Acknowledgement is also extended to Dr Hussam Sheena for dedicating his precious time and knowledge, guiding me in the chemical tests and answering all my curious questions. Furthermore, I'm very thankful to my Viva examination committee of Prof Gordon Airey, Prof Mujib Rahman, and Dr Jude Onwudili for their in insightful comments and suggestions on my thesis.

A special thanks to Schlumberger Foundation's FFTF grant and the associated staff that I came in contact with (Ms Eve Millon, Ms Regina Hand, and Ms Elisabeth Forge) for providing me with all the financial resources to complete this PhD study and attend many conferences. I am immensely grateful for believing in my abilities, and I hope to support other women in STEM fields to carry on with this noble goal. Additionally, acknowledgement is extended to the British Council on the UK-China Joint Research and Innovation Partnership fund, Newton Fund (Grant No. 351957889), for funding my research placement in China.

I'd like to extend my sincere thanks to Professor Tao Ma of Southeast University and his research team, and Professor Rong Luo of Wuhan University of Technology and her research team for facilitating my laboratory work when I was in China, and also for their kind hospitality that made that research placement memorable.

During this study, I came across wonderful people who added value to my experience at Aston University, to name a few, Dr Yang Yang, for his help with the chemical tests, Dr Ricardo da Silva, for his help with the HPC issues, Ms Joanne Reid, for her assistance in many logistics, and Dr John Elgy, Dr Moura Mehravar, and Dr Sotos Generalis, for their insightful comments on my annual reports. And of course, my colleagues in MB228 for keeping a delightful company, Dr Fan Gu, Dr Yangming Gao, Dr Dimitra Kalaitzi, Ms Parastou Marsh, Dr Evanthia Thanou, Ms Amritha Dhanya, Dr Linglin Li, Ms Shadi Fathi, and Ms Charlotte Abdy.

I would also like to thank my family for their unlimited love and support. My brothers, Dr Tareq Omairi, for always being there for me, Dr Sadik Omairey, for being my all-time life and professional mentor, friend, and problem solver, and Mr Abd Al-Azeez Omairi, for being my advisor and best friend. With them by my side, I always feel happy, safe and empowered, they are my role models. Thanks are also extended to my sister-in-law, Ms Sandrella Al Arajey, for her love and friendship. Finally, my parents, Prof Lafta Omairey and Prof Ameera Hussain, words fail to describe my gratitude for your unlimited love, encouragement and support. Your smiles and voices are what light up every day. Nothing I will ever write, say or do can express how much I love and appreciate having them as my family.

List of Contents

List of Tables

List of Figures

Chapter 1 Introduction

1.1 Background

Highways are extremely important to the economic and urban life of any country due to their direct effects on the national economic output. A quality roads network helps in reducing travel times and related costs in maintenance, operation and roads users. Asphalt pavements, which are the type of pavements surfaced by asphalt mixtures, form about 90% of the highway roads networks in the world. In Europe, the annual production of the asphalt mixtures in the past decade was estimated to be approximately 292 million tons, of which more than 7.3% of it is produced by the United Kingdom (Asphalt in Figures 2019). The global increase in truck traffic volumes has raised the need for better performing pavements. Proper performance of bituminous pavements is guaranteed if all the pavement layers (surface course, base and subbase) and the subgrade can appropriately support traffic loads under all service conditions. Deterioration or loss of pavement performance has been experienced in the form of rutting due to deformations in one or several layers, fatigue cracking due to repeated dynamic heavy vehicle loading, moisture damage-related distresses in the bituminous layers, surface wear in countries where studded tyres are used, and others (Dessouky et al. 2014, Leiva-Villacorta et al. 2016, Pan et al. 2017b, Manosalvas-Paredes et al. 2020).

These forms of deterioration are more common in "aged" pavements. Ageing in asphalt pavements is attributed to the chemical and physical changes in bituminous binders when subjected to field environment for an extended period. Bitumen is an engineering binding material mainly used for paving applications. It is produced from the refining of crude oils and generally consists of about 85% carbon, 10% hydrogen, and heteroatoms such as sulphur (0–9%), oxygen (0–2%) and nitrogen (0–2%), as well as traces of metals such as vanadium, nickel and iron (Mortazavi and Moulthrop 1993, Lu et al. 2017). Bitumen is the most widely used binding materials in road pavements all over the world due to its excellent road performance. Approximately 95% of bitumen that is produced worldwide each year is applied in the paving

industry (Lesueur 2009, Sirin et al. 2018). However, the properties of bitumen are gradually degraded with influences of heat, sunlight, oxygen or a combination of these factors (Gao et al. 2006, Feng et al. 2013).

Ageing is primarily associated with the loss of volatile components and oxidation of the bitumen during asphalt mixture construction (short-term ageing) and progressive oxidation of the in-place material in the field (long-term ageing). Both factors cause an increase in viscosity of the bitumen and consequential stiffening and hardening of the mixture (Airey 2003). The detrimental effects of hardening in asphalt pavements were first recognised by pioneering pavement engineers in the 1990s and have been studied extensively during the past decades. Ageing affects pavement performance in many ways: ageing increases asphalt complex modulus and decreases the phase angle. As a result, mixtures become stiffer while fatigue life becomes reduced. (Sirin et al. 2018)

One of the key challenges for the development of performance-based specifications for asphalt pavements is the prediction of in-time age hardening in the long term. Without having a reliable ageing model, making long-term pavement performance predictions in life cycle cost determination, risk assessment, or pavement maintenance planning will always remain erroneous (Woo et al. 2008, Das et al. 2015d). This is the to-be-addressed challenge that is focused on in this thesis.

Substantial literature available shows that the theories and causative mechanisms of oxidative ageing are complex. Most publications ascribe ageing progression to variables like bitumen properties, mixture volumetric properties, pavement structure and environmental conditions of the field, indicating the Multiphysics nature of oxidative ageing of asphalt pavements. Specifically, ageing of asphalt materials involves three Multiphysics: (1) chemical oxidation reaction in the bitumen; (2) mechanical responses (e.g., altered viscosity); and (3) physical environmental processes (i.e., heat transfer and oxygen diffusion) leading to varying environmental profiles within pavements. These processes are influenced by the microstructural morphology, including bitumen mastic film thickness, pore size and air void distribution (as shown in **Figure 1-1**). The great diversity of variables and differences in earlier research results

reported make a prediction of oxidative ageing difficult. For this reason, existing studies only focused a "one physics" approach, which studies the effect of one variable on the oxidative ageing growth with ignoring the interactions among these physics. However, the interrelationships among them are circularly dependent in the dynamic ageing process. For example, oxygen distribution affects the chemical oxidation of bitumen, resulting in increased viscosity and decreased oxygen diffusivity, which in turn affects oxygen distribution and oxidative ageing. Ignoring the Multiphysics nature of the oxidative ageing in the pavement structure leads to simplification in modelling, thereby reducing the prediction accuracy or resulting in misleading results. Thus, oxidative ageing of asphalt pavements should be modelled in a Multiphysics perspective so that the dynamic circular dependencies among these physics are solved simultaneously for an accurate prediction of ageing in the asphalt pavements. In addition, Multiphysics modelling is capable of assessing the influence of different material and environmental components on oxidative ageing of asphalt pavements from both physical and chemical perspectives.

The future of road integrity partly depends on a better understanding of the fundamental relationships between ageing and pavement mechanical response. This fundamental knowledge can be vital to pavement engineers owing to the need for a high level of risk management, customised design decisions and sustainable selection of materials.

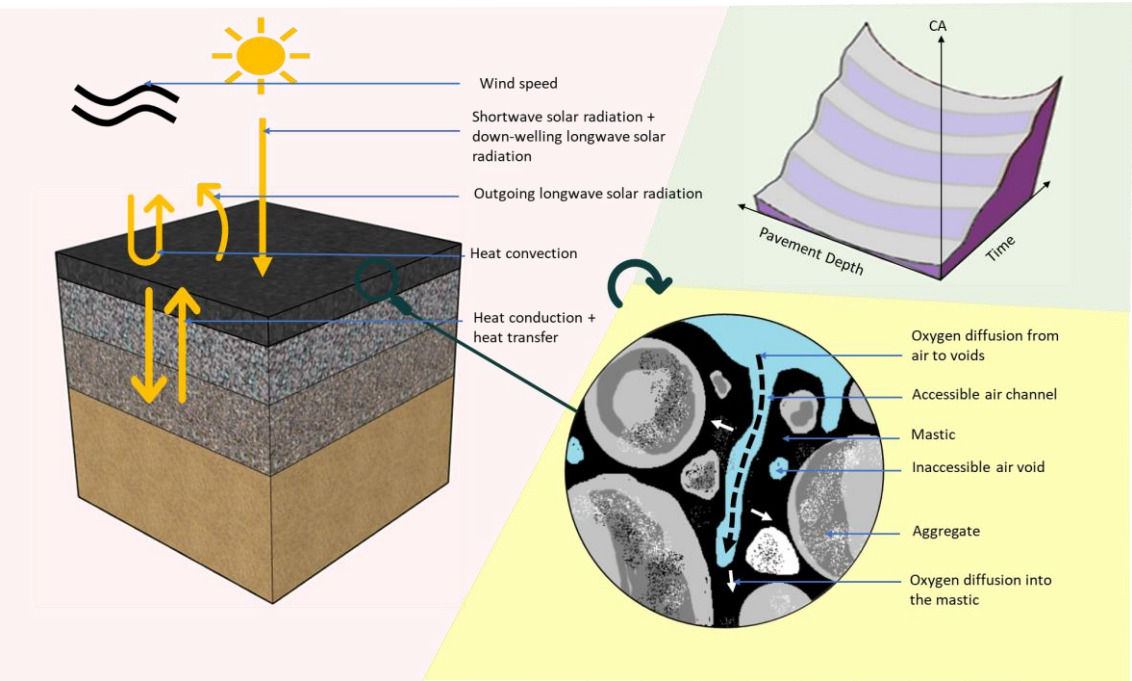

Figure 1- 1 Physical processes of oxidative ageing of asphalt pavements: (1) heat transfer (2) oxygen diffusion (3) oxidation kinetics in terms of carbonyl area (CA) growth rate.

With the objective of contributing towards this important knowledge, numerical modelling and laboratory testing presented in this thesis were undertaken to predict the oxidative field ageing of asphalt pavements, determine the influence of various variables on ageing deterioration, and develop roads to be more durable. After a comprehensive literature review, the study developed a framework for modelling oxidative ageing of asphalt pavements from a Multiphysics perspective. Specifically, a series of analytical models were identified to quantify the influence of each physics on the oxidative ageing. Then, an equation-based finite element (FE) modelling approach was employed to integrate these analytical models into the Comsol Multiphysics solver. The integrated FE model was used to compute the change of each physics during oxidative ageing simultaneously. The computational results facilitate an understanding of the oxidative ageing mechanism of asphalt pavements. Next, the oxidation kinetics of binders modified with anti-ageing compounds (AACs) were compared, and a screening method to evaluate the performance of different AACs was proposed.

1.2 Problem Statement

Ageing of bitumen is identified by the increase in its stiffness which causes adverse changes in the mechanical performance of roads and eventually leads to ageing failure in the form of block, thermal or fatigue cracking. Oxidative ageing of the bitumen is typically quantified by the development of carbonyl functional groups using the Fourier Transformation Infrared Spectroscopy (FTIR) test (Liu et al. 1996). The effect of oxidative ageing on the mechanical performance of asphalt pavements is well recognised in the literature. Yet, there are shortcomings in current long-term ageing performance prediction models of asphalt pavements. These shortcomings are summarised as follows:

1. Ageing theories and field measurements have well characterised the individual physics associated with the ageing in the asphalt pavement structures. For instance, the effects of temperature profile, oxygen diffusion or bitumen's properties on the ageing evolution in the pavements. However, applying Multiphysics models in ageing predictions, considering their circular and time-dependency, was limited due to the unclear interactions between the multiple physics as well as the Finite Element (FE) modelling restrictions. Such restrictions include limitations on specific constitutive models, non-user-friendly interfaces, and inadequate modelling abilities. Additionally, user-defined subroutines must be programmed to address different physics simultaneously. Research methods based on traditional methods has been difficult to adapt to the development of transportation infrastructure. The development of supercomputing, large-capacity storage, artificial intelligence technology, numerical simulation, and intelligent simulation have gradually become important means and approaches for theoretical research and engineering practice that can solve this issue.
2. Immense studies covered the ageing mechanism of bitumen binders and less on the ageing in asphalt pavement structures as a whole. It is impossible to accurately quantify the effect of different variables on the ageing degree and distribution without

a reliable ageing prediction model. Thus, once a Multiphysics model is established, a parametric analysis for oxidative ageing in asphalt pavements will be needed to guide a studied modification in pavement design and materials selection.

3. It is difficult to compare the ageing performance of modified binder samples of various modifiers or binders of different sources subjectively. The reason behind this is that studies adopted various ageing conditioning techniques and evaluation criteria.
4. Mechanical characterisation theories were mostly based on crude-oil based virgin bitumen and asphalt mixtures subjected to limited stress and strain conditions. However, the modern-day binder is the modified bitumen with a variety of additives. It is expected to sustain satisfactory resistance to fatigue and thermal cracking for extended periods in the field. Limited literature is available on the fatigue characterisation of bitumen modified with anti-ageing additives.

This thesis aims to address these research gaps by: (1) developing a comprehensive and integrated Multiphysics ageing prediction model sensitive to all different variables of the ageing process, making use of recent developments in supercomputing technologies, Multiphysics FE modelling capabilities, and cumulative literature on the subject; (2) prolonging the working life of pavements using anti-ageing modifiers; (3) understanding the complex ageing mechanism in asphalt pavements by a complete parametric analysis.

1.3 Research Objectives

The overall aim of this research is to establish a reliable oxidative ageing prediction model that can estimate the rate of binder oxidation within the pavement structures, with considering the multiple physics that contribute to the ageing evolution and distribution. The Multiphysics model is capable of capturing the effect of the mixture morphology, pavement structure, binder type, and environmental conditions on the degree of oxidative ageing. This will result in (1) providing a better understanding of the field ageing behaviour of asphalt pavements; (2) enabling researchers and engineers to make accurate performance deterioration prediction models of asphalt pavements; (3) performing feasibility analysis studies that can improve design

protocols and specifications to reduce or delay maintenance needs. To achieve the research aim, the following objectives are set:

1. Build a heat transfer model of asphalt pavements to forecast the hourly temperature profiles at any region, and validate this model against recorded data collected from field in different climates.
2. Build an oxygen diffusion model that predicts oxygen concentrations at any time and location within the asphalt concrete layer, particularly in air channels and mastic coating film within the asphalt mixture materials.
3. Develop an oxidation reaction model to simulate the growth rate of carbonyl functional groups in the mastic film. Then, link it to the oxygen diffusion and heat transfer models to consider the circular dependency among these three physics. After that, validate the overall ageing model against the carbonyl content of field samples collected at multiple depths within the asphalt concrete wearing layer for distinct ageing intervals.
4. Investigate the effect of different anti-ageing compounds (AACs) on the oxidation kinetics of thin-film aged bitumen samples using Fourier Transformation Infrared (FTIR) spectroscopy, and validate these observations with complete rheological and chemical testing on laboratory aged specimens. Consider the effect of AAC-inclusion on the degree and extent of field ageing of asphalt pavements using the proposed FE ageing model.
5. Run a parametric sensitivity analysis for model parameters that are: (1) affecting the oxidative ageing growth rate (e.g., the activation energy of oxidation), (2) materials properties contributing to oxidation, and (3) boundary conditions of pavement structure (e.g., the existence of porous layer under the asphalt concrete course). Moreover, study the effect of changing climatic data from one climatic region to another and their impact on the oxidative ageing growth rate.

1.4 Thesis Structure

This thesis comprised three journal papers that have been published in international peer-reviewed scientific journals and one paper that is currently under review (refer to **Appendix A**). The thesis also contains a literature review of the existing studies and collected data from the field pavements and the literature to form an integrated, standalone document about the oxidative ageing of asphalt pavement in the field. This thesis consists of seven chapters as illustrated in **Figure 1-2** and aligned as follows.

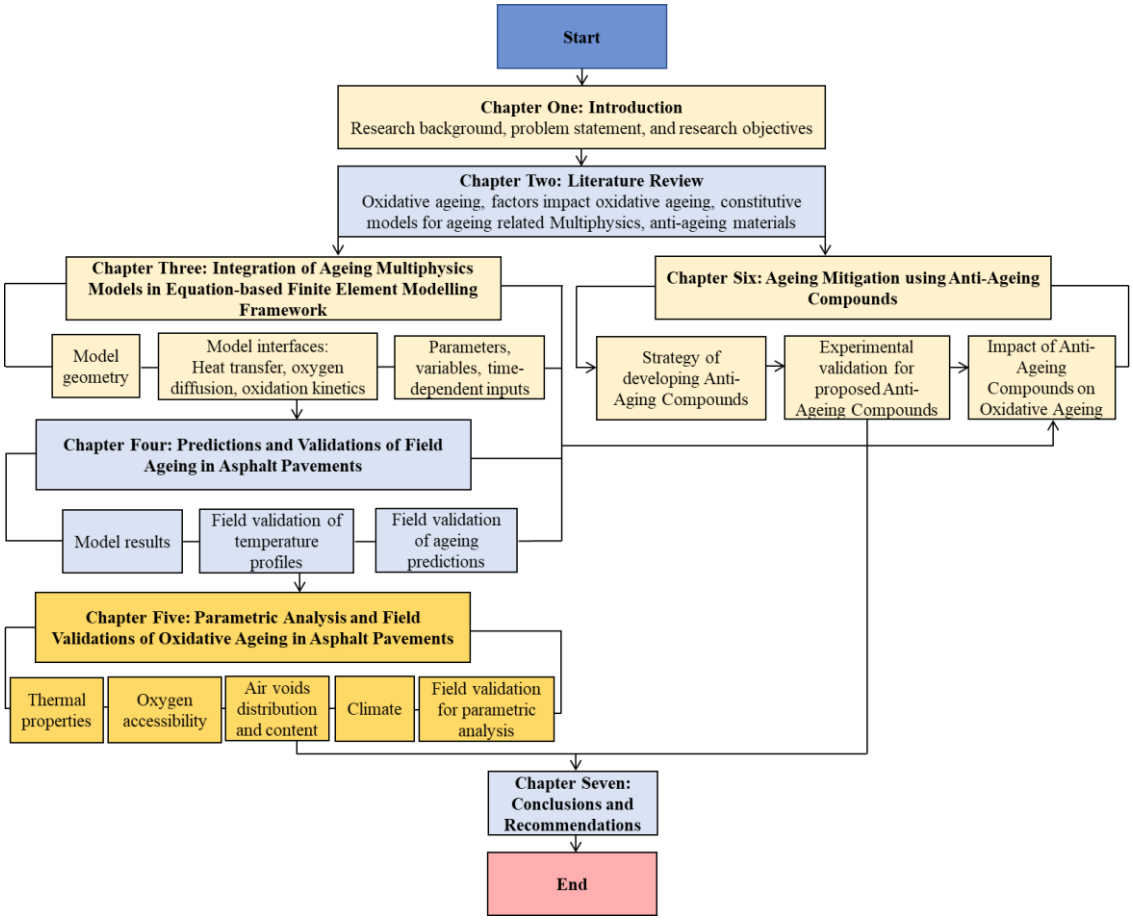

Figure 1- 2 Thesis structure and workflow chart.

Chapter One illustrated the research background, problem statement, research objectives, and chapters layout.

Chapter Two presents the main findings from the literature review covering published work from a range of scientific journals, technical reports, and professional bodies that investigate

the ageing behaviour of bituminous materials and asphalt mixtures, methods to quantify changes in the chemical and physical properties of bitumen and asphalt concrete due to ageing and proposed anti-ageing materials. The chapter is also looking into modelling techniques to predict the ageing in asphalt pavements.

Chapter Three integrates the oxidative ageing partial differential equations into one ageing model. Thus, this chapter illustrates all parts of the proposed ageing modelling framework. This includes details on the physical domain (geometry) with determining active areas for each process (physics), methods of solving the constitutive equations, initial parameters (to represent the asphalt concrete condition before subjecting it to field settings), constant and variable inputs, and time-dependent climate information.

Chapter Four presents all yielded simulation results, then it validates the model against actual available field data. The validation process is done in two stages: (1) validation of the temperature prediction model using hourly collected field data at different depth intervals. (2) validation of the integrated ageing model against carbonyl growth rate collected from field cores and recorded by previous researchers. Chapters three and four were published as a paper in the *Journal of Cleaner Production* (Omairey et al. 2021)

Chapter Five provides insights into how some of the model inputs affect ageing growth and distribution. This is especially important to reflect whether the model follows the same ageing behaviour of actual pavement in the field and identifies parameters that play a dominant role in the oxidative ageing of asphalt pavement. One test section is utilised for this purpose. The sensitivity analysis is divided into two main divisions: (1) internal variables (e.g., the effect of thermal properties, pavement morphology and structure on the oxidative ageing), and (2) external variables (e.g., the impact of climate region on the oxidative ageing). This chapter is submitted as a paper for publication in the International Journal of Pavement Engineering (under review).

Chapter Six looks into ways to reduce or mitigate the degree and extent of oxidative ageing by means of chemical additives to work as anti-ageing agents when added to bitumen

binders. First, preliminary tests are conducted to filter out ineffective anti-ageing additives. Then, detailed chemical and rheological tests are followed to ensure selected AACs can modify the bitumen with sufficient fatigue and rutting performance. Finally, the effectiveness of AACs-inclusion in mitigating field oxidative ageing was investigated using the proposed oxidative ageing modelling framework. This chapter has been published in two journal papers in the *Journal of Construction and Building Materials* (Omairey et al. 2019, Omairey et al. 2020)

Chapter Seven contains a summary of this study, the main conclusions and recommendations for future studies.

Chapter 2 Literature Review

The purpose of this chapter is to critically review relevant literature and motivate the methods used in this study. The review starts with a general introduction on bitumen binders, asphalt pavements and types of asphalt pavement deterioration, and then the review carries on introducing the oxidative ageing of binders and flexible pavements. Then it presents the internal and external factors that contribute to oxidative ageing. The chapter addresses the lack of understanding of field oxidative ageing caused by its many inputs. Following that, the available analytical models of ageing-related Multiphysics are introduced, some of which are employed in this study. The chapter also covers the current laboratory methods and techniques available to assess, quantify, and effectively reduce and mitigate the oxidative ageing.

2.1 Bitumen Binders

Bitumen-based construction materials, including bituminous binders and asphalt mixtures, are mainly used to pave roads and highways. Bitumen is a hydrocarbon product produced by removing light fractions (such as liquid petroleum gas, petrol and diesel) from crude oil during the refining process (Hunter et al. 2015, Tauste et al. 2018). It is an extremely complex material, composed of thousands of various paraffinic, aromatic, and naphthenic compounds and hydrocarbons, with varying saturations, polarity, and functional groups. This diversity in the chemical composition of bitumen causes variation in its mechanical behaviour (Petersen 2000).

From a rheological point of view, bitumen should be considered a viscoelastic material, very sensitive to temperature (Yu et al. 2015, Zakaria 2020). Even though the asphalt binder is only one component in an asphalt mixture, it is the component that provides the material with the desired viscoelastic properties. In addition to increasing driving comfort and flexible maintenance, this viscoelastic behaviour plays a prominent role in many aspects of mixture durability, such as resistance towards thermally or traffic-induced cracking and ravelling (Das et al. 2016).

2.2 Asphalt Pavement

Pavements are engineered structures and are important for our everyday life, commerce and trade. Like any other engineered structure, pavements are expected to be adequately strong and durable for their design life. They are expected to function properly by providing a smooth travelling surface for the traffic under various conditions of the environment. In order to ensure this, pavements must be designed, constructed, maintained, and managed properly.

Pavements can be broadly classified into asphalt (or flexible) and concrete (or rigid) pavement. Pavements consist of different layers, more so in the case of asphalt pavements than concrete ones. From the bottom up, these layers are known as the subgrade, subbase, base, and binder and/or surface. There are certain pavements with asphalt surface layers on top of concrete layers.

The layered structure of the pavement is meant for ensuring that the load is spread out below the tire, such that the resultant stress at the bottom layer of the pavement, the subgrade, is low enough not to cause damage. The most significant load applied to a pavement surface comes from a truck or an aircraft tire. The approach in a flexible pavement is to spread the load in such a way that the stress at the subgrade soil level is small enough so that it can sustain the stress without any major deformation (Mallick and El-Korchi 2008).

Three types of coats are used in the flexible pavement system which are seal coat, tack coat and prime coat (Zakaria 2020).

- Surface course: Surface course is also known as wearing course, is a bituminous layer that contains high-quality material to withstand direct loading from traffic. The main function of this layer is to provide skid resistance surface which vehicles can travel safely, in addition to providing friction and drainage for the pavement. The surface course is constructed using a good quality aggregate and high dense bitumen.
- Binder course: The binder course consists of aggregates and bitumen. The material used in this layer is similar to the base course but smaller aggregate size with less bitumen

content than the surface layer. The purpose of the binder course is to transfer the loads from the surface course to the base course.

- Base course: Base course is constructed either hydraulically bound (e.g. concrete) or granular, or both with larger aggregate size. Apart from structural support, the function of this layer is to distribute the loads from the top layers to the subbase and subgrade layer. Moreover, the sub surface drainage system can be provided within the base course.
- Subbase course: Subbase course is placed beneath of base course, and the function of this layer is similar between these two layers. Generally, the hydraulically bound or granular is used in this layer and the construction of subbase course is dependent on the subgrade soil. A subbase course is not needed if the soil of subgrade is strong and stiff.
- Subgrade: Subgrade layer is a foundation for the pavement system that located at the bottom layer. This layer consists of a natural soil layer that is compacted to the desired density. The main purpose of subgrade is to transfer the load from the above layers to the ground, and thus, it should be strong enough to take the stresses.
- Seal coat: Seal coat is a thin surface treatment used to waterproof the surface course and to provide skid resistance.
- Tack coat: Tack coat is a very light application of asphalt, usually asphalt emulsion diluted with water. It provides proper bonding between two layers of binder course and must be thin, uniformly cover the entire surface and set very fast.
- Prime coat: Prime coat is an application of low viscous cutback bitumen to an absorbent surface like granular bases on which a binder layer is placed. It provides bonding between two layers. Unlike tack cost, prime coat penetrates into layer below, plugs the voids, and forms a watertight surface (Zakaria 2020).

2.3 Pavement Deterioration

The major flexible pavement failure modes are fatigue cracking, rutting and thermal cracking. Fatigue failure is one of the main forms of asphalt pavement damage (You et al. 2016, Zhang et al. 2018a, Lv et al. 2020). The appearance of surface cracks is mainly due to the fatigue

cracking in the long-term perspective. Therefore, fatigue design is the critical factor of asphalt pavement structure design. So far, the ageing of asphalt mixture was not accurately considered in the current asphalt pavement design around the world, the impact of asphalt mixture ageing on the asphalt pavement fatigue life need more attention in the asphalt pavement structure design (Lv et al. 2020).

Rutting is a very common distress mechanism observed in flexible asphalt pavements under high-temperature conditions (45–85°C) (Phillips and Robertus 1996, Chen et al. 2018). Typically, rutting is characterised by depressions in the wheel path and mixture shearing can occur along the sides of the pavement. These depressions may cover extensions from some meters up to several kilometres depending on the vehicle speeds, the compaction conditions and the climate temperatures (Domingos et al. 2017).

Thermal fatigue failure as a result of heating and cooling cycles have been studied recently using an asphalt thermal cracking analyser (Marasteanu et al. 2012, Elkashef et al. 2018). Thermal shrinkage cracking in asphalt pavement occurs when the thermal tensile stress within the asphalt pavement that results from temperature drop exceeds the strength at that temperature. Thermal cracks typically appear as transverse cracks (pavement cracks perpendicular to the direction of traffic) at regular intervals in the field pavements. Low-temperature thermal cracks have been controlled historically by limiting the asphalt binder stiffness. Assuming similar asphalt binder tensile strengths and coefficients of thermal expansion/contraction, binders with a higher stiffness will crack at a higher temperature than softer binders (Kim 2005). Therefore, thermal cracking is common in aged asphalt roads because of the increase in binder stiffness upon ageing. Thermal cracking performance is derived mainly by the relaxation modulus and creep compliance of asphalt mixtures and binders.

2.4 Introduction to Oxidative Ageing

Existing studies demonstrated that the chemical composition of bitumen changes with ageing, which occurs in two phases, i.e., short- and long-term ageing (Mirza 1995, Airey 2003). Short-term ageing occurs during the initial construction phase due to volatilisation, oxidation, and

absorption of oily components in the maltenes during mixing. Long-term ageing occurs in the pavement service stage and is mainly due to the oxidation process.

Oxidative ageing is the reaction between asphalt constituents and atmospheric oxygen. Fourier transform infrared spectroscopy (FTIR) test is usually employed to identify changes in the chemical composition of bitumen due to ageing. According to existing FTIR studies, the oxidative ageing of bitumen causes the formation of carbonyl (C=O) and sulfoxide (S=O) functional group compounds (Petersen 2009, Zhao et al. 2010, Yang et al. 2018). Moreover, the formed carbonyl is much greater than the sulfoxides in terms of product quantity. Therefore, many researchers utilised carbonyl formation solely to characterise the change in the chemical composition of bitumen in the oxidative ageing process (Liu et al. 1996, Jin et al. 2011). They determined the carbonyl area (CA) from the FTIR tests to quantify the oxidative ageing of bitumen. While doing so, they found that a linear relationship exists between the carbonyl content formed and the oxygen absorbed by the bitumen. A correlation also exists between the bitumen's hardening susceptibility and the carbonyl content (Glover et al. 2014). Such a parameter was well allied to ageing time, ageing temperature and oxygen pressure. In addition to changes in chemical composition, the rheological properties of bitumen (e.g., viscosity and dynamic shear modulus) also exhibit hardening characteristics in the oxidative ageing process. The hardening leads to an increase in these properties so that the asphalt material becomes stiffer and more brittle. Many laboratory and field studies confirmed that the oxidative ageing of asphalt materials leads to the degradation of their physical, chemical, and mechanical properties, which could cause deterioration of the materials and distresses in the pavement structures, eventually resulting in the reduction of pavement durability. Thus, a comprehensive understanding and reliable prediction of the oxidative ageing performance of asphalt pavements is needed.

2.5 Oxidative Ageing-related Multiphysics and Variables

Existing studies focused on the oxidative ageing of asphalt pavements can be categorised into four groups according to the various physical fields involved in pavement ageing: oxidative

kinetics, asphalt morphology, environmental conditions, and ageing effects on mechanical responses. This literature review and dissertation is focused on the first three aspects.

2.5.1 Oxidative kinetics of bitumen and asphalt

Liu et al. (1996) and Peterson and Harnsberger (1998) found that bitumen typically oxidises in two stages, a nonlinear fast-rate and linear constant-rate stages (Liu et al. 1996, Petersen and Harnsberger 1998). To quantify this phenomenon, Jin et al. (2011) developed a two-reaction kinetics model to predict CA of bitumen in various oxidative ageing conditions (Jin et al. 2011). Luo et al. (2015, 2019) extended this model to include the change in stiffness of aged asphalts in the field (Luo et al. 2015, 2019).

Oxidation kinetics of bitumen is a well-known element determining the rate of oxidative ageing. This is particularly important because studies recognised that binders of the same temperature performance grade do not necessarily achieve the same ageing performance (Rochlani et al. 2020). The dissimilarity in behaviour can be attributed to differences in the oxidation kinetics of binders. The activation energy required to cause oxidation in binders was found to be a good indicator of their ageing susceptibility (Liu et al. 1996, Glover et al. 2009a, Liu et al. 2020). Researchers adopted similar kinetics-based ageing modelling concepts and formulations to represent the physical and chemical dynamics of pavement materials (Luo et al. 2015, Wang et al. 2015, Luo et al. 2018, Luo et al. 2019). The activation energy is a binder-source dependent parameter; it is the energy required to establish a chemical reaction between oxygen and bitumen, measured in units of (kJ/mol). A high activation energy is desirable because it means the binder is insusceptible to oxidation. In contrast, low activation energy indicates the binder can age faster, i.e., more susceptible to oxidative ageing. It is found that the activation energy can be altered by the inclusion of additives (e.g., anti-ageing compounds) to the bitumen. However, the scale of this alteration in the activation energy on the field ageing of asphalt pavements is still ambiguous, particularly under a complex environmental condition including coupled temperature and oxygen distribution in the pavement structure.

2.5.2 Influence of asphalt mixture morphology on oxidative ageing

Another main physics in the oxidative ageing process is oxygen diffusion. Oxygen diffuses from the atmospheric environment to asphalt pavements to react chemically with bitumen forming carbonyl and sulfoxide functional groups. Therefore, the availability of oxygen is essential to feed this oxidative chemical reaction. Peterson (2009) and Abu Al-Rub (2013) reported that oxygen diffuses inside asphalt pavement through the interconnected air voids in the asphalt layer (Petersen 2009, Al-Rub et al. 2013). Lower air void contents result in lower oxygen diffusivity, which will reduce the severity of oxidative ageing. Yin et al. (2017) performed a tensile stiffness test on 30 field-aged asphalt samples with different air void contents and then extracted the bitumen to conduct rheology testing. They observed less hardening in the asphalt sample with a lower interconnected air-void content (Yin et al. 2017). Oxygen diffusion can be experimentally quantified in the bitumen binder and its constituents (saturates, aromatics, resins, and asphaltenes) using the oxygen absorption ageing (OOA) (Qi et al. 2003), and the oxygen diffusion in the interconnected air voids of compacted asphalt mixtures can be quantified using the diffusion apparatus developed by Wen & Wang (2018) (Wen and Wang 2018).

The oxygen accessibility from the top and bottom boundaries of the asphalt layer is the first factor influencing the oxygen diffusion and thus affecting the oxidative ageing profile in the pavement structure. The surface of asphalt concrete commonly experiences a higher degree of oxidative ageing than that of asphalt at deeper layers (Han 2011, Glover et al. 2014, Yin et al. 2017). This is a result of higher temperatures and easy access to oxygen from atmospheric air. There is debate on the carbonyl area distribution pattern and the factors that contribute to it, such as porosity of underlying layers and air voids distribution and content in the asphalt pavements. For instance, it is believed that using a treated base or milling techniques (for new overlays) will reduce the ageing of asphalt pavement (Luo et al. 2018). Thus, it is vital to investigate the effect of oxygen accessibility at the lower boundary condition of AC layer on the carbonyl area profile.

The air voids distribution and air voids content are the second and third potential influencers on oxygen pressure distribution, leading to the variations of the oxidative ageing

profile within the asphalt concrete. Many studies were focused on characterising air voids distribution within the pavement structure in terms of air voids content, number and diameter of air voids, and availability of accessible air channels (Castelblanco Torres 2006, Caro et al. 2010, Han 2011, Glover et al. 2014, Wang et al. 2014, Rose 2016, Zhao et al. 2019). Results found a non-uniform C-shaped distribution of the air voids content along the pavement depth is commonly observed in field-compacted samples (Prapaitrakul et al. 2009, Zhao et al. 2019). Where the air voids content is less at the middle than at the top and bottom of AC because of movement constraints and lower temperatures at the top and bottom upon compaction. Digital imaging techniques and volumetric testing protocols were established to determine and thus characterise the air voids distribution. CT-scanning technique measures air voids of diameters not less than 0.0211 mm with usually 0.1 mm vertical intervals (Jiang et al. 2020). Recent advancements in quality control measures, design procedures, and materials characteristics ensure the field compaction can achieve desired specifications for the average air voids content. However, it is impossible to guarantee the air voids profile within AC depth is uniform, nor it is possible to achieve a consistent profile across the pavement depth from a point to another in the same road section. For this reason, studies adopted different approaches to model and simulate the volumetric distribution of air voids. For instance, studies that developed mechanical models to represent the asphalt pavement structures either placed air voids randomly (to achieve the desired air void content, AAV%) in pavement structures (Zhang et al. 2018c, Zhang et al. 2019) or used probabilistic distribution for the air voids sizes and numbers (Castelblanco Torres 2006, Caro et al. 2010). In both modelling conditions, there was no defined relationship between the air voids distribution and pavement depth. Therefore, the current study investigates the significance of air voids content and vertical profile of voids distribution on field oxidative ageing of asphalt pavements.

The extent of oxidative ageing is also bounded by the film thickness of asphalt mastic surrounding accessible air channels within the asphalt concrete. It could be that the thicker the mastic coating thickness, the less the average carbonyl area will be. Previous studies showed that

laboratory-mixed and compacted asphalt concrete specimens with lower mastic film thickness and better mastic distribution are more susceptible to oxidative ageing, resulting in a dramatic decrease in pavement's resistance to cracking (Jiang et al. 2020). Thus it is also essential to look into the effect of mastic film thickness on the oxidative ageing propagation under field conditions.

2.5.3 Environmental effects on ageing

Environmental factors affect oxygen transport and diffusion as well as pavement temperature profile, which further impacts oxidative ageing. Prapaitrakul et al. (2009) developed an oxygen transport model to predict asphalt oxidation in pavements, which involved oxygen pressure, oxygen concentration, oxygen diffusivity, and pavement temperature (Prapaitrakul et al. 2009). Jin et al. (2013) found that oxygen diffusivity in transport media was related to the temperature and viscosity of the material (Jin et al. 2013). Lytton et al. (1993) developed a one-dimensional heat transfer model, the Enhanced Integrated Climate Model (EICM), to calculate heat conduction in asphalt pavements (Lytton et al. 1993). They assumed a constant-temperature boundary condition (BC) well below the pavement surface. The required climatic inputs included solar radiation, ambient temperature, wind speed, pavement albedo, pavement emissivity, and thermal diffusivity. Han et al. (2011) improved the prediction accuracy of the EICM by taking into account the unsteady-state heat flux boundary condition (Han et al. 2011). The modified heat transfer model was validated by comparing prediction results to measured temperature data from 29 pavement sites across the United States.

Distribution of oxidative ageing products in pavements is strongly linked to their temperature profile. Non-uniform temperature distribution within pavement depth causes oxidative ageing and pavement modulus gradients to exist (Hall et al. 2012, Yin et al. 2017). According to Lu et al. (2009), the performance of asphalt pavements is closely related to the temperature profile, and the influence of temperature on pavement performance can be more significant than that of loading level and duration (Lu et al. 2009). Further studies revealed that reduction of the temperature by several degrees was easily possible with positive implications on pavement mechanical response and environment (Hall et al. 2012). Mallick et al. (2009) used

NCHRP 1-37A MEPDG to demonstrate that for the same traffic and pavement materials, pavement life can be extended by five years for a 5°C decline in temperature (Mallick et al. 2009).

Internal factors govern the temperature profile in the asphalt pavements, including the thermal properties of paving materials, the thickness of layers, and the presence of thermal isolation fillers. These factors can be altered to control the temperature profile to some extent. Whereas the external factors, including the atmospheric temperature, geographic location, and earth temperature, cannot be controlled. Enhancing the thermal properties of asphalt pavement (to cool down its temperature) by adding thermal modifiers or isolators to prevent excessive thermal exposure is more practical than replacing paving materials with other substances or changing the thickness of pavement layers.

Several studies have quantified the effect of thermal parameters on the temperature profile of asphalt pavements (Solaimanian and Kennedy 1993, Gui et al. 2007, Lu et al. 2009, Wang et al. 2010, Bobes-Jesus et al. 2013, Alavi et al. 2014, Chen et al. 2015a, Chen et al. 2017). However, there are limited research outputs that measure the direct impact of thermal properties of paving materials on the content and distribution of oxidation products like carbonyl and sulfoxide in the field asphalt pavements. Therefore, it is vital to understand the effect of thermal properties on the temperature profile of asphalt pavement, and subsequently on the degree and extent of oxidative ageing to mitigate performance deterioration due to long-term thermal exposure and oxidation.

2.6 Constitutive Models for Ageing Related Multiphysics

Oxidative ageing of asphalt pavements is a complex process governed by oxidation kinetics, oxygen diffusion, and heat transfer. The earliest research attempts to use the Multiphysics approach for modelling the oxidative ageing of petroleum binders could be traced back to Dickinson (1984). He linked diffusion-controlled oxidative reaction to bitumen hardening using the finite difference method for unsteady-state condition (Dickinson 1984). Herrington (2012) further developed a numerical model to predict the diffusion and reaction of oxygen in petroleum bitumen films (Herrington 2012). His model parameters for the diffusion–oxidation

process were obtained by correlating oxygen uptake of bitumen solutions to changes in carbonyl infrared spectral absorption and viscosity. The model developed predicted the average viscosity in bitumen films after exposure to a constant temperature and ageing time. Following on Herrington's mathematical models, Das et al. (2015) investigated the effect of diffusion-controlled oxidative ageing on different mixture morphologies based on oxidative ageing mechanism and diffusion-reaction of bitumen using FEM (Das et al. 2015a, Das et al. 2015b, Das et al. 2015c, Das et al. 2015d). In parallel, a comprehensive experimental investigation, field ageing data collection and detailed mathematical models were carried out by (Lunsford 1994, Glover et al. 2009b, Prapaitrakul et al. 2009, Han 2011, Han et al. 2011, Jin et al. 2011, Jin 2012, Jin et al. 2013, Glover et al. 2014, Rose 2016, Cui et al. 2018). The established constitutive models to characterise ageing physics are detailed in this section.

2.6.1 Oxidative kinetics model

Oxidative kinetics of bitumen is characterised by the formation of carbonyl (C=O) and quantified by the carbonyl area (CA) measured from FTIR results. Jin et al. (2011) developed a two-reaction kinetics model to predict the reaction rate of CA in bitumen (Jin et al. 2011), as shown in **Equation 2-1**.

$$CA = CA_{tank} + (CA_o - CA_{tank})(1 - e^{-k_f t}) + k_c t \quad (2\text{-}1)$$

where CA_{tank} is the CA of unaged tank bitumen; CA_o is the intercept of the constant-rate line, which is a unitless value; k_f and k_c are fast-rate and constant-rate reaction constants, respectively, in 1/day; and t is field ageing time. The fast and constant rate reaction constants k_f and k_c are temperature and binder-source dependent and can be predicted using the Arrhenius expression shown in **Equations 2-2** and **2-3**.

$$k_f = A_f \, e^{-E_{af}/RT} \quad (2\text{-}2)$$

$$k_c = A_c \, e^{-E_{ac}/RT} \quad (2\text{-}3)$$

where A_f and A_c are fast-rate and constant-rate pre-exponential factors, respectively, in 1/day, E_{af} and E_{ac} are fast-rate and constant-rate activation energies, respectively, in kJ/mol; R is a

universal gas constant ($R = 8.314\, J/(mol \cdot K)$); and T is the absolute temperature, in K. To consider the oxygen partial pressure (as a measure of oxygen content), **Equations 2-2** and **2-3** were expanded to **Equations 2-4** and **2-5** (Jin et al. 2013).

$$k_f = A_f\, P^{\alpha} e^{\,-E_{af}/RT} \tag{2-4}$$

$$k_c = A_c P^{\alpha} e^{\,-E_{ac}/RT} \tag{2-5}$$

where P is the oxygen partial pressure and α is the reaction order for oxygen pressure. The terms $A_f\ P^{\alpha}$ and $A_c\, P^{\alpha}$ are described in ln(1/day) units.

2.6.2 Oxygen transport model

Oxygen transported in a pavement structure can be characterised by the oxygen pressure rate with time at any location within the asphalt layer. The oxygen transport model is shown in **Equation 2-6**, a 2nd order PDE (Han et al. 2011). The more aged the bitumen is, the more oxygen has been consumed; thus, the lower oxygen pressure will be in the transport media. Therefore, the equation uses CA growth rate to quantify the oxygen consumption rate as a reducing factor to the oxygen transport process.

$$\frac{\partial P}{\partial t} = \nabla(fcf.D_o\,\nabla P) - \frac{c_o\, T\, R}{h} \cdot \frac{\partial CA}{\partial t} \tag{2-6}$$

where P is the oxygen pressure; ∇ is the location derivative $[\frac{d}{dx}, \frac{d}{dy}]$; D_o is oxygen diffusivity in pure bitumen in m^2/s; c is a factor that converts the reaction rate of CA to oxygen consumption rate (3.71×10^{-4} mol/ml); fcf is the field calibration factor for the effect of fine-graded matter in the mastic; and h is the solubility constant of oxygen in asphalt, which is a unitless value. Solubility is a temperature-sensitive parameter and can be altered for any temperature using **Equation 2-7**, where h_o is the oxygen solubility in bitumen at a standard temperature of 30 °C ($h_o = 0.0076$) (Dickinson 1984). The oxygen diffusion coefficient is a function of the temperature and the viscosity of bitumen, as shown in **Equation 2-8** (Lunsford 1994, Glover et al. 2014).

$$h = h_o(1 + 0.0215\ (T - 30)) \quad (2\text{-}7)$$

$$\frac{D_o}{T} = 5.21 \times 10^{-12} LSV^{-0.55} \quad (2\text{-}8)$$

$$LSV = e^{(m+HS.CA)} \quad (2\text{-}9)$$

where *LSV* is the low-shear-rate-limiting viscosity, which is a measurement of the rheological properties of the asphalt binder when it is undisturbed by external forces (Glover et al. 2014). *LSV* is temperature- and CA-dependent. *HS* is the asphalt hardening susceptibility which is the change in log-viscosity with respect to the change in CA, and m is an experimental parameter, which is the intercept of log-viscosity with CA. *HS* and *m* are functions of temperature, as seen in **Equations 2-10** and **2-11** (Vehrencamp 1953). T_o is the standard temperature at which HS and m are measured.

$$HS(T) = HS(T_o) + \gamma\left(\frac{1}{T} - \frac{1}{T_o}\right) \quad (2\text{-}10)$$

$$m(T) = m(T_o) + \delta(\tfrac{1}{T} - \tfrac{1}{T_o}) \quad (2\text{-}11)$$

2.6.3 Heat transfer model

One dimensional Fourier's law of heat conduction is used to determine the temperature profile across pavement depth, as shown in **Equation 2-12**. The thermal diffusivity of each pavement layer and temperature transfer rate at the bottom of the pavement are illustrated in **Equations 2-13** and **2-14**, respectively (Han et al. 2011).

$$\frac{\partial T}{\partial t} = \alpha\left(\frac{\partial^2 T}{\partial^2 y}\right) \quad (2\text{-}12)$$

$$\alpha = \frac{k}{\rho\ .C_p} \quad (2\text{-}13)$$

$$\left.\frac{\partial T}{\partial y}\right|_{3m} = constant \quad (2\text{-}14)$$

where y is the pavement depth, in meters; k is the thermal conductivity of the pavement layer, in W/(m. K); ρ is the corresponding material density, in kg/m^3; α is the heat diffusivity; and c_p is

the heat capacity in J/(kg.K). The surface boundary for the heat transfer model was defined by Han et al. (2011) and represented by **Equation 2-15**.

$$\rho\, c_p \frac{\Delta y}{2}\frac{\partial T_s}{\partial t} = Q_s - \breve{\alpha}.Q_s + Q_a - Q_r - Q_c - Q_f \quad (2\text{-}15)$$

where T_s is the pavement surface temperature, in K; y is the pavement depth; Q_s is the heat flux due to solar radiation; $\breve{\alpha}$ is the albedo of the pavement surface (the fraction of reflected solar radiation); Q_a is the down-welling long-wave radiation heat flux from the atmosphere; Q_r is the outgoing long-wave radiation heat flux from the pavement surface; Q_c is the convective heat flux; and Q_f is the heat conduction from the surface into the pavement; with all heat fluxes expressed in W/m^2 (Jin et al. 2013).

2.7 Ageing Quantification and Anti-ageing Compounds

Along with the call for developing a comprehensive Multiphysics prediction model of field ageing, ageing characterisation of bitumen binders modified with anti-ageing compounds (AACs) is also needed to mitigate the ageing and build durable flexible pavements to withstand various distresses.

2.7.1 Quantifying ageing of bituminous materials

As discussed in previous sections, at the molecular level, bitumen consists of a wide variety of hydrocarbons of aliphatic and aromatic molecules, with some molecules of both aromatic and aliphatic nature. Some of these hydrocarbons also contain one or more heteroatoms, nitrogen, sulfur, and metals. Thousands of different species may be present in the bitumen, making it a monumental task to define bitumen based on specific molecular species. It is more effective to classify the chemistry according to the molecular generic groups or types (Robertson et al. 1991, Petersen 2009). A wide range of FTIR applications for bitumen exist, including materials and ageing recognition, bitumen interaction with modifiers, and moisture effects on ageing (Ma et al. 2011, Ma et al. 2012, Ma et al. 2016). For ageing recognition and quantification, researchers have established various parameters to characterise the carbonyl-growth, one of which is carbonyl area (CA) that is defined as the area integral under the absorbance curve of the FTIR

test within a wavelength range of 1820 to 1650 cm^{-1} (Cui et al. 2018). The carbonyl area is intensively used to quantify the ageing performance of petroleum bitumen. However, it has limitations in comparing the ageing performance of modified binders. Some additives contain carbonyl functional groups in their primary chemical form that may change upon ageing, making it unclear how ageing is propagated (Ma et al. 2011). Additionally, using a constant wavelength range (1820 to 1650 cm^{-1}) to define CA can cause inaccuracy in calculating the carbonyl area due to changes encountered in the absorbance wave pattern within or around that range. This case is more pronounced when bitumen lacks carbonyl before ageing, which sometimes causes a negative value. Herrington (2012) defined carbonyl area as the ratio of area under 1640 to 1810 cm^{-1} to the area under 1600 cm^{-1} peak (using 1810 cm^{-1} as a baseline)(Herrington 2012). Liu et al. (2015) introduced a carbonyl index as the carbonyl area ratio under 1700 cm^{-1} peak to that of methylene group under 1375 cm^{-1} peak to eliminate the effect of bitumen sample thickness on the carbonyl area (Liu et al. 2015). Another practice was to divide the carbonyl area under peak 1700 cm^{-1} by summation of all absorbance areas of bitumen (Lamontagne et al. 2001) or a portion of it (Yao et al. 2013). Similarly, sulfoxide index (which is an additional oxidation measure) was calculated by the same procedures but under a peak of 1031 cm^{-1} instead of 1700 cm^{-1}. It can be seen that there is no agreed or consistent method to determine the carbonyl content, and the decision was somewhat arbitrary depending on individual choices.

The attempt to characterise the ageing quantity of modified bitumen binders such as SBS polymer modified binders by carbonyl formation adds another complexity layer. This led to adopting a new set of testing methods and conditions (Ma et al. 2017). Few attempts were made to address this issue (Ma et al. 2012). Zhao et al. (2010) studied ageing characteristics and materials interaction of polymer modified bitumen using two carbonyl parameters (Zhao et al. 2010). One parameter was carbonyl index to study the ageing properties of bitumen-polymer blend. The second parameter was carbonyl area to address the changes occurring in polymer and base bitumen individually upon ageing. However, no explanation was provided for using those two various parameters. Therefore, it is difficult to compare the ageing resistance for the bitumen

with different modifiers subjectively. It is also unclear which FTIR parameter effectively ranks anti-ageing compounds (AACs) according to their performance in reducing the bitumen's ageing. Reasons for this attributed to the adoption of various ageing conditions (such as short-term ageing, long-term ageing, different temperatures and pressure conditions), evaluation criteria (rheological properties or chemical changes), and parameters used (ageing indices).

2.7.2 Anti-ageing compounds for ageing mitigation

The oxidative ageing causes hardening of the material and increases the likelihood of fracture of a pavement due to the decreased resistance to fatigue cracking (Tauste et al. 2018). Fatigue cracking is a result of repeated traffic loads and pavement materials degradation under rigorous environmental conditions, such as exposure to heat, solar radiation, and oxygen from air. The in-service asphalt pavements are more susceptible to fatigue cracking at later stages of their life as asphalt mixtures become brittle due to ageing. Fatigue resistance of bitumen binders was found to fundamentally determine and directly correlate to the fatigue resistance of asphalt mixtures (Anderson and Kennedy 1993, Wang et al. 2016). Therefore, one solution to prolong the service life of asphalt pavements and prevent fatigue failure is by modifying the bitumen with anti-ageing compounds (AACs).

AACs are believed to reduce oxidative ageing, one of the major contributors to pavement ageing (Petersen 2009). Researchers found that these additives can reduce the growth of carbonyl and sulfoxides (Gawel et al. 2016). The development of oxidation products associates with the increase in molecular size of asphaltenes, resins and reduction of free volume space for saturates, causing less molecular diffusion and decreases the self-healing capability of bitumen, leading to bitumen hardening (Xu and Wang 2017). Therefore, inducing AACs reduces bitumen hardening, enhances fatigue resistance in asphalt pavements, and prolongs their service life. However, a consistent primary selection criterion to screen promising AACs is needed. Additionally, the effect of AACs incorporation on the ageing kinetics of bitumen (and thus, pavements) requires further investigation.

2.8 Characterisation of Anti-ageing Compounds Modified Bitumen

2.8.1 Fatigue characterisation methods for AAC-modified bitumen

The fatigue behaviour of asphalt binders is characterised using the dynamic shear rheometer (DSR) test, and the criterion of fatigue failure of bitumen binders is a subject of on-going research (Pronk and Hopman 1991, Anderson and Kennedy 1993, Bahia et al. 1999, Ghuzlan and Carpenter 2000, Anderson et al. 2001, Wang et al. 2016). Many studies stated the Superpave asphalt binder specification criterion for fatigue characterisation to be inaccurate, particularly for polymer-modified bitumen. Mainly because the Superpave fatigue parameter ($|G^*| \cdot \sin \delta$), where G* is the complex shear modulus and δ is the phase angle, relies on the linear viscoelastic properties at undamaged conditions (relatively small strain levels), producing unrepresentative results. Still, in reality, the fatigue failure occurs at high strain levels where the bitumen is in damaged conditions. Therefore, the use of undamaged viscoelastic properties alone yields inaccurate fatigue characterisation, which is more pronounced in modified bitumen (Bahia et al. 1999, Anderson et al. 2001, Wang et al. 2018). Thus, a different fatigue evaluation term called the dissipated energy ratio (DER) was employed to characterise the fatigue behaviour of asphalt binders. DER gave a better representation of the fatigue properties of a various range of binders (Pronk and Hopman 1991, Ghuzlan and Carpenter 2000, Anderson et al. 2001). DER is represented by **Equations 2-16, 2-17** and **2-18** (Pronk and Hopman 1991).

$$W_i = \pi \sigma_i \gamma_i \sin(\delta_i) \tag{2-16}$$

$$W_{\sum n} = \sum_{i=1}^{n} W_i \tag{2-17}$$

$$DER = \frac{W_{\sum n}}{W_n} \tag{2-18}$$

where W_i is dissipated energy density at load cycle i; σ_i is the stress amplitude at load cycle i; γi is the strain amplitude at load cycle i; δi is the phase angle at load cycle i; and $\sum W_i$ is the cumulative dissipated energy (W_n), up to cycle n.

A new fatigue measure for asphalt binders was proposed recently by Zhang and Gao (2021) using a DSR-based crack (DSR-C) growth model derived from dissipated strain energy equilibrium principle and damage mechanics (Zhang and Gao 2021). They employed DSR test to

determine the shear moduli and phase angles at both undamaged and damaged conditions. Two DSR testing schemes were adopted: (1) linear amplitude sweep (LAS) to obtain the undamaged material properties; (2) time sweep (TS) tests to obtain the fatigue properties at the damaged condition. Results were validated at different temperatures, frequencies and strain levels. The fatigue damage was quantified directly by a predicted crack length (c_p), illustrated in **Equation 2-19**.

$$c_p = \left[1 - \left(\frac{|G_N^*|/sin(\delta_N)}{|G_o^*|/sin(\delta_o)}\right)^{\frac{1}{4}}\right] r_o \quad (2\text{-}19)$$

where, r_o is the original radius of the sample; $|G^*_N|$ and $|G^*_o|$ are the shear moduli for the damaged and undamaged samples, respectively; δ_N and δ_o the phase angles of the damaged and undamaged samples, respectively; and c_p is the predicted crack length at the N^{th} loading cycle of time sweep fatigue test.

The crack length predicted by DSR-C model (**Equation 2-19**) was effectively validated for virgin and polymer-modified bitumen at different loading and temperature conditions. A digital visualisation approach similar to that employed by Hintz and Bahia (2013) and Shan et al. (2017) was adopted for DSR-C model validation (Hintz and Bahia 2013, Shan et al. 2017). The fatigue evaluation approaches mentioned earlier are used in the present study to investigate the fatigue performance of bitumen modified with different AACs.

2.8.2 Changes in chemical composition and fatigue resistance

Some studies attempted to recognise a link between ageing-induced chemical changes and fatigue and healing behaviour of bitumen (Wu et al. 2009, Xu et al. 2017). SARA (saturates, aromatics, resins and asphaltenes) fractionation technique was utilised for this purpose. It was observed that a higher ratio of flocculated fractions (asphaltenes and saturates) to dispersed constituents (aromatics and resins) in bitumen led to a higher $|G^*|\cdot\sin\delta$ value. This observation means the higher the flocculated content, the stiffer the bitumen will be (Sun et al. 2017, Ameri et al. 2018, Yang et al. 2018, Wang and Wang 2019). Therefore, bitumen will be more prone to fatigue cracking. Others investigated the effect of molecular size of bitumen components on the

fatigue properties of asphalt binders using Size Exclusion Chromatography test (Jennings et al. 1981, Sun et al. 2017, Wang and Wang 2019). Findings explained that the existence of small molecules within the binder is favourable for improving fatigue resistance performance, and bigger size molecules generate poor fatigue resistance. However, SARA fractionation techniques and molecular size analysis pose limitation concerns due to the continuous introduction of various new types of modifiers and chemical additives to bitumen (Wang and Wang 2019). These standard practices are designed to analyse petroleum bitumen without any modifiers. When used for modified binders, these tests can only characterise the chemical composition of their base binders rather than the combination of bitumen with chemical additives (Wang and Wang 2019). Thus, a direct correlation between oxidative ageing products and fatigue performance for aged asphalt binders (including those modified with AACs) is needed.

A few attempts correlate the fatigue behaviour of bitumen to its molecular structure using FTIR test results (Jennings et al. 1981, Sun et al. 2017). These attempts utilised FTIR absorption peaks 1600, 1460, and 1376 cm^{-1} to characterise fatigue damage behaviour of asphalt binders, where those peaks represent benzene ring, methylene CH2 and methyl CH3, respectively. These functional groups are employed to evaluate the chemical structures of bitumen, where the higher the ratio of area under peak 1460 cm^{-1} to that for peak 1376 cm^{-1}, the lower the branched-chain molecules in the sample. In contrast, the higher the area under peak 1600 cm^{-1}, the higher the molecular weight of bitumen. However, peaks 1600, 1460 and 1376 cm^{-1} remain unchanged during ageing (Xu and Wang 2017). Therefore, this FTIR analysis approach cannot evaluate ageing effects on the fatigue behaviour of bitumen binders. It is believed that pavements are more susceptible to fatigue cracking at later stages of their service lives when asphalt is severely aged (McGennis et al. 1994, Hajj and Bhasin 2018), and ageing induced growth of oxidation products affects binder-aggregate molecular adhesion properties (Gao et al. 2018, Gao et al. 2019). Therefore, further studies are needed to investigate any links between the chemical functional groups responsible for ageing and fatigue performance of long-term aged (LT-aged) modified-

asphalt binders. This would establish a step further in building a comprehensive mechanistic pavement performance prediction model.

2.9 Summary of Literature Review

This critique of the available literature has indicated that long-term ageing occurs in the pavement service stage and is mainly due to the oxidation process. Ageing of asphalt materials involves three Multiphysics (1) chemical oxidation reaction in the bitumen; (2) mechanical responses (e.g., altered viscosity); and (3) physical environmental processes (i.e., heat transfer and oxygen diffusion) leading to varying environmental profiles within pavements. These processes are influenced by the microstructural morphology, including asphalt film thickness, pore size, and air void distribution. The Multiphysics nature of ageing has been well characterised by ageing theories and field measurements, as shown in the above studies. However, applying Multiphysics models in ageing predictions, considering their circular and time-dependency, is limited due to some FE modelling restrictions.

Moreover, the existing studies evaluated the influences of pavement material properties (e.g., thermal properties and oxidation kinetics), structural parameters (e.g., air voids content and distribution, and mastic coating film) or climate conditions on the oxidative ageing in the asphalt pavements, separately. This kind of parametric evaluations is relatively isolated, which means the interactions or constrains between the material, structural, and climate variables on the ageing evolution were not accounted for. This may have already resulted in misleading conclusions on the significance of one parameter on the ageing production.

Additionally, there are recognised limitations in ageing quantification. For instance, there is no agreed or consistent method for effectively determining oxidation products content, leading to difficulties in nominating anti-ageing compounds to reduce or mitigate ageing. Finally, studies concerned with anti-ageing materials were mostly laboratory-based, and the true impact of these additives on ageing evolution and propagation is still ambiguous.

Chapter 3 Integration of Ageing Multiphysics Models in Equation-based Finite Element Modelling Framework*

The oxidative ageing process results from chemical and physical operations happening concurrently in the complex pavement structure under the influence of constantly changing environmental conditions in the field. As discussed in the previous chapter, analytical methods are incapable of accommodating a key objective in this study, which is accounting for the effect of various physics. Thus, this chapter develops a weak form partial differential equation (PDE) based finite element (FE) models as a Multiphysics tool to accurately predict the oxidative ageing growth in terms of carbonyl area production while considering the changes in environmental profiles (i.e., heat transfer and oxygen diffusion) and physical properties (i.e., viscosity). This chapter includes a brief introduction to weak form PDEs, then details of each component of the comprehensive oxidative ageing model are presented, including: (1) model geometry, (2) model interfaces, (3) model variables, (4) model parameters, (5) interpolation functions, and (6) user-defined materials properties. Finally, a database of physiochemical properties of field-oxidised asphalts will be collected from the existing literature.

3.1 Weak Form PDE based FE Modelling

The weak form partial differential equation (PDE) based FE modelling is adopted to solve time-dependent physics on a two-dimensional domain without the need for user subroutine programming. As a general-purpose FE program, Comsol Multiphysics provides an efficient computational platform to solve PDEs (Comsol Multiphysics Reference Manual 2013). The weak form of a PDE is an important mathematical analysis method to find the solutions to the PDE. A

* Models developed in this chapter are published as part of : Omairey, E. L., et al. (2021). "An equation-based Multiphysics modelling framework for oxidative ageing of asphalt pavements." Journal of Cleaner Production 280: 124401. https://doi.org/10.1016/j.jclepro.2020.124401

weak form of the differential equations is equivalent to the governing equation and boundary conditions. i.e. the strong form. In many disciplines, the weak form has specific names; e.g., it is called the principle of virtual work in stress analysis (Jacob and Ted 2007).

The major advantage of using the weak form of PDE modelling in Comsol rather than traditional FE modelling is that no user subroutine is needed, and the control/constitutive equations of different physics can be defined and solved by equation-based models. Thus the different physics such as viscoelasticity, plasticity, fracture, heat transfer and moisture diffusion can be easily modelled using weak form PDEs (Zhang et al. 2016, Zhang et al. 2018b).

To summerise how weak form PDEs work, assume a two-dimensional heat transfer equation at unsteady-state condition (temperature change with time) with a heat source. Therefore, the temperature (T) will be a function of the position (x, y) and time (t) working in a specific domain defined by x and y intervals. The equation involves the second derivative of the temperature, and its solution will give the temperature profile within the specified domain. Solving the second derivative can cause numerical issues in practical situations where the differentiability of the temperature profile may be limited (Liu 2014). For instance, at a boundary where the adjacent materials have different values of thermal conductivity, the first derivative of the temperature becomes discontinuous, and the second derivative can not be evaluated numerically (Liu 2014). This can happen when modelling the temperature profile of a pavement of different layers. The weak form role is to turn PDE into an integral equation to simplify the numerical algorithm.

To turn the differential equation (**Equation 3-1**) into an integral equation, a first approach may integrate it over the entire domain (**Equation 3-2**).

$$\frac{\partial T}{\partial t} = \frac{k}{\rho \,.C_p}\left(\frac{\partial^2 T}{\partial x^2} + \frac{\partial^2 T}{\partial y^2}\right) \tag{3-1}$$

$$\int_{\Omega} \left[-\frac{\partial T}{\partial t} + \frac{k}{\rho \,.\, C_p}\left(\frac{\partial^2 T}{\partial x^2} + \frac{\partial^2 T}{\partial y^2}\right)\right] d\Omega = 0 \tag{3-2}$$

where, Ω is the entire domain. Thus, the average value over the entire domain is zero. This is "too weak" compared to the strong form in **Equation (3-1)**. To improve this, the integrand is multiplied by a weight function or a test function, test(T), that is non-trivial only in a narrow range. Each weight function limits the contribution of the integrand to a narrow range centred around different x and y values, thus achieving the same effect as the collection of integral equations (Liu 2014). The weight function can be thought of as an enforcer: whatever it multiplies is enforced to be zero by its arbitrariness (Jacob and Ted 2007). Thus, when applying Galerkin method, **Equation (3-2)** will be;

$$\int_{\Omega}\left[-\frac{\partial T}{\partial t}+\frac{k}{\rho\,.\,C_p}\left(\frac{\partial^2 T}{\partial x^2}+\frac{\partial^2 T}{\partial y^2}\right)\right]test(T)\,d\Omega=0 \tag{3-3}$$

Or it can be written as:

$$\int_{\Omega}-\rho\,.\,C_p\frac{\partial T}{\partial t}.test(T)d\Omega+\int_{\Omega}k\left(\frac{\partial^2 T}{\partial x^2}+\frac{\partial^2 T}{\partial y^2}\right)test(T)\,d\Omega=0 \tag{3-4}$$

To reduce the order of differentiation of the second term in **Equation (3-4)**, the method of integration by parts is used. So that:

$$\frac{\partial^2 T}{\partial x^2}.test(T)=\frac{\partial}{\partial x}\left(\frac{\partial T}{\partial x}.test(T)\right)-\frac{\partial T}{\partial x}.test(Tx) \tag{3-5}$$

$$\frac{\partial^2 T}{\partial y^2}.test(T)=\frac{\partial}{\partial y}\left(\frac{\partial T}{\partial y}.test(T)\right)-\frac{\partial T}{\partial y}.test(Ty) \tag{3-6}$$

where test(Tx) and test(Ty) are derivatives of the weight function test(T) in x and y directions. By retaining these two equations in **Equation (3-4)**, it will be;

$$\begin{aligned}\int_{\Omega}-\rho\,.\,C_p\frac{\partial T}{\partial t}.test(T)d\Omega+\int_{\Omega}k\,\frac{\partial}{\partial x}\left(\frac{\partial T}{\partial x}.test(T)\right)d\Omega-\int_{\Omega}k.\frac{\partial T}{\partial x}.test(Tx)\,d\Omega\\+\int_{\Omega}k\,\frac{\partial}{\partial y}\left(\frac{\partial T}{\partial y}.test(T)\right)d\Omega-\int_{\Omega}k.\frac{\partial T}{\partial y}.test(Ty)\,d\Omega=0\end{aligned} \tag{3-7}$$

The second and fourth terms of the equation are converted to boundary elements using the divergence theorem. Thus,

$$\int_{\Omega} k\ \frac{\partial}{\partial x}\left(\frac{\partial T}{\partial x}.test(T)\right)d\Omega + \int_{\Omega} k\ \frac{\partial}{\partial y}\left(\frac{\partial T}{\partial y}.test(T)\right)d\Omega = \int_{\partial\Omega} k\ \frac{\partial T}{\partial x}.test(T).\eta_x.ds + \int_{\partial\Omega} k\ \frac{\partial T}{\partial y}.test(T).\eta_y.ds \quad (3\text{-}8)$$

where $\partial\Omega$ being the boundary of the domain, η_x and η_y are the normal vectors oriented away from the domain, and ds is a small length on the boundary. Thus, the first derivatives of the solved variables (called the natural boundary condition or the Neumann boundary condition) can be represented in the weak form PDE. The fixed boundary condition (i.e., Dirichlet boundary condition) can be specified too. The weak formulation uses the exact mechanism of test functions and its natural boundary conditions to construct additional terms for the fixed boundary conditions so that the overall flux at a particular boundary generates a constant value for the variable.

The other parts of **Equation (3-7)** represents the weak form of the equation, and it is also the overall equation if there was no flux at the boundaries. It is written as;

$$\int_{\Omega}\left[-\rho\ .C_p\frac{\partial T}{\partial t}.test(T) - k.\frac{\partial T}{\partial x}.test(Tx) - k.\frac{\partial T}{\partial y}.test(Ty)\right]d\Omega = 0 \quad (3\text{-}9)$$

Therefore, the weak formulation can be implemented by enforcing test functions to clamp down the solution, then integrating the weak form by parts to provide the numerical benefit of reduced differentiation order and provide a natural way to specify boundary conditions. In the following sections, a framework is proposed to model the oxidative ageing of asphalt pavements in the field using the PDE solver, Comsol. The proposed finite element framework consists of (1) model geometry (physical domains) with specified materials properties for each domain; (2) model physics (represented by the weak form of PDEs); and (3) model parameters, variables, and time-dependent interpolation functions.

3.2 Model Geometry for Ageing Simulation in Asphalt Pavements

A two-dimensional geometry was developed in this study (**Figure 3-1**). The dimensions of the geometry are customised according to pavement structure and volumetric properties of the asphalt mixture. The geometry consists of three main domains: (1) interconnected air channels in the asphalt concrete (AC) layer, (2) mastic coating film and, (3) underlying pavement layers (base, subbase and subgrade). Herein, the thickness of the mastic coating film is defined as the diffusion depth (d_D) which is different from the conventional film thickness, in that it is the bitumen mastic coating film thickness that surrounds the interconnected air channels, not the aggregate particles (Glover et al. 2014). **Figure 3-2** illustrates the idea of diffusion depth, where oxygen diffuses horizontally in a hollow cylinder from the air channel along the mastic coating thickness towards the mastic-aggregate interface. The diffusion depth approach is more realistic in reflecting the nature of the pavement structure in that the diffusion of oxygen into the mastic occurs via the surface area of the mastic exposed to air (i.e., surrounding air channels), rather than that surrounding the aggregate particles. The diffusion depth is defined in **Equation 3-10** (Glover et al. 2014).

$$d_D = \frac{V_{be}}{S_{ea}} \tag{3-10}$$

where V_{be} is the volume of effective binder (total volume of bitumen in the mix excluding the volume absorbed by aggregate), and S_{ea} is the exposed surface area of binder to the accessible air voids. The overall two-dimensional mesh consists of 15625 elements with 1550 edge elements and 12 vertex elements.

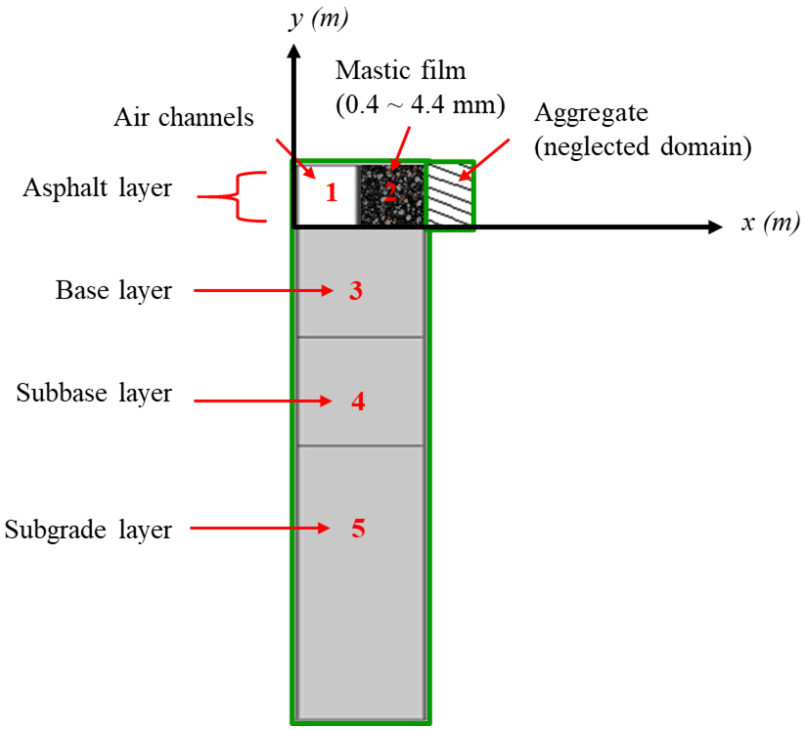

Figure 3- 1 Geometry of the integrated ageing model (not plotted to a scale). The domains of the geometry are identified by numbers (domain 1: interconnected air channels, domain 2: mastic coating film, domain 3: base layer, domain 4: subbase layer, and domain 5: subgrade layer). Domain 2 has two vertical interfaces, air-mastic interface and mastic-aggregate interface. Aggregate is not included in the geometry.

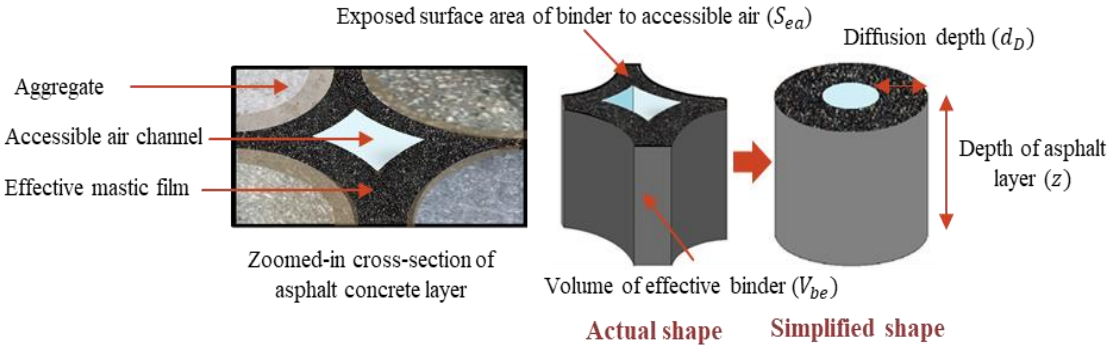

Figure 3- 2 Graphic illustration of the diffusion depth of oxygen in the asphalt pavement.

The heat transition rate among the different pavement layers affects the temperature profile in the topmost layer (AC layer); consequently, it affects the overall oxidative ageing process in asphalt. Therefore, to accurately simulate the heat transfer, the proposed geometry

includes the entire pavement structure even though underlying layers (i.e., base, subbase and subgrade layers) do not suffer from oxidative ageing.

3.3 Model Interfaces for Ageing Multiphysics

This section describes the model interfaces to couple the constitutive models discussed earlier in **Chapter 2 (Section 2.6)** into one integrated Multiphysics ageing model. Specifically, five interfaces are coupled together to form the oxidative ageing model. These interfaces and their active domains on the geometry are shown in **Figure 3-3**. In this figure, there are five interfaces (heat transfer in pavement, vertical diffusion of oxygen in the interconnected air voids, horizontal diffusion of oxygen in the asphalt mastic, carbonyl area growth at the air-mastic contact surface, and carbonyl area growth in the asphalt mastic), each work at a certain domain in the geometry, called the active domain (represented by red highlights in **Figure 3-3**). For example, the interface, horizontal diffusion of oxygen in the asphalt mastic, will make use of the oxygen diffusion equation (**Equation 2-6**), and it will be held active in the asphalt mastic (domain 2 of the geometry). More details on this are mentioned in the following sub-sections.

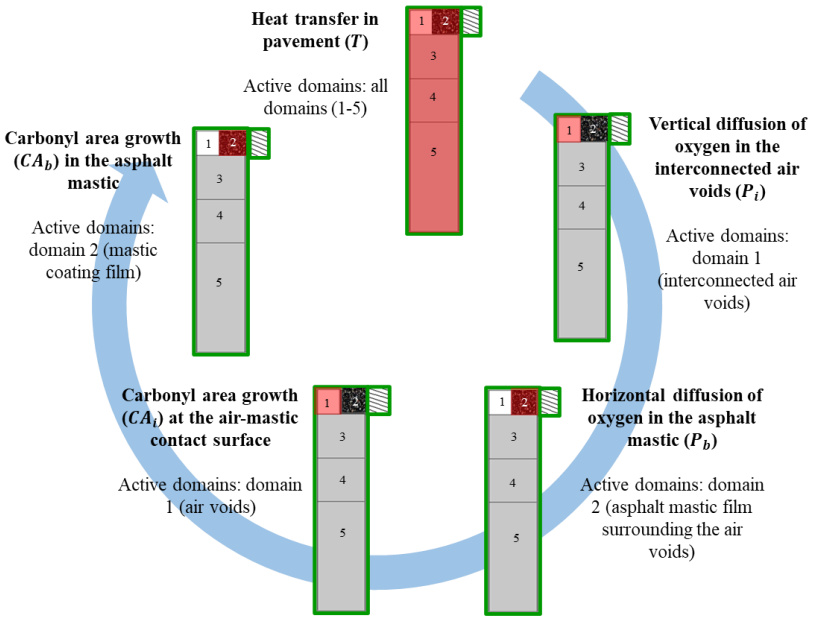

Figure 3- 3 Model interfaces and their active domains in the geometry (highlighted in red colour). The model interfaces work simultaneously and circularly with each other.

3.3.1 Heat transfer in pavement layers interface (T)

The time-dependent pavement temperature profile uses the weak form interface. Comsol solver can simulate any physics with this interface as it provides a blank platform to construct mathematical models, as shown in **Equation 3-11**.

$$\int_{\Omega} [weak\ expression\ to\ be\ input] d\Omega = 0 \tag{3-11}$$

The pavement heat transfer process (i.e., conduction, convection and radiation) are simulated with weak contributions at the active boundaries. Fourier's law equation at unsteady heat transfer in a two-dimensional domain (**Equation 3-1**) is converted into the weak form with some added customised inputs (i.e., heat sources) (Comsol Multiphysics Reference Manual 2013). The weak expression of the equation is input as:

$$\begin{aligned} -Tt * test(T) * material.rho * material.Cp * 1[m] - material.k\_iso * Tx \\ * test(Tx) * 1[m] - material.k\_iso * Ty * test(Ty) * 1[m] \end{aligned} \tag{3-12}$$

where Tt is time derivative of temperature in K/s; test(T) is a test function of temperature; material.rho is the prespecified density of each domain; material.Cp is the prespecified heat capacity for each domain; material.k_iso is the isotropic thermal conductivity at each domain; Tx is derivative of temperature in x-direction; and Ty is temperature derivative in y-direction.

Since the heat transfer interface is held active for all the domains (active domain=all domains in the geometry), the thermal properties for each domain are defined. The thermal properties are described in material components (**Section 3.4**).

The initial temperature in the geometry (at $t = 0$) is set to be the mean annual subsurface soil temperature (T=T0), which is the temperature measured at a depth of three meters (Dickinson 1984). The initial temperature was found to have negligible short-term effects on the heat transfer model and no impact on the overall ageing model. In addition, the initial rate of heat transfer is set at zero (initial conditions: $\frac{\partial T}{\partial t} = 0$).

The temperature at the lower boundary is also considered a constant, equals to the mean annual subsurface soil temperature (Dirichlet boundary condition at the bottom boundary of the geometry: T=T0). Therefore, the bottom boundary for the heat transfer interface depends on the climatic region where the road section is located. This assumption provides more area-specific inputs that can increase the accuracy of the temperature profile. The subsurface soil temperatures at different depths are available in the Climate Tool at the Long-Term Pavement Performance (LTPP) database. They are originally collected from the National Aeronautics and Space Administration (NASA), for the project Modern-Era Retrospective analysis for Research and Applications, Version 2 (MERRA-2), where the depths of the subsurface temperatures are available in detail.

Heat fluxes at the top boundary condition of the geometry (boundary condition at the surface of the pavement) are defined as:

$$((1 - albedo(t)) * Qsolar(t)) * 1[m] + ((hc * 1[W/m\text{^}2/degC]) * (Tair(t) - T)) * 1[m] + (5.67E - 8[W/m\text{^}2/K\text{^}4] * (ac * (Tair(t))\text{^}4 - emissivity(t) * T\text{^}4)) * 1[m] \quad (3\text{-}13)$$

where, albedo(t) is prespecified hourly albedo values input in the model as time-dependent interpolation function; Qsolar(t) is the hourly time-dependent shortwave solar radiation; hc is the coefficient of heat transfer at the surface of asphalt pavement; Tair(t) is hourly recorded air temperature introduced as a time-dependent interpolation function; and emissivity(t) is hourly emissivity values which are also time-dependent.

The external vertical boundaries of the overall geometry are considered thermally insulated (no heat flux across the vertical borders); thus, the temperature gradient across the boundary is zero. The topmost boundary of the pavement (which makes up the upper borders for the air voids and mastic domains) is defined according to Han et al. (2011) in **Equation 2-15** (Han et al. 2011). This equation is broken down in the current model into several general inward heat flux equations. The convective heat flux is defined in the model using the equation:

$$Q_c = (T_{air} - T)\, h_c \tag{3-14}$$

where T_{air} is the air temperature at the road section, in K; and h_c is the heat transfer coefficient obtained by Vehrencamp's empirical equation (**Equation 3-15**) and employed by Lytton et al. (1993) and Han et al. (2011) for the determination of pavement temperature profiles by using the finite difference method (Vehrencamp 1953, Lytton et al. 1993, Han et al. 2011).

$$h_c = 698.24 * 1.4\,(0.00144\,\left(abs\left(\frac{T+T_{air}}{2}\right)\right)^{0.3} * U_{wind}^{0.5} + 9.7 * 10^{-4} * \left(abs(T - T_{air})\right)^{0.3}) \tag{3-15}$$

where U_{wind} is the wind speed above the road section, in m/s. T_{air} and U_{wind} are hourly inputs, therefore they are introduced to the model as interpolation functions (refer to **Section 3.4**).

The down-welling and ongoing long-wave radiations are defined as:

$$Q_a - Q_c = 5.67 * 10^{-8} * (ac * {T_{air}}^4 - ec * T^4) \tag{3-16}$$

where ac is the absorption coefficient of the pavement. It is a climatic region-dependent model parameter, and ec is the emission coefficient of the pavement, which is a time-dependent coefficient; therefore, it is introduced in **Section 3.4** using time interpolation function tool.

Finally, the heat flux within the pavement at the surface is expressed by Fourier's law:

$$Q_f = -k\frac{\partial T}{\partial y} \tag{3-17}$$

The heat transfer physics employs the LTPP Climate Tool to obtain site-specific hourly air temperature, wind speed, solar radiation, albedo and emissivity values. Therefore, this model covers more time-dependent parameters, such as albedo and emissivity coefficient, which were considered constants or seasonal variables in the previous pavement profile prediction model (Han 2011). Additionally, the previous model calculates the hourly heat flux on the surface and the temperature at different depths using the finite-difference approximation. In contrast, this model measures the temperature profile at any point simultaneously. Another improvement is that

the current model uses the field mean subsurface soil temperature as a bottom boundary, which is location-dependent, rather than using a fixed decline rate or a constant value for all the climate regions.

3.3.2 Oxygen diffusion along interconnected air channels interface (P_{air})

Oxygen diffuses from the ambient air into the interconnected air channels first, before it spreads into the bitumen mass. Therefore, it is imperative to simulate oxygen diffusion from the air to the accessible air channels. In Comsol solver, the weak form and the coefficient form PDE interfaces can be used to simulate oxygen diffusion in the air voids. The coefficient form PDE interface is a general interface that can solve one dependent variable in up to second-order derivatives in both time and space (Comsol Multiphysics Reference Manual 2013). Comsol converts this equation into weak-form internally before solving it. The general form of the equation is:

$$\frac{\partial^2 u}{\partial t^2} + d_a \frac{\partial u}{\partial t} + \nabla.(-c\,\nabla u - \propto u + \gamma) + \beta.\nabla u + au = f \tag{3-18}$$

$$\nabla = [\frac{\partial}{\partial x}, \frac{\partial}{\partial y}] \tag{3-19}$$

where u is the dependent variable to solve for, and d_a, c, γ, β, a and f are user-defined coefficients. To utilise the general form PDE in **Equation 3-18** to determine oxygen diffusion in the interconnected air channels as expressed in **Equation 2-6**: u is defined as the partial pressure of oxygen (P_{air}); c is defined as the coefficient of oxygen diffusion in the air voids (D_{o_2}) which is related to the air voids percentage in the AC mix; γ, β, and a are all substituted by zero; and d_a is replaced by 1. The source term f is expressed by:

$$f = -\frac{c_o RT}{h} . \frac{\partial CA}{\partial t} \tag{3-20}$$

This interface is held active for the interconnected air channels domain only (domain 1 in **Figure 3-1**). The amount of oxygen in the AC matrix is measured and represented by the oxygen partial pressure, as described in **Equation 2-6**. According to **Equation 2-6**, the oxygen consumption rate is inversely proportional to the CA-growth rate. The same also applies to the

oxygen content in the air channels; therefore, the carbonyl area considered in this physics is CA at the air channel-mastic interface, namely, CA_i. The approximate diffusion coefficient (D_{o_2}) in the air channels is obtained from the work of Wen and Wang (2018) by correlating D_{o_2} to the air voids content in the asphalt mixture (Wen and Wang 2018). Therefore, D_{o_2} is a constant that is dependent on the asphalt morphology. Moreover, the field correction factor fcf mentioned in **Equation 2-6** is given a value of 1 for the diffusion of oxygen in the air channels.

The initial value for the oxygen partial pressure is considered equal to the oxygen pressure in the ambient air (0.2 atm), while the initial oxygen partial pressure rate (at $t = 0$) is zero. Additionally, since the air channel is connected to the atmospheric air, the boundary condition of the oxygen partial pressure at the topmost surface of the air voids channel is taken to be 0.2 atm at any time. The same applies to the AC-base course interface, where the unbound base layer is assumed to be porous, thus allowing free access of the air to the AC layer (Wang et al. 2014). Therefore, oxygen partial pressure at the bottom surface boundary of the air voids channels (domain 1 in **Figure 3-1**) equals 0.2 atm (Han 2011). When a treated base is used, such as cement or asphalt treated base, access to free air is constrained, leading to the unavailability of oxygen; thus, the oxygen partial pressure at any time will be zero. The effect of using an impermeable base layer on oxidative ageing is discussed in **Chapter 5**. One additional BC is considered here: the interface between the air channel and the bitumen coating surface (bounds domain 1 from the right side in **Figure 3-1**). The partial pressure here is interchangeable (circularly dependent) between the air-channels and the mastic coating. Therefore, the boundary condition is defined as ($P_{air} = P_b$), where P_b is the oxygen partial pressure in the AC mastic.

Now that the coefficient form interface was discussed in detail, the weak form interface is illustrated. The advantages of using the weak form over the coefficient form interface are that the weak form is more simplified/generalised and can be implemented to solve any mathematical model. Therefore, it can be used to simulate all model physics with minimum user training. The weak expression is defined as:

$$Pairt * test(Pair) + (if(Pair < 0.0001[atm],0, c0 * T * R/h * d(CAi, TIME))) * test(Pair) + Pairx * test(Pairx) * Do2 + Do2 * Pairy * test(Pairy) \quad (3\text{-}21)$$

where Pairt is the time derivative of oxygen pressure in air channels; test(Pair) is the test function of oxygen pressure in air channels; Pair is the oxygen pressure in air channels measured in Pa; CAi is carbonyl area at the air channels-mastic interface; Pairx and Pairy are Pair derivatives in x and y directions, respectively; Do2 is the coefficient of oxygen diffusion in the air channels (function of air voids content); test(Pairx) and test(Pairy) are derivatives of Pair test function for x and y, respectively; and Pb is oxygen pressure in the mastic coating.

Similar to the coefficient form interface, the active domain is specified as domain 1 (shown in **Figure 3-1**), with Pair initial (at t=0) is 0.2 atm, and $\frac{\partial Pair}{\partial t} = zero$. The boundary condition at the air channel-bitumen coating interface (vertical line between domains 1 and 2) is defined as a Dirichlet boundary with ($P_{air} = P_b$) at the air channel-bitumen coating interface. Finally, at the top and bottom of domain 1 (at the top and bottom of the air pores domain), a Dirichlet boundary condition is also defined as ($P_{air} = 0.2\ atm$).

3.3.3 Oxygen diffusion inside the mastic coating film interface (P_b)

When oxygen diffuses into the interconnected air channels, it then spreads into the bitumen mastic and causes oxidation. The coefficient form PDE and weak form interfaces can be utilised to simulate the diffusion process of oxygen in the mastic phase, and the latter is detailed here. The equation is activated in domain 2 (shown in **Figure 3-1**), representing the AC mastic coating film. In this interface, the oxygen partial pressure (P_b) describes the oxygen content by using **Equation 2-6**. The coefficient of diffusion here is CA- and temperature-dependent variable (D_o) according to **Equation 2-8,** unlike the coefficient of oxygen diffusion in the air channels (D_{o2}) which was a constant value and dependent on the structure of the mixture (air voids content-dependent). Since D_o is not constant; it is introduced to the model as a variable (**Section 3.4**). Additionally, since oxygen diffusion is carbonyl area dependent (**Equation 2-6**), the carbonyl

area considered here is the stationary carbonyl area inside the mastic film (domain 2 in **Figure 3-1**), namely (CA_b). Whereas the field calibration factor fcf was given a value of 1 because all the AC volumetric properties are available. The weak expression will be:

$$Pbt * test(Pb) + \left(if\left(Pb < 0.0001[atm], 0, c0 * T * \frac{R}{h} * d(CAb, TIME) \right) \right) * test(Pb) + Pbx * test(Pbx) * D * fcf + D * fcf * Pby * test(Pby) \quad (3\text{-}22)$$

where Pbt is time derivative of oxygen pressure in the mastic coating film; test(Pb) is the test function for oxygen pressure in mastic; CAb is carbonyl area in the mastic coating film; Pbx and Pby are Pb derivatives in x and y directions, respectively; and test(Pbx) and test(Pby) are derivatives of Pb test function with respect to x and y.

The boundary conditions of this interface are defined as follows. The initial partial oxygen pressure is considered to have a small initial value of 0.0001 atm, and the initial rate of oxygen partial pressure is set to zero. Since the topmost and bottom surfaces of mastic are freely exposed to the ambient atmospheric air, the oxygen partial pressure at these two BCs is defined as 0.2 atm at any time. The BC at the mastic-air channels interface (shown in **Figure 3-1** as a vertical line between domains 1 and 2) is defined as ($P_b = P_{air}$). Therefore, this interface is circularly dependent on the vertical diffusion of oxygen in the air channels interface. In other words, the oxygen partial pressure in the air channels model serves as a line BC for the oxygen partial pressure in the mastic interface.

Oxygen diffusion within the asphalt layer is a central component of modelling the oxidation process. However, the rate and extent of oxidation are bitumen-source dependent; therefore, the following two model interfaces are employed to simulate oxidation kinetics. Two different interfaces for the oxidation rate are necessary because it is also oxygen pressure dependent. Furthermore, since the air channels possess a coefficient of oxygen diffusion different from that in the bitumen mastic, an interface is needed to simulate the carbonyl growth at the

mastic-air channel interface and use it as a boundary condition for the growth of carbonyl inside the mastic.

3.3.4 Carbonyl area at the mastic-air channels interface (CA_i)

This interface is held active at domain 1 (shown in **Figure 3-1**) to determine the growth of carbonyl at the mastic-air channels interface. The model uses the differential form of **Equation 2-1**, shown in the kinetics **Equation 3-23** (Jin et al. 2013) to predict the carbonyl area (CA_i).

$$\frac{\partial CA_i}{\partial t} = M_{RTFO} k_f e^{-k_f t} + k_c \tag{3-23}$$

where M_{RTFO} is the limiting amount of carbonyl formation due to the first-order reaction after hot mix production. To convert **Equation 3-23** into the weak form, the weak expression is defined as:

$$CAit * test(CAi) - (if(Pair < 0.0001[atm], 0, M * Kf * exp(-Kf * t) + Kc)) * test(CAi) \tag{3-24}$$

where CAit is the time derivative of CA at air channel-mastic interface; test(CAi) is a test function of CA at the air channel-mastic interface; Kf and Kc are fast-rate and constant-rate exponential functions of CA growth; M is the limiting amount of carbonyl formation due to the first-order reaction after hot mix production; CAb is CA in the mastic (domain 2); and CA0 is the initial carbonyl content in mastic before ageing.

The initial value for CA_i can be obtained by conducting an FTIR scanning test for the unaged bitumen binder, so that (CAi= CA0, CA0 is CA of unaged binder), and the initial carbonyl rate (at $t = 0$) is defined to be zero. The carbonyl area CA_i at the BC where the air channels and mastic meet is made equal to CA in the mastic domain (CA_b) so that the two domains will have circular dependency (i.e., $CA_i = CA_b$ at the BC).

3.3.5 Ageing kinetics for carbonyl area in the asphalt mastic interface (CA_b)

The weak form interface is employed to simulate the oxidation kinetics inside the mastic (domain 2 shown in **Figure 3-1**). Similar to **Equation 3-23** that is being used to simulate the

carbonyl growth at the mastic-air channels interface, **Equation 3-25** is implemented to predict the growth of carbonyl functional groups in the mastic CA_b (domain 2 in **Figure 3-1**).

$$\frac{\partial CA_b}{\partial t} = M_{RTFO} k_f e^{-k_f t + k_c} \tag{3-25}$$

Thus, the weak expression is defined as:

$$CAbt * test(CAb) - (if(Pb < 0.0001[atm], 0, M * kf * exp(-kf * t) + kc)) * test(CAb) \tag{3-26}$$

where CAbt is time derivative of CA in the mastic; test(CAb) is a test function of CA at the air channel-mastic interface; and kf and kc are fast-rate and constant-rate exponential functions of CA growth.

The initial value (at $t = 0$) is set to be the carbonyl area in the virgin (unaged) bitumen. The bitumen-air channels interface (domain 1-domain 2 interface) is defined as ($CA_b = CA_i$) to allow the circular-dependency between the two carbonyl interfaces.

3.4 Model Variables, Parameters and Material Properties as Model Inputs

3.4.1 Model variables defined in the PDE-FE model

The following variables are defined:

1. The coefficient of heat convection at the surface boundary (h_c), as defined in **Equation 3-15**. The equation is expressed in the following format:

$$hc = 697.33 * (0.000144 * (if(Tav == 0, abs(Tav + 0.00001), abs(Tav)))^0.3 * (Uwind(t)/1[m/s])^0.7 + 0.00097 * (if(Tdiff == 0, abs(0.00001 + Tdiff), abs(Tdiff)))^0.3) \tag{3-27}$$

$$Tav = (T/1[K] + Tair(t)/1[K])/2 \tag{3-28}$$

$$Tdiff = (T/1[K] - 273.15) - (Tair(t)/1[K] - 273.15)) \tag{3-29}$$

2. Oxidation kinetics coefficients (k_f and k_c), as defined in **Equations 2-2 and 2-3**. Since k_f and k_c are oxygen pressure-dependent; they are defined separately for the air-channels (domain 1) and mastic (domain 2) as follows:

   At the air channels-mastic interface:

$$Kf = Af * (Pair/101325[Pa])\text{^}aa * exp(-Eaf/R/T) \quad (3\text{-}30)$$

$$Kc = Ac * (Pair/101325[Pa])\text{^}aa * exp(-Eac/R/T) \quad (3\text{-}31)$$

   In the mastic:

$$kf = Af * (Pb/101325[Pa])\text{^}aa * exp(-Eaf/R/T) \quad (3\text{-}32)$$

$$kc = Ac * (Pb/101325[Pa])\text{^}aa * exp(-Eac/R/T) \quad (3\text{-}33)$$

3. Diffusion of oxygen in the bitumen coefficient (D_o), defined in **Equation 2-8**, and its corresponding variables (shown in **Equations 2-9, 2-10**, and **2-11**) are expressed in the following format:

$$D = ((5.21E-12) * (LSV\text{^} - 0.55) * T)/1[K * s/m\text{^}2] \quad (3\text{-}34)$$

$$LSV = exp(m + HS * CAb) \quad (3\text{-}35)$$

$$m = m\_T0 + Delta * ((1/T) - (1/333.3[K])) \quad (3\text{-}36)$$

$$HS = HS\_T0 + Gamma * ((1/T) - (1/333.3[K])) \quad (3\text{-}37)$$

4. Coefficient of oxygen solubility in the bitumen (h), as defined in **Equation 2-7** and written in the following format:

$$h = h0 * (1 + 0.0215 * (T/1[K] - 273.15 - 30)) \quad (3\text{-}38)$$

5. Coefficient of oxygen diffusion in the air channels (D_{o2}). The pavement structure is employed to estimate the coefficient of oxygen diffusion in the air channels (D_{o2}). To do so, a correlation between the average air voids (AAV) in the pavement and the coefficient of diffusion in the air pores is established based on an empirical set of laboratory

measurements provided by Wen and Wang (2018) (Wen and Wang 2018). This correlation is shown in **Equation (3-39)**, with an R^2 value of 0.8725.

$$D_{o2}\left(\frac{cm^2}{s}\right) = 10^{1.7866*\log(\text{AAV})-7.3139} \quad (3\text{-}39)$$

The equation is input into the FE model, as follows:

$$Do2 = 10\text{^}(1.7866 * log(AAVav) - 7.3139) * 1[cm\text{^}2/s] \quad (3\text{-}40)$$

where AAVav is the average air voids content in the field.

6. Average carbonyl area (CA_y). It is necessary to calculate the average CA from the model predictions at the specific pavement depth. There are two factors to consider when determining the average predicted CA at any depth of the AC layer: (1) the oxygen diffusion depth is employed based on the model illustrated in **Figure 3-2** such that oxygen diffuses horizontally in a hollow cylinder from the air channel along the mastic coating thickness toward the mastic-aggregate interface; (2) the carbonyl area is decreasing and non-uniformly distributed across the mastic film thickness (as will be shown in **Figure 4-7 (c)**). Therefore, the volumetric integration in **Equation 3-41** was adopted to calculate the average predicted carbonyl area at a certain depth.

$$CA_y = \frac{\int_{r_{air}}^{R} 2\,\pi CA(r)\,r\,dr}{\pi\,(R^2 - r_{air}^2)} \quad (3\text{-}41)$$

where CA_y is the average predicted carbonyl area at a certain depth of the AC layer (y), $CA(r)$ is the predicted carbonyl area at a radius of (r), r is the radius calculated from the centre of the air channels, the minimum radius would be the radius of the air channels (r_{air}), and the maximum radius would be the radius of the air channels plus the oxygen diffusion depth (d_D) in the mastic coating film, i.e., $R = r_{air} + d_D$. The average carbonyl area at any depth is set in the model's variables by means of General Projection operator, which uses path integrals of CA_b in a preset direction and domain. In this case, it is domain 2 (mastic film shown in **Figure 3-1**) in the x-

direction. For example, the equation for average CA (CAav) for US277 (which will be discussed in **Chapter 4**) will be:

$$CAav = genproj1(CAb * 2 * Pi * (Radair + x * min(1, if(y >= 0.0508[m], 0.000386[m]/x, if(y >= 0.0381[m], 0.000615[m]/x, if(y >= 0.0254[m], 0.000748[m]/x, if(y >= 0.0127[m], 0.000706[m]/x, 0.000462[m]/x)))))) / genproj1(2 * Pi * (Radair + x * min(1, if(y >= 0.0508[m], 0.000386[m]/x, if(y >= 0.0381[m], 0.000615[m]/x, if(y >= 0.0254[m], 0.000748[m]/x, if(y >= 0.0127[m], 0.000706[m]/x, 0.000462[m]/x)))))) \quad (3\text{-}42)$$

where, $genproj1$ is a predefined general projection operator, $Radair$ is the mean radius of air voids. CAav is also dependent on the average diffusion depth, as seen in **Equation 3-41**, where mean diffusion depth values at each AC layer (values for road section US277 shown in **Chapter 4 , Table 4-3**) were input into the equation.

Other variables were input into the model to examine the model sensitivity to certain parameters. These additional parameters will be discussed in **Chapter 5**.

3.4.2 Model parameters and materials properties defined as model inputs

The model parameters that are associated with the ageing Multiphysics and defined the PDE-FE model include:

1. Geometry dimensions (obtained from the structural design specifications of the pavement and the volumetric characteristics of the AC mix).
2. Oxidation kinetics constants $M_{RTFO}, CA_o, A_c, A_f, E_{af}, and\ E_{ac}$. These parameters can be obtained by performing laboratory ageing tests (rolling thin film oven and pressurised ageing vessel tests), rheological tests, and FTIR to obtain CA at different ageing stages (Glover et al. 2014).

3. The temperature at the bottom of the pavement and the initial temperature (at $t = 0$). These temperatures are considered equal to the subsurface soil temperature at a depth of 3 meters, available in the LTPP Climate Tool database for various regions.
4. The field correction factor, fcf, is utilised to correct the coefficient of oxygen diffusion in the mastic in case there is not enough information about the binder absorbed by the aggregate and the existence of fine matter in the mastic.

   An example of parameter inputs for road section US277 located in Laredo, Texas, USA are shown in **Table 3-1**.

Table 3- 1 Model parameters for road section US277 in Laredo, Texas.

Name	Value	Description
Ac	0.75	absorption coefficient
Eac	103.8[kJ/mol]	activation energy of constant-rate oxidation
Eaf	75.4[kJ/mol]	activation energy of fast-rate oxidation
AAV	7.27	air voids content
c0	3.71E-4[mol/ml]	carbonyl content to pressure conversion factor
m_T0	5.84	CA-viscosity intercept at standard temperature
Ac	5.034E13[1/day]	coefficient of constant-rate oxidation
Af	5.0497E10[1/day]	coefficient of fast-rate oxidation
Tas	0.0762[m]	depth of asphalt layer (domains 1 and 2 in **Figure 3-1**)
Tlowerbase	0.15[m]	depth of lower base layer

Tsubgrade	2[m]	depth of subgrade layer
Tupperbase	0.3[m]	depth of the base layer
Fcf	1	field correction factor
R	8.314[J/K/mol]	gas constant
HS_T0	3.97	hardening susceptibility at standard temperature
CA0	0.942	initial CA value
Pi	0.0001[atm]	initial oxygen pressure
T0	22.5[degC]	initial temperature
M	0.05	limiting amount of CA due to the first-order reaction
Was	1[mm]	maximum width of mastic coating
h0	0.0076	oxygen solubility inside the mastic at a standard temperature
Aa	0.27	reaction order of oxygen pressure in the Arrhenius equation of CA growth
Gamma	1656[K]	temperature shift factor
Delta	20360[K]	temperature shift factor
Wair	0.5124[mm]	width of air channels

The materials properties are values assigned to specific domains in the geometry. Heat transfer in the pavement depends on the thermal properties of the pavement materials. Therefore, the thermal characteristics of the pavement layers are introduced to the model in this section. The inputs for each layer (for each domain in **Figure 3-1**) include thermal conductivity, density and

heat capacity. The thermal properties of the air channels (domain 1) and the mastic coating film (domain 2) are similar as they both represent the AC layer in the heat transfer interface. The sensitivity and significance of each parameter on the pavement temperature prediction model were assessed in previous studies. It was found that the thermal diffusivity (α) of AC, which is a term that combines thermal conductivity, density, and heat capacity (**Equation 2-13**), had negligible effects on model accuracy if it was kept in the range of $4.4 - 6.4\ x\ 10 - 7$ m^2/s (Luca and Mrawira 2005, Han et al. 2011).

Due to the lack of field measurements, the thermal properties of pavement layers were collected from the literature (Highter 1984, Yavuzturk et al. 2005, Gui et al. 2007, Nguyen et al. 2012, Alawi and Helal 2014, Shi 2014, Bai et al. 2015, Chen et al. 2015b, Hassn et al. 2016a, Hassn et al. 2016b, Alavi et al. 2017, Pan et al. 2017a) (listed in **Table 3-2**) and employed in the current model. **Table 3-3** lists the thermal properties used for each pavement layer in this study. There is no evidence of significant changes to the thermal properties of asphalt pavement upon ageing (Pan et al. 2017a); therefore, the materials thermal properties are kept constant. A parametric sensitivity analysis is conducted (detailed in **Chapter 5)** to assess the effect of these parameters on field oxidative ageing growth rate.

Table 3- 2 Thermal properties of the asphalt pavement layers recorded in the literature.

Material	Thermal conductivity, k (W/m.K)	Heat capacity, c_p (J/kg.K)	Density, ρ, (kg/m^3)	Thermal diffusivity (m^2/s) ($* 10^{-7}$)	Reference
Asphalt concrete	2.89-0.14	2570-628	2250	5.9	(Highter 1984)
	1.21	924	2238	-	(Gui et al. 2007)
	0.82-1.16	945-963.7	1906-2371		(Hassn et al. 2016a, Hassn et al. 2016b)

	1.86	959	2282	8.53	(Bai et al. 2015)
	1.35	823	-	-	(Nguyen et al. 2012)
	0.5-2.5	2000	-	-	(Yavuzturk et al. 2005)
	1.548-1.622	-	-	7.44-7.59	(Pan et al. 2017a)
	1.5	921	2550	-	(Alavi et al. 2017)
Asphalt binders	0.169-0.191	-	-	1.23-1.28	(Pan et al. 2017a)
	0.8	-	-	-	(Chen et al. 2015b)
Aggregate	2.86	-	-	-	(Chen et al. 2015b)
Wearing layer	2.5	1003	2300	-	(Alawi and Helal 2014)
Base layer , bound base (old HMA)	1.21	924.37	2238	-	(Gui et al. 2007)
Base (unbound base)	1.8	1100	2200	-	(Alawi and Helal 2014)
	1.5	805	2370	-	(Alavi et al. 2017)
Portland cement	0.53	-	-	-	(Shi 2014)
Subbase	1.8	900	2200	-	(Alawi and Helal 2014)
Subgrade	1.5	850	1500	-	(Alawi and Helal 2014)

1.7	1100	2200	-	(Alavi et al. 2017)
1	1906	1500	-	(Gui et al. 2007)

Table 3- 3 Thermal properties of pavement layers used in this study.

Pavement layer	Thermal conductivity, k (W/m.K)	Heat capacity, c_p (J/kg.K)	Density, ρ, (kg/m^3)
Asphalt concrete	2.3	960	2450
Base and subbase	1.5	805	2350
Subgrade	1.7	1100	2200

3.4.3 Time-dependent parameters as model inputs

The time-dependent inputs are introduced into the Comsol program by tables or files containing discrete points, called interpolation functions (Comsol Multiphysics Reference Manual 2013). Therefore, they can be generated to introduce the time-dependent climate inputs needed for the pavement temperature model. These inputs include the hourly records of shortwave solar radiation, air temperature, wind speed, emissivity, and albedo values. These hourly climate data are available in the LTPP Climate Tool for different climatic regions. An example of these inputs is shown in **Table 3-4**, in which site specific-data for road section US277 in Laredo -Texas, USA, collected from climate station (MERRA 130881) for only 10 hours, are shown in the table. The implemented model for this road section (US277) used collected inputs for 30720 hours (i.e., 3.5 years), as explained in **Chapter 4**.

Table 3- 4 An example of time-dependent hourly climate data for road section US277 located in Laredo, Texas, USA, collected from the LTPP database at station MERRA 130881.

Date (dd/mm/yyyy), time (h)	Time, (h)	Albedo	Air temperature (°C)	Wind speed (m/s)	Solar radiation (W/m/s)	Emissivity
	t			f(t)		
01/07/2008 0	1	0	28.3	4	0	0.972393
01/07/2008 1	2	0	27.6	4	0	0.972387
01/07/2008 2	3	0	27	3	0	0.972243
01/07/2008 3	4	0	26.5	3	0	0.97238
01/07/2008 4	5	0	26.1	3	0	0.972374
01/07/2008 5	6	0	25.7	2	0	0.972367
01/07/2008 6	7	0.18859	26	2	1.1	0.97236
01/07/2008 7	8	0.187919	27.3	3	59.1	0.972354
01/07/2008 8	9	0.18499	29	3	200.5	0.972347
01/07/2008 9	10	0.174064	30.4	3	328.1	0.972341

3.5 Summary of Ageing Multiphysics Modelling Framework

A Multiphysics finite element (FE) framework is developed in this chapter to integrate the ageing physics (heat transfer in the pavement, oxygen diffusion in the asphalt layer, and oxidation reaction in the asphalt mastic) into one model to solve them simultaneously.

The proposed FE framework consists of (1) model geometry (physical domains) with specified materials properties for each domain; (2) model physics (represented by the weak form of partial differential equations (PDEs)); and (3) model parameters, variables, and time-dependent interpolation functions. A two-dimensional geometry with a high computational efficiency is developed with customised dimensions according to pavement structure and volumetric properties of asphalt mixture. A time-dependent simulation is built using five circularly dependent

physics that work simultaneously at certain geometry domains by converting the PDEs into weak-form physics in Comsol Multiphysics solver.

Finally, information such as pavement structure, oxidation kinetics of bitumen, and morphology of mixture is input into the model as parameters, variables, shape functions, and materials properties. Site-specific hourly climatic data were obtained from the Climate Tool at the Long-Term Pavement Performance (LTPP) database and input into the model as time-dependent interpolation functions. Compared to other models, the model is built to rely more on site-specific climatic data, such as albedo, emissivity, and subsurface soil temperatures.

Chapter 4 Predictions and Validations of Field Ageing in Asphalt Pavements*

In this chapter, the results of the integrated ageing model are analysed and compared against field measurements. Results confirm the circular dependency among the four physics of ageing (temperature change, oxygen diffusion, oxidative reaction, and viscosity change). The validation process is carried out in two stages: (1) validation of the pavement temperature model, (2) validation of the integrated ageing model.

4.1 Integrated Ageing Multiphysics Model for Asphalt Pavements

Two road sections were selected to run the integrated ageing model: US277 and US83, both located in Texas, USA, in different climate regions. They were chosen in this study due to the availability of the Carbonyl Area (CA) values in the binder at different ageing periods, which will be used to validate model predictions. Ageing data were collected from the Federal Highway Administration (FHWA) reports (Glover et al. 2014). In addition to CA, properties of binders, mixtures, and pavement structures were also recorded. Aged binders were extracted and recovered from field-aged cores, sliced into several pieces with a thickness of 12.7 mm and then tested using FTIR to determine CA values (Han 2011, Jin et al. 2013, Glover et al. 2014). **Table 4-1** shows general information of the mixture and binder types as well as the environmental zones for these sections.

Table 4-2 lists the oxidation kinetics and viscosity hardening properties of the virgin binders. The volumetric properties of the asphalt concrete layers were obtained from CT-scan images (Han 2011, Han et al. 2011, Jin et al. 2013, Glover et al. 2014) and listed in **Table 4-3**.

* Findings derived from this chapter are published as part of : Omairey, E. L., et al. (2021). "An equation-based Multiphysics modelling framework for oxidative ageing of asphalt pavements." Journal of Cleaner Production 280: 124401. https://doi.org/10.1016/j.jclepro.2020.124401

Mean values of diffusion depths and air voids radiuses were employed as geometry inputs; for air channel thickness (thickness of domain 1 in **Figure 3-1**) and mastic film thickness (thickness of domain 2 in **Figure 3-1**).

Table 4- 1 General Information on mixture and binder types used for road sections US277 and US83 (Han 2011, Han et al. 2011, Jin et al. 2013, Glover et al. 2014)

Road Section - Location	Climate zone	AC cores thickness (mm)	Binder supplier	PG (modifier)	AAV (%)	Construction date
US277 - Laredo, Texas	Dry-Warm	76.2	Valero	70-22 (SBS)	7.27	2008
US83 - Childress, Texas	Dry-Cold	50.8	SEM	PG 70-28	7.7	06/2008

Table 4- 2 Oxidation kinetics parameters for road sections US277 and US83 (Han 2011, Han et al. 2011, Jin et al. 2013, Glover et al. 2014).

Road	$A_c P^{\propto}$ (CA/ Day)	$A_f P^{\propto}$ (CA/ Day)	HS (1/CA)	m (ln(Pa.s))	CA_o	fcf	M_{RTFO}	E_{af} (kJ/mol)	E_{ac} (kJ/mol)
US277	$3.26 * 10^{13}$	$3.27 * 10^{10}$	3.970	5.84	0.826	1.2	0.05	75.4	103.8
US83	$1.03 * 10^{9}$	$3.34 * 10^{7}$	4.530	7.89	0.594	12	0.12	49.1	072.5

Table 4- 3 Mixture volumetric properties for the extruded field cores for sections US277 and US83 (Han 2011, Han et al. 2011, Jin et al. 2013, Glover et al. 2014).

Road	Air voids radius mm)/ No. air voids in the topmost layer	Av. air voids radius in the uppermost layer (mm)	Layer No./ Diffusion depth d_D (mm) at the wheel path (1st core)	Layer No./ Diffusion depth d_D (mm) at the wheel path (2nd core)	Layer No./ Diffusion depth d_D (mm) at the shoulder path (1st core)	Layer No./ Diffusion depth d_D (mm) at the shoulder path (1st core)
US277	0.140/034	0.5124	1/ 0.386	1/ 1.167	1/ 0.663	1/ 0.592
	0.332/672		2/ 0.615	2/ 3.072	2/ 0.636	2/ 2.710
	0.697/211		3/ 0.748	3/ 0.575	3/ 0.790	3/ 1.579
	1.338/083		4/ 0.706	4/ 0.510	4/ 0.603	4/ 0.675
	2.400/014		5/ 0.462	5/ -	5/ 0.344	5/ 0.700
US83	-	0.400	1/ 0.847	1/1.297	-	1/ 0.966
	-		2/ 4.405	2/2.346	-	2/ 3.032
	-		3/ 3.146	3/1.802	-	3/ 2.778
	-					4/ 2.026
	-					5/ 1.267

Figure 4-1 illustrates the pavement structures for road sections US277 and US83 (Sebesta et al. 2006, Martin et al. 2013). In addition to setting up the geometry for the ageing models, the pavement structure is also employed to estimate the coefficient of oxygen diffusion in the air channels (D_{o2}). Since AAV% is recorded in FHWA reports (**Table 4-1**), the coefficients of oxygen diffusion in the interconnected air channels for road sections US277 and US83 were calculated using **Equation (3-39).**

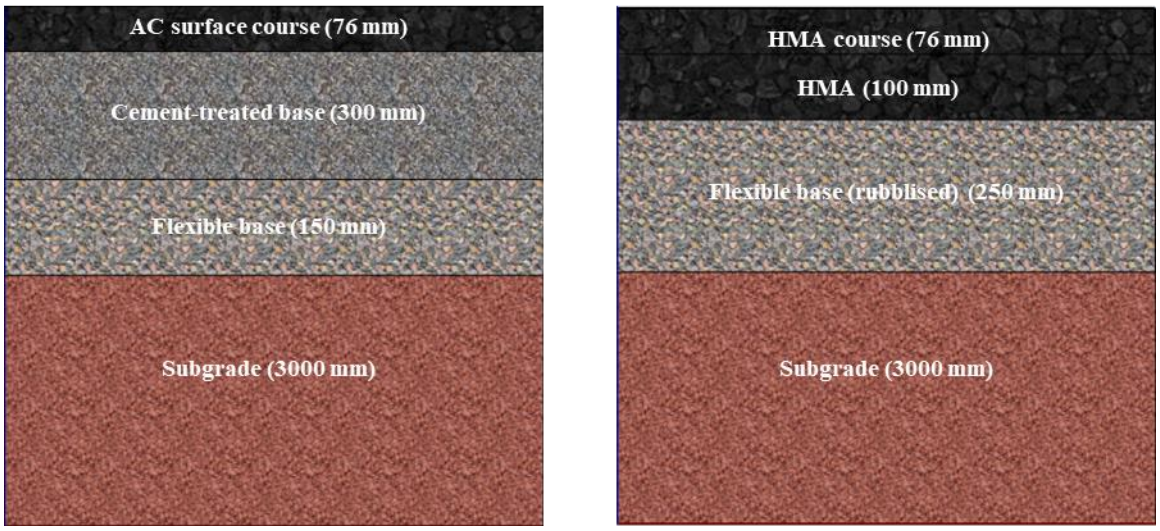

(a) **(b)**

Figure 4- 1 Pavement profiles of (a) road section US277 in Laredo, Texas, USA; and (b) road section US83 in Childress, Texas, USA.

Other inputs for the model include hourly climate data (air temperatures, wind speed, shortwave solar radiation, albedo, and emissivity) obtained from the Climate Tool in the LTPP database. The ageing models can be run for any duration; however, for model validation purposes in the current study, the durations were limited by the availability of field carbonyl data. Therefore, hourly climate data were collected for July 2008 - January 2012 for road section US277 when the last coring sample was extruded in January 2012. For road section US83, hourly climate data were collected for July 2008 – November 2011. Since the selected road sections are located in different environmental regions, the absorption coefficients (ac) will differ. Absorption coefficients were obtained from the environmental parametric study conducted by Han (2011), with values of 0.75 and 0.70 for road sections US277 and US83, respectively (Han 2011).

4.2 Simulation Results of Ageing Multiphysics in Asphalt Pavements

After developing the equation-based modelling framework for oxidative ageing of asphalt pavements and collecting all climatic data, binder properties, and pavement structure inputs, two pavement models were run. Data were collected for every one-hour interval, with outputs

including the pavement temperature profile, partial oxygen pressure in the air channels, partial oxygen pressure inside the mastic, and the carbonyl area within the mastic.

4.2.1 Pavement temperature profiles (T)

The heat transfer interface predicted pavement temperature at any depth across the pavement profile. Outputs for each hour at any location within the pavement structure were obtained and employed simultaneously in the other interfaces (i.e., oxygen diffusion and oxidation kinetics). The temperature profile is a one-way process which means it is not affected by the oxygen pressure distribution or the carbonyl area growth within the pavement structure; however, it plays a significant role in the pressure distribution and the growth rate of the oxidation products. **Figure 4-2** shows temperature change plotted against time for road section US277 at different depths of the AC layer and the temperature variation with AC depth at different time intervals. Since the topmost layers are closer to atmospheric seasonal changes, temperatures at the surface show more seasonal variation than those in deeper layers. Additionally, the daily temperature variation between daytime and nighttime is more pronounced at the pavement surface than at greater depths.

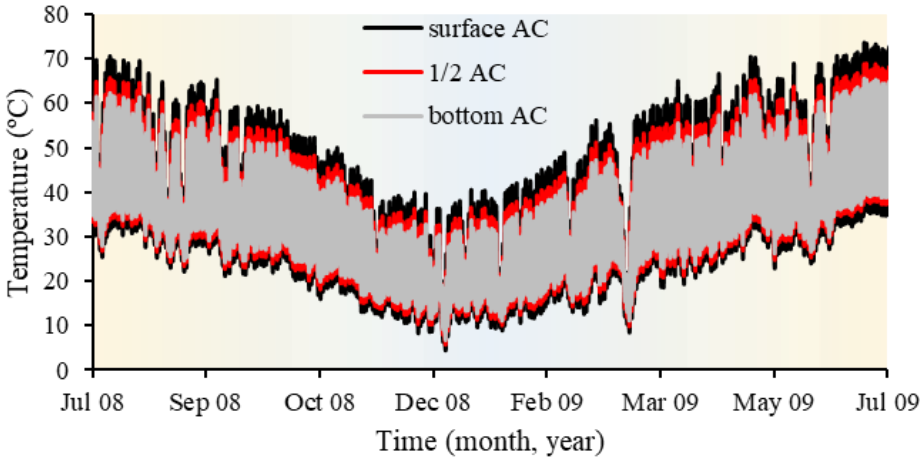

(a) Temperature versus ageing time.

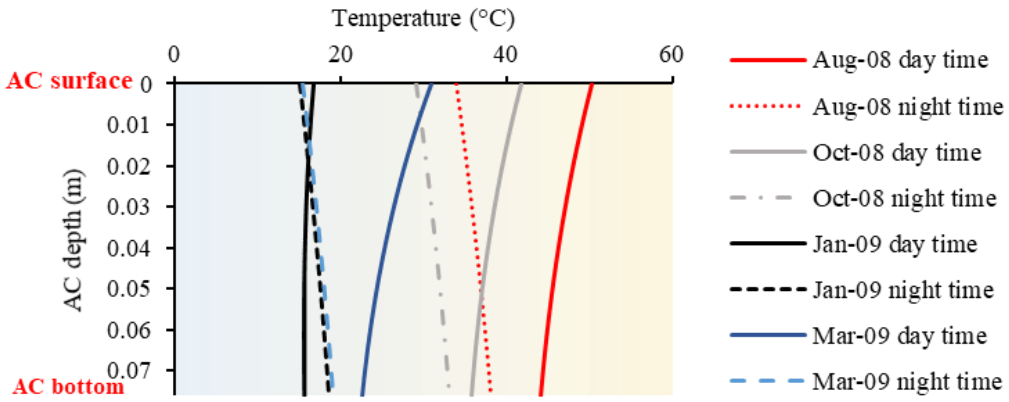

(b) Temperature profile of asphalt layer.

Figure 4- 2 Temperature profile for road section US277, located in Laredo, Texas, USA. (a) Temperature plotted against time at three asphalt concrete (AC) depths (surface, ½ AC, and bottom of AC layer) for one year. (b) Temperature profile for the AC layer at four different times throughout the year. Winter and summer seasons are highlighted with blue and yellow colours, respectively.

4.2.2 Partial oxygen pressure along interconnected air channels (P_{air})

The accessibility and distribution of oxygen within the pavement play a vital role in the oxidative ageing of asphalt pavement. Without a continuous supply of oxygen from the surrounding atmosphere into interconnected air channels and then to the bitumen in the mastic film, the oxidation process will stop. The coefficient of oxygen diffusion in the air channels is a constant value with time that depends on the percentage of air voids, whereas the coefficient of oxygen diffusion in the mastic is a function of CA and temperature; thus, it is changing with ageing time. While the coefficient of oxygen diffusion in the air channels is approximately 1000 times greater than that in the mastic, oxygen distribution in the air and the mastic are circularly linked. Oxygen in the air channels is supplied by the ambient atmosphere, and it will be consumed by the binder in the asphalt mastic due to oxidation; therefore, more oxygen will transport from the air into the air voids and then into the mastic.

Figure 4-3 shows the partial oxygen pressure distribution in the air channels (domain 1 in **Figure 3-1**) for road section US277 over a period of 3.5 years. As expected, the oxygen pressure

varies between 0 – 0.2 atm, as the oxygen pressure in the atmosphere is 0.2 atm. The oxygen partial pressure is low with high daily variations during the summer season because the surrounding mastic consumes more oxygen in the oxidation process in summer. In contrast, the oxygen pressure is high with low daily variations in the winter because the oxidation rate is low in this season due to low temperatures. Similar patterns were observed for road section US83.

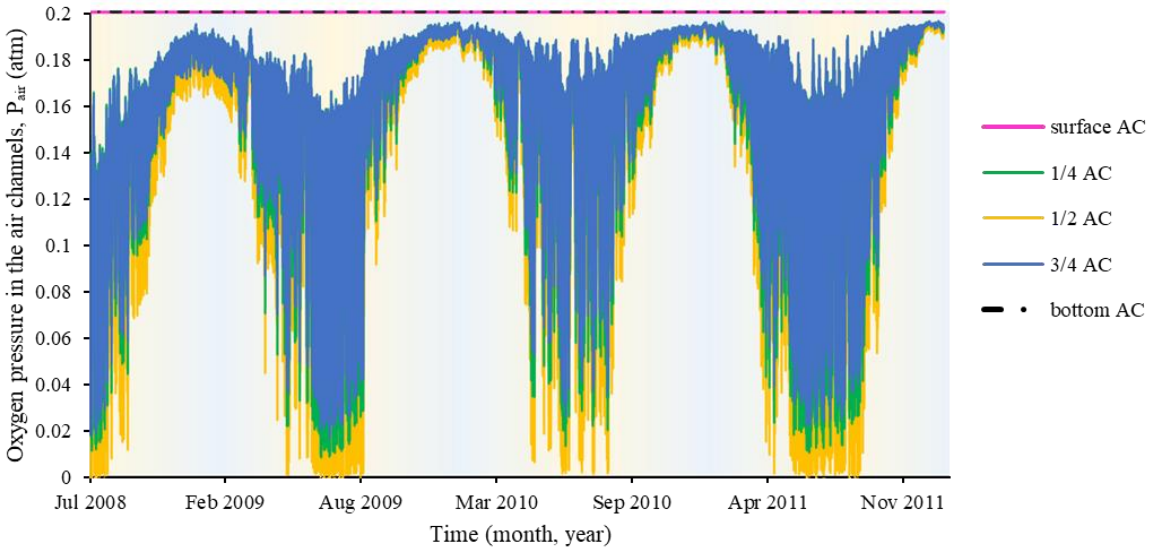

(a) Oxygen partial pressure in the air channels versus ageing time.

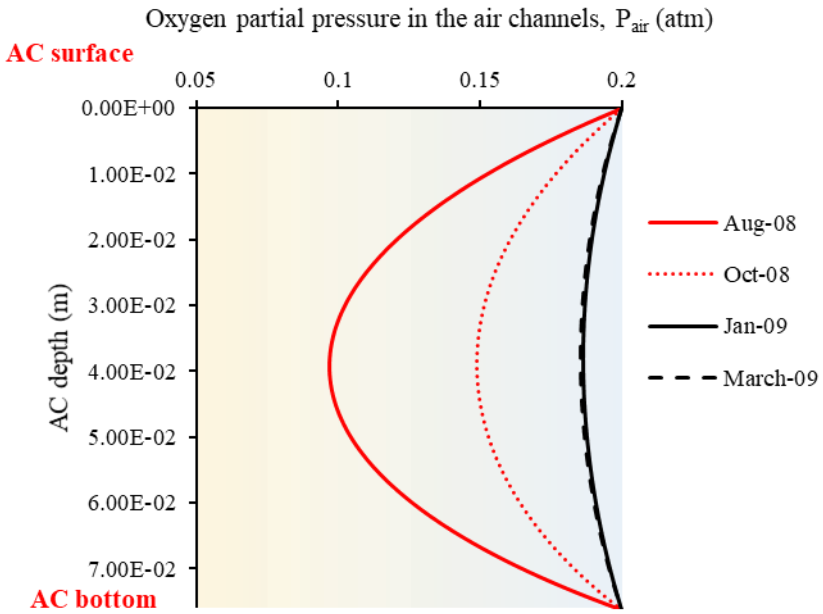

(b) Profile of oxygen pressure in the air channels.

Figure 4- 3 Oxygen partial pressure distribution in the air channels for road section US277, located in Laredo, Texas, USA. (a) Oxygen partial pressure in the air channels plotted against ageing time at different asphalt concrete (AC) depths (surface, ¼ AC, ½ AC, ¾ AC, and bottom of AC layer). (b) Oxygen pressure in the air channels against the depth of AC layer at different field ageing times. Winter and summer seasons are highlighted in blue and yellow colours, respectively.

In this model, oxygen can diffuse freely from the air into the interconnected air channels from both the topmost surface and the bottom of the asphalt layer, assuming the base material is crushed stones of high porosity. Therefore, complete access of oxygen into the pavement is assumed (Han 2011, Wen and Wang 2018). Consequently, **Figures 4-3 (a)** and **(b)** show that the oxygen pressure in the middle of the AC layer (1/2 AC) is low and it becomes higher at the top and bottom of the AC layer due to the boundary conditions; this forms a clear C-shaped curve across the pavement depth. This observation is consistent with the oxygen distribution in the field observed by Wang et al. (2014) (Wang et al. 2014).

Although the oxygen movement is two-dimensional, due to the *relatively* high diffusivity of oxygen in the air channels, there is no clear difference in the oxygen partial pressure in the horizontal direction (x-direction) within the air channels domain (domain 1 in **Figure 3-1**). However, there is a considerable difference in the vertical direction as oxygen was supplied from the top and bottom surfaces of the AC layer. For this reason, this interface is referred to as the *vertical* diffusion of oxygen in the interconnected air channels.

4.2.3 Partial oxygen pressure inside asphalt mastic coating film (P_b)

When exposed to oxygen and high temperatures, the bitumen in the asphalt mastic will suffer from oxidation. As a result, it will consume the oxygen that diffused into the mastic. When the temperature is low, the oxidation process will be halted as the energy required to initiate oxidation is not reached; therefore, the oxygen will not be consumed, and the oxygen pressure will increase in the mastic due to continuous oxygen diffusion. **Figure 4-4** shows the oxygen pressure distribution in the asphalt mastic (labelled as domain 2 in **Figure 3-1**). **Figure 4-4 (a)**

shows that the oxygen pressure in the mastic follows the same pattern as that in the air channels (**Figure 4-3**) but with lower oxygen pressures in the mastic. This is reasonable as the oxygen from the air diffuses through more steps to reach the mastic and oxygen is consumed by the oxidative reactions. As shown in **Figure 4-4 (b)**, the oxygen pressure in the mastic forms a C-shaped curve where the middle AC layer (1/2 AC) has low oxygen pressure, while the top and bottom surfaces of the AC layer have much higher oxygen pressures as they are exposed to atmospheric air pressure. The oxygen pressure in winter is consistently higher than in summer as oxygen is consumed due to severe oxidation in summer.

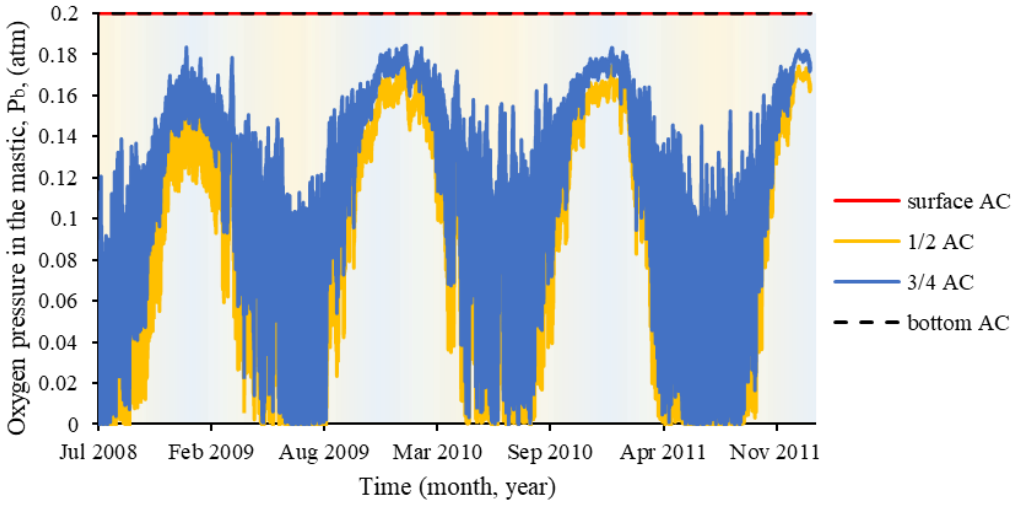

(a) Oxygen partial pressure in the mastic plotted against ageing time at different asphalt concrete (AC) depths at points located at 1/3 the mastic thickness.

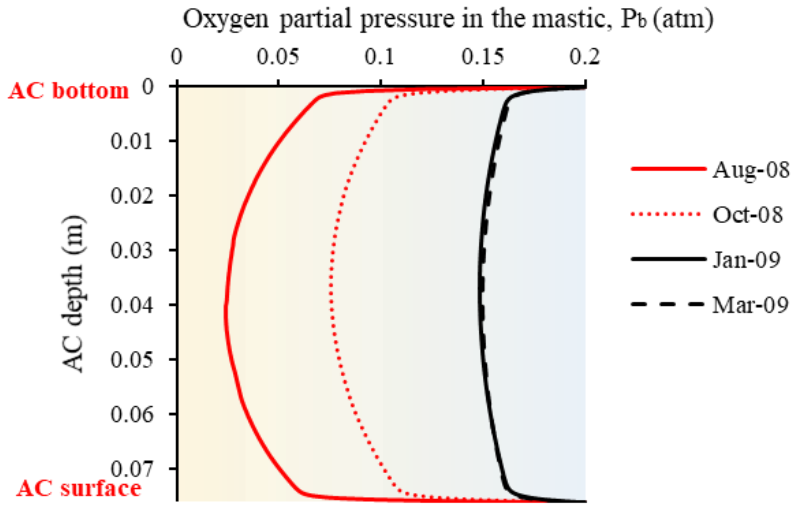

(b) Profile of oxygen pressure in the mastic.

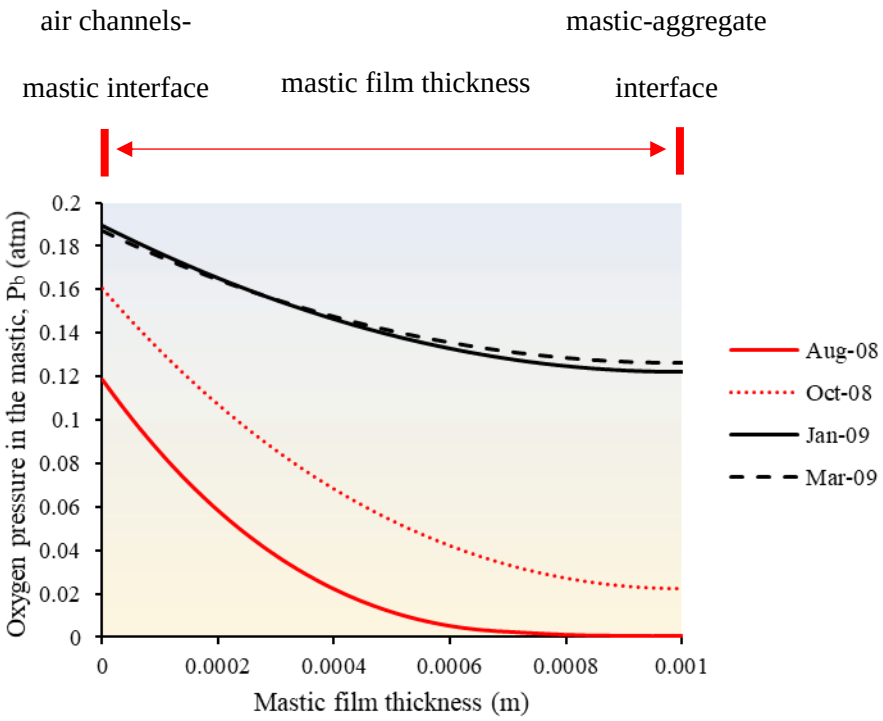

(c) Oxygen partial pressure distribution in the mastic across the mastic coating film.

Figure 4- 4 Oxygen partial pressure distribution in the mastic for road section US277, located in Laredo, Texas, USA. (a) Oxygen partial pressure in the mastic plotted against ageing time at different asphalt concrete (AC) depths (surface, ½ AC, ¾ AC, and bottom AC layer), at points located at 1/3 the mastic thickness. (b) Oxygen pressure in the mastic plotted against depth of AC layer at different time intervals for points located at 1/3 the mastic thickness. (c) Oxygen partial pressure distribution in the mastic plotted against width of mastic coating film at different field ageing times at 1/3 AC depth. Winter and summer seasons are highlighted in blue and yellow colours, respectively.

Since the coefficient of oxygen diffusion inside the mastic is low, the oxygen pressure distribution will be non-uniform across the mastic film thickness at any time interval (when $t > 0$). As shown in **Figure 4-4 (c)**, the oxygen pressure is higher at the air-mastic interface but decreases horizontally along the mastic thickness toward the mastic-aggregate interface. The non-uniform distribution of the oxygen pressure along the film thickness suggests that the carbonyl

area growth will follow a similar pattern even if the temperature is constant across the mastic film thickness.

Moreover, the coefficient of oxygen diffusion D_o is inversely proportional to the carbonyl content (as illustrated in **Equations 2-8** and **2-9**). Therefore, it will decline with ageing time, as shown in **Figure 4-5**. This suggests that oxygen diffusion will limit the oxidation process gradually with progressive ageing. **Figure 4-5** also shows that the coefficient of oxygen diffusion changes periodically with temperature due to the fact that oxygen diffusivity in the mastic is highly associated with the viscosity of the binder, which is affected by temperature and oxidative hardening. Therefore, neglecting the ageing effect, the oxygen diffusivity would be expected to be higher in summer due to low apparent viscosity and lower in winter when high apparent viscosity is high. However, when considering the ageing effect, as shown in **Figure 4-5**, the coefficient of oxygen diffusion decreases in summer due to the increase in CA and maintains a relatively constant value during winter due to the lack of oxygen consumption.

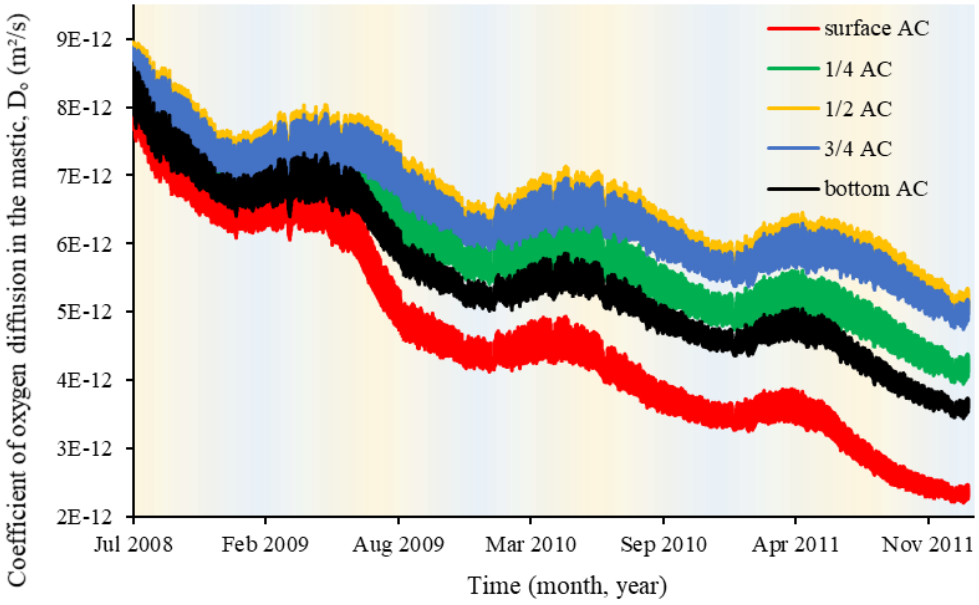

Figure 4- 5 Coefficient of oxygen diffusion in the mastic plotted against ageing time at different asphalt concrete (AC) depths (surface, ¼ AC, ½ AC, ¾ AC, and bottom of AC layer) for road section US277, located in Laredo, Texas, USA. Points are located at 1/3 the

mastic thickness. Winter and summer seasons are highlighted in blue and yellow colours, respectively.

4.2.4 Carbonyl area at the air channels-mastic interface (CA_i)

The bitumen at the air-mastic interface is in direct contact with the oxygen in the air channels; therefore, it experiences more ageing than the bitumen at the same pavement depth inside the mastic film. Carbonyl production at this location relies on the availability of oxygen pressure in the air channels. The physical domain, domain 1 (illustrated in **Figure 3-1**), was employed in the modelling framework to measure CA at the air channels-mastic interface. Results for the CA growth with time at different depths are shown in **Figure 4-6 (a)**. The growth pattern of the CA was affected by both temperature and oxygen pressure changes, displaying a faster growth rate in summer and a slower (or zero) growth rate in winter. This behaviour is attributed to the accelerated oxidation due to high temperatures in summer, leading to a faster generation of carbonyl. Moreover, carbonyl growth declines with field ageing time, as a result of decreased oxygen diffusivity due to the increase in CA and oxidation hardening in the mastic. **Figure 4-6 (b)** shows that the CA pattern with depth forms an unsymmetrical C-shaped curve with higher CA values at the surface and the bottom of the AC layer and lower CA values in the middle of the AC layer. This pattern follows that of the oxygen pressure distribution in the air channels but with slightly higher CA values at the top surface than at the bottom due to higher surface temperatures that result in higher oxidative reactions. **Figure 4-6** shows that, compared to deeper asphalt layers, the AC surface layer ages severely due to high temperatures and complete oxygen availability.

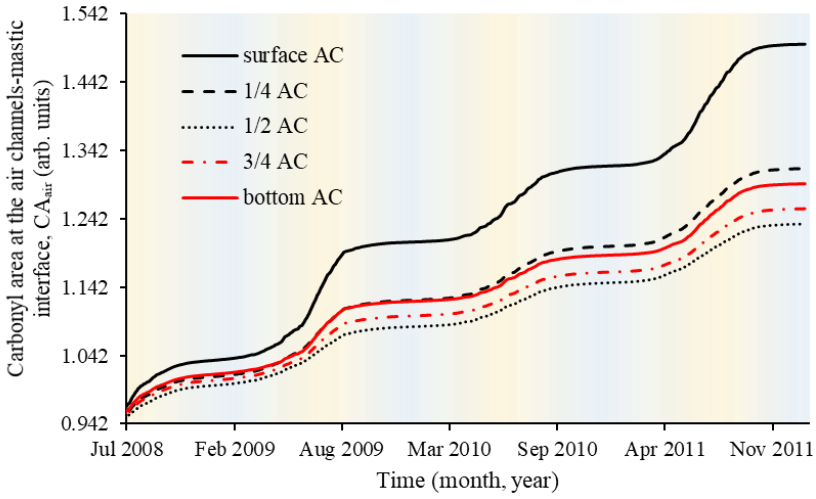

(a) Carbonyl area growth versus ageing time at different asphalt concrete (AC) depths.

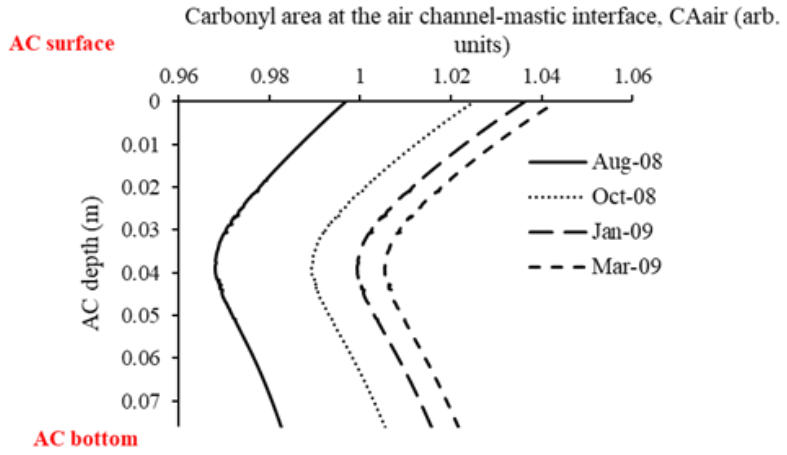

(b) Carbonyl area profile across asphalt concrete (AC) depth.

Figure 4- 6 Carbonyl area at the air channels-mastic interface for road section US277, located in Laredo, Texas, USA. (a) Carbonyl area plotted against ageing time at different AC depths (surface, ¼ AC, ½ AC, ¾ AC, and bottom of AC layer). Winter and summer seasons are highlighted in blue and yellow colours, respectively. (b) Carbonyl area plotted against depth of AC at different ageing times.

4.2.5 Carbonyl area within the asphalt mastic coating film (CA_b)

Predicted results for road section US277 are detailed in this section. **Figure 4-7 (a** and **b)** shows that the carbonyl growth in the mastic follows the same pattern as that at the air-mastic interface; namely, the carbonyl grows quickly in summer due to high temperatures but increases

at a very slow or zero rate in winter. The carbonyl area at the surface and bottom is higher than that in the middle due to high oxygen availability at the surface and bottom, leading to the C-shaped curve of the carbonyl profile along the pavement depth, as shown in **Figure 4-7 (b)**. The CA values in the asphalt mastic are much less than those at the air-mastic interfaces, at the same pavement depth, although they have the same temperature profile. This observation shows that the availability of oxygen constrains carbonyl growth.

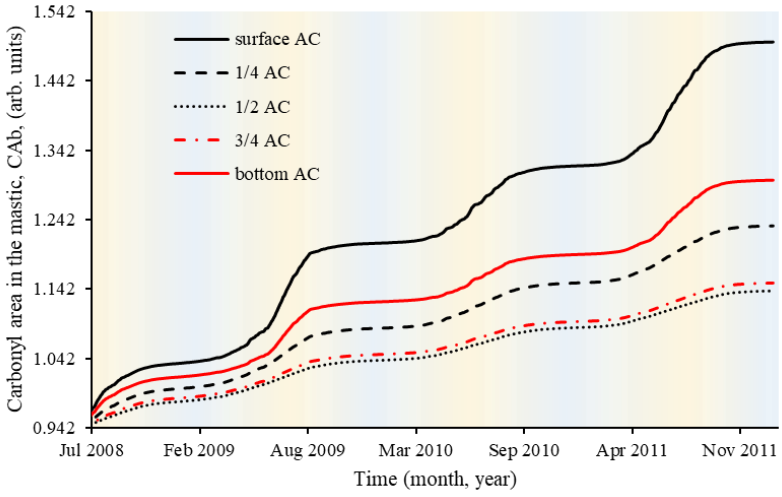

(a) Carbonyl area in the mastic plotted against ageing time at different AC depths.

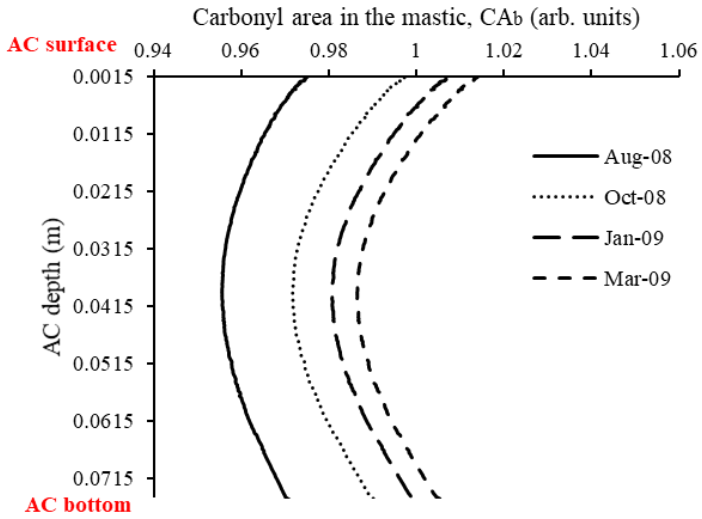

(b) Carbonyl area in the mastic plotted against depth of AC layer at different time intervals.

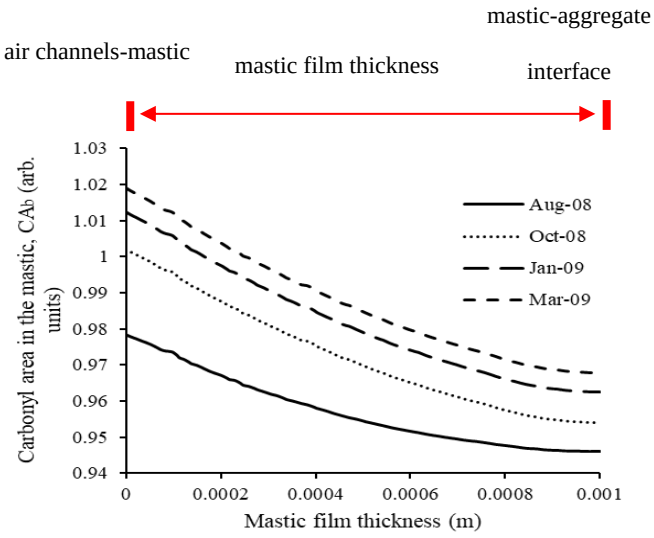

(c) Carbonyl area in the mastic plotted against thickness of mastic coating film.

Figure 4- 7 Carbonyl area in the mastic (CA_b) for road section US277, located in Laredo, Texas, USA. (a) CA_b plotted against ageing time at different AC depths (surface, ¼ AC, ½ AC, ¾ AC, and bottom of AC layer), at points located at 1/3 the mastic thickness. Winter and summer seasons are highlighted in blue and yellow colours, respectively. (b) Carbonyl area in the mastic plotted against depth of AC layer at different time intervals. Points are located at 1/3 the mastic thickness. (c) Carbonyl area in the mastic plotted against thickness of mastic coating film at different field ageing times at 1/3 AC depth.

Figure 4-7 (c) shows the carbonyl area across the mastic coating film thickness at a certain depth of the AC layer (1/3 AC depth). CA is not produced equally across the width of the mastic coating film but decreases quickly along the film thickness, moving away from the air-mastic interface. This observation is particularly important when calculating the average carbonyl area at a certain pavement depth. As shown in the simplified air/mastic structure in **Figure 3-2,** the perimeter of asphalt mastic surrounding the air channels is much less than that in contact with the aggregate. This material distribution should be considered when calculating the average carbonyl area at a certain pavement depth.

4.3 Field Validations of Temperature Profiles in Asphalt Pavements

The temperature profile of flexible pavement plays a vital role in the oxidative ageing process. When the temperature increases, the diffusivity of oxygen in the mastic increases, and oxidation accelerates, which subsequently leads to more oxidative ageing in the pavement. Similarly, when the temperature drops, the bitumen in the asphalt mixture will experience a temporary physical hardening (increase in viscosity), which blocks or decreases oxidation of the pavement, leading to a slower oxidative ageing rate. Therefore, it is crucial to ensure the accuracy of predicted temperature profiles.

Since the time-dependent heat transfer interface is independent of the other physics of ageing, it can be run and validated individually before combining it into the integrated ageing model. The LTPP database contains the hourly field temperatures of 82 road sections in different climate regions across the United States. The field temperatures were collected using thermistors installed at various pavement depths, and the collected data are available for specified time intervals.

This study selected three road sections from different climate regions, including (1) road section 48-1068 in Lamar, Texas, USA (in wet, no freeze region); (2) road section 27-1028 in Otter Tail, Minnesota, USA (in wet, freeze region); and (3) road section 16-1010 in Idaho, USA (in dry, freeze region). **Figure 4-8** shows the location of the selected sections, and **Table 4-4** contains their pavement structures (layers types and thicknesses). The predicted pavement temperature profiles were compared against the hourly recorded temperatures from five thermistors installed at different pavement depths. **Table 4-5** lists the depths of the thermistor locations measured from the surface of the pavement for road sections 48-1068, 27-1028 and 16-1010.

Figure 4- 8 Distribution map of selected road sections to predict and validate the pavement temperature profiles.

Table 4- 4 Pavement structures of the selected sections obtained from the Long-term Pavement Performance (LTPP) database.

Layer description	Layer code	Layer type	Representative thickness (mm)
Road section 48 – 1068 in Lamar, Texas			
Asphalt overlay	AC	asphalt concrete layer	80
Original asphalt layer	AC	asphalt concrete layer	198
Base layer	GB	unbound (granular) base	152
Subbase layer	TS	bound (treated) subbase	203
Subgrade	SS	subgrade (untreated)	N/A
Road section 27- 1028 in Otter Tail, Minnesota			
Asphalt overlay	AC	asphalt concrete layer	41
Original AC layer	AC	asphalt concrete layer	51

AC treated base layer	AC	asphalt concrete layer	152
Subgrade	SS	subgrade (untreated)	N/A
Road section 16-1010 in Idaho			
Asphalt overlay	AC	asphalt concrete layer	132
Original AC layer	AC	asphalt concrete layer	145
Base layer	GB	unbound (granular base)	137
Subgrade	SS	subgrade (untreated)	N/A

Table 4- 5 Location of thermistors for the selected sections obtained from the Long-term Pavement Performance (LTPP) database.

Thermistor identification number	Depth from the pavement surface (m)
Road Section 48-1068 in Lamar, Texas	
1	0.025
2	0.128
3	0.232
4	0.321
5	0.397
Road Section 27-1028 in Otter Tail, Minnesota	
1	0.025
2	0.115
3	0.205
4	0.623

5	0.696
Road Section 16-1010 in Idaho	
1	0.023
2	0.13
3	0.25
4	0.34
5	0.42

In addition to the pavement structure, the hourly air temperatures, wind speed, short-wave solar radiation, albedo, and emissivity were collected from the LTPP database and incorporated into the temperature prediction models. Optimised absorption coefficients were employed by region. For road sections 48-1086, 27-1028, and 16-1010, Han et al. (2011) determined the following absorption coefficients: 0.7, 0.75, and 0.7, respectively (Han et al. 2011). The mean subsurface soil temperatures obtained from MERRA-2 were 17, 5.3 and 6.3°C for road sections 48-1068, 27-1028, and 16-1010, respectively. These subsurface soil temperatures were also considered the bottom Dirichlet boundary condition for the temperature prediction models. Previous studies regarded temperature as a constant value (33.5ºC) or changing at a constant rate for depths below three meters (Han et al. 2011). Therefore, using actual site-specific soil temperatures is expected to provide greater accuracy, especially for deeper pavement layers.

The empirical equation proposed by Vehrencamp (**Equation 3-15**) (Vehrencamp 1953) causes the heat transfer coefficient of conduction (h_c) to drop in freezing conditions, which creates a divergence between predicted and measured temperatures during the winter season (shown in **Figure 4-9**) and causes a maximum mean absolute error (MAE) of more than 12ºC. Thus, the error was likely caused by using empirical parameters for the heat transfer equation, specifically the heat conduction coefficient between the pavement surface and air, (h_c). These parameters were obtained experimentally under ideal conditions where the surface temperature is

always higher than the air temperature with a variance range of 6.3 to 26 ºC (Vehrencamp 1953). Field conditions do not always match this assumption. For example, in regions susceptible to freezing, the air temperature is sometimes higher than pavement temperature during the winter season. This causes heat to transfer from the air to the pavement, not in the opposite direction (pavement to air). Physically, the heat conduction rate is assumed to be the same regardless of the route of heat transfer (air to/from pavement surface); however, there are no data to support this assumption.

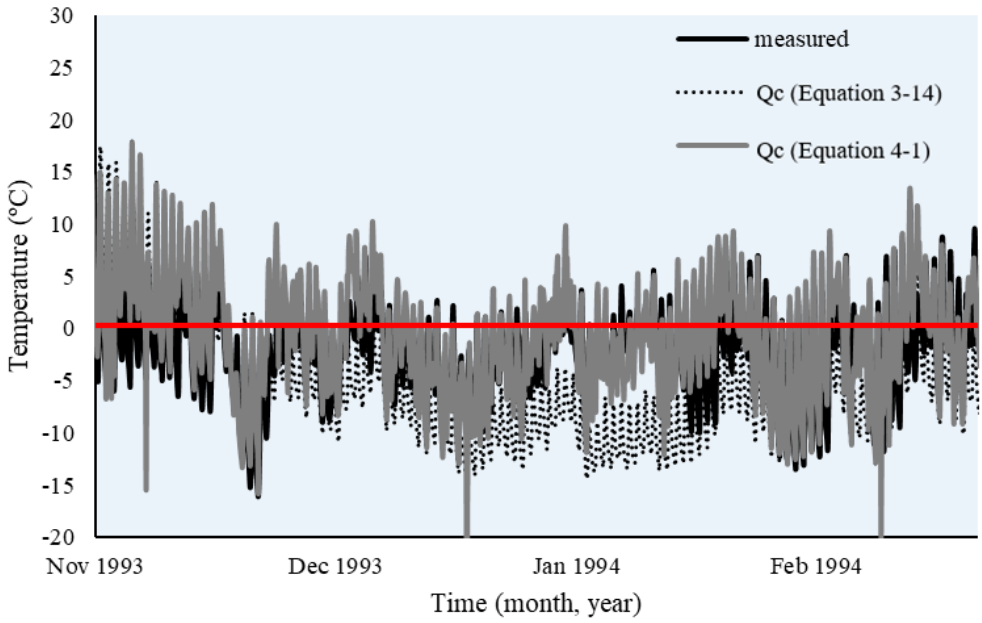

Figure 4- 9 Divergence between predicted and measured temperatures before and after applying a minimum limit to the coefficient of heat conduction (h_c).

Therefore, a limitation is proposed for the heat conduction equation so that if the difference in temperature between the air and pavement surface exceeds -4ºC, it will not cause the heat conduction to drop radically (as shown in **Equation 4-1**). This constraint ensures a certain level of heat conduction is achieved even during the freezing condition, a condition which the empirical conduction equation (**Equation 3-15**) did not cover.

$$Q_c = (if\ (T_{air}(t) - T) > -4, -4, (T_{air} - T))\ h_c \tag{4-1}$$

Figures 4-10, **4-11**, and **4-12** compare predicted hourly pavement temperatures with field-measured temperatures at different pavement depths over time for road sections 48-1068, 27-1028 and 16-1010, respectively. These figures show that predicted temperatures at various pavement depths are comparable to those measured in the field. Daily temperature variations are reduced as pavement depth increases. For validation purposes, the models were run for a minimum of one year to capture temperatures in all seasons. The time interval is also bounded by the availability of field measurements in the LTPP database. The mean absolute error (MAE) is measured at five pavement depths for each road section and detailed in **Figures 4-10**, **4-11**, and **4-12**. In which, MAE= $\frac{1}{number\ of\ values(n)}\sum_{i=1}^{n}|measured\ temperature - pedicted\ temerature|$).

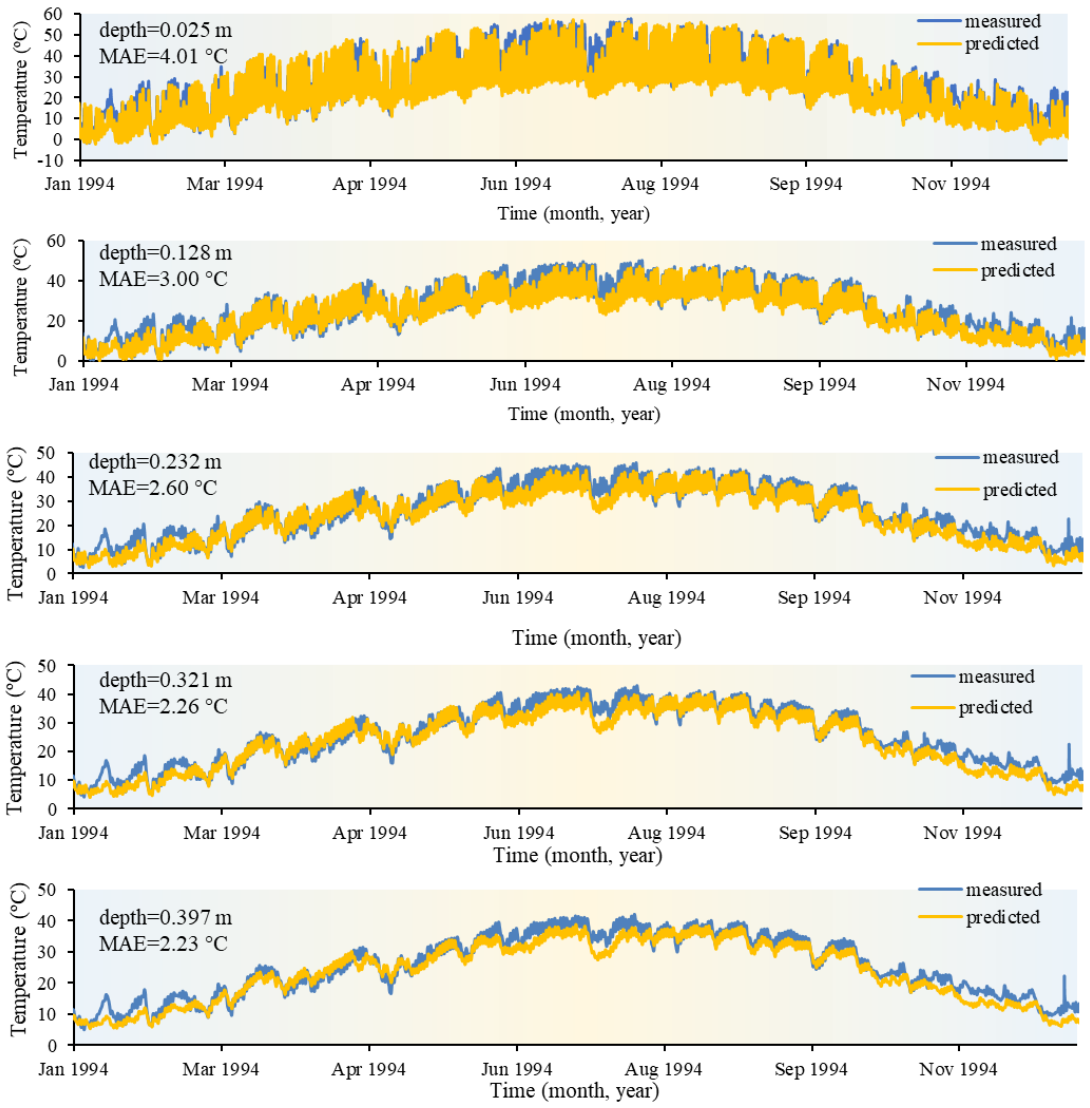

Figure 4- 10 Predicted and field-measured temperatures for road section 48-1068 in Lamar, Texas, USA, for one year (January 1994-December 1994) at depths of 0.025, 0.128, 0.232, 0.321, and 0.397 m, respectively, measured from the surface of the pavement with the mean absolute error (MAE) at different depths. Winter and summer seasons are highlighted in blue and yellow colours, respectively.

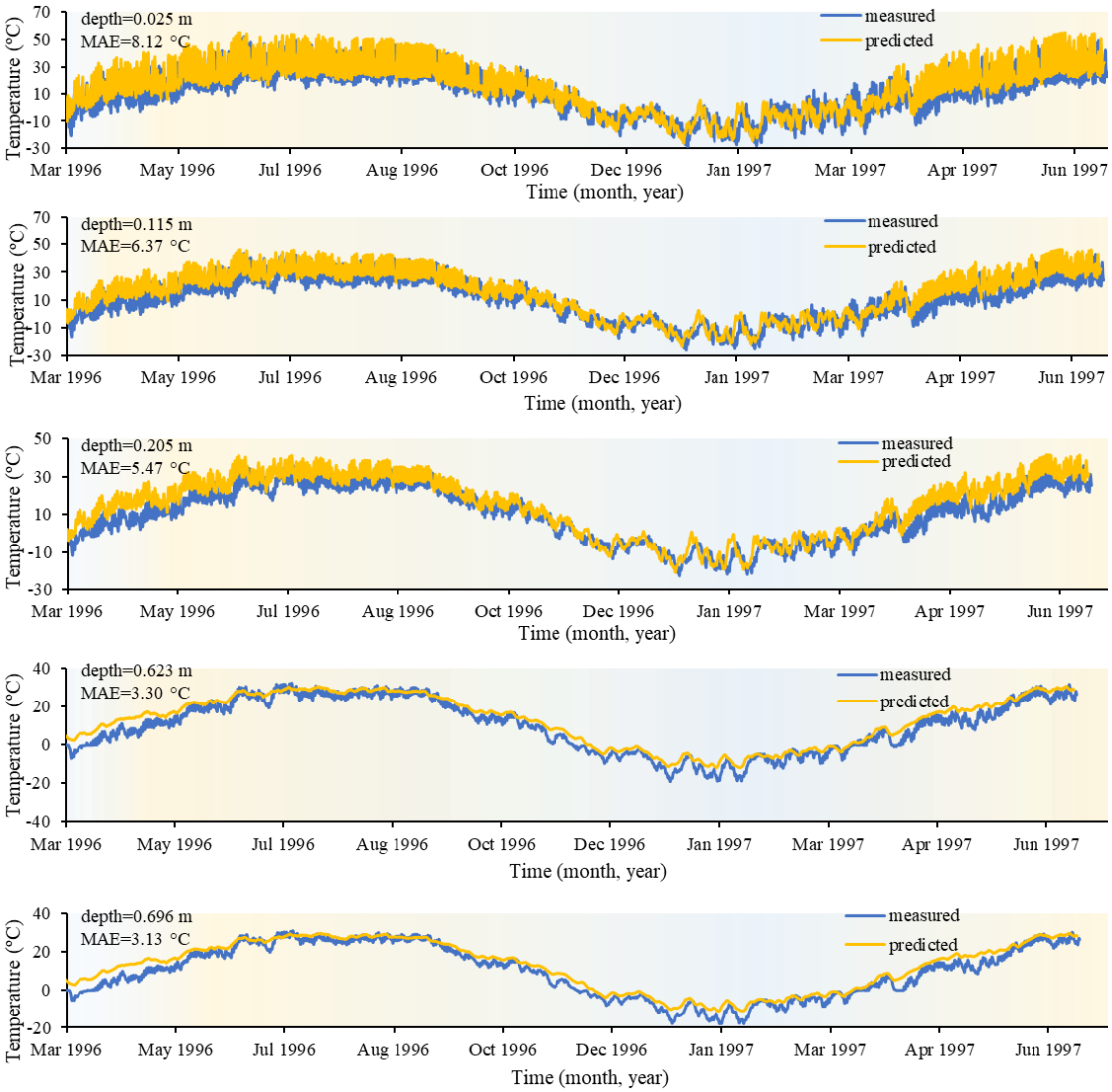

Figure 4- 11 Predicted and field-measured temperatures for road section 27-1028 in Otter Tail, Minnesota, USA, for the period (March 1996-June 1997) at depths of 0.025, 0.115, 0.205, 0.623, and 0.696 m, respectively, measured from the surface of the pavement with the mean absolute error (MAE) at different depths.

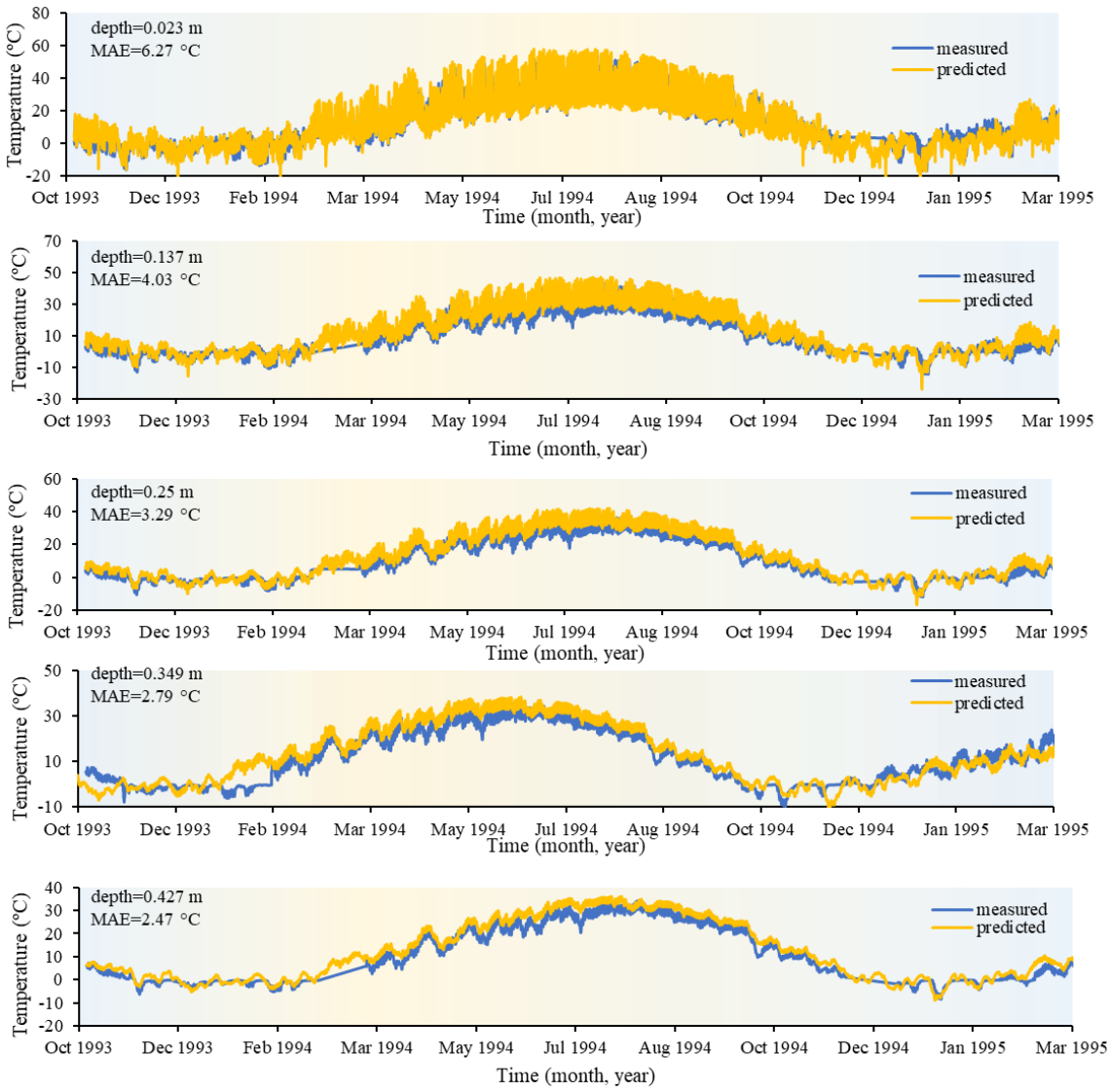

Figure 4- 12 Predicted and field temperatures for road section 16-1010 in Idaho, USA, for the period (October 1993-March 1995) at depths of 0.023, 0.137, 0.25, 0.349, and 0.427 m, respectively, measured from the surface of the pavement with the mean absolute error (MAE) at different depths.

The maximum mean absolute error (MAE) values of 8.12ºC and 6.27ºC were encountered close to the pavement surface at 0.025 m and 0.023 m in the cold (freeze) regions (Minnesota and Idaho), and the error was more distinct in the winter season. Nonetheless, the model appears to have sufficient accuracy, particularly for ageing prediction purposes where ageing occurs at high temperatures and stops when the temperature is low, suggests that the small divergence during cold seasons will not affect oxidative ageing.

4.4 Field Validations of Ageing Predictions in Asphalt Pavements

To verify the ageing model results, predicted carbonyl area values were compared with CA measurements of the binder extracted from field cores. The FHWA reports show that the cores were extruded from field sections at various ageing intervals. Cores were assembled and analysed for air voids percentage and accessible air voids by using air voids determination procedures and X-ray CT scans; then binders were extracted and recovered from sliced asphalt concrete samples at different pavement depths. The recovered binders were then analysed for oxidation products, specifically the carbonyl area, using FTIR (Glover et al. 2014). This process is illustrated in **Figure 4-13**.

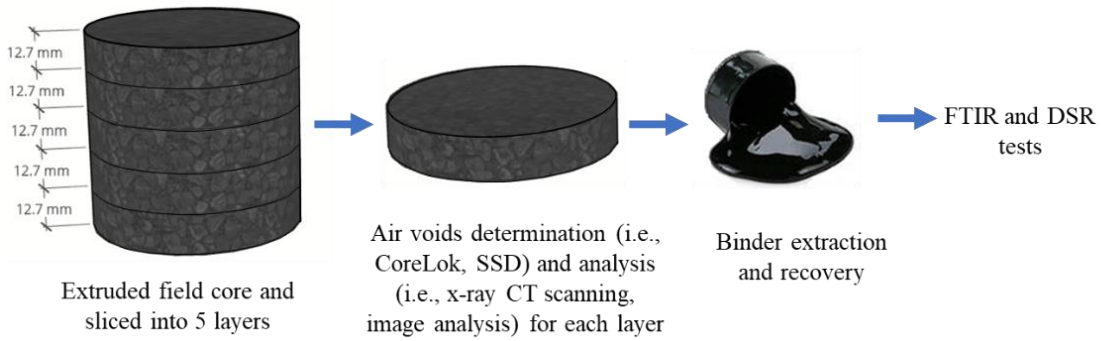

Figure 4- 13 Illustration of field sample extraction and binder recovery processes.

The measured CA at a specific pavement depth is an overall representation of the carbonyl contents of the sliced asphalt samples at that depth.The average predicted carbonyl area was obtained for each AC layer at different pavement depths using **Equations 3-41 and 3-42** and compared against field measurements (shown in **Table 4-6**). **Figure 4-14** shows a comparison between the predicted carbonyl content and the carbonyl content measured in the field for cores recovered at the wheel path. The field data seem to have unsystematic patterns across the pavement depth; for example, the field measurements of CA for road section US277 form an S-shaped ageing gradient across the pavement depth. Nonetheless, in general, there is a meaningful agreement between the field measurements and the predicted values obtained by the comprehensive oxidative ageing models, and the predicted carbonyl profile shows a consistent increase with ageing year and a C-shaped curve along the pavement depth.

Table 4- 6 Carbonyl area for field aged recovered binders collected at the wheel bath for road sections US277 and US83 (Han 2011, Jin et al. 2013, Glover et al. 2014)

Road section - Area	Date of cores extraction	Measured carbonyl area				
Depth		**Layer 1/ 0.0064 m**	**Layer 2/ 0.0191 m**	**Layer 3/ 0.0318 m**	**Layer 4/ 0.0445 m**	**Layer 5/ 0.0572 m**
US277-Laredo	07/2008	0.936	0.937	0.971	0.954	0.930
	12/2009	1.206	1.004	0.970	0.886	-
	12/2010	1.116	1.013	1.104	1.079	-
	01/2012	1.135	1.026	1.175	1.053	-
Depth		**Layer 1/ 0.0085 m**	**Layer 2/ 0.0254 m**	**Layer 3/ 0.0423 m**		
US83-Childress	08/2008	0.968	0.867	0.871		
	10/2009	1.129	1.012	1.029		
	08/2010	1.097	1.043	0.934		
	11/2011	1.134	0.971	0.946		

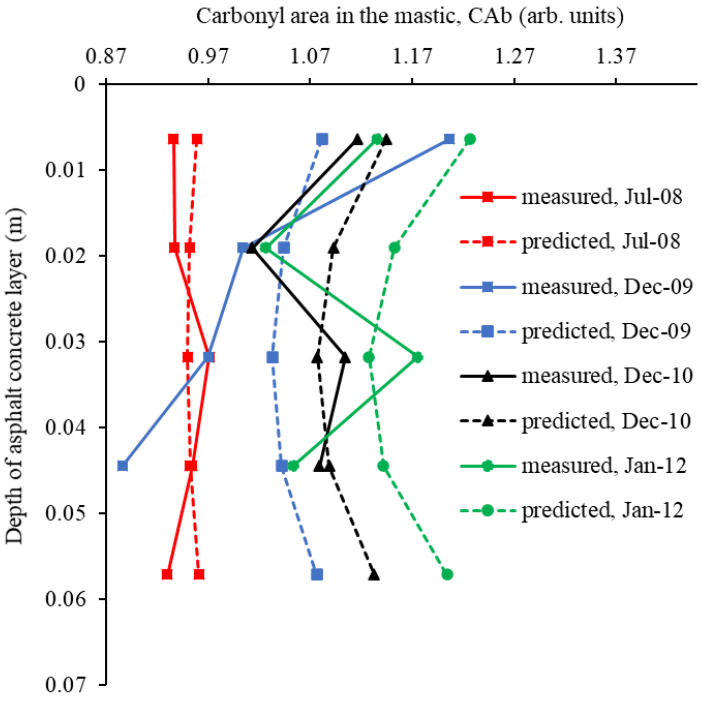

(a) Carbonyl area for road section US277 in Laredo, Texas, USA

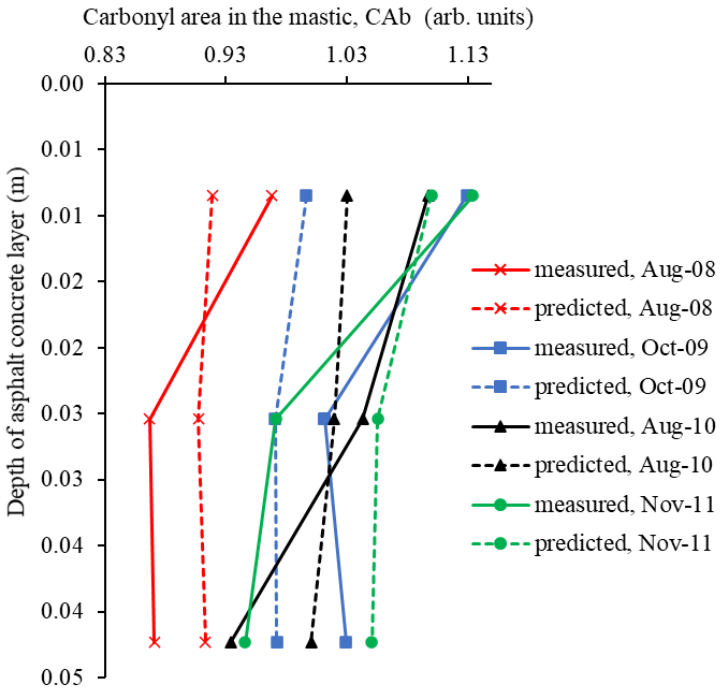

(b) Carbonyl area for road section US83 in Childress, Texas, USA.

Figure 4- 14 Comparison between the carbonyl area of recovered field cores and the predicted carbonyl area in the mastic (CA_b) obtained from the proposed oxidative ageing models (a) for road section US277 in Laredo, Texas, USA; and (b) for road section US83 in Childress, Texas, USA.

4.5 Summary of Field Ageing Predictions and Validations

In this chapter, ageing predictions for selected road sections were provided using the integrated Multiphysics ageing modelling framework. The circular dependency among ageing-related physics was addressed, and the proposed ageing prediction model was validated using available field measurements of the temperature and ageing profiles in the asphalt pavements.

Ageing model input data such as climate, material and structural information were collected from the Long-term Pavement Performance (LTPP) database and the Federal Highway Administration (FHWA) reports and imported into the finite element model (FEM). It is found that the model can effectively address the circular dependency among ageing-related Multiphysics (i.e., heat transfer, oxygen diffusion, and oxidation kinetics). Partial differential

equations (PDEs)-based FEM can reliably predict annual hourly profiles of temperature, oxygen pressure, and oxidation products growth across the pavement depth, in different climate zones. Oxygen pressure within the asphalt structure frequently changes due to seasonal and daily temperature variation, and it is affected by the oxidation process. Modelling results in this study support that oxidative ageing is non-uniform and decreasing in general across pavement depth because it is highly sensitive to oxygen pressure and temperature profiles. This unique behaviour cannot be observed without using the circular-dependent Multiphysics model.

The temperature profiles in asphalt pavements were validated using field temperatures for three road sections at different pavement depths. The proposed comprehensive ageing model was also validated using field measurements of the oxidation products (the carbonyl area) for two road sections located in Texas, USA, by comparing the predictions with the carbonyl area from field samples collected by the FHWA.

Chapter 5 Parametric Analysis and Field Validations of Oxidative Ageing in Asphalt Pavements*

In this chapter, a parametric study is conducted using the Multiphysics modelling approach to predict the field ageing and evaluate the effects of material thermal properties, air voids content and distribution, mastic coating thickness, oxygen accessibility, and climate region on the spatial and temporal evolution of oxidative ageing in the asphalt pavements. The findings are validated using available literature results as well as field data from 14 European road sections.

First, a suitable range of values is identified for each parameter based on the experimental data extracted from an extensive literature search. Parameters covered include **internal parameters** associated with paving materials properties (thermal conductivity and heat capacity), pavement structures (bound and unbound base layers), and morphology of asphalt concrete (mastic coating film, and air voids content and distribution); and **external factors** (climate region). Then ageing predictions for each set of parameters are made for one year of field ageing simulations, analysed and compared with field measurements for validation. The overall aim is to investigate model inputs effect on ageing growth and distribution to identify parameters that play a vital role in the oxidative ageing of asphalt pavement.

5.1 Effects of Thermal Properties on Ageing in Pavements

The thermal diffusivity of a material is a term that combines all three pillars of thermal behaviour, that is, thermal conductivity, heat capacity, and density together. It plays a chief role in the heat transfer process. This parametric study focuses on thermal conductivity and heat capacity, without considering the effect of density on ageing evolution. This is because the density

* Findings of this chapter are summarised in a journal paper: Omairey, E., Zhang Y., Soenenb H., and Carbonneauc, X. (submitted in March 2021). "Parametric Analysis and Field Validations of Oxidative Ageing in Asphalt Pavements using Multiphysics Modelling Approaches" under peer reviewal by International Journal of Pavement Engineering.

falls within a narrow range (i.e., it does not change significantly for the same material type); for example, density ranges for asphalt concrete, base and subbase layers are 2100-2350 kg/m^3, 1800-2375 kg/m^3, and 1500-2350 kg/m^3, respectively (Luca and Mrawira 2005, Han 2011, Alawi and Helal 2014, Hassn et al. 2016a, Alavi et al. 2017, Li et al. 2019). Thus, the density will not originate a significant change in the temperature profile when altered. Additionally, there are several design limitations and performance implications that are linked to asphalt materials. Therefore, changing this material property merely to mitigate oxidative ageing is not applicable from a practical point of view. It should also be noted that the influence of thermal properties on the temperature profile of pavement is bounded by the thickness of paving layers. However, just like density, changing layers thicknesses has many economic and design implications; thus, it is kept constant. It should be kept in mind that the results of this parametric study (in terms of the influence of thermal properties on the temperature profile and oxidative ageing products) are sensitive to changes in layers thicknesses. For instance, the temperature at the bottom AC layer becomes less influenced by the temperature of outside atmosphere when increasing the pavement thickness, because of the increased thermal mass of AC materials (Gui et al. 2007, Alavi et al. 2014).

First, thermal conductivity and heat capacity values for all pavement materials are collected from the literature (Luca and Mrawira 2005, Gui et al. 2007, Han 2011, Alawi and Helal 2014, Hassn et al. 2016a, Alavi et al. 2017, Li et al. 2019). Then, a range of thermal conductivity and heat capacity values is considered in this parametric study. There is no evidence of important changes in the thermal properties of pavement materials upon ageing (Pan et al. 2017b); accordingly, the thermal properties are kept constant with time.

Road section US277, located in dry-warm environmental zone, is employed to carry out the parametric analysis. Such warm climatic regions have more implications on oxidative ageing than cold areas, where oxidative ageing damage is less of a problem in the latter. The model is run for one year to consider temperature variations in all seasons.

5.1.1 Thermal conductivity

Thermal conductivity is a material property and a measure of its ability to transfer heat. Materials with low thermal conductivity values have a low heat transfer rate (e.g., thermal isolators); whereas, materials of high thermal conductivity values experience a high heat transfer rate (e.g., metals). The thermal conductivity of the asphalt mixtures can be altered by adding fillers. Chen et al. (2015, 2017) found that the thermal conductivity of dense asphalt mixtures increased by 0.5 W/m/K by adding 20% graphite powders to bitumen (Chen et al. 2015a, Chen et al. 2017). Furthermore, aggregate type predominantly influences the thermal conductivity of asphalt concrete mixtures (Qin 2016), where it can be reduced by 0.5 W/m/K by replacing 40% of coarse granites with ceramic aggregates.

Table 5-1 contains the typical range of thermal conductivity values for all pavement layers (AC, base, and subgrade layers). Three thermal conductivity values are considered for each pavement layer in the parametric sensitivity study. These are the maximum, minimum and mid-range values. One parameter is tested at a time while keeping others at the mid-range. Thus, nine field ageing simulations are set to run.

Table 5- 1 Typical range of thermal conductivity values for different layers of asphalt pavement.

Material	Thermal conductivity (W/m/K)	Low	Middle	High
Asphalt concrete	1.00– 2.88	1.00	1.94	2.88
Base layer	1.00- 2.50	1.00	1.75	2.50
Subgrade layer	0.19 – 2.50	0.19	1.345	2.50

Figure 5-1 shows the predicted pavement temperature profile for all thermal conductivity values; results are collected during peak temperatures in the daytime in the summer season. One profile pattern is observed for all thermal conductivity of the asphalt layer (k_{as}) values in this figure, with a temperature variation of 2.5°C at one depth. The peak temperature is recorded at the top surface of AC layer. It then declines gradually in the base layer, rises again at the base-

subgrade interface (making an S-shaped pattern), and then decreases in the subgrade to reach the pre-determined earth temperature. This S-shaped formation can be attributed to the existence of higher thermal conductivity value of the base layer compared to that of the subgrade. When this happens, the temperature will easily transport from the heat source (outside atmosphere) into the asphalt concrete and base at a fast rate. Then, the heat transfer rate will drop at the subgrade-base interface. Any excess heat will be trapped in the middle of the AC layer due to the low thermal conductivity of subgrade, causing such a unique pattern. This perhaps designates that a consistent thermal conductivity along pavement depth is desirable to prevent additional temperature absorption and heat storage.

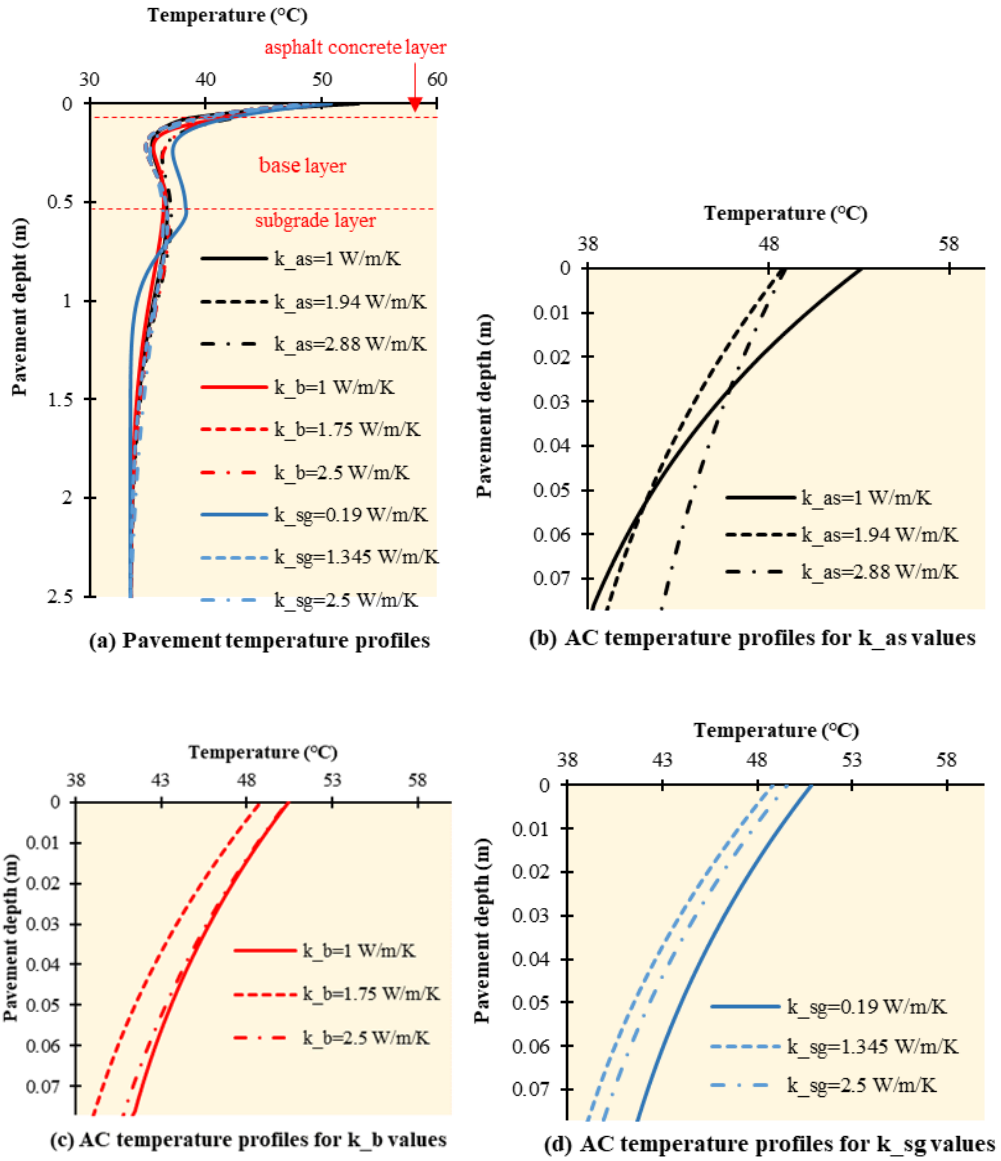

(a) Pavement temperature profiles

(b) AC temperature profiles for k_as values

(c) AC temperature profiles for k_b values

(d) AC temperature profiles for k_sg values

Figure 5- 1 Predicted temperature profiles for road section US277 for different thermal conductivity values at peak daily temperature in summer. (a) Temperature profiles across the pavement, (b) asphalt concrete (AC) temperature profiles for different k_{as} values (c) AC temperature profiles for different k_b values, (d) AC temperature profiles for different k_{sg} values. The yellow highlight of the figure indicates data are collected in warm intervals (summer, peak daily temperatures).

The observed temperature gradient in relation to changes in asphalt thermal conductivity (k_{as}) agrees well with others' findings, in that the surface temperature declines with increasing the thermal conductivity of AC while the temperature rises as depth increases (Solaimanian and Bolzan 1993, Solaimanian and Kennedy 1993, Wang et al. 2010, Bobes-Jesus et al. 2013). Increasing k_{as} lowers the surface temperature and increases the bottom temperature, thus lead to a less temperature gradient in asphalt layer, this can benefit the reduction of the ageing gradient and cracking damage.

Results also suggest reducing the thermal conductivity of base and subgrade layers did not cause a significant improvement (temperature reduction < 2°C) within the AC layer.

Figure 5-2 shows the temperature prediction for pavements with different asphalt thermal conductivity values (k_{as}) for four days intervals in the summer and winter seasons at the surface and bottom of AC layer. A nonlinear correlation exists between the AC temperature and thermal conductivity values. The minimum thermal conductivity in the AC layer ($k_{as} = 1\ W/m/K$) yielded greater day-to-night surface temperature variations and overall lower variations at AC bottom. This behaviour is predictable because the heat will be accumulated at the near-surface depths because it cannot transport deeper, due to low heat transfer rate caused by this small k_{as}. While at the bottom of AC layer, the temperature is more stable and less affected by the outer atmosphere for the same reason, which is the low heat transfer rate. Chen et al. (2015) recorded similar observations, the day-to-night temperature gradient decreases by increasing the pavement thermal conductivity (Chen et al. 2015a). To conclude, increasing k_{as} reduces the peak

temperature in summer, which can help to minimise rutting damage. At the same time, increasing k_{as} will increase the bottom temperature (**Figure 5-2 (d)**), which softens the bitumen, leading to less fatigue damage.

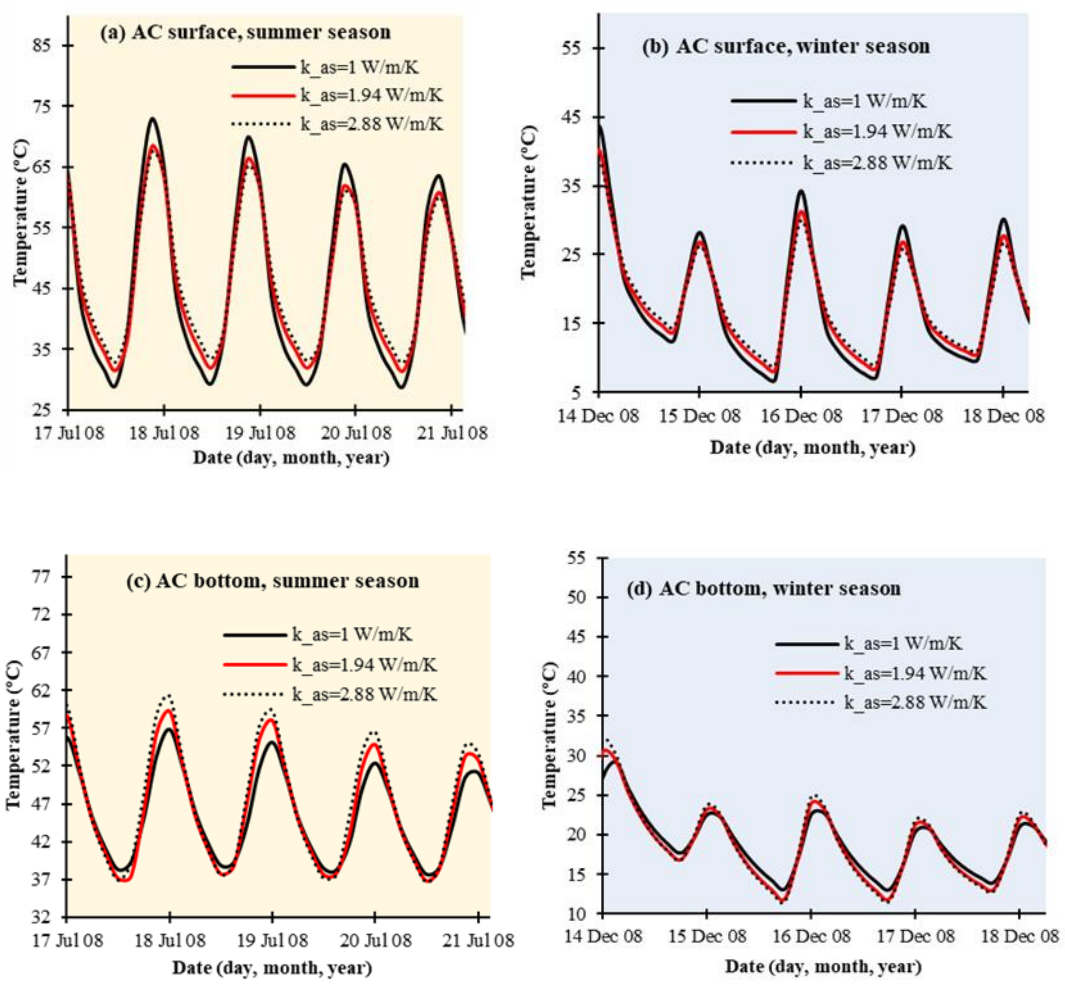

Figure 5- 2 Temperature variation with time in asphalt concrete (AC) layer with thermal conductivity (k_{as}= 1, 1.94, and 2.88 W/m/K) for summer and winter time intervals at (a) AC surface during summer (b) AC surface during winter (c) AC bottom during summer, and (d) AC bottom during winter. The yellow and blue highlights indicate warm and cold intervals, respectively.

The mean increase in the daily maximum temperature at the top surface of AC layer due to reducing k_{as} from 2.88 W/m/K to 1 W/m/K is 5°C, and the mean decline in the daily maximum temperature at the bottom of the asphalt layer is 4.1°C. The change in the daily maximum

temperature is particularly important to the field oxidative ageing growth level and extent. To explain, Mallick et al. (2009) demonstrated that for the same traffic and pavement materials, the pavement life could be extended by five years for a 5°C decline in temperature, using NCHRP 1-37A MEPDG (Mallick et al. 2009). Thus, the change in carbonyl growth with ageing time is investigated. **Figure 5-3** shows the carbonyl growth rate at the surface-mastic interface at the top, middle and bottom of the AC layer. The carbonyl indices (CI) (where, CI= (CA of aged binder - CA of unaged binder)*100/CA of unaged binder) at the surface of asphalt pavement at air-mastic interface for k_{as} of 1 W/m/K and 2.88 W/m/K are 22.2% and 17%, respectively after one year of field ageing simulation. The difference in CI makes up a 5% increase per ageing year due to reducing k_{as} value from the maximum to minimum thermal conductivity values.

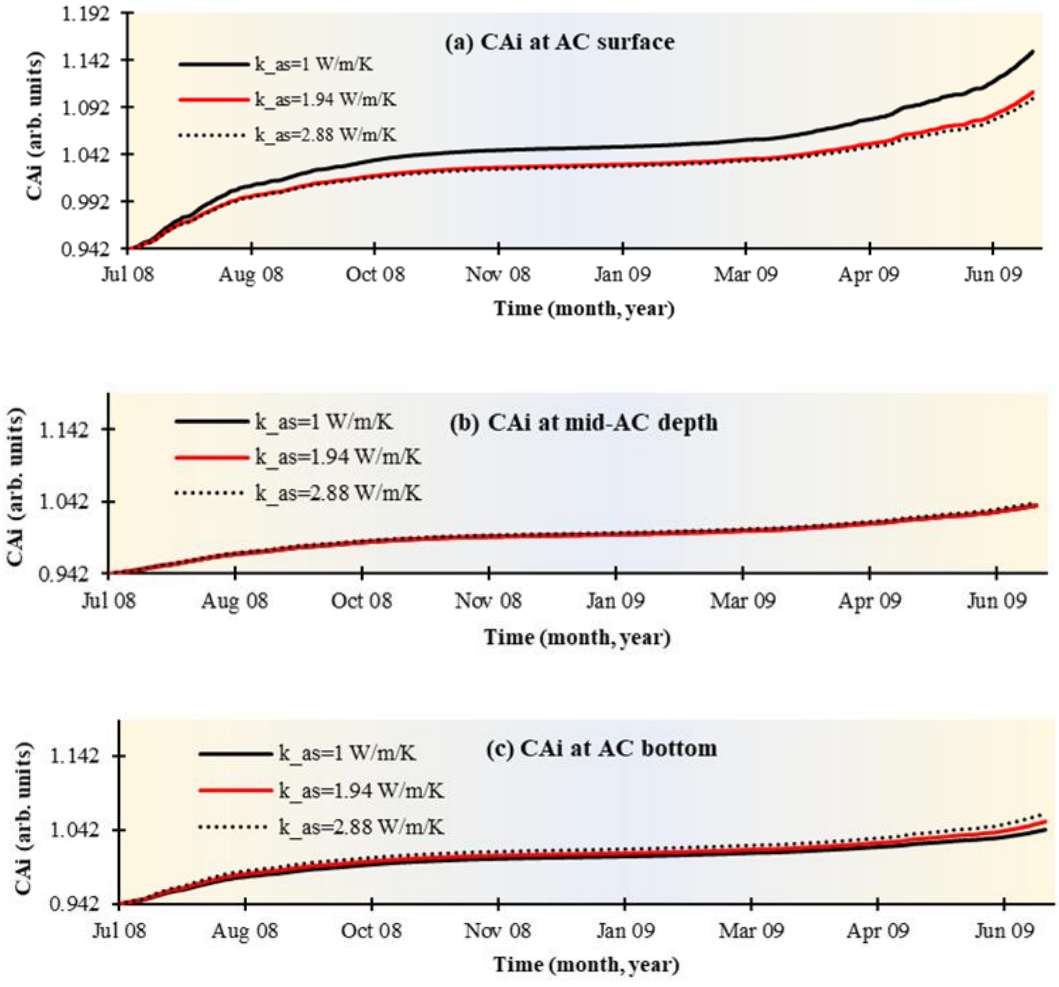

Figure 5- 3 Carbonyl area at the air channels-mastic interface (CA_i) versus ageing time, for different thermal conductivity values (k_{as}= 1, 1.94, and 2.88 W/m/K) at three asphalt concrete (AC) depths (a) AC surface, (b) mid-AC depth, and (c) AC bottom.

Figure 5-4 shows the average predicted carbonyl content in the mastic within AC depth for the thermal conductivity values (1, 1.94, and 2.88 W/m/K) for one year of field ageing. The average carbonyl content within the depth after one year of ageing is consistent with its corresponding temperature profile. It seems that maintaining a low thermal conductivity at the AC layer will cause higher oxidative ageing at the surface that declines gradually at deeper levels. Results for **Figure 5-4** suggest that increasing k_{as} reduces the ageing gradient, which may help on reducing thermal and top-down cracking.

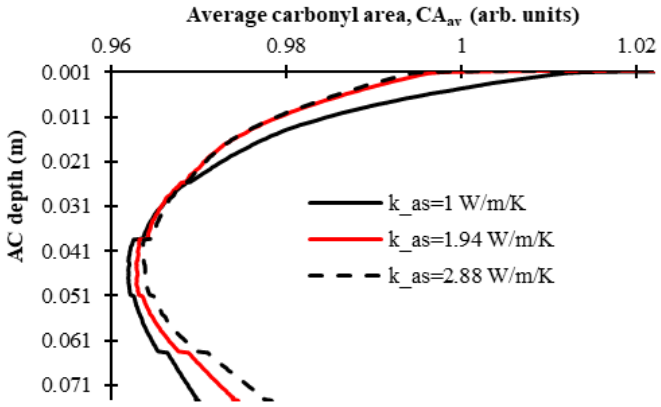

Figure 5- 4 Average carbonyl area across the asphalt concrete (AC) depth after one year of field ageing simulation using different thermal conductivity values (k_{as}). Small sudden jumps/ changes in the curve are attributed to using different mastic film thicknesses across the asphalt depth when calculating the average carbonyl content.

The thermal conductivity of underlayers (base and subgrade) is shown to have a minimal effect on the temperature profile and carbonyl content within the asphalt concrete layer.

5.1.2 Heat capacity of pavement materials

The heat capacity of a material is its ability to store heat. It is measured by the energy required to change the temperature of a certain mass of material by one degree. A high heat capacity value indicates a better ability of the material to maintain its temperature.

Table 5-2 contains the typical range of heat capacity values for all pavement layers (asphalt concrete, base, and subgrade layers). Three heat capacity values are considered for each pavement layer in the parametric sensitivity study. One heat capacity value is tested at a time while keeping other parameters at mid-range values. Therefore, nine ageing simulation tests are set to run.

Table 5- 2 Typical range of heat capacity values for different asphalt pavement layers.

Material	Heat capacity (J/kg/K)	Low	Middle	High
Asphalt concrete	700-1200	700	950	1200
Base layer	700-1100	700	900	1100
Subgrade layer	600-1100	600	850	1100

Altering heat capacity caused a limited change in the temperature (maximum difference of 2°C), as shown in **Figure 5-5**. Higher temperatures are observed for low HC_{as} (HC_{as} =700 J/kg/K), caused by the rapid change in temperature and the layer's low ability to store or maintain its heat conditions. This suggests using low heat capacity at the surface layer is undesirable. Asphalt pavements with high heat capacity need more time to reach maximum temperatures than those with low heat capacities, which agrees well with other research findings (Yavuzturk et al. 2005, Bobes-Jesus et al. 2013).

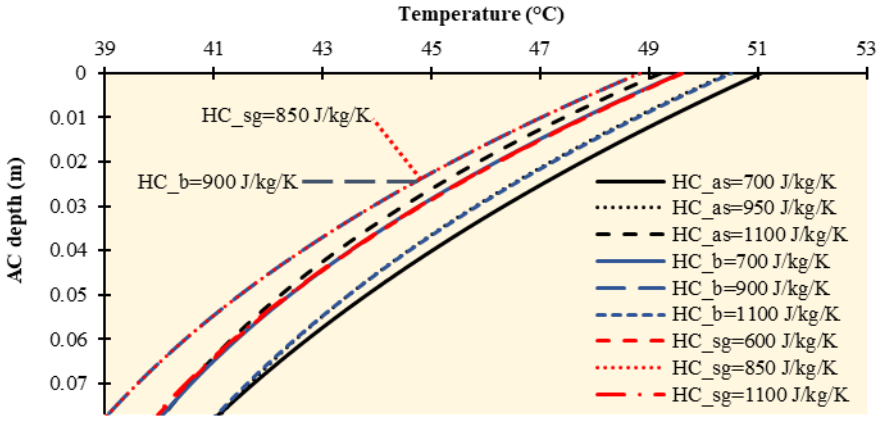

Figure 5- 5 Temperature profiles within the asphalt concrete (AC) layer collected at same peak daytime hour in summer for different heat capacity values at asphalt concrete (HC_{as}), base (HC_b) and subgrade (HC_{sg}) layers.

It can also be seen from **Figure 5-5** that changing HC_b and HC_{sg} is correlated nonlinearly with the temperature change in AC. This is because the temperature at AC layer is only a small fraction of the overall profile of the pavement, and the resultant temperature profile is affected by how all layers are working together to transport and store heat. It is therefore recommended to run a temperature simulation analysis when designing a pavement of specific thermal requirements.

The heat capacity of AC layer (HC_{as}) has more impact on the temperature profile than heat capacities of underlying layers; thus HC_{as} results are going to be discussed in more detail. **Figure 5-6** shows the day-to-night temperature variations at different locations of AC in the summer and winter seasons. The temperature fluctuation is a bit more intense at $HC_{as} = 700\ J/kg/K$ compared to that at higher heat capacity values, with an average difference of 1 to 2°C, and the fluctuation is more pronounced in the summer. Bobes-Jesus et al. (2013) noticed similar behaviour, in that the temperature variations decreases as asphalt pavement specific heat increases (Bobes-Jesus et al. 2013) due to the greater heat storage capacity of the pavement.

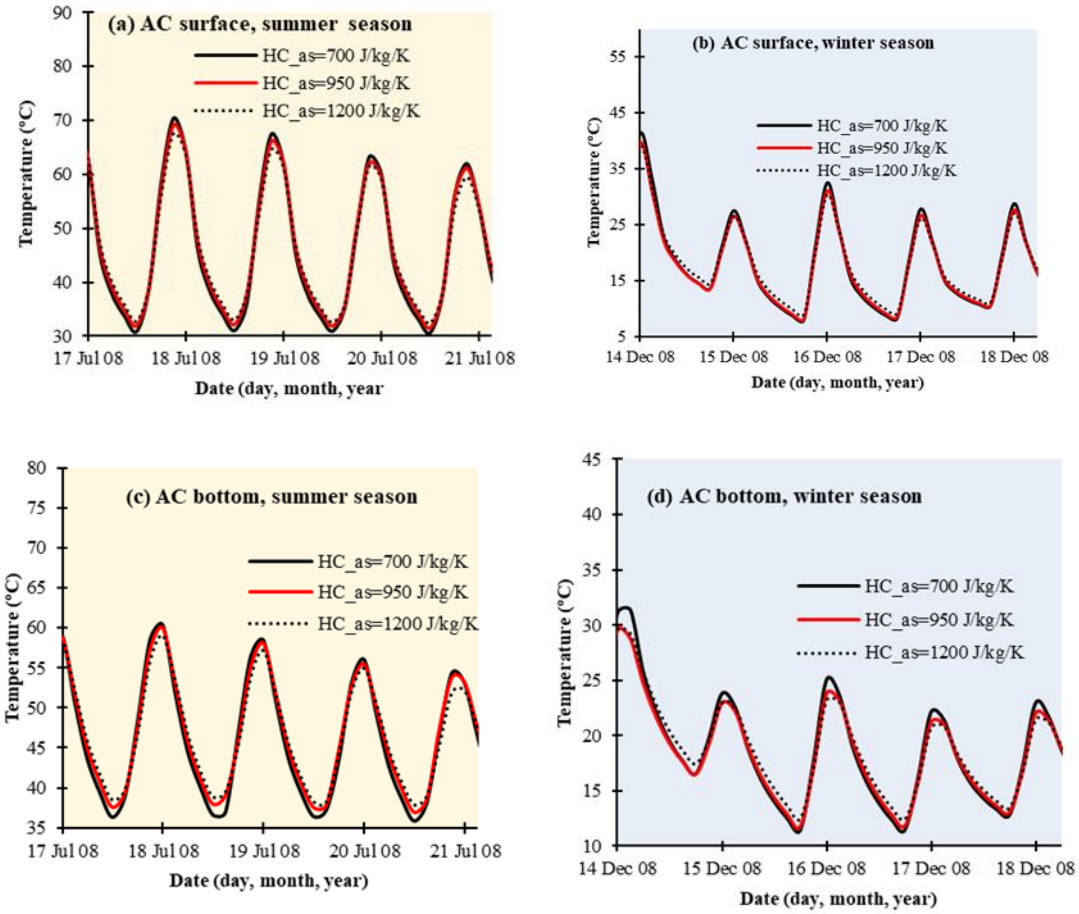

Figure 5- 6 Temperature variation with time at asphalt concrete (AC) with heat capacity values of (HC_{as}= 700, 950, and 1200 J/kg/K) at (a) AC surface in summer (b) AC surface in winter (c) AC bottom in summer, and (d) AC bottom in winter.

Figure 5-7 shows the carbonyl growth with time for different heat capacity values in the AC layer. Asphalt pavement with lower heat capacity ($HC_{as} = 700\,J/kg/K$) experienced more oxidative ageing compared to greater heat capacity values. However, the difference in the carbonyl index after one year of field ageing due to decreasing HC_{as} from 1200 to 700 J/kg/K did not exceed one percent of increase at the surface of AC. Furthermore, the impact of heat capacity of underlying layers (base and subgrade) on the oxidative ageing growth rate is also negligible.

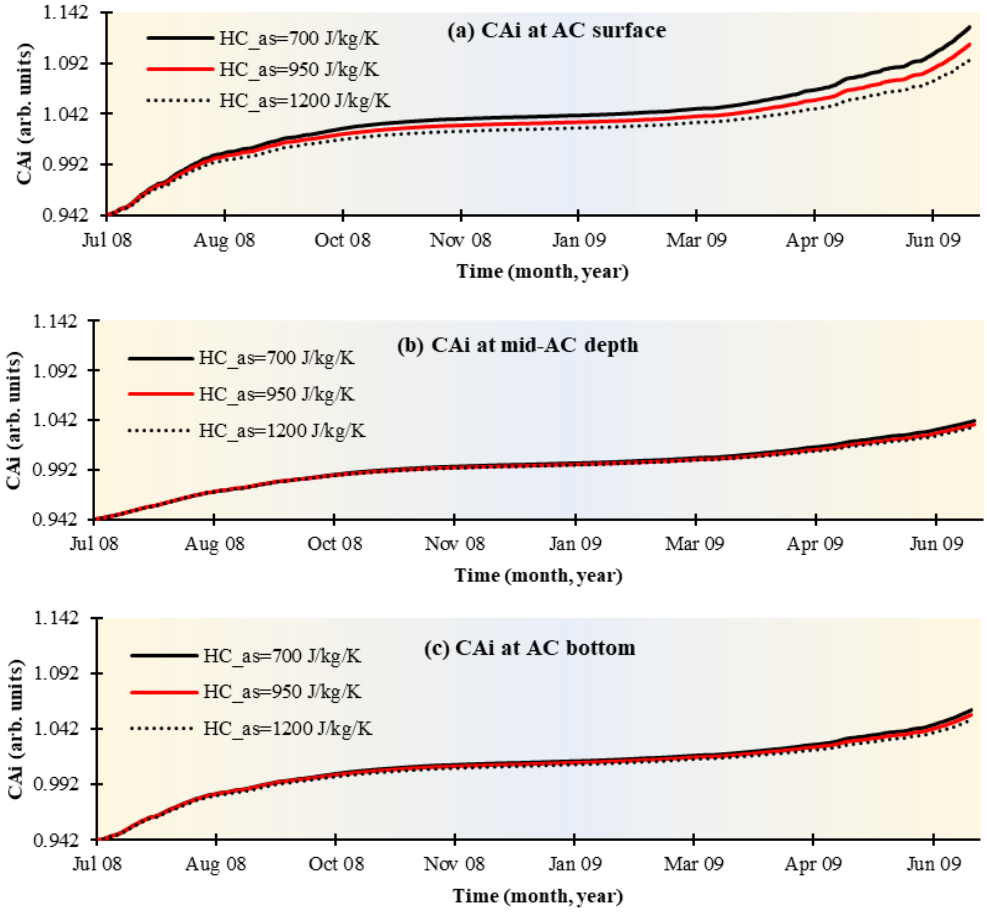

Figure 5- 7 Carbonyl area at the air channels-mastic interface (CA_i) versus ageing time, for different heat capacity values (HC_{as}=700, 950, and 1200 J/kg/C) at three asphalt concrete depths (AC) (a) AC surface, (b) mid-AC depth, and (c) AC bottom.

To conclude, the thermal properties of underlying layers (base and subgrade) causes little to no effects on the temperature profile and oxidative ageing products content and distribution for this data set. Thus, any values within the range can be safe to use in future modelling. The most notable effect was caused by changing the thermal conductivity and heat capacity of the AC. The maximum daily surface temperature can be reduced by a maximum of 5°C, which according to previous literature, can extend the service life by five years when considering all distress factors, not that caused by oxidative ageing alone.

5.2 Effect of Oxygen Accessibility on Ageing in Pavements

The porosity of underlying layers may affect oxygen supply and the ageing process in the AC. This section covers the influence of bottom boundary condition on oxygen pressure

distribution and CA growth rate. Two extreme scenarios are considered: (1) oxygen can diffuse freely from the lower boundary (i.e., presence of porous base layer), and (2) there is no access of oxygen from the lower boundary (i.e., presence of treated base layer). The first case (free access to oxygen) is predefined in the existing ageing model. The second condition (no access to oxygen) is achieved by adjusting the boundary condition of oxygen diffusion in both air channel and mastic in the ageing model. To explain, in **Section 3.3**, amend oxygen diffusion interfaces at the interconnected air channels and inside the mastic film thickness by removing the *bottom domain* of Dirichlet boundary condition ($P_{air} = 0.2\ atm$, and $P_b = 0.2\ atm$). Thus, oxygen pressure of 0.2 atm is supplied at the top surface only.

Figure 5-8 shows oxygen pressure distribution in the air channels at two different time intervals: (1) at peak daytime during summer season when rapid oxidation is expected to occur, (2) at night-time during winter when the oxidation is unlikely to occur. It is noted that the oxygen pressure (P) at the bottom boundary is more than 0 even for a predefined Dirichlet boundary condition of zero, it is because the oxygen pressure is dependent on the coefficient of oxygen diffusion in the air channels (D_{o_2}) (where the latter is considerably high in the air channels). Thus, oxygen can still reach the bottom boundary for this data set (mixture morphology, internal structure, and climate data).

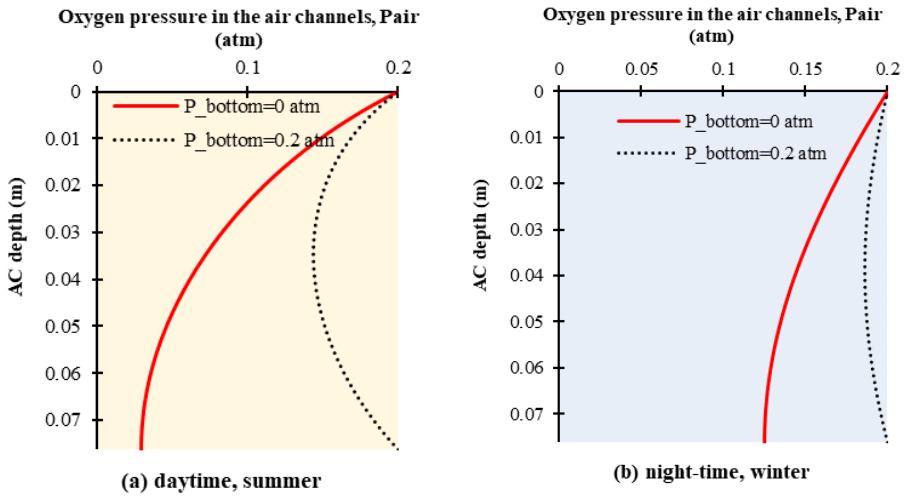

Figure 5- 8 Oxygen pressure in the air channels (P_{air}) across asphalt concrete (AC) depth at (a) peak daytime in summer, (b) peak night-time in winter.

Figure 5-9 shows the oxygen pressure distribution within the mastic coating at different AC depths. More oxygen diffused into the asphalt mastic when the lower boundary condition is made accessible to air (oxygen pressure at the bottom boundary of AC = 0.2 atm).

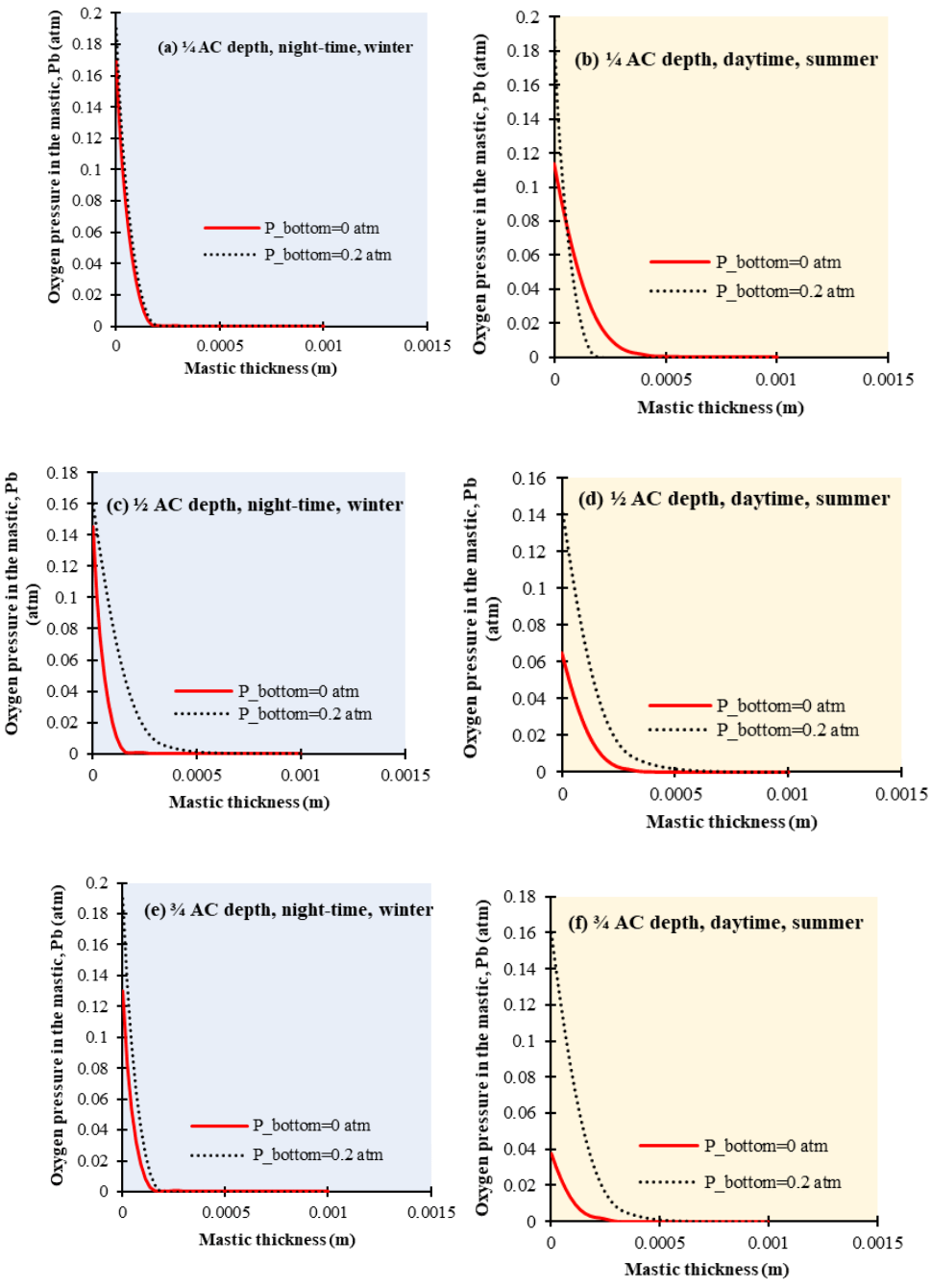

Figure 5- 9 Oxygen pressure profile across mastic coating thickness at different asphalt concrete (AC) depths (1/4, 1/2 and 3/4 depth from AC top surface), collected in two seasonal conditions (winter and summer seasons).

Oxygen pressure within the asphalt mastic plays a vital role on the level and distribution of oxidative ageing. **Figure 5-10** shows the carbonyl area at the air channels-mastic interface (CA_i), and that at one third the asphalt mastic coating thickness (CA_b) after one year of field ageing simulation. The pavement with free access to oxygen from top and bottom (e.g., an unbound granular base is used) is forming carbonyl area profile of a C-shaped curve, and pavement with access to oxygen from top surface only but no access to oxygen from the bottom surface (e.g., treated base is used) is creating an r-shaped carbonyl area profile. Moreover, pavement with access to oxygen from both top and bottom sides experienced more overall ageing, as seen in **Figure 5-10 (a).** Wang et al. (2014) placed oxygen sensors at different locations in asphalt pavement layer in the field (Wang et al. 2014). They observed that the sensor located in the middle of the asphalt pavement slab shows reduced oxygen concentration compared with one not covered by the slab, and one closer to the slab edge (has less accessibility to air). They stated that the difference in oxygen content at the pavement's upper and bottom layers creates an oxygen pressure gradient, contributing to the variations of asphalt ageing in a pavement structure. These conclusions agree with the obtained simulation results in this study. Because the ageing gradient is more significant for ($P_{bottom} = 0\ atm$), it *may* lead to a more severe top-down cracking, but less bottom-up cracking.

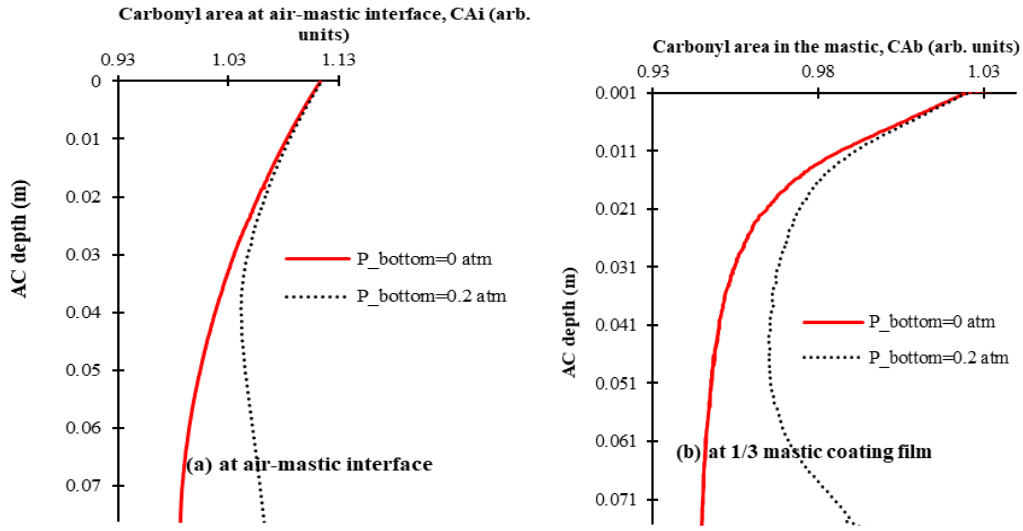

Figure 5- 10 Carbonyl area across the pavement depth for one year of field ageing simulation at (a) air channels-mastic interface, (b) 1/3 mastic film thickness.

Figure 5-11 shows CA's growth at the air channels-mastic interface for one year of field ageing simulation. The pattern agrees with **Figure 5-10** in that CA values at the surface are identical for both bottom boundary conditions, but they start to diverge when going deeper in AC.

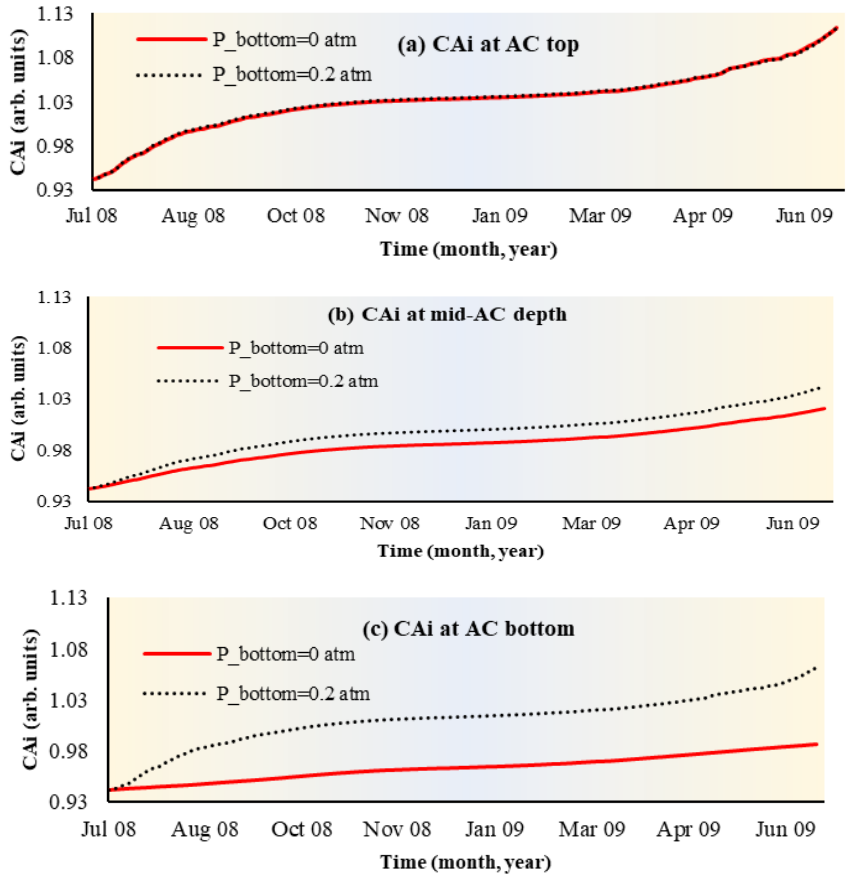

Figure 5- 11 Carbonyl area at the air channels-mastic interface (CA_i) versus ageing time, for two oxygen accessibility conditions (P_{bottom}=0 or 0.2 atm) at (a) AC surface, (b) mid-AC depth, and (c) AC bottom.

5.3 Effect of Mastic Coating Film Thickness on Ageing in Pavements

The extent of oxidative ageing in asphalt mastics is bound by the coating film thickness surrounding accessible air channels (i.e., diffusion depth of oxygen). The current ageing model uses CT-scan and imaging analysis to determine the coating thickness from extracted field cores across the AC layer. The mastic thickness is then used as a geometric parameter to measure the average carbonyl area (CA) profile across the AC layer. Thus, the extent of CA is not a function of diffusion depth. **Figures 5-12 (a and b)** show that there is a volumetric relationship between

CA and diffusion depth using three mastic coating thicknesses (2.55, 3.40 and 5.00 mm) for one year of field ageing simulation. All tested samples experienced similar behaviour, and the oxidative ageing did not extend beyond 0.07 mm of coating thickness after one year of exposure to field ageing simulation for all three samples for this specific data set.

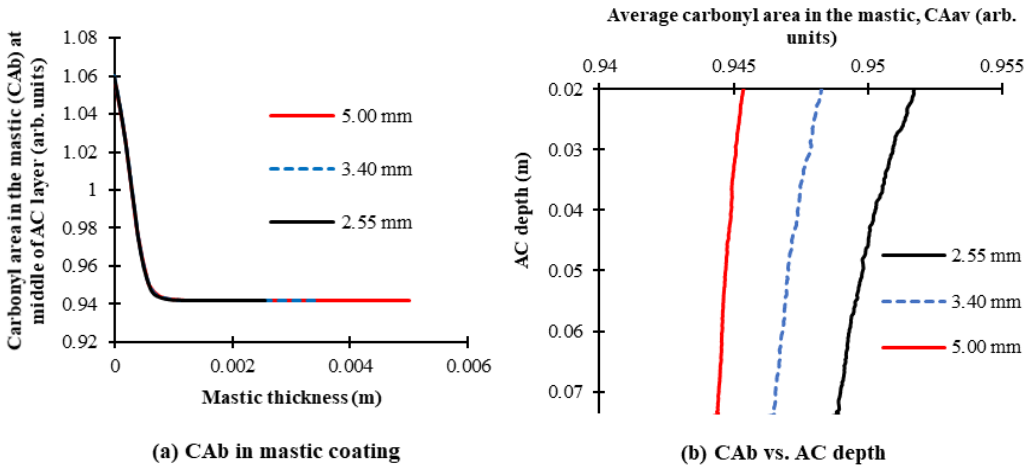

Figure 5- 12 (a) Carbonyl area profile in the binder mastic film (CA_b) measured at the middle depth of AC layer after one year of field ageing simulation. (b) Average carbonyl area in asphalt mastic for AC with different mastic coating film thicknesses (2.55, 3.40, and 5.00 mm) after one year of field ageing.

Thus, the thicker the mastic coating film, the less the average carbonyl area will be. These findings agree well will previous studies, where it was found that asphalt pavements of less mastic coating film and better mastic distribution are more susceptible to oxidative ageing, resulting in a dramatic decrease of pavement's resistance to cracking (Jiang et al. 2020).

5.4 Effect of Air Voids Distribution and Content on Ageing in Pavements

In this section, the effect of a simplified C-shaped distribution of air voids on the oxidative ageing profile will be considered and compared with results from the constant air voids approach. Then, the effect of average air voids percentage on oxidative ageing is investigated.

5.4.1 Effect of air void distribution on ageing in pavements

The role of air voids in the proposed equation-based ageing model is manifested in three parts (1) model geometry: the average air voids radius is forming the width of air channels (domain 1); (2) coefficient of oxygen diffusion in the air channels (D_{o2}): the coefficient of oxygen diffusion in the air channels is linked to the average air voids content (AAV) as seen in **Equation 5-1** and **Figure 5-13** (derived from the experimental results of Wen and Wang (2018) (Wen and Wang 2018); (3) average carbonyl content at a certain depth (CA_y): the predicted carbonyl area at any depth is calculated using the volumetric integration of mastic surrounding air voids channels (as can be seen in **Equation 5-2**).

$$D_{o2}(cm^2/s) = 10^{1.7866*\log(\text{AAV\%})-7.3139}, R^2 = 0.8725 \quad (5\text{-}1)$$

$$CA_y = \frac{\int_{r_{air}}^{R1} 2\,\pi CA(r)\,r\,dr}{\pi\,(R^2 - r_{air}^2)} \quad (5\text{-}2)$$

where R_1 equals the air voids diameter (r_{air}) plus the average diffusion depth at a certain AC depth, *CA(r)* is the carbonyl area at a specific point, and r is the horizontal coordinate of the point.

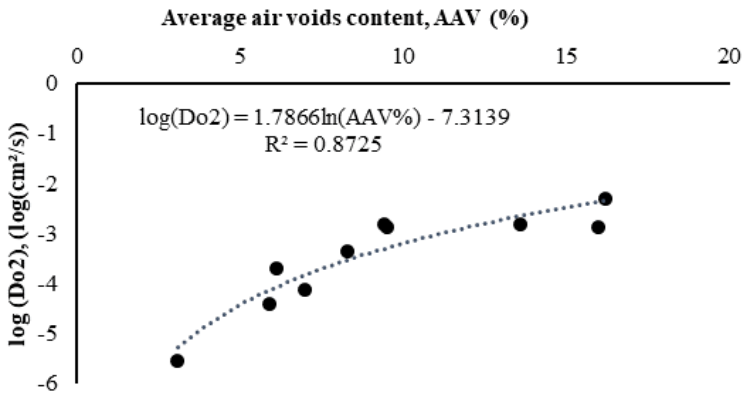

Figure 5- 13 Correlation between the coefficient of oxygen diffusion (D_{o2}) and air voids content (AAV%) (derived from experimental measurements of (Wen and Wang 2018)).

Two parameters linked to air voids distribution were employed in the proposed ageing model, that is (1) air voids content and (2) average radius of air voids. The air voids distribution (number and diameter) were obtained using x-ray CT-scan technique (Glover et al. 2014), however, the accuracy of CT-scan data (i.e., number, distribution and diameter of air voids) is

highly dependent on the number and location of extracted core samples. Additionally, it is unclear how many cores can be considered representative of the volumetric properties of the actual road section in the field. Thus, a relationship between air voids content and diameter (or radius) is employed to replace any dependency of the proposed ageing model on the air voids diameter from CT-scan images. This relationship was recognised empirically by Zhang et al. (2014) as displayed in **Figure 5-14** and **Equation 5-3** (with $R^2 = 0.7431$) (Zhang et al. 2014). It is worth to mention that this relationship may not apply to dense-graded mixtures (air voids content is less than 2%), as appears in **Figure 5-14**, the equation would still generates air voids radius even for zero air voids content. This error is attributed to limitations in air voids measuring techniques.

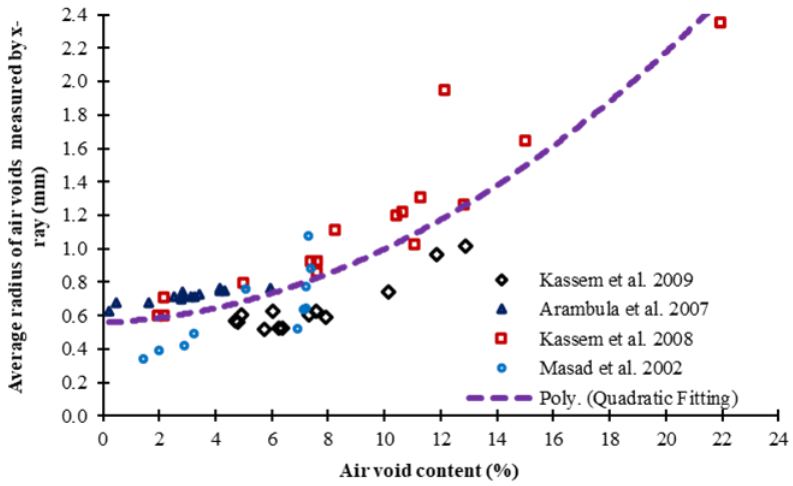

Figure 5- 14 Empirical correlation between average air void radius and air void content of asphalt mixtures based on laboratory and field samples (Zhang et al. 2014).

$$r_{air} = 0.0037(AAV\%)^2 + 0.0071(AAV\%) + 0.5583 \quad (5\text{-}3)$$

To study ageing sensitivity to air voids distribution, a C-shaped distribution pattern will be imposed in the model. The minimum value of air voids content is located at the middle of AC layer, and the maximum value is located at the top and bottom. To quantify these two extreme AAV values in relationship to the average air voids content, data collected from 48 field cores at 19 road sections located in the United States were employed to estimate the standard deviation from the mean of air voids content across depth. The air voids profiles for these road sections are documented in (Glover et al. 2014). Although these sections did not necessarily demonstrate a C-

shaped distribution, they give insight into the nature of variation in air voids content in the AC structure. **Figure 5-15** shows that 30% of studied core samples had a 1.5% to 2% deviation in the air voids content from the mean AAV. Therefore, the estimated minimum and maximum air voids content for the C-shaped distribution will have 2% to 1.5% deviation from the mean value in the current study.

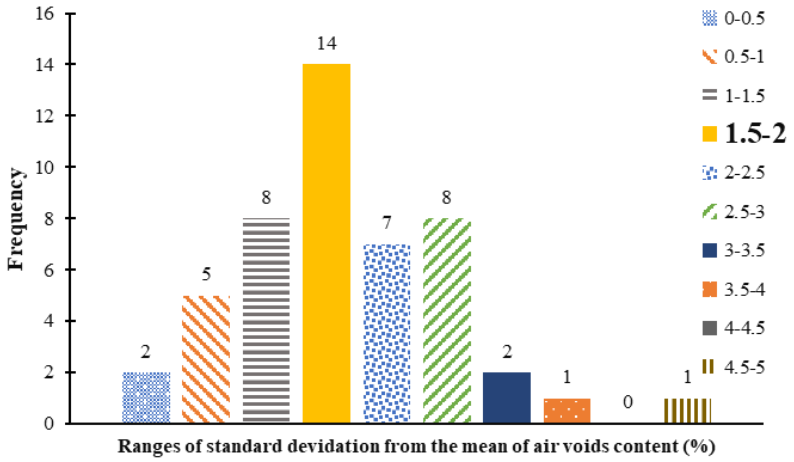

Figure 5- 15 Ranges of standard deviation from the mean of air voids across pavement depth for 48 field cores collected from 19 road sections in the United States (based on collected field data in (Glover et al. 2014))

Accordingly, the parabolic general formula is employed to form a C-shaped distribution of air voids, as seen in **Equation 5-4**.

$$AAV = \frac{AAV_{max} - AAV_{min}}{\left(-\frac{T_{as}}{2}\right)^2}\left(y - \frac{T_{as}}{2}\right)^2 + AAV_{min} \quad (5\text{-}4)$$

where, AAV is the air voids content at any AC depth (y), AAV_{max} and AAV_{min} are the maximum and minimum air voids contents, respectively, and T_{as} is the total depth of AC measured in meters. AAV_{max} and AAV_{min} are calculated using **Equations 5-5** and **5-6**, they ensure that average value of air voids content calculated from the proposed C-shaped curve equals the mean air voids of asphalt pavement.

$$AAV_{max} = AAV\% + 2\,a \quad (5\text{-}5)$$

$$AAV_{min} = AAV\% - a \quad (5\text{-}6)$$

where, a is equal or less than 1% to maintain a standard deviation from the mean within the range (2 to 1.5%), as discussed in **Figure 5-15**.

The oxygen pressure distribution in the air channels is expected to undergo changes when air voids distribution is altered because the coefficient of oxygen diffusion in air channels (D_{o2}) is air voids dependent. Increasing the air voids content at the top and bottom of AC by forcing a C-shaped arrangement caused a slight increase in the oxygen pressure, as shown in **Figure 5-16**. Consequently, there is a uniform increase in the carbonyl area growth across AC depth (**Figure 5-17**). Thus, although the average air voids content is kept the same, a non-uniform air voids distribution allowed more oxygen access to AC and increased the oxidative ageing across the pavement depth.

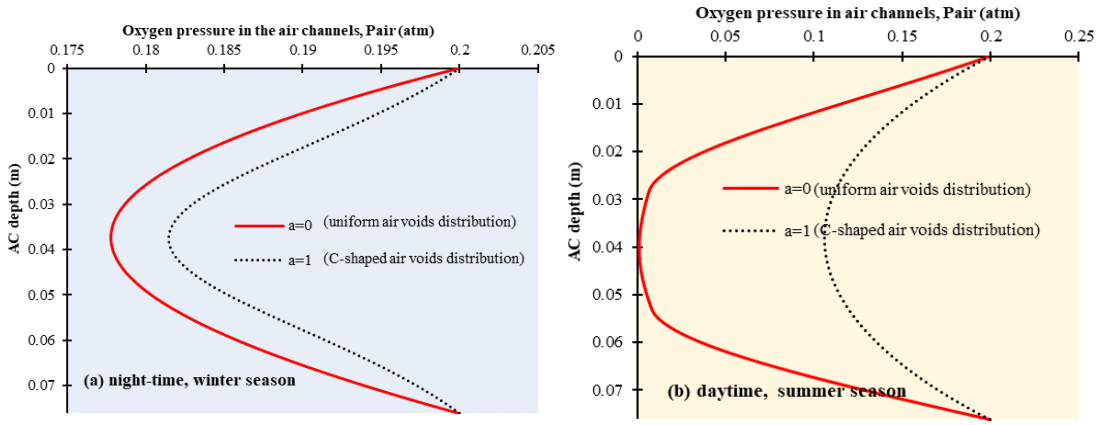

Figure 5- 16 Oxygen pressure profile in the air channels (P_{air}) for a uniform air voids distribution (a=0) and C-shaped air voids distribution (a=1) at an average air voids ratio of 8%, at (a) peak night-time in winter, (b) peak daytime in summer.

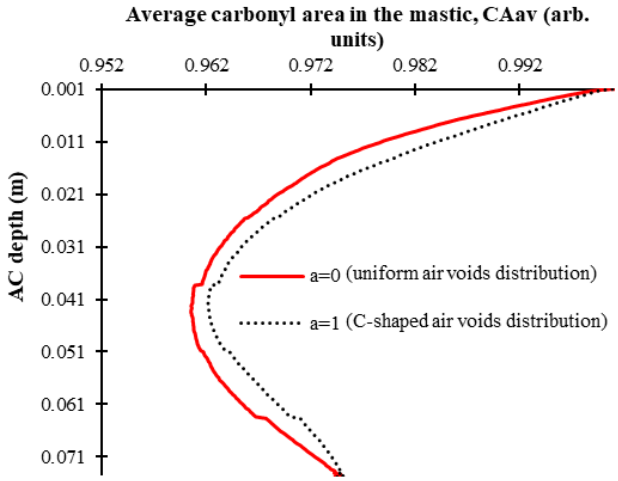

Figure 5- 17 Average carbonyl area profile for a uniform air voids distribution (a=0) and C-shaped air voids distribution (a=1) at average air voids ratio of 8%, for one year of field ageing simulation.

5.4.2 Effect of air voids content on ageing in pavements

A wide range of air void contents (AAV) from 2 to 14% with 1% increment was set in this parametric study. The variation in AAV distribution across depth was set as a C-shaped distribution (a=1). **Figure 5-18** shows carbonyl growth at the air-mastic interface for one year of field ageing simulation in the middle of the AC course. The results indicate a nonlinear change in carbonyl content with air voids content and the existence of two air voids thresholds. Pavements with air voids content of 5% and less experienced limited to no oxidative ageing. Altering the air voids from 5% to 9% caused a constant increase in CA, whereas increasing the air voids by more than 9% did not increase carbonyl formation rate. Thus it can be concluded: (1) dense AC of low air voids content (<5%) will experience little to no ageing especially in the middle of AC layers; (2) asphalt pavements with air voids content of (5-9%) will experience AAV-dependent oxidative ageing, where higher AAV leads to a higher ageing rate; (3) pavements with air voids of (>9%) will have a full access to oxygen from the atmosphere, and thus the oxidative ageing is very significant and will not be constrained by AAV. **Figure 5-19** shows the average CA content across pavement depth for AC with various AAVs. The results confirm that of **Figure 5-18**. The average carbonyl content for (AAV > 9%) is uniform across AC depth (i.e., no clear C-shaped or r-shaped ageing gradient).

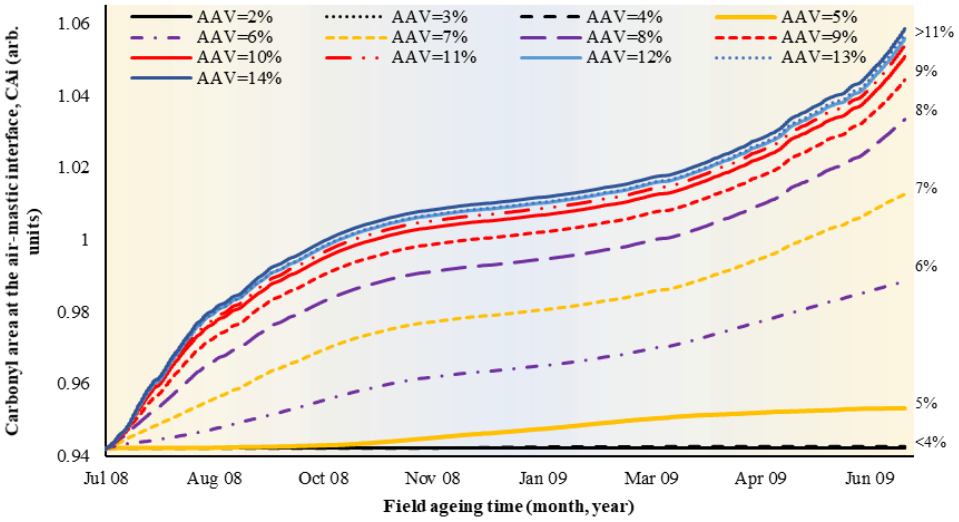

Figure 5- 18 Carbonyl area at air-mastic interface (CA_i) for one year of field ageing simulation, for asphalt layer of various air voids contents (AAV= 2%-14%).

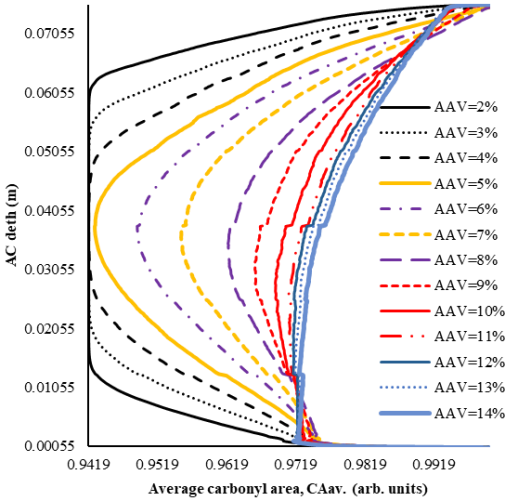

Figure 5- 19 Carbonyl area profile in asphalt layer with various air voids contents (AAV=2%-14%) after one year of field ageing simulation.

5.5 Effect of Climate on Field Oxidative Ageing of Asphalt Pavements

For a systematic improvement in pavements' thermal performance, customised pavement design and materials selection based on predicted pavement temperature profile or based on the experimental oxidative behaviour of materials is desirable. A better practice is forecasting the pavement response in terms of oxidative ageing growth rate directly upon changes in the climatic region. However, making customised field ageing predictions is not an easy task because

oxidative ageing is a multi-physical process. Interactions or constraints between the material, structural and climate variables on the ageing evolution must be accounted for when the ageing is modelled. The proposed PDEs-based FE model makes such multi-physical ageing predictions possible. With this framework, it becomes possible to comprehensively evaluate and determine the influence of climate conditions on field ageing distribution and evolution over the years in asphalt pavement.

In this section, climate data for two regions and pavement structural and materials information for one road section (road section US277) were collected. Then, oxidative ageing predictions for one year of field simulation were made using the proposed framework. Thus, binder information and pavement structure were kept identical, but the collected climate data varied to measure the impact of climate region on the oxidative ageing performance.

Hourly climate data from South Texas and South Washington States were collected for one year (starting from July). Information includes hourly data (air temperature, wind speed, solar radiation, albedo, and emissivity), average annual earth temperature at 3 meters depth, and coefficients of absorption were collected for these two locations.

The stations, both located in wet, no-freeze regions, were selected to have the same moisture and freezing conditions but with a clear difference in temperature profiles. South Texas has a higher temperature than South Washington, and this is reflected in the predicted pavement surface temperatures, as shown in **Figure 5-20**, with a mean annual difference in pavement temperature of 14°C at any depth across the AC layer.

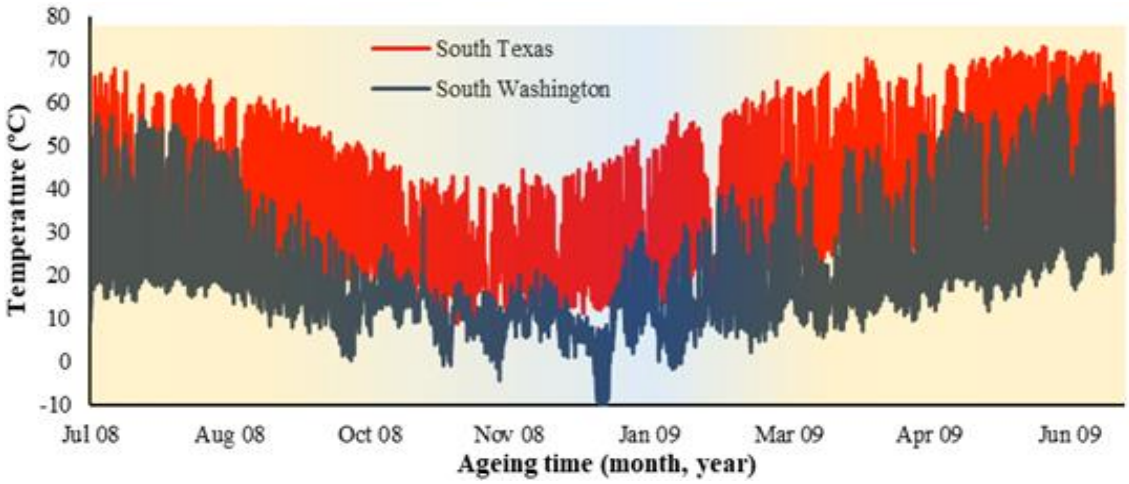

Figure 5- 20 Predicted pavement surface temperature for road section US277 at two climate regions.

Figure 5-21 shows the oxygen pressure distribution in the air channels for one year of field ageing simulation. Although the pressure profile in both climatic regions is high (0.19-0.2 atm), there is a clear difference between them, with lower oxygen pressure for the warmer region (Laredo, Texas).

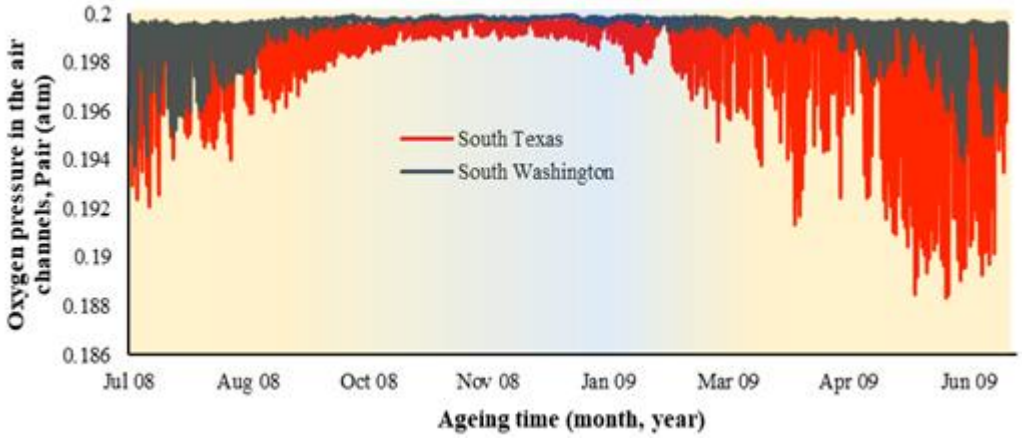

Figure 5- 21 Predicted oxygen pressure distribution in air channels measured at the middle of the asphalt concrete (AC) layer for one year of field ageing.

The oxygen consumption rate in Texas is more significant than that in Washington due to having a higher temperature profile along the pavement. Consequently, carbonyl builds up in

Texas at a higher rate than that in Washington, even after only one year of field ageing, as shown in **Figures 5-22** and **5-23**.

Figure 5-22 shows that the predicted carbonyl area growth at the air-mastic interface has decreased from 17.6% in the warm region to 5.58% growth for the colder region at any AC depth after one year of field ageing simulation. This difference makes up a 68% drop in the produced CA for these specific pavement properties and climates.

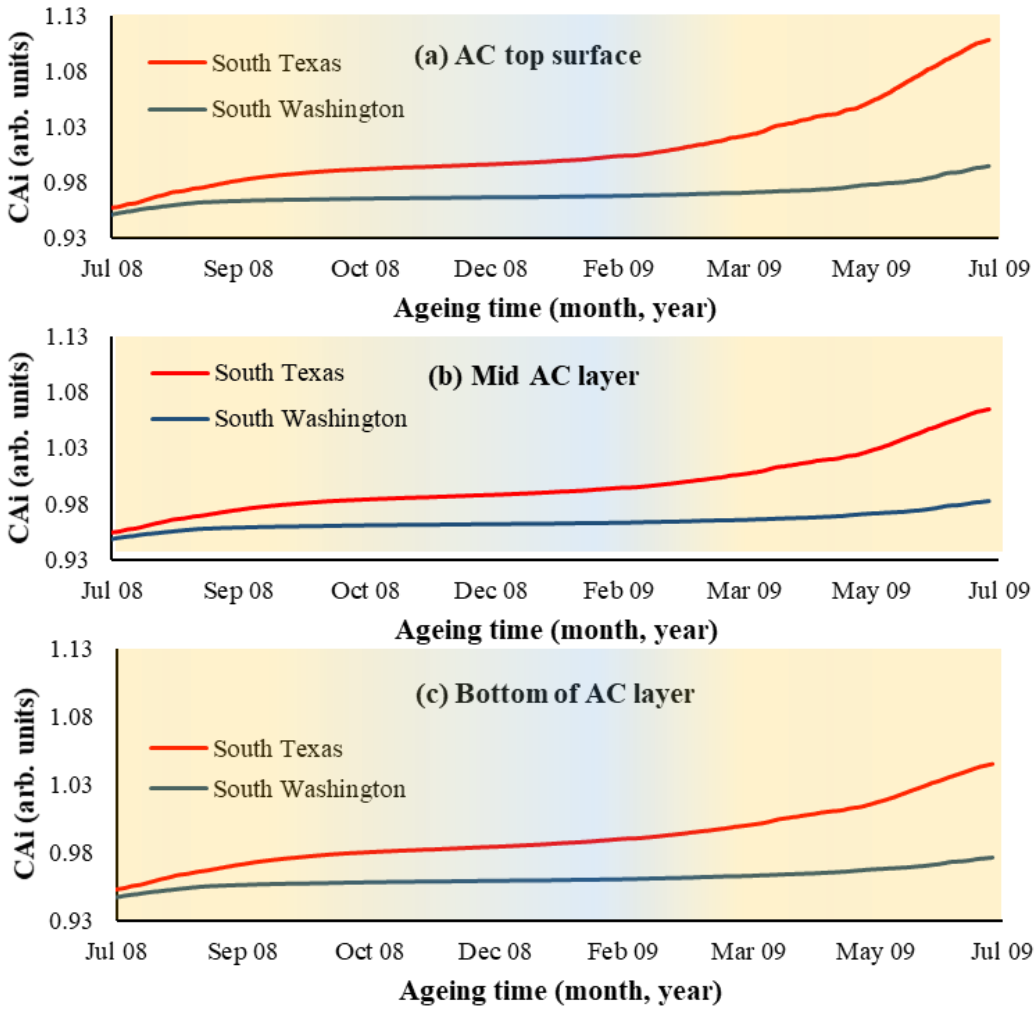

Figure 5- 22 Predicted carbonyl area (CA_i) at the air-mastic interface at three depths of asphalt concrete (AC) layer (surface, middle and bottom) for one year of field ageing simulation in two climate regions.

Similarly (but on a smaller scale of that for CA_i), CA at 1/3 mastic coating thickness has declined by 7% at the surface of AC and 4% at the bottom when shifting climate data from Texas to Washington after one year of ageing simulation. **Figure 5-23** shows a notable CA gradient in South Texas region, causing binder hardening at the surface and increased susceptibility to top-down cracking. In contrast, there is no clear gradient in South Washington section. This suggests that the climatic region will not only affect the degree of oxidation (and thus the degree of damage), but it will also change the form or type of this damage.

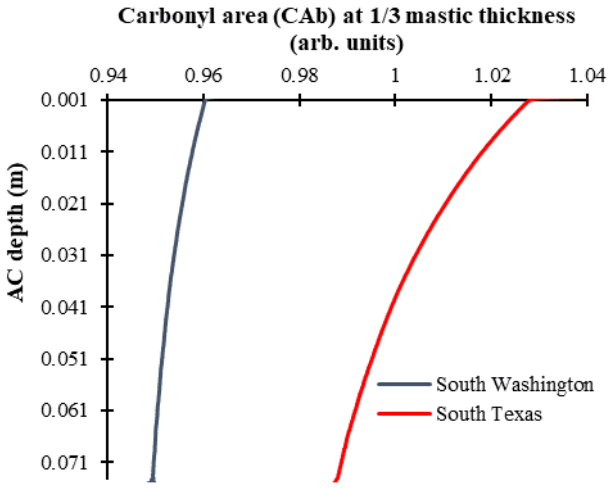

Figure 5- 23 Predicted carbonyl area (CA_b) at 1/3 of the mastic thickness across the asphalt layer depth after one year of field ageing simulation in two climate regions.

5.6 Validation of Parametric Analysis using Field Ageing Data

Extracted site cores data are collected from Soenen et al. (2020a, 2020b, 2021) and analysed to identify a potential link between air voids content and oxidation products content. Fourteen road sections with field ageing ranged from 8 to 21 years were considered (Soenen et al. 2020a, Soenen et al. 2020b, Soenen et al. 2021). The sections are located in various sites across Europe. **Figure 5-24** illustrates undergone process to obtain the average air voids and carbonyl functional groups. Binders from the surface course are recovered. This is conducted after cutting the cores into thin layers or slices. Typically, the top slice is 5 mm, and the lower slices are 1 cm thick. Depending on the wearing course thickness, the total number of slices varied between 2

and 5. The void percentage is measured using nuclear density device, and the average value for all layers is considered.

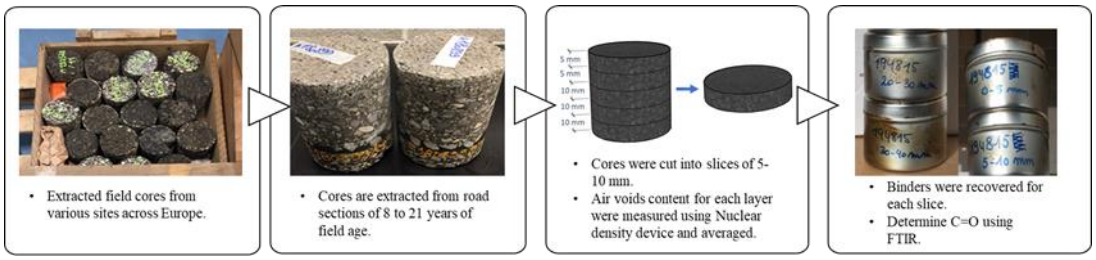

Figure 5- 24 Field cores extraction and binder recovery from aged asphalt pavements.

Figure 5-25 shows the carbonyl area content and the corresponding average AAV for all 14 field road sections. Generally, it is observed that top AC layers experience more ageing than that at deeper layers, validating the modelling results shown in **Figures 5-10, 5-11, 5-18, and 5-19** in this study. Some sections experienced a non-uniform C-shaped ageing profile, where mid-layers maintained low oxidative ageing, where others show a decreasing r-shaped ageing profile along pavement depth. This can be attributed to the presence of porous course or non-porous course (e.g., unbound or treated base) below the AC layer.

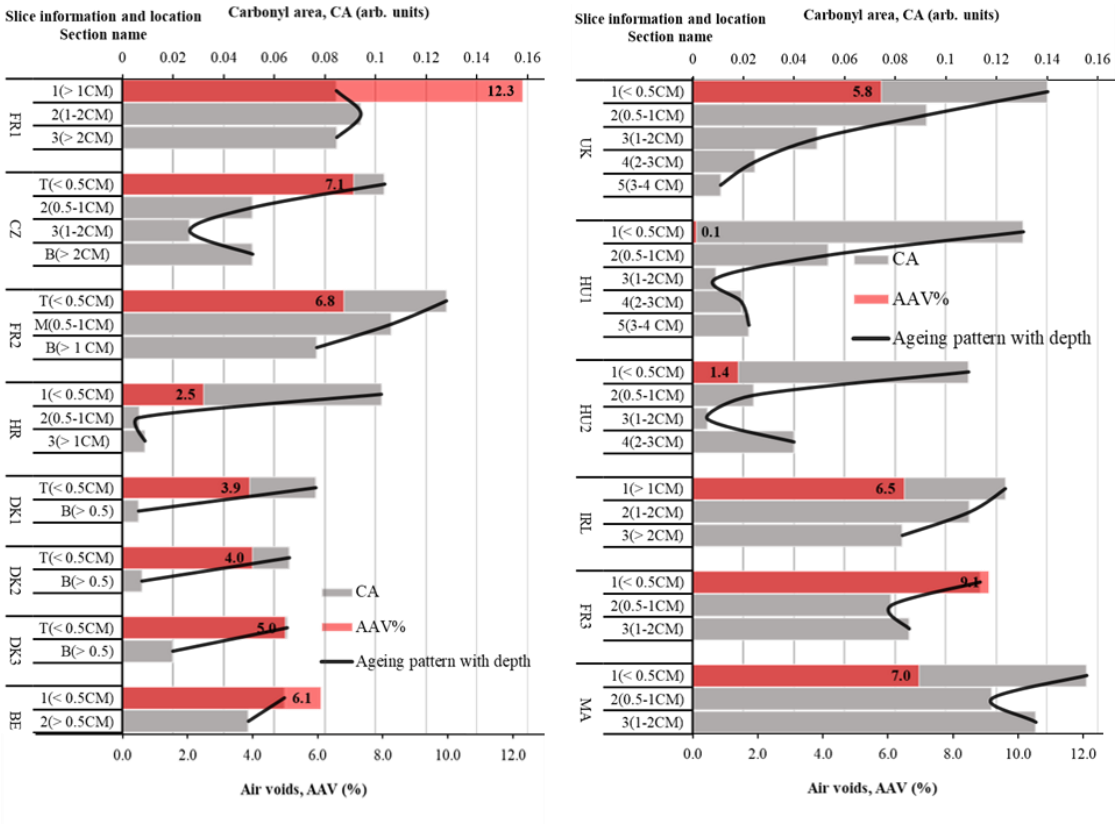

Figure 5- 25 Carbonyl area (CA) values and air voids contents of field cores for 14 road sections across Europe (the solid curves show the ageing pattern and CA profile along pavement depth).

Figure 5-26 shows the carbonyl area difference (ΔCA, determined using the carbonyl content at the top and bottom slices of the asphalt layer), against air voids content. A higher ΔCA indicates a greater gradient in the CA profile along pavement depth. A lower ΔCA means the ageing profile is close to uniform along depth. When the AAV < (5~6)%, there is severe ageing on the top surface but minimal ageing below the asphalt top surface; thus ΔCA is close to one. There is a gradually increasing ageing when the AAV is above this threshold (5~6%); thus ΔCA decreases and ranges from 0.6 to 0.2. When the AAV > (9~10)%, the ageing is severe, and uniform across the whole asphalt layer depth and ΔCA is close to zero. A noticeable decrease in ΔCA for AAV at (5~6)% exists, agreeing well with the model results from **Figures 5-18 and 5-19**.

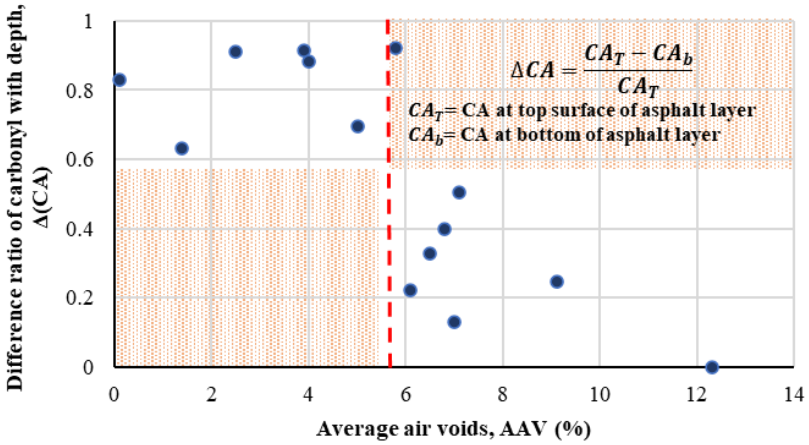

Figure 5- 26 Correlation between air voids (AAV) and carbonyl content difference between top and bottom of asphalt layer (ΔCA) for 14 European road sections

5.7 Summary of Parametric Analysis for Field Ageing

This parametric analysis study uses the Multiphysics modelling approach developed in **Chapter 3** for ageing simulation of asphalt pavements in the field to assess the effects of material properties on the ageing evolutions. The focused material properties include thermal properties

of asphalt, base and subgrade layers, air voids content and distribution in the asphalt layer, coating thickness of asphalt mastic, and oxygen accessibility of the base layers. The effect of climate region on ageing growth is also studied. The ageing evolutions were examined on the spatial and temporal distribution of the oxidative products (carbonyl area) in the asphalt pavement structures.

Results of altering the thermal properties show that increasing the thermal conductivity of asphalt layers lowers the surface temperature and increases the bottom temperature in the asphalt layer up to 5°C. Increasing the heat capacity of the asphalt layer generates slightly reduced daily temperature variations due to the greater heat storage capacity of the pavement. In comparison, the variations of the thermal properties of underlying layers (base and subgrade) cause little or no effects on the temperature profile and oxidative ageing amount and distribution in the asphalt layers.

Results of altering the pavement structure (base contents) show that asphalt layers built on unbound granular base (free access to oxygen at both top and bottom of the asphalt layer) will experience greater overall ageing with a C-shaped ageing gradient compared to that built on treated base (access to oxygen at the top but none at the bottom of the asphalt layer) which lead to a r-shaped ageing gradient along pavement depth.

The extent of oxidative ageing in asphalt mastics is also bound by the mastic film thickness surrounding accessible air channels (i.e., diffusion depth). The thicker the mastic coating film, the less the average carbonyl area will be, resulting in a potentially increased pavement resistance to cracking.

The air voids content and distribution plays a vital role in limiting oxidative ageing. A non-uniform (i.e., C-shaped) air voids distribution within the asphalt layer allows more oxygen access. It increases the oxidative ageing across the pavement depth, causing binder hardening and aged pavements prone to more fatigue damage. Additionally, Dense asphalt pavements with a low air voids content (<5%) experience little to no ageing, whereas asphalt pavements with air void content of 5-9% experience a growing oxidative ageing rate with an increasing air void

content. Pavements with high air voids (>9%) will have full access to oxygen from the atmosphere, thus the average carbonyl content is high and uniform across asphalt pavement depth with no clear C-shaped or r-shaped ageing gradient.

The climate region at which the road is constructed can significantly affect the oxidative ageing growth; for instance, differences in temperature within the same environmental region (e.g., wet, no-freeze) can still generate significant variation in field ageing performance. In addition, the temperature gradient and oxidation growth rate is more significant in hot regions, such as Texas than the cold regions, such as Washington. Thus, changing the climatic region *may* cause variations in thermal and oxidative damage degree and failure type.

Chapter 6 Ageing Mitigation using Anti-Ageing Compounds*

The effect of adding anti-ageing compounds (AACs) on the oxidative ageing of binders and asphalt pavements in the field to prevent or reduce ageing is investigated in three stages. The first stage, based on laboratory testing, aims to nominate potential effective AACs, and propose a measuring parameter to quantify the improvement in ageing reduction. In this stage, twenty different AACs are mixed with bitumen to fabricate thin film samples of AAC-modified bitumen and subject them to laboratory oven ageing at 100ºC for different ageing periods. Then, changes in the oxidation kinetics of bitumen upon the addition of various AACs are analysed using Fourier transformation infrared (FTIR) spectroscopy.

The second stage, based on detailed laboratory testing, investigates the effects of nominated AACs from the first stage on the mechanical performance of bitumen subjected to standard laboratory ageing conditions. The AAC-modified bitumen binders were tested by dynamic shear rheometer (DSR) and FTIR at different ageing conditions, including unaged, short-term ageing by thin film oven test (TFOT) and long-term ageing by pressure ageing vessel (PAV).

Based on the PDEs-based FE ageing modelling approach, the third stage investigates the scale at which the AACs reduce or prevent the oxidative ageing of asphalt pavements in the field under a complex environmental condition, including coupled temperature and oxygen distribution in the pavement structure. **Figure 6-1** shows the workflow of the three stages of ageing mitigation using AACs.

---

* Findings of this chapter are published in:

(1) Omairey, E. L., et al. (2019). "Impact of anti-ageing compounds on oxidation ageing kinetics of bitumen by infrared spectroscopy analysis." 223: 755-764. https://doi.org/10.1016/j.conbuildmat.2019.07.021

(2) Omairey, E. L., et al. (2020). "Rheological and fatigue characterisation of bitumen modified by anti-ageing compounds." 265: 120307. https://doi.org/10.1016/j.conbuildmat.2020.120307

Figure 6- 1 Workflow of ageing mitigation

6.1 Strategy of Developing Anti-Ageing Compounds

In this section, the effect of different anti-ageing compounds (AACs) on the oxidation kinetics of bitumen is investigated using Fourier transformation infrared (FTIR) spectroscopy.

6.1.1 Materials and testing methods

Bitumen of grade 40/100, according to BSEN14023:2010, was used as a base (control) binder, and its engineering specifications are listed in **Table 6-1**. Using one source/type of bitumen will withdraw binder-source effects when examining AAC related changes. Others have

used a similar approach to neglect the binder type variances on ageing kinetics (Yu et al. 2007, You et al. 2011, Yao et al. 2013, Liu et al. 2015).

Table 6- 1 Binder specifications.

Property	Value
Penetration @ 25°C (0.1 mm)	45-80
Softening point (°C)	≥45
Flash point (°C)	>250
Force ductility @ 5°C (J/cm^2)	>3

The selection of AACs is based on four aspects: (1) materials proven effective in previous studies but require further investigation, (2) polymer modifiers not tested for bitumen modification before, (3) multifunctional nanomaterials (i.e., materials in nanoscale size range in at least one dimension, that could potentially work as exfoliators/intercalators, hydroxyl groups providers, metal fillers, etc.), and (4) common AACs added for comparison. The selected AACs vary in their anti-oxidation functionality, structure and chemical behaviour to ensure the study covers a wide range of anti-ageing materials. The mixing ratio of AACs in the binder is based on two aspects, (1) availability of materials to be used in large quantities, and (2) previous findings and mixing recommendations. Some additives were tested at different concentrations to determine the best mixing ratio. A list of AACs and their concentrations are shown in **Table 6-2** and details of these additives are discussed in this section.

Table 6- 2 Anti-ageing compounds and concentrations.

Additive	Concentration of added additive (% by mass of bitumen binder)
Irganox acid	5, 10, 15
Tetramethylthiuram disulphide	1

Cloisite C20A	10
Bentonite HCT	10
Sodium montmorillonite	10, 15
TRIS (hydroxymethyl-aminomethane)	5, 10
Calcium hydroxide	10
(3:1:1) TRIS (hydroxymethyl-aminomethane): bentonite: calcium hydroxide	10
Irganox 1076	15
MD1024	0.1
(3:2) sodium montmorillonite: Irganox acid	25
(1:1) calcium hydroxide: TRIS (hydroxymethyl-aminomethane)	20
(4:3) furfural: DLTDP ((Dilauryl) Thiodipropionate)	3.5
Furfural	2
(1:5) furfural: Irganox 1076	12
Trimethylolpropane TMP	10

The compounds, Furfural (2-Furaldehyde) and (Dilauryl) Thiodipropionate (DLTDP) (didodecyl 3, 3'-thiopropionate) were added to the bitumen and tested for improvements in rheological properties by Apeagyei (2011). A percentage of 3.5% (4:3 furfural: DLTDP) achieved a 40% reduction in the ageing hardening when added to bitumen compared to the control binder. However, the chemical properties and ageing kinetics were not investigated (Apeagyei 2011).

No studies were found covering the usage of Irganox 1076 (Octadecyl-3-(3,5-di-tert. butyl-4-hydroxyphenyl)-propionate) for bitumen modification purposes. Irganox 1076 is a commercial polymer additive with low volatility, good resistance to extraction and thermo-oxidative degradation (i.e., the process of oxygen-containing groups formation that occurs under the comprehensive effects of light, heat and oxygen).

Two other types of Irganox additives are also included in this study, MD1024 and Irganox acid. MD 1024 (Benzenepropanoic acid, 3,5-bis(1,1-dimethylethyl)-4-hydroxy-, 2-[3-[3,5-bis(1,1-dimethylethyl)-4-hydroxyphenyl]-1-oxopropyl] hydrazide) is commonly used for protection against metals and minerals contamination at high temperatures. Irganox acid is a hindered phenol organic (3,5-di-tert-butyl-4-hydroxyphenylpropionic acid) that has been synthesized at Aston University Chemical Engineering laboratories and currently being tested as a polymer antioxidant.

Hydrated lime is commonly known for reducing the rate of age hardening of bitumen (Plancher et al. 1976, Dickinson 1984, Edler et al. 1985, Petersen 2009, Ameri et al. 2013). This reduction is attributed to the absorption of asphalt components by lime that would otherwise increase the asphalt sensitivity to the oxidation (Petersen 2009). The use of emulsifiers such as lime is a common practice, especially in cold recycled asphalt pavements (Gu et al. 2019). The end result of using lime emulsifier in pavements is hydrated lime. For this reason, it has been included as a potential AAC in this study.

Nanomaterials, such as Cloisite C20A, bentonite HCT and sodium montmorillonite are included in the testing program. Ghile (2006), Hassan et al. (2012), Yao et al. (2013), Kumar and Suman (2017), and Ortega et al. (2017) reported the beneficial effects of adding nanomaterials to bitumen, including the increase of bitumen's thermal stability, resistance against permanent deformations and strengthening of bitumen's bonding with rubber modifiers. These nanomaterials are also believed to reduce oxygen diffusion into the binder and halt or reduce ageing. However, there is debate on whether these improvements can justify their application in the field (Ghile 2006, Hassan et al. 2012, Yao et al. 2013, Kumar and Suman 2017, Ortega et al. 2017).

Other additives, such as Tetramethyl thiuram disulphide, TRIS, and trimethylolpropane, are also included. Tetramethyl thiuram disulphide is used as a polymerization initiator and accelerator in the rubber industry (Ferington and Tobolsky 1955). TRIS (hydroxymethyl-aminomethane), according to Wilkes and Davies (2010), is a dispersant for asphaltene inhibition of hydrocarbon fluids such as bitumen and crude oil (Wilkes and Davies 2010). Trimethylolpropane, a stable compound under different environmental and light exposure conditions, is included due to its ability to reduce the oxidation of trimethylolpropane esters based on a study conducted on palm oil palm kernel oils (Yunus et al. 2004).

AAC-modified bitumen samples were prepared by mixing the additives with 1-3 g of bitumen by solvent blending method, i.e., mother liquor melting, to achieve better dispersion of the AACs into bitumen and create a thin-film sample on the FTIR sodium chloride testing plates (Li et al. 2017). Dichloromethane was used as a solvent for its high bitumen dissolving ability at low temperature (i.e., room temperature), high evaporation rate and low viscosity (Lamontagne et al. 2001). Other solvents, such as kerosene, were also used by others due to its low cost and availability (Li et al. 2017).

Samples were prepared by mixing additives, bitumen and equal concentrations of dichloromethane by means of an ultrasonic shaker for at least 30 minutes to ensure complete dispersion at room temperature (20ºC).

Afterwards, thin-film samples (0.5 mm thick) are laid on newly-polished salt plates sitting in metallic frames to be scanned using FTIR. The solvent is left to evaporate in a nitrogen environment. Then, it is placed in a temperature-controlled oven at 100ºC for 10 minutes to ensure complete solvent evaporation (Yang et al. 2018).

Temperature-controlled oven, set at 100ºC under atmospheric air conditions (0.2 atm oxygen pressure), is used to age the thin-film specimens for extended periods up to 504 h. The isokinetic temperature of bitumen binders is recorded to be 100°C (Liu et al. 1996). At this temperature, the oxidation activation energies are independent of the binder source; therefore, the

oven-ageing temperature is set to be 100°C to eliminate the binder source effects. Additionally, at 100°C temperature, the bitumen suffers detectable but reasonable ageing at short ageing periods since the temperature lies within the pressurised ageing vessel (PAV) testing temperature range (90-110°C) (ASTM 2019)

FTIR spectroscopy tests are then carried out at different ageing periods of 0 (unaged), 12, 24, 48, 72, 96, 120, 144, 168, 336 and 504 h using a PerkinElmer spectrum 100 spectrometer. The device is set to scan in a range of 450-4000 cm^{-1}, with a scanning frequency of 32 and 4 cm^{-1} resolution. Background scans are made prior to scanning samples. The tests are run in duplicates to ensure repeatability of results, and the maximum percent of error obtained is found to be 11%.

6.1.2 Analysis of Fourier transformation infrared spectroscopy of anti-ageing compounds modified bitumen

Figure 6-2 shows the FTIR results for two replicates of unaged control bitumen samples. There is a considerable difference between the two replicates at the areas of carbonyl and sulfoxide functional groups (peaks 1700 cm^{-1} and 1031 cm^{-1}, respectively), even though they are prepared at identical conditions from the same binder source. This suggests that the areas between the two valleys (the range between 1820 to 1650 cm^{-1} and 1080 to 980 cm^{-1}, for carbonyl and sulfoxide, respectively) are not representative measures for oxidation. This variation between replicates is attributed to the differences in sample film thickness, causing divergence in absorption percentages; another reason can be the heterogeneity nature of the bitumen.

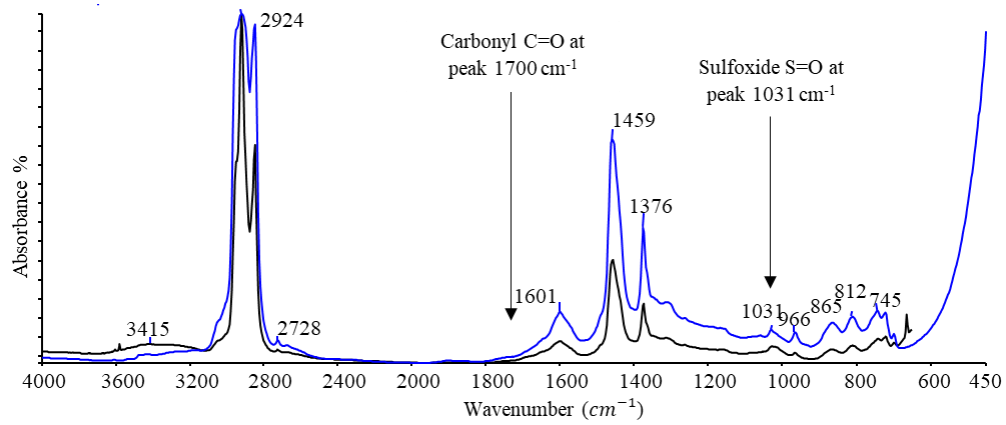

Figure 6- 2 FTIR spectrum of control bitumen samples (no additives) at a wave range of 450-4000 cm^{-1}.

Figure 6-3 shows the FTIR spectrum for the control bitumen sample after different oven ageing periods. There are no peaks in the carbonyl range (1820 to 1650 cm^{-1}) for the unaged bitumen. This suggests that considering a constant range (1820 to 1650 cm^{-1}) for CA can cause measuring errors or originate negative values of CA. Thus, in this study, each absorption curve is examined individually to set appropriate ranges for both CA and SA by connecting the left valley's bottom of the peak to the right valley's bottom.

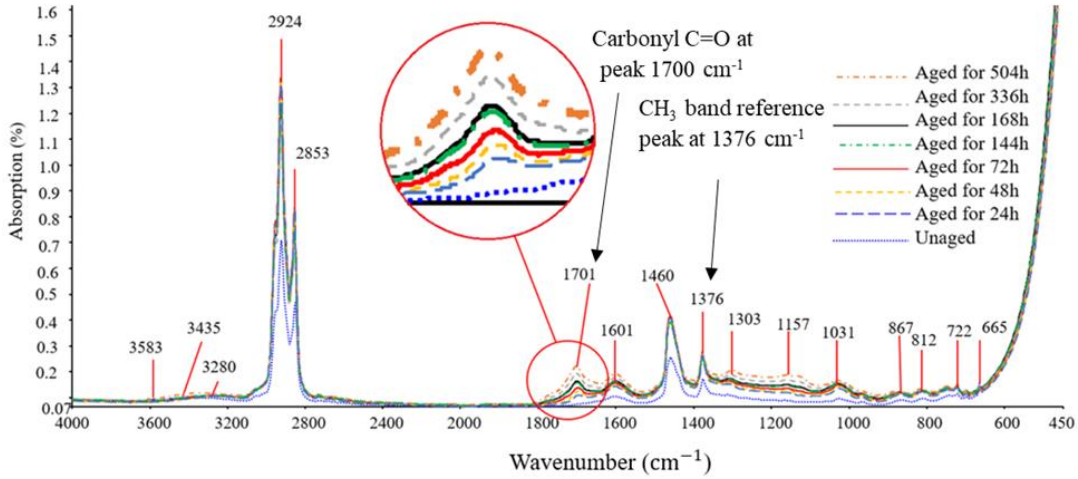

Figure 6- 3 FTIR spectrum of control bitumen sample (no additives) for different age periods, at a wavelength range of 450- 4000 cm^{-1}.

A reference peak that maintains its area unchanged during ageing must be selected to eliminate the sample film thickness effects from the ageing parameters (CA and SA). One potential reference peak is that at wavelength 2924 cm^{-1}, with shoulders at 2853 and 2953 cm^{-1} that belongs to the alkyl C-H functional group. Although it was selected previously as a reference peak (Zhao et al. 2010), it can cause inaccuracy due to its high absorption compared to CA. Another potential reference is peak 1601 cm^{-1}; however, it can also cause inaccuracy in calculating the ageing index because it shares a shoulder with the carbonyl. Other recognisable peaks are 1460 cm^{-1}, 1377 cm^{-1} and 813 cm^{-1} representing CH_2 alkanes, CH_3 alkanes, and

aromatics. The carbonyl index (CI) is measured using **Equation 6-1** for these three different peaks and shown in **Figure 6-4** for the control bitumen samples.

$$CI = \frac{CA}{Area\ under\ reference\ peak} \tag{6-1}$$

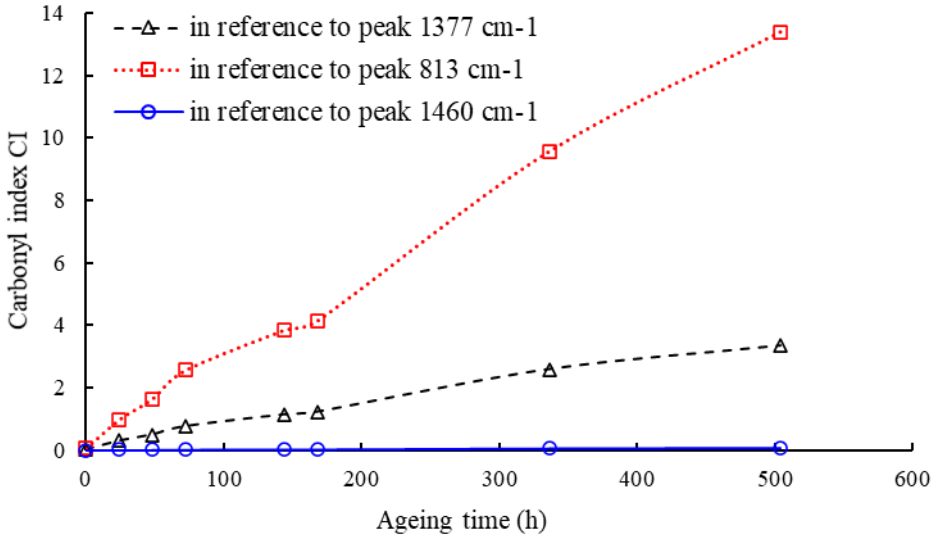

Figure 6- 4 Carbonyl ageing index for control bitumen at different ageing periods measured for different reference peaks.

Peak 1377 cm^{-1} is selected as the reference peak due to its relatively compatible wave height compared to the carbonyl peak, causing less measurement error. More importantly, it maintained a consistently stable condition when bitumen was mixed with other additives. On the other hand, 1460 cm^{-1} peak seemed to be less stable during the initial ageing period, particularly with additives containing aromatics, such as Irganox acid, Irganox 1076, MD1024 and calcium hydroxide. Finally, 813 cm^{-1} peaks may interfere with the polymer modifiers functional groups, thus was not selected.

Similar to the carbonyl index, the sulfoxide index (SI) ageing growth is also observed. SI is the ratio of area under peak 1031 cm^{-1} to the area under the reference peak for the same ageing period (shown in **Equation 6-2**). **Figure 6-5** shows that SI of the control bitumen maintained the same CI pattern (**Figure 6-4**) at different reference peaks, but unlike the carbonyl, sulfoxide's growth rate started to decline after 24 hours of ageing at 100ºC.

$$SI = \frac{SA}{Area\ under\ reference\ peak} \quad (6\text{-}2)$$

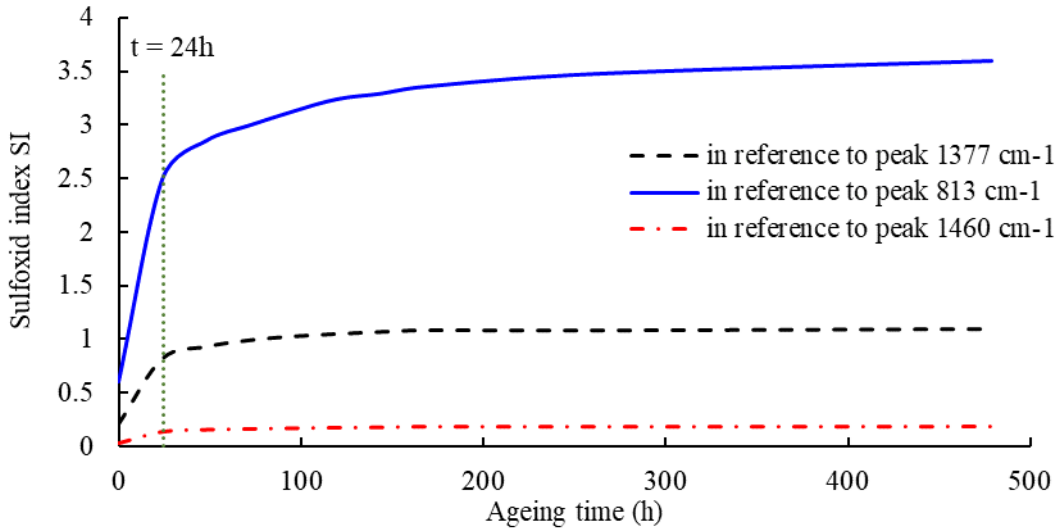

Figure 6- 5 Sulfoxide index at different ageing periods for the control bitumen without additives, measured for different reference peaks.

Figure 6-6 shows the carbonyl and sulfoxide indices (CI and SI) of the control bitumen sample (no additives) versus the oven ageing time. Carbonyl and sulfoxide indices are measured as the CA and SA ratio to a reference peak 1377 cm^{-1}. Gradual growth in the carbonyl index along the ageing period is observed in **Figure 6-6**, in contrast to the sulfoxide index, which stabilised with time after an initial sudden shift at the first 24 hours of ageing. This behaviour agrees with Zhao et al. (2010) and Ma et al. (2012) findings, where they used the Rolling Thin Film Oven (RTFO) ageing test to characterise the ageing properties of SBS polymer modified bitumen (Zhao et al. 2010, Ma et al. 2012).

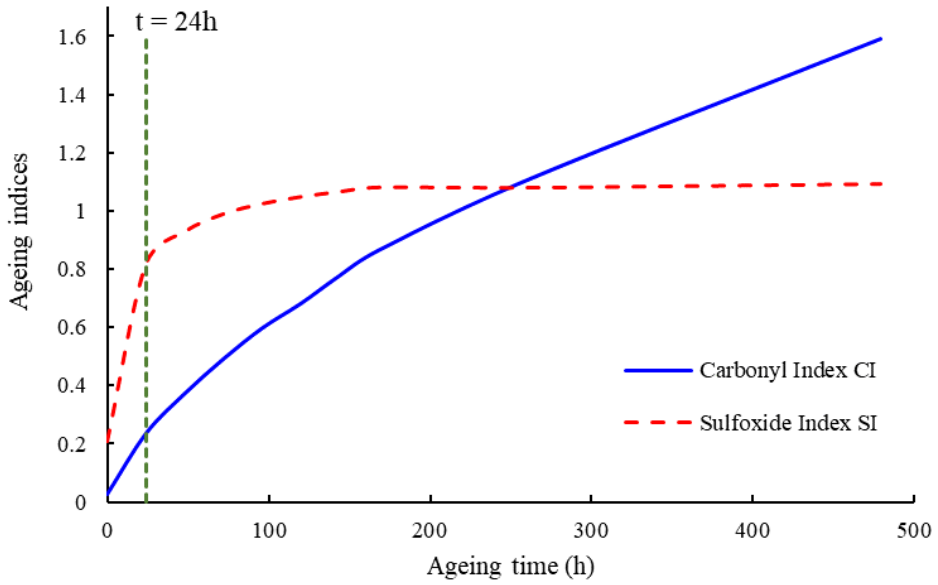

Figure 6- 6 Carbonyl and sulfoxide indices of control bitumen sample (no additives) measured with respect to the reference peak 1377 cm^{-1} versus the oven ageing time.

The initial values of CI prior to oven ageing (shown in **Figure 6-4**) are approximately zero due to the lack of carbonyl functional groups in the virgin bitumen. However, this is not necessarily the case for different bitumen sources. It is also very common to encounter carbonyl and sulfoxide in the virgin bitumen due to the ageing in the early processing, refining, and mixing operations (Zafari et al. 2014). Therefore, CI and SI plotted against ageing time to compare the ageing growth rate of different binders may not be practical. Likewise, CI plotted against ageing time for the AAC-modified bitumen cannot be utilised as an AAC selection criterion due to the inherent existence of the carbonyl functional group in these compounds**. Figure 6-7** shows CI for the AAC-modified and unmodified bitumen versus ageing time for a 100ºC oven ageing temperature. It is clear that the CI values have different initial values and can decrease when AAC-modified bitumen ages. Thus, CI cannot be directly used for comparing the AAC-modified bitumen in terms of its anti-ageing performance.

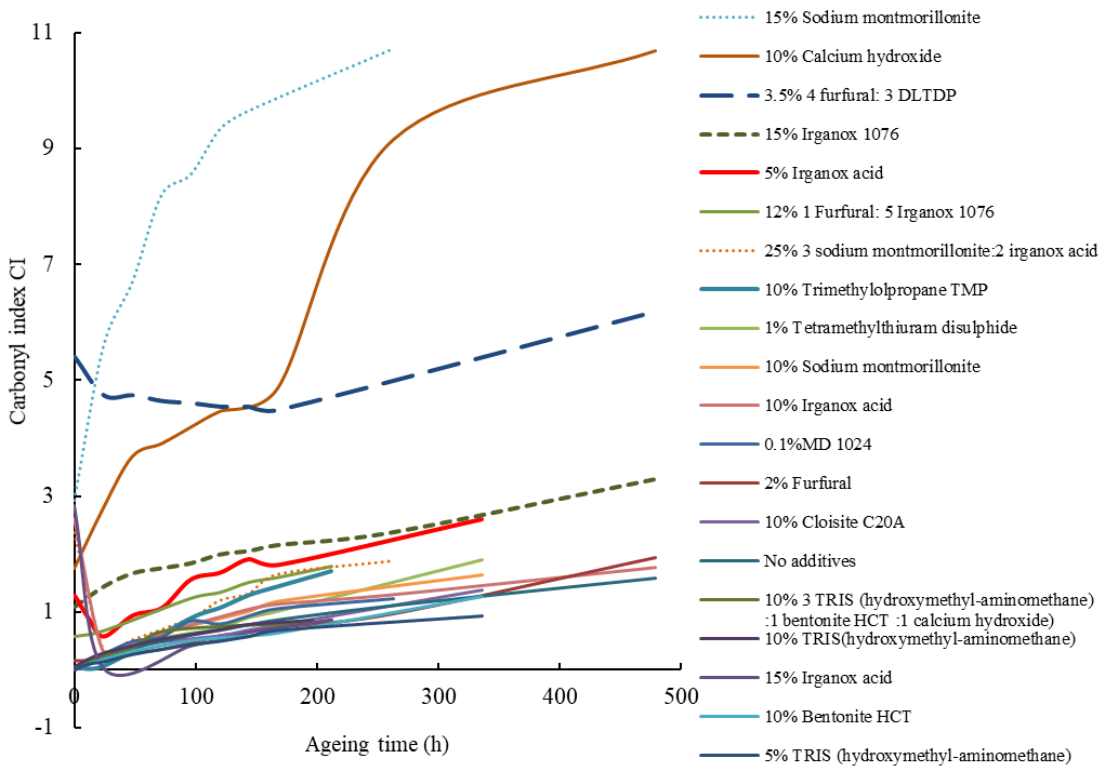

Figure 6- 7 Carbonyl index against oven ageing time at 100ºC for AAC-modified and unmodified (control) samples measured for a reference peak of 1377 cm^{-1}.

To overcome the drift at the initial values of the CI, another term was adopted to compare the efficiency of AACs, called the Normalised Carbonyl Index (NCI), explained as the ratio of the difference between carbonyl index at any ageing time (CI_t) and that before ageing CI_o to the carbonyl index at time zero (CI_o), as shown in **Equation 6-3**.

$$NCI = \frac{CI_t - CI_o}{CI_o} \tag{6-3}$$

Thus, NCI will start from zero before ageing, regardless of the bitumen's chemical composition and its containing additives. **Figure 6-8** shows the change in NCI with ageing time. NCI can drop with ageing to become a negative value for some of the AAC-modified bitumen specimens that contained carbonyl in their chemical composition. During ageing, this carbonyl decrease led to a drop in NCI, causing negative values, as shown in **Figure 6-8**.

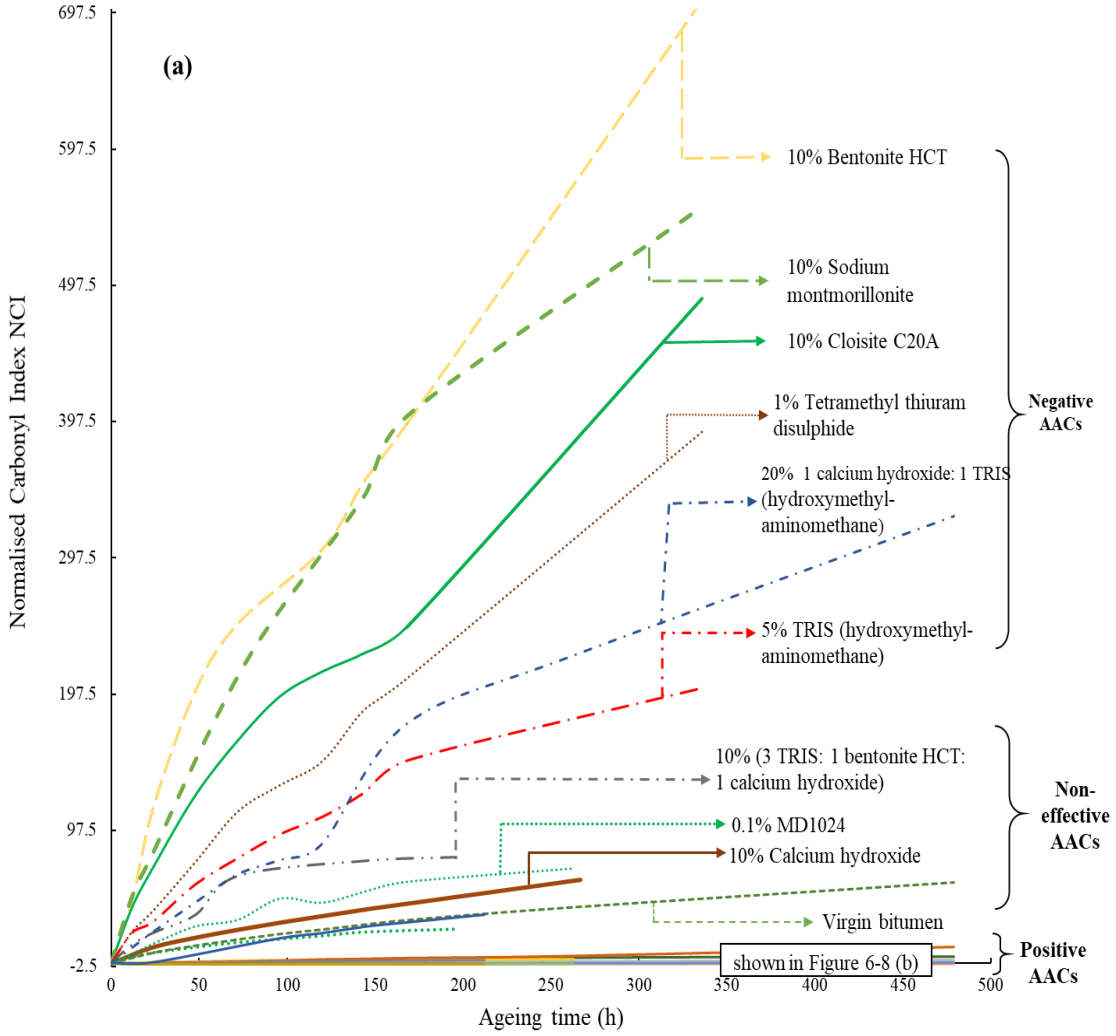
(a)
Normalised Carbonyl Index NCI
697.5
597.5
497.5
397.5
297.5
197.5
97.5
-2.5
0
50
100
150
200
250
300
350
400
450
500
Ageing time (h)
10% Bentonite HCT
10% Sodium montmorillonite
10% Cloisite C20A
1% Tetramethyl thiuram disulphide
20% 1 calcium hydroxide: 1 TRIS (hydroxymethyl-aminomethane)
5% TRIS (hydroxymethyl-aminomethane)
Negative AACs
10% (3 TRIS: 1 bentonite HCT: 1 calcium hydroxide)
0.1% MD1024
10% Calcium hydroxide
Virgin bitumen
Non-effective AACs
shown in Figure 6-8 (b)
Positive AACs

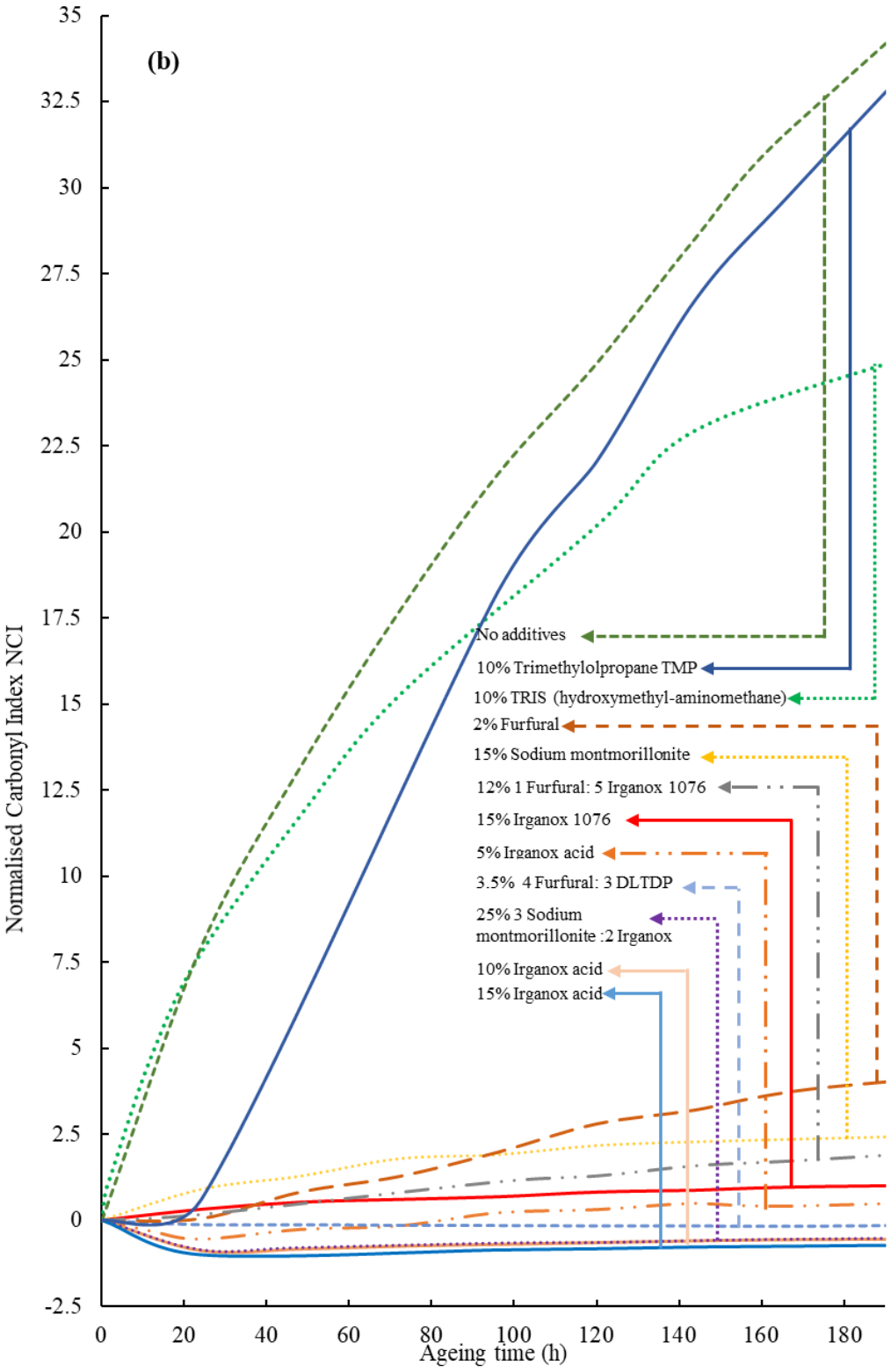

Figure 6- 8 Normalised carbonyl index with ageing time at 100ºC ageing temperature for AAC-modified and unmodified (control) bitumen samples measured for reference peak of 1377 cm^{-1} (a) all samples, (b) bitumen samples with positive anti-ageing AACs.

Figure 6-8 (a and b) shows the NCI against ageing time for all samples, according to these results, AACs are divided into three categories in terms of their anti-ageing effectiveness: (1) negative AACs, work to accelerate the ageing of bitumen, (2) non-effective AACs that did not alter the ageing of bitumen significantly, and (3) positive AACs, inhibit the formation of carbonyl and reduce bitumen ageing.

Negative additives include sodium montmorillonite, low concentrations of TRIS and the combination of TRIS with nanomaterials and calcium hydroxide. Generally, all the tested nanomaterials did not experience any positive impacts in inhibiting the carbonyl formation upon ageing. This may be attributed to the nature of samples preparation and testing because the bitumen samples were thin-film slides and assumed to be completely exposed to air oxidation. Therefore, the nanomaterials added to the bitumen will introduce no resistance to the oxygen diffusion in the bitumen sample. Thus, additives that work towards reducing diffusion will have no effect in such thin film sample, and further testing is needed for the anti-ageing mechanism of the nanomaterials on the bitumen (covered in **Section 6.2**)

Non-effective additives of no contribution to ageing resistance include TMP, calcium hydroxide and 10% concentration of TRIS. The bitumen modified with those additives shows similar NCI growth to that of the control virgin bitumen. However, increasing TRIS concentration in the binder from 5 to 10% led to a minor decrease in ageing progression.

Positive additives that proved effective in reducing bitumen's ageing include Irganox 1076, furfural, DLTDP with furfural combination, and 10 and 15% of Irganox acid, shown as the overlapped curves at the bottom of **Figure 6-8 (a)**, and shown separately in **Figure 6-8 (b)**. The bitumen modified by those additives have shown a significant reduction in the growth of the NCI compared to that of the control bitumen.

6.1.3 Ageing kinetics analysis of anti-ageing compounds-modified bitumen

It can be observed from the ageing pattern of the control sample, the carbonyl formation is time-dependent throughout the entire ageing period, suggesting the binder is still in the fast-

term ageing stage. Therefore, **Equation 6-4** is formulated by replacing CA with NCI to model the fast-term ageing of the bitumen modified with the AACs.

$$\frac{dNCI}{dt} = Mk_f e^{-k_f t} \tag{6-4}$$

$$k_f = A_f P^{\alpha} e^{-\frac{E_f}{RT}} \tag{6-5}$$

where, M is the limiting amount of the carbonyl formation due to the first-order reaction following the hot mix production; A_f is frequency factor for fast-term ageing, it is bitumen-type dependent, measured by (1/day) units; P is the partial pressure of oxygen (0.2 atm under current oven ageing settings); α is the reaction order due to oxygen partial pressure; E_f is the oxidation activation energy; T is the absolute temperature measured in K; t is ageing time (days); R is the universal gas constant which equals 8.314 J/K/mol and k_f is a reaction constant which depends on the pressure and temperature.

Equation 6-5 can be simplified using A'_f (an earlier approach for modelling oxidation (Lau et al. 1992)), where,

$$A'_f = A_f P^{\alpha} \tag{6-6}$$

Jin (2012) correlated the fast-term frequency factor and activation energy (Jin 2012), such that;

$$A'_f = 2.031 e^{0.3076 E_f} \tag{6-7}$$

Substituting **Equation 6-7** into **Equation 6-5** gives

$$k_f = 2.031\, e^{0.3076 E_f}\ e^{-\frac{E_f}{RT}} \tag{6-8}$$

Equation 6-8 is used along with **Equation 6-4** to determine the rate of NCI. By curve-fitting the testing data into **Equation 6-9**, k_f and M are obtained. Then E_f is determined using **Equation 6-8.**

$$NCI = M(a - e^{-k_f t}) \tag{6-9}$$

where *a* equal 1±0.02, is the initial error resulting from the curve fitting process, and *M* value is a binder source-related parameter. Since one type of bitumen is used in this study, therefore the variations in *M* and k_f values are a result of AACs inclusion.

Table 6-3 shows the oxidation kinetics parameters obtained with R^2 of more than 0.95 for all samples, excluding bitumen sample with 2% furfural and 1.2% DLTDP (which achieved R^2 of 0.77) due to its low oxidation rate. The samples 10% and 15% of Irganox acid-modified bitumen did not show any signs of oxidation initiation; thus, they did not fit into the Arrhenius model for fast-term ageing (**Equation 6-8**). On the contrary, the carbonyl amount characterised by NCI remained unchanged along the entire ageing period, indicating an excellent anti-ageing performance of the AACs.

Table 6- 3 Oxidation kinetics model coefficients for all tested AAC modified bitumen samples.

AAC modified bitumen samples	k_f (1/day)	E_f (kJ/mol)	R^2	Effectiveness of the AACs
10% Trimethylolpropane TMP	0.980	49	0.9888	Negative AACs (increase the ageing of virgin bitumen)
10% (3:1:1) TRIS (hydroxymethyl-aminomethane): bentonite HCT: calcium hydroxide	0.351	119	0.9830	
15% Sodium montmorillonite	0.336	122	0.9940	

10% TRIS (hydroxymethyl-aminomethane)	0.286	133	0.9953	
5% Irganox acid	0.154	175	0.9761	
10% Sodium montmorillonite	0.124	190	0.9988	
5% TRIS (hydroxymethyl-aminomethane)	0.116	194	0.9961	
10% Calcium hydroxide	0.088	213	0.9453	Non-effective AACs (not alter the ageing of virgin bitumen)
Virgin bitumen with no additives (control)	0.076	222	0.9962	
12%(1:5) furfural: Irganox 1076	0.075	223	0.9953	
20% (1:1) calcium hydroxide: TRIS (hydroxymethyl-aminomethane)	0.049	253	0.9839	
10% Cloisite C20A	0.046	257	0.9833	
15% Irganox 1076	0.045	258	0.9710	
0.1% MD 1024	0.033	278	0.9703	
10% Bentonite HCT	0.031	283	0.9803	
1% Tetramethylthiuram disulphide	0.023	305	0.9972	Positive AACs (reduce
2% Furfural	0.001	567	0.9914	

25% 3:2) sodium montmorillonite: Irganox acid	0.001	596	0.9653	the ageing of virgin bitumen)
3.5% (4:3) furfural: DLTDP	0.001	664	0.7672*	
10% Irganox acid*	--	--	--	
15% Irganox acid*	--	--	--	

*****No notable oxidation was observed for those AACs modified bitumen samples, indicating excellent anti-ageing performance.

Samples in **Table 6-3** are arranged according to their fast-term activation energy in ascending order. Samples of small activation energies tend to have fast oxidation, while those with greater oxidation energies are expected to have better anti-ageing performance; thus, they develop fewer carbonyl compounds under the accelerated ageing conditions. Samples such as 10% and 15% Irganox acid that performed superiorly compared to others did not fit into the kinetics equation. They show no signs of ageing under 100ºC oven temperature conditions for a thin-film binder in ambient atmospheric pressure. It is, therefore, recommended to use activation energy to group the AACs in terms of their effectiveness in anti-ageing performance.

There was a great variation in *M* values for the tested specimens attributed to the existence of carbonyl and varying chemical composition of the AACs. **Figure 6-9 a** and **b** shows the chemical composition of Irganox acid and DLTDP. A well-defined peak for the carbonyl functional groups can be observed at the range 1710 to 1737 cm^{-1}. These AAC-induced carbonyl functional groups led to the negative values on the initial portion of the NCI versus ageing time curves, especially during the ageing period of less than one day (t =1 day). This time portion was neglected in the curve-fitting process since it makes nonsense to fit the negative NCI values to the suggested ageing kinetics model in **Equation 6-8**. Therefore, *M* values cannot be used as an

ageing indicator for the screening purposes of variable AAC additives to evaluate the anti-ageing performance of the AAC modified bitumen.

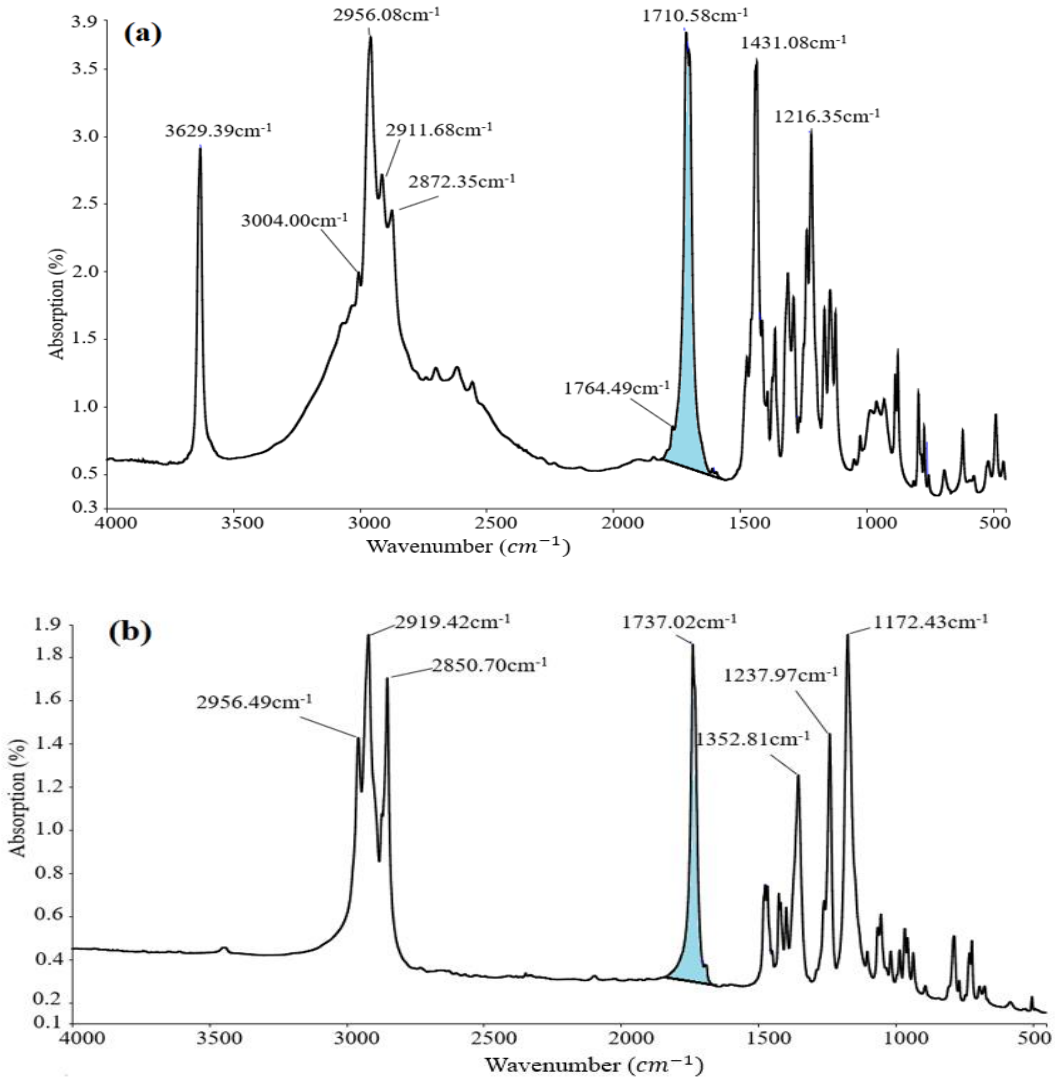

Figure 6- 9 FTIR spectrum for (a) Irganox acid and (b) DLTDP at a waves range of 450-4000 cm^{-1}.

6.2 Experimental Validation for Proposed Anti-Ageing Compounds

Following the initial screening of AACs in **Section 6.1**, a detailed performance evaluation of AAC-modified bitumen at the long-term ageing conditions is addressed in this section.

The AAC-modified bitumen binders that proven effective in **Section 6.1** were tested by dynamic shear rheometer (DSR) and Fourier transform infrared spectroscopy test (FTIR) at different ageing conditions, including unaged, short-term ageing by thin film oven test (TFOT)

and long-term ageing by pressure ageing vessel (PAV). Because fatigue failure is commonly encountered in aged pavements, it was evaluated and characterised for the AAC-modified bitumen. The fatigue performance of the AAC-modified bitumen was thus characterised by the dissipated energy ratio (DER), SHRP fatigue parameter, and the DSR-cracking (DSR-C) approaches, discussed in **Section 2.8**.

The study also examines the high-temperature performance and the thermal stability of nominated AAC-modified bitumen to cover more aspects concerning the effects of AACs on bitumen. Differential scanning calorimetry (DSC) test was employed to examine the oxidation onset temperature (OOT) of the AAC-modified bitumen, and the multiple stress creep and recovery (MSCR) test was utilised to measure the rutting susceptibility of AAC-modified bitumen at high temperatures.

6.2.1 Materials preparation

A control bitumen with a standard penetration grade of 60 was used as a base (control) sample. **Table 6-4** lists the standard engineering specifications of the binder.

Table 6- 4 Binder specifications.

Test index	Value
Penetration (15ºC) 0.1 mm	24.6
Penetration (25ºC) 0.1 mm	60.7
Penetration (30ºC) 0.1mm	106.27
Softening point ºC	48.6
Ductility (5ºC) cm	5.7
Ductility (15ºC) cm	>150
Viscosity (135ºC) Pa.s	0.4363

The AACs selection criteria were based on a preliminary AAC screening method, discussed in **Section 6-1**. A list of the selected AACs and their concentrations are summarised in

Table 6-5. The specimens identification numbers listed in **Table 6-5** will be used to refer to the samples in this study.

Table 6- 5 Anti-ageing compounds and concentrations in modified bitumen.

Specimen ID	Additive	Additive concentration (% by mass of bitumen binder)
1	Control bitumen	N/A
2	Trimethylolpropane TMP	10
3	Furfural	2
4	Sodium montmorillonite	15
5	(1:5) Furfural: Irganox 1076	12
6	Irganox 1076	15
7	(3:4) DLTDP ((Dilauryl) Thiodipropionate): furfural	3.5

The bitumen and AACs were blended using a high-speed shear mixer (FLUKO FM300) at a rotation speed of 4000 rpm for 90 minutes under controlled temperature conditions to ensure full dispersion of the additives. The temperature was kept in a 120-150°C range during the mixing process to prevent excessive ageing. The control bitumen sample (without additives) was subjected to the same mixing process to ensure that all samples experience identical mixing and ageing conditions. Following mixing, part of the binder-AAC mixture was stored in air-tight containers to be tested under unaged conditions. The remaining specimens were cast into flat containers to be subjected to short-term ageing (ST) and long-term ageing (LT) conditions using Thin Film Oven test (TFOT, ASTM standard D1754-97) and Pressurised Ageing Vessel test (PAV, ASTM standard D6521-18), respectively (ASTM 2002, 2019)

6.2.2 Dynamic shear rheometer (DSR) tests

The dynamic shear rheometer (DSR) is used to determine the rheological properties of asphalt binder using Malvern Instruments Kinexus device. Bitumen samples are heated to 130°C and poured into 8 mm diameter moulds (2 mm vertical gap) or 25 mm diameter moulds (1 mm vertical gap). The samples are prepared using silicone moulds. The hot bitumen from a heated container is poured into the mould to form a convex surface, and then the filled mould is cooled to room temperature without chilling. Then, the bitumen is loosened from the mould by flexing the rubber mould and is adhered to the preheated lower test plate by gently pressing the convex (top) surface of the pellet. After that, the upper test plate is moved until the gap between the plates equals the testing gap, plus the gap closure required to create a slight bulge at the outside face of the test specimen. The excess bitumen is trimmed by moving a heated trimming tool around the edges of the plates to level the bitumen with the outer diameter of the plates. When the trimming is complete, the gap is decreased to the testing value. Finally, the bitumen is heated to the testing temperature and then remained for 5 min before loading (Zhang et al. 2019).

A series of DSR tests were conducted on unaged and LT-aged bitumen samples. **Table 6-6** shows the testing schemes used in this study. The tests were run in duplicates, and in case of inconsistent results for the repeats, they were run in triplicates.

Table 6- 6 Dynamic shear rheometer (DSR) testing schemes.

Test*	Temperature (°C)	Frequency (Hz)	Strain level	Number of cycles
LAS	20 64	10	0.1%-15%	N/A
TS	20	10	5%	24000
HT-PG	Standard test (AASHTO T 315)			
MSCR	64	Standard test (AASHTO T 350)		

*LAS = linear amplitude sweep test; TS = time sweep test; HT-PG = high temperature Performance Grading test; MSCR = multiple stress creep and recovery test

6.2.2.1 Linear amplitude sweep test

The Linear Amplitude Sweep (LAS) strain-controlled tests were conducted at an intermediate temperature of 20°C with 10 Hz frequency and 0.1% - 15% strain values. The initial shear complex moduli (G_o^*) and phase angles (δ_o) were obtained at undamaged condition (where the shear moduli and phase angles remain unchanged with low strain levels). To investigate the high-temperature performance due to AACs modification, LAS tests at high temperature (64°C) are conducted solely for bitumen samples that demonstrate good fatigue cracking behaviour. The same testing parameters (i.e., load frequency and strain level) used in LAS tests at 20°C temperature were employed for high-temperature tests.

The initial phase angles δ_o and shear moduli G_o^* at undamaged condition are obtained using LSA test, where the shear modulus and phase angle remain unchanged at relatively low strain levels (e.g., <1%), as shown in **Figure 6-10**.

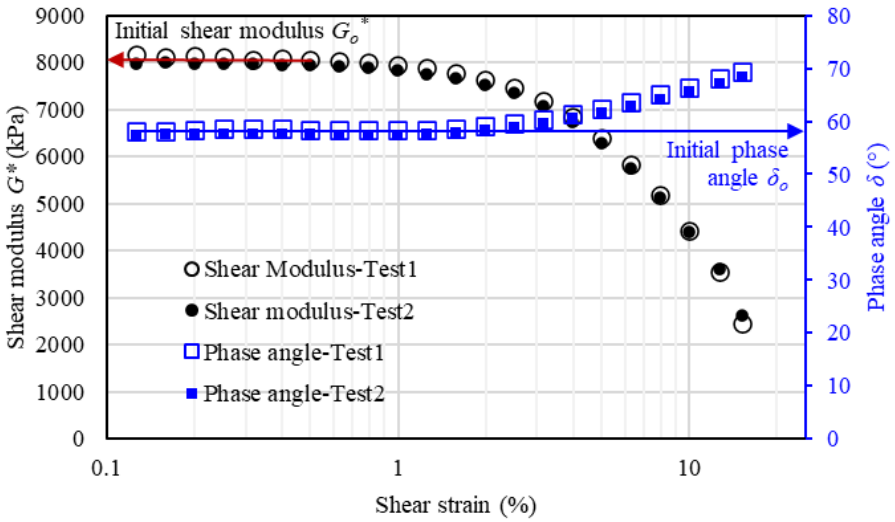

Figure 6- 10 Linear amplitude sweep (LAS) test results with the shear modulus G_o^* and phase angle δ_o of the unaged bitumen with 10% TMP (sample 2) under a strain level of 0.1 %- 15%. The test is conducted at 20°C temperature and loading frequency of 10 Hz for two replicates.

The tests are performed at different ageing conditions (unaged, ST-aged by TFOT and LT-aged by PAV). The initial shear modulus (at undamaged conditions) varied significantly due to AACs inclusion, as can be seen in **Figure 6-11**. Compared with the control sample (sample 1), samples 2, 3 and 4 caused an increase in stiffness at ST-ageing and LT-ageing conditions. In contrast, samples 5 and 6, containing Irganox 1076 as a main anti-ageing compound, shown a considerable decrease in stiffness at all ageing stages. Sample 7, containing 3.5% DLTDP: furfural (3: 4), maintained the same complex modulus as in the control sample (sample 1) after the ageing conditioning. The combination of furfural and DLTDP works as primary and secondary anti-oxidants, where furfural works as a free-radical scavenger and DLTDP as a peroxide inhibitor, prevents oxidation. Furfural is a liquid with low viscosity and DLTDP is a material of low melting point (39-42°C), thus, explaining the slight reduction in the initial shear modulus and increase in phase angle for sample 7.

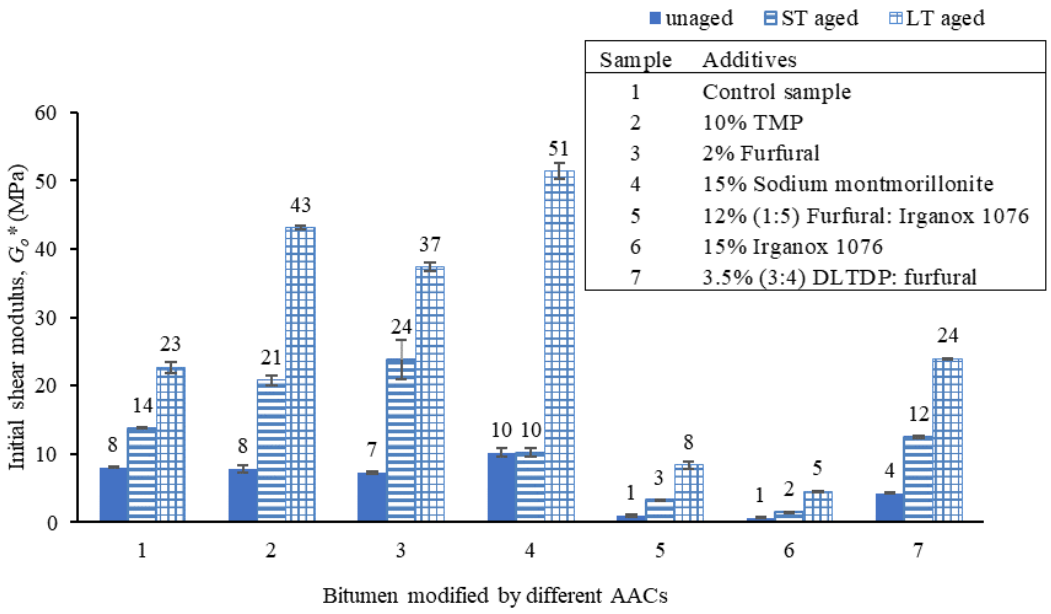

Figure 6- 11 Initial shear moduli G_o^* measured using the linear amplitude sweep (LAS) test. The test is conducted on unaged, short-term (ST, by TFOT) aged and long-term (LT, by PAV) aged bitumen samples modified by different AACs at a temperature of 20°C and loading frequency of 10 Hz.

The initial phase angles (shown in **Figure 6-12**) demonstrated negligible changes upon the inclusion of AACs, excluding samples 5 and 6 (containing Irganox 1076), which experienced increases in phase angles.

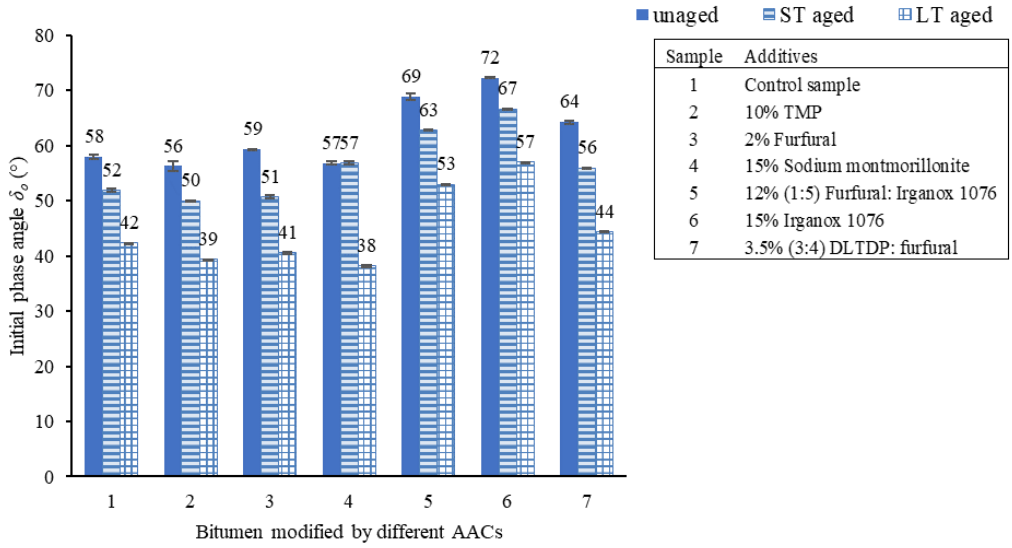

Figure 6- 12 Initial phase angles δ_o measured using the linear amplitude sweep (LAS) test. The test is conducted on unaged, short-term (ST, by TFOT) aged and long-term (LT, by PAV) aged bitumen samples modified by different AACs at a temperature of 20°C and the loading frequency of 10 Hz.

The oxidation ageing occurs when oxygen removes hydrogen atoms from carbon atoms, thereby causing a rise in the proportion of asphaltenes and a reduction in the content of resins and most of the aromatic compounds in the bitumen (Tauste et al. 2018). Irganox 1076 is hindered phenol organic ester anti-oxidant, works as a primary anti-oxidant and prevents thermal oxidation by donating hydrogen atoms for the free radicals that cause oxidation (Dessouky et al. 2015, Tauste et al. 2018). Irganox 1076 has a low molecular weight of approximately 531 g/mol and low melting temperature (50-55°C). The low molecular weight is similar to that for the dispersing medium (aromatics) and the non-polar viscous oil (saturates) in the bitumen (300-800 g/mol). Therefore, Irganox 1076 can reduce the viscosity for modified bitumen, leading to a significantly reduced modulus and increased phase angle, as shown in **Figures 6-11** and **6-12**. Based on these results, one may deduce that modified bitumen with Irganox 1076 alone may not be a suitable

anti-ageing additive with satisfying engineering performance. However, it can be feasible to use Irganox 1076 in combination with high-surface-area fillers, such as nano-silica (which can improve the rutting resistance and reduce susceptibility to oxidation by interacting with the polar aromatics and asphaltenes (Tauste et al. 2018)).

One of the common problems encountered with AACs is that they can perish with time due to ageing and exposure to environmental conditions. It is noted from **Figures 6-11** and **6-12** that the long-term aged AAC-modified bitumen samples maintained a different behaviour than that for the long-term aged control sample, suggesting the additives still affect the material behaviour even after exposure to long-term ageing. This behaviour indirectly indicates good stability for these anti-ageing compounds, although chemical tests are needed to confirm this theory.

6.2.2.2 Time sweep fatigue test

The time sweep (TS) test is a strain-controlled fatigue test utilised to determine the complex shear moduli (G^*) and phase angle (δ) at damaged condition (at 24,000 loading cycle) to evaluate the fatigue performance of the modified binders. The tests are conducted at an intermediate temperature of 20°C for 10 Hz frequency and 5% strain level and up to 24,000 cycles (40 minutes). The plate used in this test is 8 mm in diameter (2 mm vertical gap). The high strain (5%) was selected as the strain level at which virgin bitumen and AAC-modified bitumen demonstrate significant damage, as indicated by the decreased modulus and increased phase angle from LAS test results.

The image analysis method (IAM) is used to measure the fatigue cracking extent (crack length) at the end of the TS test. When the DSR completes 24,000 loading cycles, loading is stopped, and the temperature is set to cool down automatically to 3 °C to prevent the sample from melting and therefore preserve cracks morphology and geometry. The sample is then pulled apart axially by separating the top-loading plate from the bottom plate, and the cracking pattern on the bitumen sample is photographed. **Figure 6-13** displays the cross-section of a damaged bitumen sample. The effective and original radiuses of samples are measured, where the effective radius

(r_E) is the radius of remained uncracked area at the centre of the sample. The effective radius is measured about the original radius (r_o); the latter represents the radius of DSR sample at undamaged condition (4 mm standard radius). Then the crack length is measured as ($c_p = r_0 - r_E$). Detailed steps to determine the crack length are reported in the literature (Zhang and Gao 2021). The measured crack length is employed to validate predicted crack length by DSR-C model in **Equation 2-19**.

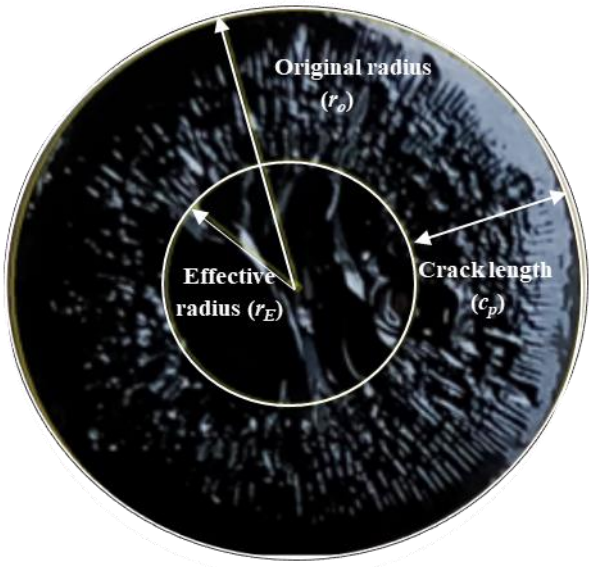

Figure 6- 13 Crack morphology of bitumen under shear fatigue loading. The effective radius calculated by the image analysis method.

The reason for selecting loading cycles (n) to be 24,000 cycles is to verify the cracking damage magnitude obtained by the IAM. If the loading cycle at failure (N_f at which the DSR versus the loading cycle curve becomes nonlinear) was utilised to measure the crack length, it would not be possible to inspect the actual damage at that point (Pronk and Hopman 1991, Ghuzlan and Carpenter 2000). Therefore, the number of loading cycles at which the test ends were selected based on two aspects. The first aspect for selecting (n=24,000) to be the loading cycle at which TS test stops is that it was found previously that an intermediate crack length was formed at this stage of loading for two types of binders (Zhang and Gao 2021). The second aspect is that measured cracks did not reach a complete failure (c_m < 4 mm). In other words, the sample

is not completely separated into two parts at this stage of loading, although it shows measurable crack damage.

The time sweep (SW) test is conducted for unaged and LT-aged samples at intermediate temperature conditions (20°C) to evaluate the fatigue performance of AAC-modified bitumen. The phase angles and shear moduli are recorded up to 24,000 loading cycles, as can be seen in **Figure 6-14**.

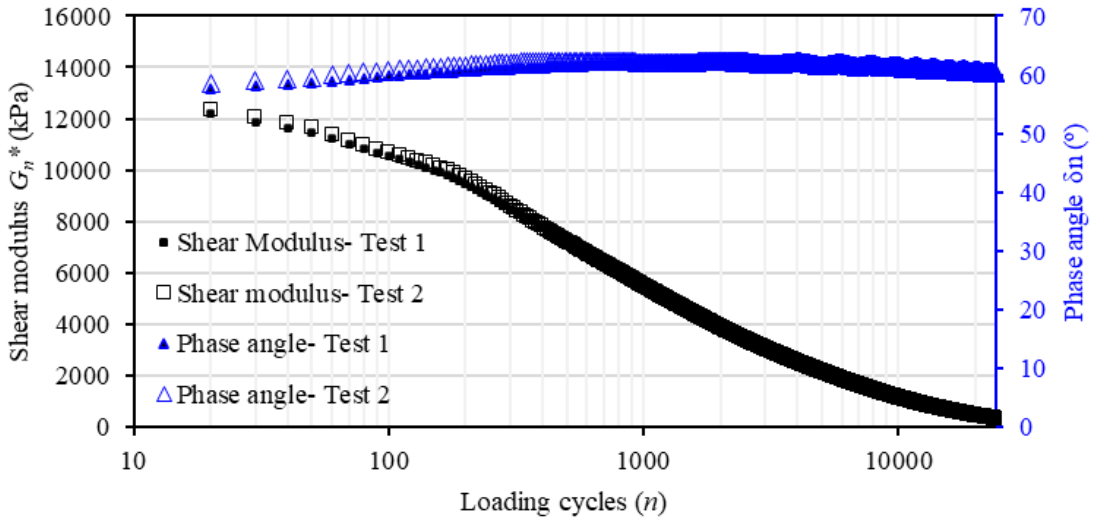

Figure 6- 14 Time sweep (TS) test results for sample 2 (bitumen with 10 % TMP) for the unaged condition. The test is conducted at 20°C temperature, 10 Hz loading frequency, 5% strain level, and up to 24,000 cycles.

The parameters phase angle $\delta_{n=24,000}$ and shear modulus $|G^*_{n=24,000}|$ at (n=24,000) loading cycles are obtained by TS tests for LT-aged samples. The crack length at (n=24,000) is calculated using DSR-C model in **Equation 2-19**. Both LAS and TS results are used to obtain predicted crack length values (c_p). For comparison, measured crack length (c_m) at (n=24,000 loading cycles) for all AAC-modified bitumen samples is determined by IAM, as shown in **Figure 6-15**. The figure shows the predicted and measured crack lengths are in good and consistent agreement, and there is a proportional correlation between calculated and measured crack lengths at all ages (for unaged, ST-aged and LT-aged samples) with an R^2 value of 0.7602. The correlation between measured and calculated crack lengths is better for LT-aged samples with an R^2 value of 0.9567,

this is a promising finding because it is more vital for measuring fatigue resistance performance since asphalt pavements are susceptible to fatigue failure at later ageing stages of their service life, and the method proved effective in measuring this value. It is expected that the variation between predicted and measured crack lengths is caused by (1) possible errors in measuring the crack length by IAM, (2) the high healing capacity for unaged and ST-aged samples. Generally, results indicate that the crack length predicted by DSR-C model (**Equation 2-19**) can effectively evaluate and differentiate the fatigue performance of bitumen modified by AACs, particularly for those at long-term ageing conditions.

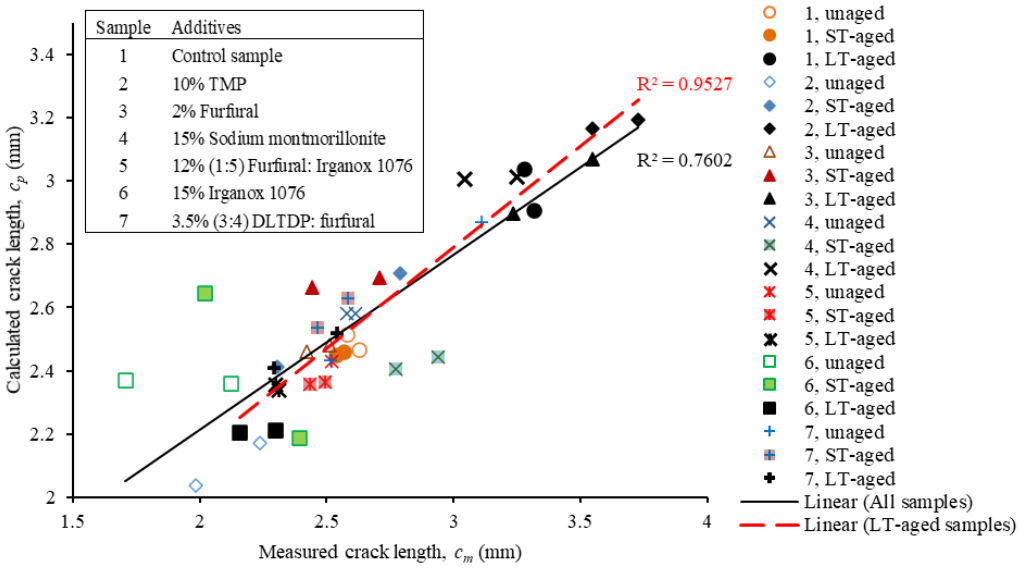

Figure 6- 15 Predicted crack length (c_p) versus measured crack length (c_m). The predicted crack length is obtained using DSR-C method, and measured crack length obtained by image analysis method (IAM) using time sweep (TS) and linear amplitude sweep (LAS) tests for samples at different ageing conditions (unaged, ST-ageing, LT-ageing) at 20°C temperature and 10 Hz loading frequency. IAM is conducted at 24,000 loading cycles. Tests are replicated.

It is also observed in **Figure 6-15** that samples 2, 3 and 4 at LT-aging condition show larger crack lengths compared with the control sample (sample 1). This behaviour means that even if the AACs in samples 2, 3 and 4 can reduce the oxidation of bitumen, they are unable to reduce fatigue damage. Moreover, samples 5 and 6 experienced the least fatigue damage among

other samples; however, the shear modulus for these two samples is significantly reduced due to the addition of AACs, meaning they may be unable to provide stiffness modulus. Sample 7 performed better resistance to fatigue cracking than that for the control bitumen, while still maintained adequate stiffness as indicated by LAS test. Thus, only sample 7 (bitumen modified by (3:4) DLTDP: furfural) has demonstrated a great anti-oxidation and fatigue-resistance performance without significantly reducing stiffness.

To compare the different fatigue characterisation approaches, DER values at n= 24,000 loading cycle are obtained using **Equation 2-18**. DER values are compared to the measured crack lengths (c_m) and shown in **Figure 6-16**. There is a weak correlation between DER and measured crack length for bitumen samples at different ages (unaged, ST-aged and LT-aged) with an R^2 value of 0.2329, with DER having a bit better correlation to the measured crack lengths for LT-aged samples, with an R^2 value of 0.4418.

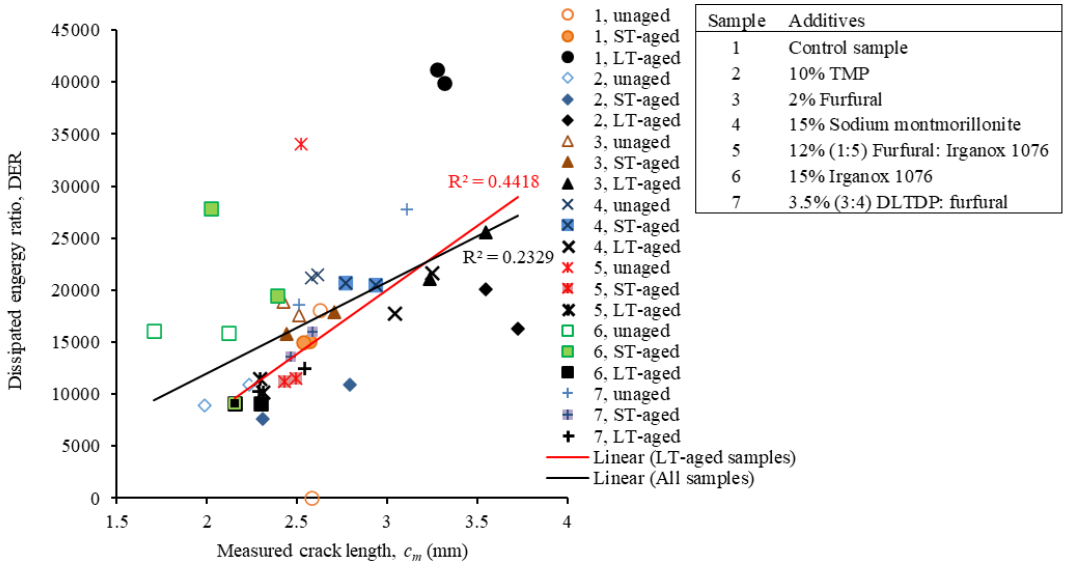

Figure 6- 16 Dissipated energy ratio (DER) versus measured crack length (c_m). DER and cm are obtained by time sweep (TS) test for samples at different ageing conditions (unaged, ST-ageing, and LT-ageing) at a temperature of 20°C and 10 Hz loading frequency. IAM is conducted at 24,000 loading cycles. Tests are replicated.

To examine the fatigue performance against other known parameters, measured crack lengths are plotted against the Superpave fatigue parameter ($|G_o^*|.sin\ \delta_o$) developed by the Strategic Highway Research Program (SHRP) (Anderson and Kennedy 1993). Low ($|G_o^*|.sin\ \delta_o$) indicates good resistance to fatigue cracking. **Figure 6-17** shows that the correlation between measured crack lengths and Superpave fatigue parameter at the initial (undamaged) state is weak, with an R^2 value of 0.5206 for samples at different ageing conditions (unaged, ST-aged and LT-aged) and an R^2 value of 0.6115 for samples tested at LT-ageing conditions.

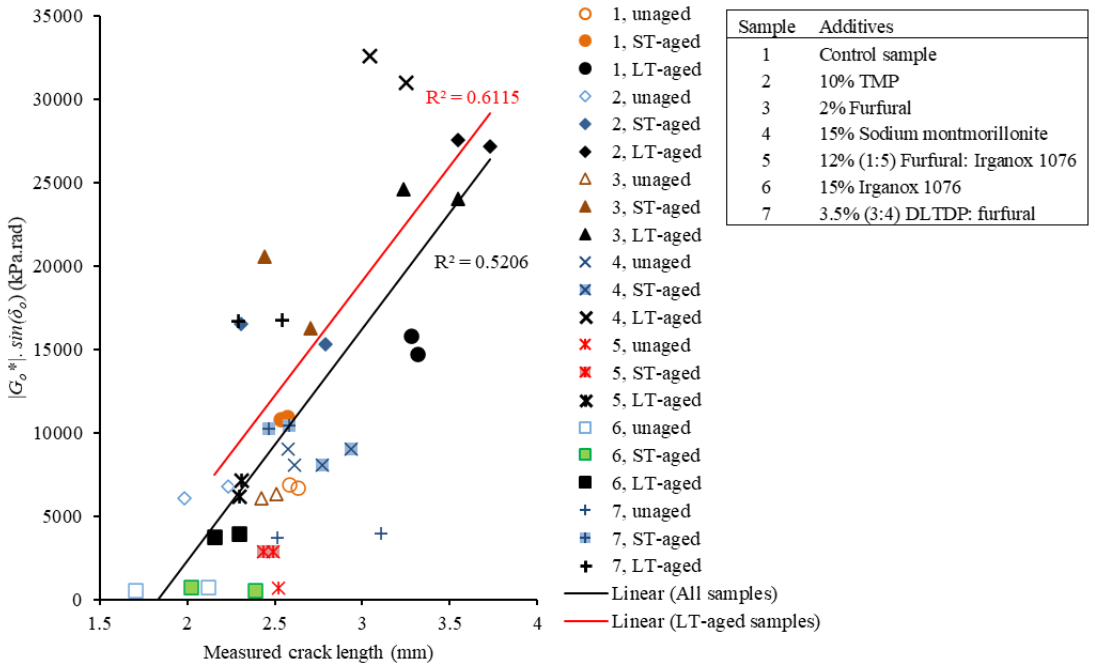

Figure 6- 17 Superpave fatigue parameter at the undamaged state versus measured crack length (c_m). The undamaged fatigue parameter is obtained by linear amplitude sweep (LAS) test for samples at different ageing conditions (unaged, ST-aged, and LT-aged) at intermediate temperature (20°C), 5% strain level and 10 Hz loading frequency. The measured crack length was obtained by time sweep (TS) test for samples at different ageing conditions (unaged, ST-ageing, and LT-ageing at 20°C temperature and 10 Hz loading frequency. IAM is conducted at 24,000 loading cycles. Tests are replicated.

Comparing **Figures 6-15, 6-16** and **6-17**, it can be concluded the fatigue cracking for AAC-modified bitumen quantified by laboratory-induced and measured crack lengths correlates the best (highest R^2 values) with the calculated crack length determined by DSR-C model.

6.2.2.3 Multiple stress creep and recovery test

The multiple stress creep and recovery (MSCR) test is a standard test (ASTM standard D7405-15, AASHTO T 350), used to measure rutting susceptibility of bitumen at high temperatures (ASTM 2015). This test is conducted solely on bitumen samples that demonstrates good fatigue resistance characteristics. The plate used in this test is the 25 mm diameter plate (1 mm vertical gap). The temperature for MSCR test is set to be Performance Grade (PG) high-temperature. The PG high-temperature is determined by the DSR device and high-temperature standard evaluation test (HT-PG) (using the standards AASHTO T-315) (AASHTO 2012).

The fatigue cracks propagation behaviour at intermediate temperatures and the carbonyl growth (**Section 6.2.3**) suggested that samples 5, 6 and 7 contain promising AACs. However, samples 5 and 6, containing Irganox 1076, suffered a considerable decrease in the initial complex shear modulus (**Figure 6-11**). Therefore, samples 5 and 6 considered improper AACs. Nonetheless, the addition of Irgnox 1076 may still be considered for specific applications with lower PG-grade or when combined with other additives after further testing.

Sample 7 demonstrated good fatigue cracking resistance and anti-oxidative action (**Sections 6.2.2.2** and **6.2.3**). However, OOT test (detailed in **Section 6.2.4**) indicated a decrease in the melting temperature of sample 7 compared to the control sample. For this reason, it is necessary to investigate the rutting susceptibility of the modified sample.

To investigate the high-temperature behaviour (e.g., rutting) of sample 7, first, the high-temperature performance grade (HT-PG) is determined, then it was implemented later for MSCR and LAS tests both at high-temperature conditions. It is found that HT-PG for sample 7 is 64°C, and HT-PG for the control binder was 70 °C. This finding contradicts with Apeagyei (2011) for DLTDP/furfural additives, as they observed an increase in HT-PG from 64°C at control binder to 70°C at the modified binder, this variation may be attributed to differences in sample preparation,

where Apeagyei (2011) introduced an acid catalyst to mix furfural into the binder (Apeagyei 2011). It may also be a result of using a different sample preparation procedure as they mixed the binder at a lower mixing rate of 750 rpm but for four hours, whereas in this study, the mixing time was 90 minutes with mixing rate of 4000 rpm, which can cause less volatilisation of light compounds.

MSCR test is performed to measure the non-recoverable deformations. The test is usually conducted for rolling thin-film oven aged samples (Subhy 2017), but since the additive caused ageing retardation, the test was also conducted for LT-aged samples as rutting damage may become potential distress when induction of the AACs reduces the ageing.

Figure 6-18 shows MSCR results for ST-aged and LT-aged samples (sample 1 and 7). Sample 7 demonstrated increased non-recoverable creep compliance and an unchanged per cent recoverable strain at ST-ageing condition, compared to the control bitumen (sample 1). At ST-ageing condition, a negative recovered strain value is obtained; this occurs when strain increases in unloading phase, in the absence of load, especially when the sample is very soft, and there is almost no recovery. The slight increase in strain curve is enough to give a negative value for the total recovery; this slight increase in loading could be a result of rheometer errors at unloading condition (Soenen et al. 2013). At LT-ageing condition, sample 7 demonstrated a slight increase in the non-recoverable creep compliances and a reduced per cent recoverable strain. This means bitumen samples 7 have less rutting resistance compared to the control bitumen (sample 1) at high temperature. Increased rutting potential can be attributed to the addition of low molecular mass components (furfural and DLTDP), or due to reduction in polarity due to the reaction of these primary and secondary anti-oxidants with bitumen reducing viscosity and thermal dependency.

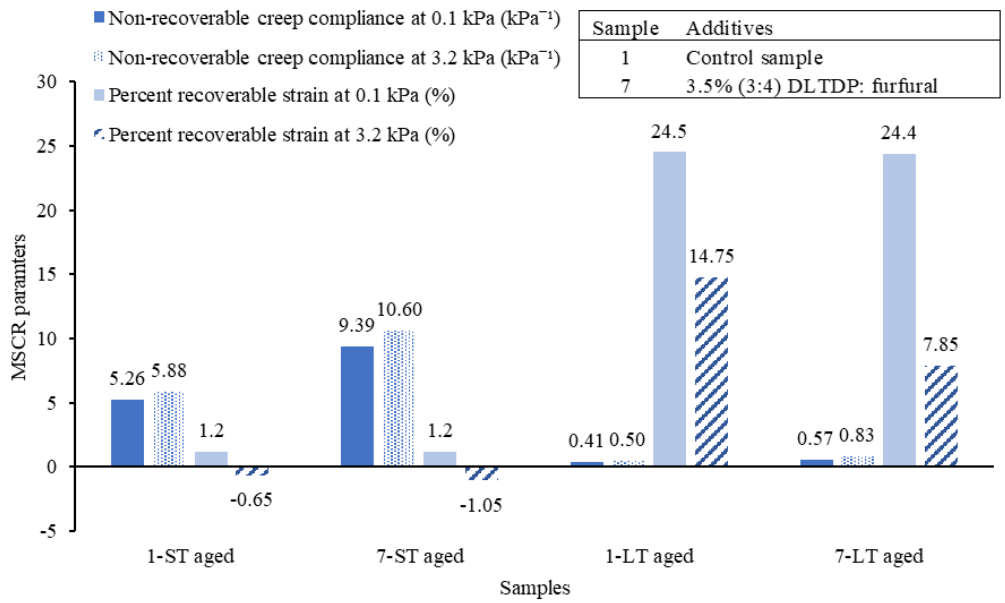

Figure 6- 18 Multiple stress creep and recovery (MSCR) test parameters at 64°C temperature for short-term (ST, by TFOT) aged and long-term (LT, by PAV) aged samples (samples 1 and 7)

6.2.3 Fourier transform infrared spectroscopy (FTIR) test

Fourier transform infrared spectroscopy (FTIR) tests were carried out for unaged and LT-aged bitumen samples using Thermo Scientific Nicolet iS10 spectrum. The device is set to scan in a range of (500-4000) cm^{-1}, with a scanning frequency of 16 and 4 cm^{-1} resolution. KBr scanning plates with a 12 mm diameter are prepared by compressing KBr powder into thin discs (about 1 mm thickness). Then, a small amount of bitumen is placed close to the edge of newly prepared KBr plates and heated to 100±5 ºC. A clean steel spatula also heated, then when the bitumen melts, it is levelled by the spatula into a thin layer and cooled before scanning by FTIR, to observe the changes of chemical functional groups due to ageing in bitumen samples modified by AACs.

To correlate the oxidation products growth and fatigue performance for AAC-modified bitumen samples, **Figure 6-19** shows NCI (defined by **Equation 6-3**) against the ratio of change in fatigue crack lengths ($\Delta c/c_{unaged}$) between the LT-aged sample and the corresponding unaged sample, as defined in **Equation 6-10**.

$$\Delta c/c_{unaged} = \frac{c_{LT\ aged} - c_{unaged}}{c_{unaged}} \quad (6\text{-}10)$$

where, $c_{LT\ aged}$ is the predicted crack length for LT-aged samples, c_{unaged} is the predicted crack length for unaged samples.

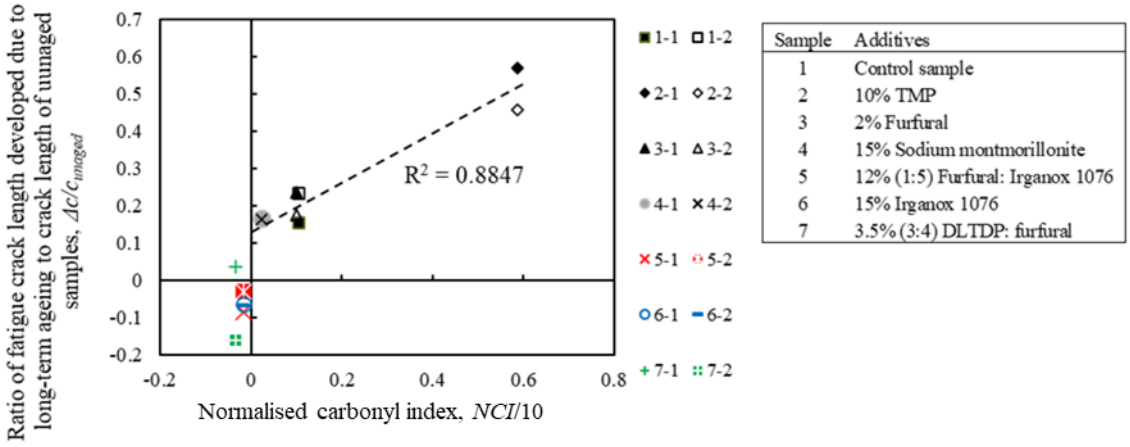

Figure 6- 19 The normalised carbonyl index (NCI) of LT-aged samples versus the ratio of change in the crack length propagation due to long-term laboratory ageing for all tested samples. In legends label, the first number represents AAC sample number and the second number represents the number of tests replicates).

Results show a good linear correlation between ageing products (represented by NCI) and the fatigue resistance of AAC-modified binders, with R^2 value of 0.8847 is found for samples 1, 2, 3, and 4 (samples that show less effectiveness in anti-ageing, represented by black marks in **Figure 6-19**).

Figure 6-19 also shows that samples 5, 6 and 7 (shown to have high effectiveness in anti-ageing, represented with coloured markers in **Figure 6-19**) shown a decrease in both normalised carbonyl index (*NCI*) and cracking lengths propagation ratio upon LT-ageing. This observation means the AACs in samples 5, 6 and 7 can reduce both oxidation and fatigue damage by preventing build-up of asphaltene and resin fractions upon exposure to oxygen from ageing conditioning. The NCI retardation (remains unchanged and close to zero) in samples 5, 6 and 7 can be attributed to the high carbonyl content in the additives prior to ageing. Whereas AACs in

samples 3 and 4 did not affect the fatigue resistance and carbonyl development when compared to the control sample (sample 1).

Results suggest that adding furfural alone as a primary anti-oxidant (sample 3) and sodium montmorillonite (sample 4) are ineffective in retarding the oxidation. Recent researches reported many beneficial effects of adding nanomaterials to bitumen (Ghile 2006, Yao et al. 2013, Ortega et al. 2017), including improvements in thermal stability, resistance against rutting, and strengthening bonding with rubber modifiers. However, there is no evidence that nanomaterials can hinder oxygen diffusion into binder film during ageing, thus retard oxidation by preventing oxygen from the air to reach the free-radicals in the bitumen binder. Sample 2 (containing TMP) demonstrated poor performance, thus agreeing well with the findings in **Section 6-1** regarding the low oxidation activation energy. TMP esters are reaction blocks used in polymer production and lubrication applications (Cuellar Jr 1977, Yunus et al. 2004). TMP is added to bitumen to retard oxidation by assuming a reaction of OH- will occur with the acidic compounds of bitumen. Due to the unclear behaviour of TMP in the preliminary testing stage, it was included in the current study for further investigation. The high crack length values (especially that at LT-ageing condition) and high initial shear modulus obtained for sample 2 suggest that the TMP is an ineffective anti-oxidant. TMP alone crystallises at medium/low temperatures; therefore, it led to more susceptibility to fatigue cracking when added to bitumen. Additionally, TMP melts at high temperatures, causing low viscosity for the modified binder.

Samples 5 and 6 possessed high initial phase angles and low shear moduli due to the decrease in viscosity upon the addition of AACs; therefore, they are not recommended, although they achieved good anti-ageing performance, confirming Irganox 1076 is effective in retarding oxidative ageing of bitumen. Sample 7 with 3.5% (3 DLTDP/4 furfural) demonstrated a better initial shear strength with minimum ageing and fatigue failure compared to other additives.

6.2.4 Oxidation onset temperature (OOT) test

The differential scanning calorimetry (DSC) was reported to characterise the thermal properties of asphalt binders (Harrison et al. 1992) and measure the thermal stability of polymeric

materials (Focke and Van Der Westhuizen 2010). The oxidation onset temperature (OOT) is a testing scheme that examines the oxidation initiation temperature of materials in controlled temperature and pressure conditions. Therefore, it is used in this study to assess the thermal stability of AACs-modified bitumen in oxygen-exposed conditions and at a temperature range similar to that in the field. A higher OOT indicates better thermal stability at the oxygen-exposed condition for AAC-modified bitumen.

The OOT is performed using the DSC Netzsch high-temperature device. The test measures the temperature at which the oxidation process initiates by observing the change in heat flux for a sample placed inside oxygen gas chamber. Oxidation is an exothermic process that involves a decrease in heat flow (release of energy) when initiated (such as the burning process of hydrocarbon materials). In other words, the machine will release less heat flow to maintain the control temperature level during an exothermic process. Bitumen samples of 0.05 g mass are placed in oxygen gas controlled-environmental cell and subjected to a 5°C/min temperature rate starting at 20°C room temperature. The tests are stopped at a temperature of 150°C to avoid reaching the flashpoint.

The OOT test results are illustrated in **Figure 6-20** for unaged and LT-aged samples. Results are averaged for two replicates. Sample 2 is not tested because it demonstrates negative impacts on fatigue resistance and carbonyl growth retardation. Results indicate initiation of endothermic reaction; meaning the oxidation initiation process did not commence at this temperature range or that the energy released from the endothermic reaction is more significant than that of any exothermic reactions. The endothermic reaction is initiated at lower temperatures for samples 5, 6 and 7 compared to that of the control sample (sample 1), as shown in **Figure 6-20**. The endothermic reaction can be a result of the melting of waxy components in bitumen. It is argued that samples 5, 6 and 7 contain fewer asphaltene fractions and higher aromatics content; therefore, this influenced the chemical structure and led to lower melting temperatures (Harrison et al. 1992).

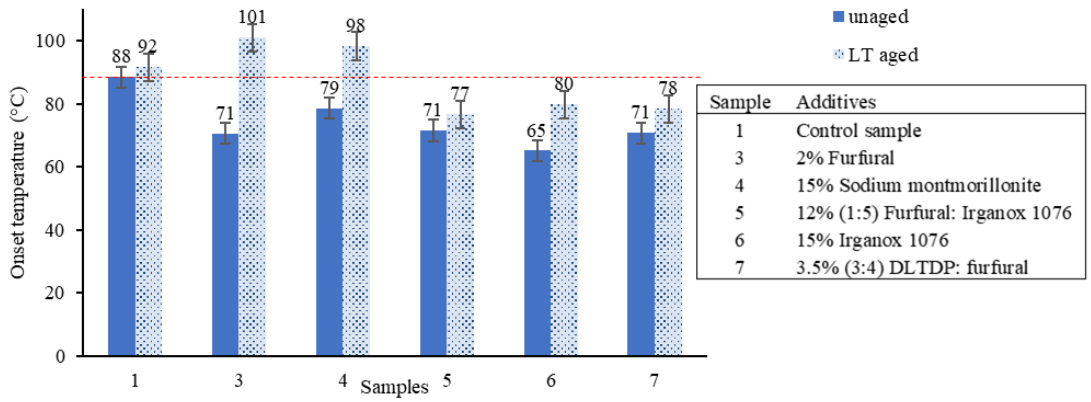

Figure 6- 20 Endothermic reaction initiation temperature for unaged and long-term (LT, by PAV) aged bitumen samples.

6.3 Impact of Anti-Ageing Compounds on Oxidative Ageing of Asphalt Pavements in the Field using Multiphysics Modelling Approach

Research findings confirm the importance of activation energy at the fast-rate ageing on the overall ageing process of binders. The effect of activation energy on field ageing of asphalt pavements is investigated in this section. Jin et al. (2011) found a linear correlation between the activation energies of the fast and constant oxidation stages based on the tests of 15 asphalt binders aged in laboratory using thin-film oven conditions at atmospheric air pressure (1 atm) (Jin et al. 2011), as shown in **Equation 6-11**.

$$E_{af} = 0.85E_{ac} - 10.4 \quad (6\text{-}11)$$

Additionally, they established an exponential relationship between the pre-exponential factor A_c and constant-term activation energy E_{ac}, and between A_f and E_{af} as seen in **Equations 6-12** and **6-13**.

$$A_c = 0.0315\, e^{0.3325E_{ac}} \quad (6\text{-}12)$$

$$A_f = 0.20\, e^{0.3328\, E_{af}} \quad (6\text{-}13)$$

Thus, it is possible to predict binder-source dependent oxidation kinetics from the oxidative activation energy of the fast-term ageing stage.

In the technical report FHWA/TX-14/0-6009-2, a number of 15 binders were tested, and their activation energy values for the fast-term ageing stage were ranging from 35.2kJ/mol to 75.4 kJ/mol. The activation energies for the constant-term ageing were ranging from 64.9 kJ/mol to 103.8 kJ/mol for unmodified and polymer modified binders (Glover et al. 2014). For the current study, a suitable range of oxidative activation energy values (74-226 kJ/mol) is identified for anti-ageing compounds (AACs) modified bitumen, based on **Section 6-1**. The improvement in anti-ageing performance is presented in the form of a ratio between E_f of AAC-modified specimen and that for the control specimen. It was observed that some AACs caused an increase in E_f from 222 kJ/mol to 664 kJ/mol, achieving a ratio of improvement of 3.0. Thus, a ratio of 3 is considered as the upper limit, and a ratio of 1 (i.e., control bitumen without improvement in E_f) was considered as the lower limit. Some AAC-modified binders did not show any signs of oxidation when tested under thin-film oven ageing conditions; therefore, it was impossible to determine their oxidative activation energies.

Climate data, pavement structure and mixture morphology for road section US277 located in Laredo – Texas were employed to conduct the parametric study. The model is let to run for one year of field ageing simulation. The original value of E_f for road section US277 is 75.4 kJ/mol. Thus, values ranging from 75.4 kJ/mol to 226 kJ/mol are selected to maintain an improvement ratio in the activation energy of 1 to 3.

Figure 6-21 (a-c) shows the carbonyl area content at the mastic-air channel interface (where there is a minimum constraint on oxygen diffusion) for one year of field ageing simulation at three asphalt concrete depths. There is an evident growth in carbonyl content for bitumen binders of activation energies 75.4 kJ/mol and 80 kJ/mol. In contrast, for high activation energy values of 151 kJ/mol and 226 kJ/mol (assuming these are AAC-modified binders), there is no ageing. This suggests the following: (1) the activation energy at fast-rate ageing is a prime parameter for ageing extent and growth in asphalt binders, and subsequently, asphalt pavements; and (2) the addition of anti-ageing materials can mitigate or prevent oxidative ageing of asphalt concrete pavements.

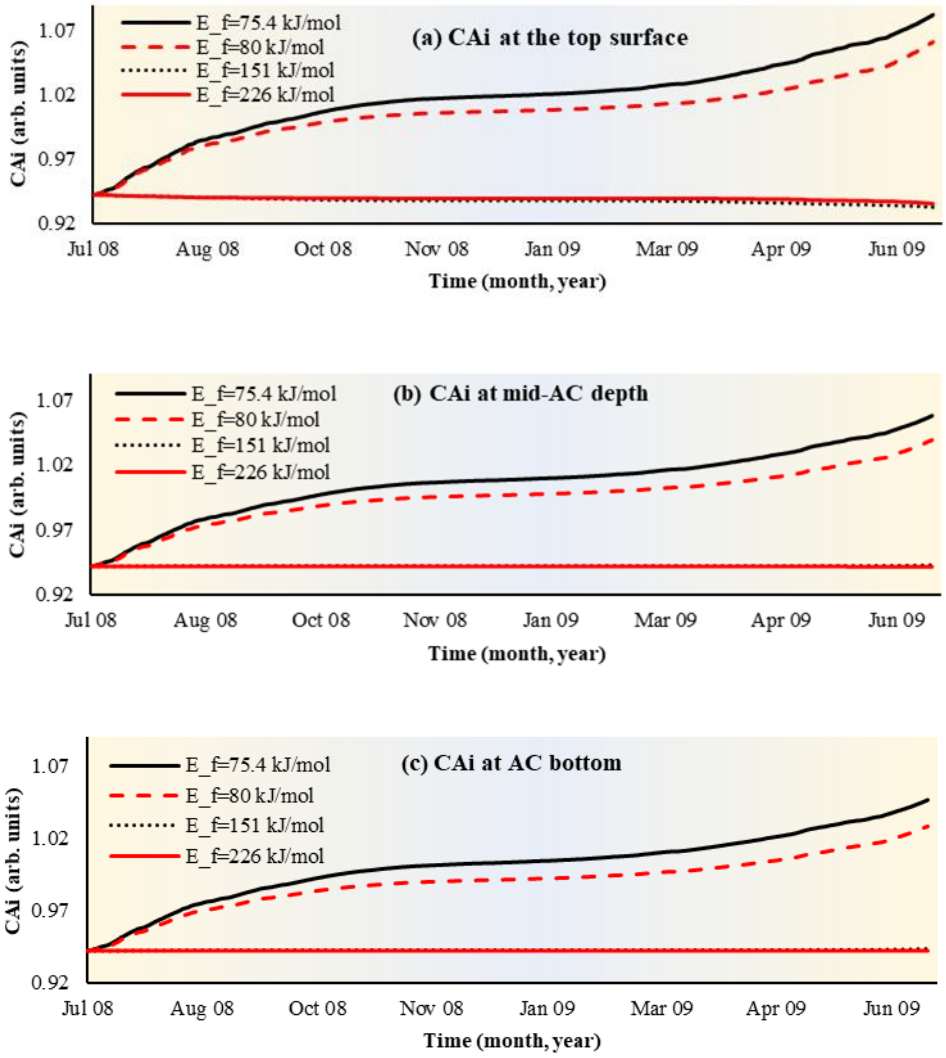

Figure 6- 21 Carbonyl area at the air channels-mastic interface (CA_i) versus ageing time, using different fast-term activation energy values (E_f=75.4, 80, 151, and 226 kJ/mol) at (a) asphalt concrete (AC) surface, (b) mid-AC depth, and (c) AC bottom.

By looking at the increase in carbonyl index with time, it was found that there is a 14.9% increase in the carbonyl index for a binder with an activation energy of 75.4 kJ/mol and a 12.6% increase in the carbonyl index for the binder with an activation energy of 80 kJ/mol at the exact location (at the top of AC layer). That is 2.3% change in carbonyl index (without accounting for the effect of oxygen diffusion) due to a considerably small change in the oxidation kinetics.

6.4 Summary of Ageing Mitigation using Anti-Ageing Compounds

This chapter investigated methods of reducing and mitigating oxidative ageing using chemical additives to work as anti-ageing agents. First, up to 20 different anti-ageing compounds (AACs) were added to the bitumen binder and subjected to laboratory thin-film oven ageing condition at 100°C. Then preliminary tests were conducted using Fourier transform infrared spectroscopy (FTIR) test to examine the impact of AACs on the oxidative ageing kinetics and filter out ineffective anti-ageing additives. A screening method for AACs was proposed, and a normalised carbonyl index (NCI) was adopted to quantify the oxidative ageing. Additionally, the fast rate activation energy (E_f) is decided to be a good indicator for the AACs effectiveness.

Then, detailed chemical and rheological tests followed to ensure selected AACs can improve the bitumen anti-ageing performance while maintaining sufficient fatigue and rutting performance. The effectiveness of six AACs is compared in terms of the resistance to fatigue cracking at intermediate temperatures. FTIR tests are conducted to link the chemical structure of bitumen samples with their fatigue performance. The fatigue behaviour is measured by using several approaches (Dynamic Shear Rheometer (DSR), actual crack length method, predicted crack length, and fatigue parameter). Further tests were carried out at high temperature for the sample with the nominated anti-oxidant to verify their resistance to rutting at high temperatures. DLTDP/furfural AACs have shown a good anti-ageing performance without sacrificing the stiffness of bitumen, and AACs maintained their performance on bitumen even after exposure to long-term laboratory ageing conditions. It was also found that the DSR-C model can effectively evaluate the fatigue performance of AAC-modified binder, and NCI correlates well with the fatigue of AACs-modified binders.

Finally, the effectiveness of AACs- inclusion in mitigating field oxidative ageing was investigated using the proposed oxidative ageing modelling framework. It was concluded that the activation energy at fast-rate ageing is a prime parameter for ageing extent and growth in asphalt binders, and subsequently, asphalt pavements. Increasing the fast-rate activation energy by only 5 kJ/mol caused a reduction in carbonyl index of up to 2.3% per one year of ageing, and asphalt

binders with very high activation energies due to the inclusion of AACs generate little oxidative ageing in the field.

Chapter 7 Summaries, Conclusions and Recommendations

7.1 Summaries

Bitumen binders can oxidise with air and cause ageing deterioration of asphalt pavements in the form of hardening, cracking and an overall decline in the mechanical performance. The degree of oxidative ageing is governed by many coupled internal and external physics and variables, making it difficult to predict. Mathematical models were established to represent the multiple physics that contribute to oxidative ageing of asphalt pavements. When coupled together, these models can simultaneously simulate heat transfer, oxygen diffusion and oxidation kinetics to predict the oxidative ageing of asphalt pavements. The challenge lies in the non-linearity and circular dependency of these physics, making them difficult to solve and converge in numerical applications.

The current study establishes a partial differential equation (PDE) based Finite Element (FE) modelling framework to solve these multiple physics using a weak form method. The framework is validated using field measurements of within-pavement temperatures and oxidative ageing products at various ageing time and different pavement depths. A laboratory-based experimental investigation is conducted to select anti-ageing compounds (AACs) to mitigate oxidative ageing of bitumen binders effectively. Thin-film oven ageing and Fourier Transform Infrared Spectroscopy (FTIR) tests are used primarily to select potential AACs. Detailed rheological and chemical tests are followed to detect any effects of these AACs on the long-term ageing performance of bitumen binders.

7.2 Conclusions

The specific conclusions drawn from this study are summarised as follows:

7.2.1 Development of an equation-based Multiphysics modelling framework for oxidative ageing of asphalt pavements

1. The model can effectively address the circular dependency among ageing-related Multiphysics (i.e., heat transfer, oxygen diffusion, and oxidation kinetics). PDE-based

FEM can reliably predict annual hourly profiles of temperature, oxygen pressure, and oxidation products growth across the pavement depth in different climate zones.

2. The model overcomes some of the encountered uncertainties in oxidative ageing prediction. For instance, it relies more on site-specific climatic data, such as albedo, emissivity, and subsurface soil temperatures; and it does not require field calibration factor fcf to calibrate oxygen diffusion process in the pavement. Moreover, the heat transfer model was calibrated to predict the temperature profile in regions susceptible to freezing.
3. Oxygen pressure within the asphalt structure frequently changes due to seasonal and daily temperature variation, and it is affected by the oxidation process. Oxygen pressure becomes low with high daily flocculation during summer because asphalt mastic ages and consumes more oxygen when subjected to high temperatures. In contrast, oxygen pressure becomes high with low daily flocculation in winter because there is a low oxidation rate in this season due to low temperatures. This unique behaviour cannot be observed without using circular-dependent Multiphysics model.
4. Design and materials selection of pavement directly impacts the severity and extend of oxidative ageing. For example, carbonyl area distribution takes a C-shaped curve along AC depth (high oxidation rate at top and bottom boundaries), in case there is free air-accessibility through the underlying layer. If the underlying layer is inaccessible to air, such as cement/asphalt treated base, carbonyl area will be high at AC surface and low at bottom. Not to forget that this pattern is also affected by temperature profile, which causes irregular or different carbonyl area distribution pattern along pavement depth. Another example on the impact of pavement structure on oxidative ageing is the effect of interconnected air channels. Presence of accessible air channels is proportional with oxidation rate (i.e., the higher the radius and number of air channels, the higher the exposed surface area of mastic to air, and the higher the ageing rate).
5. There has been a long debate regarding the uniformity and distribution of oxidative ageing products along pavement depth. Modelling results in this study support that

oxidative ageing is non-uniform and decreasing in general across pavement depth because it is highly sensitive to oxygen pressure and temperature profiles.

7.2.2 Parametric analysis and field validations of oxidative ageing in asphalt pavements using Multiphysics modelling approaches

1. Increasing the thermal conductivity of asphalt layers lowers the surface temperature and increases the bottom temperature in the asphalt layer up to 5°C. It is therefore causing less temperature gradient in asphalt layer, which can cause an up to 5% per year reduction of the ageing gradient and potential less cracking damage.
2. Increasing the heat capacity of the asphalt layer generates slightly reduced daily temperature variations due to the greater heat storage capacity of the pavement. The maximum daily surface temperature can be reduced by 2°C upon increasing the heat capacity, generating a one per cent decrease in carbonyl index.
3. The variations of the thermal properties of underlying layers (base and subgrade) cause little or no effects on the temperature profile and oxidative ageing amount and distribution in the asphalt layers. The most notable changes of temperature or ageing profiles are caused by changing the thermal conductivity and heat capacity of the asphalt layers.
4. The asphalt layers built on unbound granular base (free access to oxygen at both top and bottom of the asphalt layer) will experience greater overall ageing with a C-shaped ageing gradient compared to that built on treated base (access to oxygen at the top but none at the bottom of the asphalt layer) which lead to a r-shaped ageing gradient along pavement depth.
5. The extent of oxidative ageing in asphalt mastics is bound by the mastic film thickness surrounding accessible air channels (i.e., diffusion depth). The thicker the mastic coating film, the less the average carbonyl area will be, resulting in a potentially increased pavement resistance to cracking.
6. A non-uniform (i.e., C-shaped) air voids distribution within the asphalt layer allows more oxygen access. It increases the oxidative ageing across the pavement depth, causing binder hardening and aged pavements prone to more fatigue damage.

7. The air void content plays a vital role in limiting oxidative ageing. Dense asphalt pavements with a low air voids content (< 5%) experience little to no ageing, whereas asphalt pavements with air void content of 5-9% experience a growing oxidative ageing rate with an increasing air void content. Pavements with high air voids (> 9%) will have a full access to oxygen from the atmosphere, thus the average carbonyl content is high and uniform across asphalt pavement depth with no clear C-shaped or r-shaped ageing gradient.
8. The climate region may not only cause different levels or degrees of oxidative ageing but it can also cause a considerable difference in the ageing pattern, potentially causing different type or pattern of damage. Additionally, differences in temperature within the same environmental region (e.g., wet, no-freeze) can still generate significant variation in field ageing performance.

7.2.3 Ageing mitigation using anti-ageing compounds

1. Normalised carbonyl index (NCI) was proposed to quantify the oxidative ageing of bitumen modified by AACs. It eliminates the impact of the initial carbonyl content of the binders or AACs, thus reveals the carbonyl growth rate pattern to evaluate the AACs' anti-ageing performance. NCI may be a reliable parameter to reflect the impact of ageing products on the fatigue resistance of AAC-modified binders.
2. The activation energy of fast-term ageing (E_f) is a suitable parameter to differentiate the anti-ageing efficiency of the AACs.
3. The compounds (DLTDP/furfural), Irgnaox 1076 and (furfural/Irganox 1076) demonstrated a good anti-ageing behaviour by retarding carbonyl content growth and decreasing fatigue damage caused by the cyclic loading and long-term ageing conditions. In contrast, the additive Trimethylolpropane TMP caused adverse impacts on the binder in terms of fatigue resistance. Sodium montmorillonite and furfural alone did not show a pronounced effect in terms of fatigue cracking and anti-oxidation activity. The addition

of Irgnaox 1076 caused a drop in the initial complex shear modulus. Therefore, it should be used with precaution for certain applications after conducting further tests.

4. The long-term aged AAC-modified bitumen maintained different linear viscoelastic properties than those for the long-term aged control bitumen, suggesting that the AACs can tolerate the long-term laboratory ageing conditions. This behaviour indirectly indicates good stability for these anti-ageing compounds.
5. Compared to existing fatigue parameters for bitumen, the predicted crack length based on DSR-C model demonstrated a good agreement with the measured crack lengths, suggesting it is a promising fatigue cracking evaluation criterion for AAC-modified binders.
6. The activation energy at fast-rate ageing is a prime parameter for ageing extent and growth in asphalt binders, and subsequently, asphalt pavements. Increasing the fast-rate activation energy by only 5 kJ/mol caused a reduction in carbonyl index of up to 2.3% per one year of ageing. The asphalt binder with high activation energies due to the inclusion of anti-ageing additives generates minor oxidative ageing in the field.

7.3 Recommendations for Future Work

In this study, a Multiphysics modelling framework for predicting oxidative ageing in the field was developed and validated. However, the model did not consider other ageing types, such as UV radiation ageing and moisture-induced ageing. The future work can couple the current oxidative ageing with other types of ageing in one integrated model with considering the water effects on the ageing Multiphysics model.

Additionally, a lifetime ageing modelling is needed (e.g., more than ten years of ageing), with given consideration to the optimised computational load. The challenge lies in how to optimise the finite element models and the ageing-related constitutive models to minimise the computational load. The parallellevel computation on supercomputer will be a strong tool to reduce the total computational time.

Moreover, a three-dimensional stress-induced damage and pavement mechanical response model can be integrated with the current two-dimensional time-dependent oxidative ageing model to work as a circularly dependent unit. Such that, the interactions between the ageing evolution and the damage growth can be coupled and predicted in a more realistic method. The changes in the air voids due to mechanical stress can be incorporated in the current ageing model, and vice versa, the present ageing gradient along the pavement depth can cause a stiffness modulus gradient.

This study investigated the effect of anti-ageing compounds (AACs) experimentally on bitumen binders under different laboratory ageing conditions and levels, then implemented the observations on asphalt pavements in the field. The next step is to evaluate the AACs' efficiency on asphalt pavements aged in field conditions. The improved mechanical performance of the asphalt due to the addition of the AACs need to be validated using different types of the asphalt mixtures and verified in various pavement strucutures at different climate regions.

List of References

AASHTO (2012). T315-12-UL, Standard method of test for determining the rheological properties of asphalt binder using a dynamic shear rheometer (DSR).

Airey, G. (2003). "State of the art report on ageing test methods for bituminous pavement materials." International Journal of Pavement Engineering **4**(3): 165-176.

Al-Rub, R. K. A., M. K. Darabi, S.-M. Kim, D. N. Little and C. J. Glover (2013). "Mechanistic-based constitutive modeling of oxidative aging in aging-susceptible materials and its effect on the damage potential of asphalt concrete." Construction and Building Materials **41**: 439-454.

Alavi, M., E. Y. Hajj and P. E. Sebaaly (2017). "A comprehensive model for predicting thermal cracking events in asphalt pavements." International Journal of Pavement Engineering **18**(9): 871-885.

Alavi, M. Z., M. R. Pouranian and E. Y. Hajj (2014). "Prediction of asphalt pavement temperature profile with finite control volume method." Transportation Research Record **2456**(1): 96-106.

Alawi, M. H. and M. M. Helal (2014). "A mathematical model for the distribution of heat through pavement layers in Makkah roads." Journal of King Saud University-Engineering Sciences **26**(1): 41-48.

Ameri, M., S. Kouchaki and H. Roshani (2013). "Laboratory evaluation of the effect of nano-organosilane anti-stripping additive on the moisture susceptibility of HMA mixtures under freeze–thaw cycles." Construction and Building Materials **48**: 1009-1016.

Ameri, M., A. Mansourkhaki and D. Daryaee (2018). "Evaluation of fatigue behavior of high reclaimed asphalt binder mixes modified with rejuvenator and softer bitumen." Construction and Building Materials **191**: 702-712.

Anderson, D. A. and T. W. Kennedy (1993). "Development of SHRP binder specification (with discussion)." Journal of the Association of Asphalt Paving Technologists **62**.

Anderson, D. A., Y. M. Le Hir, M. O. Marasteanu, J.-P. Planche, D. Martin and G. Gauthier (2001). "Evaluation of fatigue criteria for asphalt binders." Transportation Research Record **1766**(1): 48-56.

Apeagyei, A. K. (2011). "Laboratory evaluation of antioxidants for asphalt binders." Construction and Building Materials **25**(1): 47-53.

Asphalt in Figures (2019). Brussels, Belgium.

ASTM (2002). ASTM D1754-97(2002), Standard Test Method for Effect of Heat and Air on Asphaltic Materials (Thin-Film Oven Test). West Conshohocken, PA, 1997.

ASTM (2015). ASTM D7405-15, Standard Test Method for Multiple Stress Creep and Recovery (MSCR) of Asphalt Binder Using a Dynamic Shear Rheometer. ASTM International, West Conshohocken, PA.

ASTM (2019). D6521-19a, Standard Practice for Accelerated Aging of Asphalt Binder Using a Pressurized Aging Vessel (PAV). West Conshohocken, PA.

Bahia, H. U., H. Zhai, K. Onnetti and S. Kose (1999). "Non-linear viscoelastic and fatigue properties of asphalt binders." Journal of the Association of Asphalt Paving Technologists **68**.

Bai, B. C., D.-W. Park, H. V. Vo, S. Dessouky and J. S. Im (2015). "Thermal properties of asphalt mixtures modified with conductive fillers." Journal of Nanomaterials **2015**.

Bobes-Jesus, V., P. Pascual-Muñoz, D. Castro-Fresno and J. Rodriguez-Hernandez (2013). "Asphalt solar collectors: a literature review." Applied Energy **102**: 962-970.

Caro, S., E. Masad, A. Bhasin, D. Little and M. Sanchez-Silva (2010). "Probabilistic modeling of the effect of air voids on the mechanical performance of asphalt mixtures subjected to moisture diffusion." Asphalt Paving Technology-Proceedings Association of Asphalt Technologists **79**: 221.

Castelblanco Torres, A. (2006). Probabilistic analysis of air void structure and its relationship to permeability and moisture damage of hot mix asphalt, Texas A&M University.

Chen, J., H. Wang and L. Li (2015a). "Determination of effective thermal conductivity of asphalt concrete with random aggregate microstructure." Journal of Materials in Civil Engineering **27**(12): 04015045.

Chen, J., H. Wang and H. Zhu (2017). "Analytical approach for evaluating temperature field of thermal modified asphalt pavement and urban heat island effect." Applied Thermal Engineering **113**: 739-748.

Chen, J., M. Zhang, H. Wang and L. Li (2015b). "Evaluation of thermal conductivity of asphalt concrete with heterogeneous microstructure." Applied Thermal Engineering **84**: 368-374.

Chen, Y., C. Ji, H. Wang, Y. J. C. Su and B. Materials (2018). "Evaluation of crumb rubber modification and short-term aging on the rutting performance of bioasphalt." **193**: 467-473.

Comsol Multiphysics Reference Manual (2013). C. Multiphysics. COMSOL: Grenoble, France**:** 1084.

Cuellar Jr, J. (1977). Degradation studies of a trimethylolpropane triheptanoate lubricant basestock, SOUTHWEST RESEARCH INST SAN ANTONIO TX.

Cui, Y., C. J. Glover, J. Braziunas and H. Sivilevicius (2018). "Further exploration of the pavement oxidation model–diffusion-reaction balance in asphalt." Construction and Building Materials **161**: 132-140.

Das, P. K., H. Baaj, S. Tighe, N. J. R. M. Kringos and P. Design (2016). "Atomic force microscopy to investigate asphalt binders: A state-of-the-art review." **17**(3): 693-718.

Das, P. K., R. Balieu, N. Kringos, B. J. M. Birgisson and Structures (2015a). "On the oxidative ageing mechanism and its effect on asphalt mixtures morphology." **48**(10): 3113-3127.

Das, P. K., B. Birgisson, D. Jelagin, N. J. M. Kringos and Structures (2015b). "Investigation of the asphalt mixture morphology influence on its ageing susceptibility." **48**(4): 987-1000.

Das, P. K., N. Kringos, H. Baaj and S. TIGHE (2015c). Investigation of Diffusion-Controlled Oxidative Aging in Asphalt Mixture. Proceedings of the Sixtieth Annual Conference of the Canadian Technical Asphalt Association (CTAA): Winnipeg, Manitoba.

Das, P. K., N. Kringos and B. J. I. J. o. P. E. Birgisson (2015d). "Numerical study on the effect of mixture morphology on long-term asphalt mixture ageing." **16**(8): 710-720.

Dessouky, S., D. Contreras, J. Sanchez and D. Park (2015). Anti-Oxidants' Effect on Bitumen Rheology and Mixes' Mechanical Performance. Innovative materials and design for sustainable transportation infrastructure**:** 8-18.

Dessouky, S. H., I. L. Al-Qadi and P. J. Yoo (2014). "Full-depth flexible pavement responses to different truck tyre geometry configurations." International Journal of Pavement Engineering **15**(6): 512-520.

Dickinson, E. (1984). "The diffusion controlled reaction of oxygen with films of bituminous binders." Australian Road Research **14**(3).

Domingos, M. D. I., A. L. Faxina, L. L. B. J. C. Bernucci and B. Materials (2017). "Characterization of the rutting potential of modified asphalt binders and its correlation with the mixture's rut resistance." **144**: 207-213.

Edler, A., M. Hattingh, V. Servas and C. Marais (1985). USE OF AGING TESTS TO DETERMINE THE EFFICACY OF HYDRATED LIME ADDITIONS TO ASPHALT IN RETARDING ITS OXIDATIVE HARDENING (WITH DISCUSSION). Association of Asphalt Paving Technologists Proc.

Elkashef, M., R. C. Williams and E. J. I. J. o. F. Cochran (2018). "Investigation of fatigue and thermal cracking behavior of rejuvenated reclaimed asphalt pavement binders and mixtures." **108**: 90-95.

Feng, Z., J. Yu, D. J. P. S. Kuang and Technology (2013). "The physical properties and photostability of bitumen with different ultraviolet absorbers." **31**(2): 113-120.

Ferington, T. and A. Tobolsky (1955). "Organic disulfides as initiators of polymerization: tetramethylthiuram disulfide." Journal of the American Chemical Society **77**(17): 4510-4512.

Focke, W. and I. Van Der Westhuizen (2010). "Oxidation induction time and oxidation onset temperature of polyethylene in air: testing Gimzewski's postulate." Journal of thermal analysis and calorimetry **99**(1): 285-293.

Gao, M., B. Xiao, K. Liao, Y. Cong, Y. J. P. s. Dai and technology (2006). "Aging behavior of colored paving asphalt." **24**(6): 689-698.

Gao, Y., Y. Zhang, F. Gu, T. Xu and H. Wang (2018). "Impact of minerals and water on bitumen-mineral adhesion and debonding behaviours using molecular dynamics simulations." Construction and Building Materials **171**: 214-222.

Gao, Y., Y. Zhang, Y. Yang, J. Zhang and F. Gu (2019). "Molecular dynamics investigation of interfacial adhesion between oxidised bitumen and mineral surfaces." Applied Surface Science **479**: 449-462.

Gawel, I., F. Czechowski and J. Kosno (2016). "An environmental friendly anti-ageing additive to bitumen." Construction and Building Materials **110**: 42-47.

Ghile, D. B. (2006). "Effects of nanoclay modification on rheology of bitumen and on performance of asphalt mixtures."

Ghuzlan, K. A. and S. H. Carpenter (2000). "Energy-derived, damage-based failure criterion for fatigue testing." Transportation Research Record **1723**(1): 141-149.

Glover, C. J., R. Han, X. Jin, N. Prapaitrakul, Y. Cui, A. Rose, J. J. Lawrence, M. Padigala, E. Arambula and E. S. Park (2014). Evaluation of binder aging and its influence in aging of hot mix asphalt concrete: Technical report.

Glover, C. J., A. E. Martin, A. Chowdhury, R. Han, N. Prapaitrakul, X. Jin and J. Lawrence (2009a). Evaluation of binder aging and its influence in aging of hot mix asphalt concrete: literature review and experimental design, Texas Transportation Institute.

Glover, C. J., A. E. Martin, A. Chowdhury, R. Han, N. Prapaitrakul, X. Jin and J. Lawrence (2009b). "Evaluation of binder aging and its influence in aging of hot mix asphalt concrete: literature review and experimental design."

Gu, F., W. Ma, R. C. West, A. J. Taylor and Y. Zhang (2019). "Structural performance and sustainability assessment of cold central-plant and in-place recycled asphalt pavements: a case study." Journal of Cleaner Production **208**: 1513-1523.

Gui, J., P. E. Phelan, K. E. Kaloush and J. S. Golden (2007). "Impact of pavement thermophysical properties on surface temperatures." Journal of Materials in Civil Engineering **19**(8): 683-690.

Hajj, R. and A. Bhasin (2018). "The search for a measure of fatigue cracking in asphalt binders–a review of different approaches." International Journal of Pavement Engineering **19**(3): 205-219.

Hall, M. R., P. K. Dehdezi, A. R. Dawson, J. Grenfell and R. Isola (2012). "Influence of the thermophysical properties of pavement materials on the evolution of temperature depth profiles in different climatic regions." Journal of Materials in Civil Engineering **24**(1): 32-47.

Han, R. (2011). Improvement to a transport model of asphalt binder oxidation in pavements: Pavement temperature modeling, oxygen diffusivity in asphalt binders and mastics, and pavement air void characterization, Texas A&M University.

Han, R., X. Jin and C. J. Glover (2011). "Modeling pavement temperature for use in binder oxidation models and pavement performance prediction." Journal of Materials in Civil Engineering **23**(4): 351-359.

Harrison, I. R., G. Wang and T. Hsu (1992). A differential scanning calorimetry study of asphalt binders.

Hassan, Z., D. Hassan, B. Rezvan and A. Ali (2012). "Influence of bentonite additive on bitumen and asphalt mixture properties." World Academy of Science, Engineering and Technology **6**.

Hassn, A., M. Aboufoul, Y. Wu, A. Dawson and A. Garcia (2016a). "Effect of air voids content on thermal properties of asphalt mixtures." Construction and Building Materials **115**: 327-335.

Hassn, A., A. Chiarelli, A. Dawson and A. Garcia (2016b). "Thermal properties of asphalt pavements under dry and wet conditions." Materials & Design **91**: 432-439.

Herrington, P. R. (2012). "Diffusion and reaction of oxygen in bitumen films." Fuel **94**: 86-92.

Highter, W. (1984). Thermal properties of some asphaltic concrete mixes. International Air Transportation Conference.

Hintz, C. and H. Bahia (2013). "Understanding mechanisms leading to asphalt binder fatigue in the dynamic shear rheometer." Road Materials and Pavement Design **14**(sup2): 231-251.

Hunter, R. N., A. Self, J. Read and E. Hobson (2015). The shell bitumen handbook, ICE Publishing London, UK:.

Jacob, F. and B. Ted (2007). A first course in finite elements, Wiley.

Jennings, P., J. A. Pribanic, K. Dawson and C. Bricca (1981). "HPLC and NMR spectroscopy to characterize asphaltic materials." Am. Chem. Soc., Div. Pet. Chem., Prepr.;(United States) **26**(CONF-810813-(Vol. 2)).

Jiang, J., Y. Li, Y. Zhang and H. U. Bahia (2020). "Distribution of mortar film thickness and its relationship to mixture cracking resistance." International Journal of Pavement Engineering: 1-10.

Jin, X. (2012). Asphalt oxidation kinetics and pavement oxidation modeling.

Jin, X., Y. Cui and C. Glover (2013). "Modeling asphalt oxidation in pavement with field validation." Petroleum Science and Technology **31**(13): 1398-1405.

Jin, X., R. Han, Y. Cui and C. J. Glover (2011). "Fast-rate–constant-rate oxidation kinetics model for asphalt binders." Industrial & Engineering Chemistry Research **50**(23): 13373-13379.

Kim, S.-S. J. J. o. m. i. c. e. (2005). "Direct measurement of asphalt binder thermal cracking." **17**(6): 632-639.

Kumar, A. and S. K. Suman (2017). "Experimental Investigations on Nanoclay (Cloisite-15A) Modified Bitumen." International Journal of Civil and Environmental Engineering **11**(2): 172-177.

Lamontagne, J., P. Dumas, V. Mouillet and J. Kister (2001). "Comparison by Fourier transform infrared (FTIR) spectroscopy of different ageing techniques: application to road bitumens." Fuel **80**(4): 483-488.

Lau, C., K. Lunsford, C. Glover, R. Davison and J. Bullin (1992). "Reaction rates and hardening susceptibilities as determined from pressure oxygen vessel aging of asphalts." Transportation Research Record(1342).

Leiva-Villacorta, F., A. Vargas-Nordcbeck, J. P. Aguiar-Moya and L. Loría-Salazar (2016). Development and calibration of permanent deformation models. The roles of accelerated pavement testing in pavement sustainability, Springer**:** 573-587.

Lesueur, D. (2009). "The colloidal structure of bitumen: Consequences on the rheology and on the mechanisms of bitumen modification." **145**(1-2): 42-82.

Li, R., F. Xiao, S. Amirkhanian, Z. You and J. Huang (2017). "Developments of nano materials and technologies on asphalt materials–A review." Construction and Building Materials **143**: 633-648.

Li, R., L. Zhao, T. Wu, Q. Wang, Y. Ding, J. Yao, X. Wu, G. Hu, Y. Xiao and Y. Du (2019). "Soil thermal conductivity and its influencing factors at the Tanggula permafrost region on the Qinghai–Tibet Plateau." Agricultural and Forest Meteorology **264**: 235-246.

Liu, C. (2014). "A Brief Introduction to the Weak Form." from https://uk.comsol.com/blogs/brief-introduction-weak-form/.

Liu, F., Z. Zhou and X. Zhang (2020). "Linking chemical to rheological properties of asphalt binder with oxidative aging effect." Road Materials and Pavement Design: 1-15.

Liu, H., H. Zhang, P. Hao and C. Zhu (2015). "The effect of surface modifiers on ultraviolet aging properties of nano-zinc oxide modified bitumen." Petroleum Science and Technology **33**(1): 72-78.

Liu, M., K. Lunsford, R. Davison, C. Glover and J. J. A. J. Bullin (1996). "The kinetics of carbonyl formation in asphalt." **42**(4): 1069-1076.

Lu, X., P. Sjövall and H. J. F. Soenen (2017). "Structural and chemical analysis of bitumen using time-of-flight secondary ion mass spectrometry (TOF-SIMS)." **199**: 206-218.

Lu, Y., P. Wright and Y. Zhou (2009). "Effect of temperature and temperature gradient on asphalt pavement response." Road & Transport Research: A Journal of Australian and New Zealand Research and Practice **18**(1): 19.

Luca, J. and D. Mrawira (2005). "New measurement of thermal properties of superpave asphalt concrete." Journal of Materials in Civil Engineering **17**(1): 72-79.

Lunsford, K. M. (1994). The effect of temperature and pressure on laboratory oxidized asphalt films with comparison to field aging, Texas A&M University. Libraries.

Luo, X., F. Gu and R. L. Lytton (2015). "Prediction of field aging gradient in asphalt pavements." Transportation Research Record **2507**(1): 19-28.

Luo, X., F. Gu and R. L. Lytton (2019). "Kinetics-based aging prediction of asphalt mixtures using field deflection data." International Journal of Pavement Engineering **20**(3): 287-297.

Luo, X., F. Gu, Y. Zhang, R. L. Lytton and B. Birgisson (2018). "Kinetics-based aging evaluation of in-service recycled asphalt pavement." Journal of Cleaner Production **200**: 934-944.

Lv, S., X. Peng, C. Liu, D. Ge, M. Tang, J. J. C. Zheng and B. Materials (2020). "Laboratory investigation of fatigue parameters characteristics of aging asphalt mixtures: A dissipated energy approach." **230**: 116972.

Lytton, R., D. Pufahl, C. Michalak, H. Liang and B. Dempsey (1993). "An integrated model of the climatic effects on pavements."

Ma, T., X.-m. Huang, E. Mahmoud and E. Garibaldy (2011). "Effect of moisture on the aging behavior of asphalt binder." International Journal of Minerals, Metallurgy, and Materials **18**(4): 460.

Ma, T., X. Huang, Y. Zhao and H. Yuan (2012). "Aging behaviour and mechanism of SBS-modified asphalt." Journal of Testing and Evaluation **40**(7): 1186-1191.

Ma, T., H. Wang, L. He, Y. Zhao, X. Huang and J. Chen (2017). "Property characterization of asphalt binders and mixtures modified by different crumb rubbers." Journal of Materials in Civil Engineering **29**(7): 04017036.

Ma, T., Y. Zhao, X. Huang and Y. Zhang (2016). "Characteristics of desulfurized rubber asphalt and mixture." KSCE Journal of Civil Engineering **20**(4): 1347-1355.

Mallick, R. B., B.-L. Chen and S. Bhowmick (2009). "Harvesting energy from asphalt pavements and reducing the heat island effect." International Journal of Sustainable Engineering **2**(3): 214-228.

Mallick, R. B. and T. El-Korchi (2008). Pavement engineering, CRC Press, NY.

Manosalvas-Paredes, M., N. Lajnef, K. Chatti, K. Aono, J. Blanc, N. Thom, G. Airey and D. Lo Presti (2020). "Data Compression Approach for Long-Term Monitoring of Pavement Structures." Infrastructures **5**(1): 1.

Marasteanu, M., W. Buttlar, H. Bahia, C. Williams, K. H. Moon, E. Z. Teshale, A. C. Falchetto, M. Turos, E. Dave and G. Paulino (2012). "Investigation of low temperature cracking in asphalt pavements national pooled fund study–phase II."

Martin, A. E., E. Arambula, M. E. Kutay, J. Lawrence, X. Luo and R. Lytton (2013). Comparison of fatigue analysis approaches for hot-mix asphalt to ensure a state of good repair, Southwest Region University Transportation Center (US).

McGennis, R., S. Shuler and H. Bahia (1994). BACKGROUND OF SUPERPAVE ASPHALT BINDER TEST METHODS. FINAL REPORT.

Mirza, M. W. (1995). "Development of a global aging system for short and long term aging of asphalt cements."

Mortazavi, M. and J. S. Moulthrop (1993). "The SHRP materials reference library."

Nguyen, Q. T., H. Di Benedetto and C. Sauzéat (2012). "Determination of thermal properties of asphalt mixtures as another output from cyclic tension-compression test." Road Materials and Pavement Design **13**(1): 85-103.

Omairey, E. L., F. Gu and Y. Zhang (2021). "An equation-based multiphysics modelling framework for oxidative ageing of asphalt pavements." Journal of Cleaner Production **280**: 124401.

Omairey, E. L., Y. Zhang, S. Al-Malaika, H. Sheena, F. J. C. Gu and B. Materials (2019). "Impact of anti-ageing compounds on oxidation ageing kinetics of bitumen by infrared spectroscopy analysis." **223**: 755-764.

Omairey, E. L., Y. Zhang, F. Gu, T. Ma, P. Hu, R. J. C. Luo and B. Materials (2020). "Rheological and fatigue characterisation of bitumen modified by anti-ageing compounds." **265**: 120307.

Ortega, F. J., F. J. Navarro, M. García-Morales and T. McNally (2017). "Effect of shear processing on the linear viscoelastic behaviour and microstructure of bitumen/montmorillonite/MDI ternary composites." Journal of industrial and engineering chemistry **48**: 212-223.

Pan, P., S. Wu, X. Hu, G. Liu and B. Li (2017a). "Effect of material composition and environmental condition on thermal characteristics of conductive asphalt concrete." Materials **10**(3): 218.

Pan, P., S. Wu, X. Hu, P. Wang and Q. Liu (2017b). "Effect of freezing-thawing and ageing on thermal characteristics and mechanical properties of conductive asphalt concrete." Construction and Building Materials **140**: 239-247.

Petersen, J. C. (2000). Chemical composition of asphalt as related to asphalt durability. Developments in petroleum science, Elsevier. **40:** 363-399.

Petersen, J. C. (2009). "A review of the fundamentals of asphalt oxidation: chemical, physicochemical, physical property, and durability relationships." Transportation Research Circular(E-C140).

Petersen, J. C. and P. M. Harnsberger (1998). "Asphalt aging: dual oxidation mechanism and its interrelationships with asphalt composition and oxidative age hardening." Transportation Research Record **1638**(1): 47-55.

Phillips, M. and C. Robertus (1996). Binder rheology and asphaltic pavement permanent deformation; the zero-shear-viscosity. EURASPHALT & EUROBITUME CONGRESS, STRASBOURG, 7-10 MAY 1996. VOLUME 3. PAPER E&E. 5.134.

Plancher, H., E. Green and J. Petersen (1976). Reduction of oxidative hardening of asphalts by treatment with hydrated lime--a mechanistic study. Association of Asphalt Paving Technologists Proc.

Prapaitrakul, N., R. Han, X. Jin and C. J. Glover (2009). "A transport model of asphalt binder oxidation in pavements." Road Materials and Pavement Design **10**(sup1): 95-113.

Pronk, A. and P. Hopman (1991). Energy dissipation: the leading factor of fatigue. Highway research: Sharing the benefits, Thomas Telford Publishing**:** 255-267.

Qi, Y., F. J. P. s. Wang and technology (2003). "Study and evaluation of aging performance of petroleum asphalts and their constituents during oxygen absorption. I. Oxygen absorption behaviors and kinetics." **21**(1-2): 283-299.

Qin, Y. (2016). "Pavement surface maximum temperature increases linearly with solar absorption and reciprocal thermal inertial." International Journal of Heat and Mass Transfer **97**: 391-399.

Robertson, R. E., J. Branthaver, H. Plancher, J. Duvall, E. Ensley and P. Harnsberger (1991). Chemical properties of asphalts and their relationship to pavement performance, Strategic Highway Research Program, National Research Council Washington, DC.

Rochlani, M., S. Leischner, G. C. Falla, P. Goudar and F. Wellner (2020). Influence of Source and Ageing on the Rheological Properties and Fatigue and Rutting Resistance of Bitumen Using a DSR. Proceedings of the 9th International Conference on Maintenance and Rehabilitation of Pavements—Mairepav9, Springer.

Rose, A. A. (2016). Pavement Air Void Property Determination and Incorporation of Pavement Air Void Properties in Pavement Oxidation Modeling with an Emphasis on X-Ray CT Image Analysis.

Sebesta, S., T. Scullion and C. Von Holdt (2006). Rubblization for Rehabilitation of Concrete Pavement in Texas: Preliminary Guidelines and Case Studies, Texas Transportation Institute, Texas A & M University System.

Shan, L., S. Tian, H. He and N. Ren (2017). "Internal crack growth of asphalt binders during shear fatigue process." Fuel **189**: 293-300.

Shi, X. (2014). Controlling thermal properties of asphalt concrete and its multifunctional applications.

Sirin, O., D. K. Paul and E. J. A. i. C. E. Kassem (2018). "State of the art study on aging of asphalt mixtures and use of antioxidant additives." **2018**.

Soenen, H., T. Blomberg, T. Pellinen and O.-V. Laukkanen (2013). "The multiple stress creep-recovery test: a detailed analysis of repeatability and reproducibility." Road Materials and Pavement Design **14**(sup1): 2-11.

Soenen, H., X. Carbonneau, A. Lorserie, X. Lu, M. Lobert and C. Robertus (2020a). "Rheological Parameters of Durability of Binders Extracted from Road Pavements." Research and innovation(974).

Soenen, H., X. Carbonneau, X. Lu, C. Robertus and B. Tapin (2020b). Evaluation of the properties of bituminous binders recovered from various sites in Europe ISBM 2020.

Soenen, H., X. Lu, C. Robertus, X. Carbonneau and G. Durand (2021). Durability paramterts evaluated on binders recovered from various field sites in Europe. 7th E&E Congress, Madrid, Spain, Eurasphalt and Eurobitume.

Solaimanian, M. and P. Bolzan (1993). Analysis of the integrated model of climatic effects on pavements, Strategic Highway Research Program, National Research Council.

Solaimanian, M. and T. W. Kennedy (1993). "Predicting maximum pavement surface temperature using maximum air temperature and hourly solar radiation." Transportation Research Record: 1-1.

Subhy, A. (2017). "Advanced analytical techniques in fatigue and rutting related characterisations of modified bitumen: Literature review." Construction and Building Materials **156**: 28-45.

Sun, D., F. Yu, L. Li, T. Lin and X. Zhu (2017). "Effect of chemical composition and structure of asphalt binders on self-healing." Construction and Building Materials **133**: 495-501.

Tauste, R., F. Moreno-Navarro, M. Sol-Sánchez and M. Rubio-Gámez (2018). "Understanding the bitumen ageing phenomenon: A review." Construction and Building Materials **192**: 593-609.

Vehrencamp, J. E. (1953). "Experimental investigation of heat transfer at an air-Earth interface." Eos, Transactions American Geophysical Union **34**(1): 22-30.

Wang, C. and Y. Wang (2019). "Physico-chemo-rheological characterization of neat and polymer-modified asphalt binders." Construction and Building Materials **199**: 471-482.

Wang, C., W. Xie and B. S. Underwood (2018). "Fatigue and healing performance assessment of asphalt binder from rheological and chemical characteristics." Materials and Structures **51**(6): 1-12.

Wang, C., H. Zhang, C. Castorena, J. Zhang and Y. R. Kim (2016). "Identifying fatigue failure in asphalt binder time sweep tests." Construction and Building Materials **121**: 535-546.

Wang, H., S. Wu, M. Chen and Y. Zhang (2010). "Numerical simulation on the thermal response of heat-conducting asphalt pavements." Physica Scripta **2010**(T139): 014041.

Wang, P. Y., Y. Wen, K. Zhao, D. Chong and A. S. Wong (2014). "Evolution and locational variation of asphalt binder aging in long-life hot-mix asphalt pavements." Construction and Building Materials **68**: 172-182.

Wang, Y., L. Sun and Y. Qin (2015). "Aging mechanism of SBS modified asphalt based on chemical reaction kinetics." Construction and Building Materials **91**: 47-56.

Wen, Y. and Y. Wang (2018). "Determination of oxygen diffusion coefficients of compacted asphalt mixtures." Construction and Building Materials **160**: 385-398.

Wilkes, M. F. and M. C. Davies (2010). Asphaltene inhibition. U. USA. **7,795,183**.

Woo, W. J., A. Chowdhury and C. J. J. T. r. r. Glover (2008). "Field aging of unmodified asphalt binder in three Texas long-term performance pavements." **2051**(1): 15-22.

Wu, S.-p., L. Pang, L.-t. Mo, Y.-c. Chen and G.-j. Zhu (2009). "Influence of aging on the evolution of structure, morphology and rheology of base and SBS modified bitumen." Construction and Building Materials **23**(2): 1005-1010.

Xu, G. and H. Wang (2017). "Molecular dynamics study of oxidative aging effect on asphalt binder properties." Fuel **188**: 1-10.

Xu, G., H. Wang and H. Zhu (2017). "Rheological properties and anti-aging performance of asphalt binder modified with wood lignin." Construction and Building Materials **151**: 801-808.

Yang, Y., Y. Zhang, E. Omairey, J. Cai, F. Gu and A. V. Bridgwater (2018). "Intermediate pyrolysis of organic fraction of municipal solid waste and rheological study of the pyrolysis oil for potential use as bio-bitumen." Journal of Cleaner Production **187**: 390-399.

Yao, H., Z. You, L. Li, C. H. Lee, D. Wingard, Y. K. Yap, X. Shi and S. W. Goh (2013). "Rheological properties and chemical bonding of asphalt modified with nanosilica." Journal of Materials in Civil Engineering **25**(11): 1619-1630.

Yavuzturk, C., K. Ksaibati and A. Chiasson (2005). "Assessment of temperature fluctuations in asphalt pavements due to thermal environmental conditions using a two-dimensional, transient finite-difference approach." Journal of Materials in Civil Engineering **17**(4): 465-475.

Yin, F., A. E. Martin, E. Arámbula-Mercado and D. Newcomb (2017). "Characterization of non-uniform field aging in asphalt pavements." Construction and Building Materials **153**: 607-615.

You, L., K. Yan, Y. Hu, D. G. J. C. Zollinger and Geotechnics (2016). "Spectral element solution for transversely isotropic elastic multi-layered structures subjected to axisymmetric loading." **72**: 67-73.

You, Z., J. Mills-Beale, J. M. Foley, S. Roy, G. M. Odegard, Q. Dai and S. W. Goh (2011). "Nanoclay-modified asphalt materials: Preparation and characterization." Construction and Building Materials **25**(2): 1072-1078.

Yu, J., X. Zeng, S. Wu, L. Wang and G. Liu (2007). "Preparation and properties of montmorillonite modified asphalts." Materials Science and Engineering: A **447**(1-2): 233-238.

Yu, R., C. Fang, P. Liu, X. Liu and Y. J. A. C. S. Li (2015). "Storage stability and rheological properties of asphalt modified with waste packaging polyethylene and organic montmorillonite." **104**: 1-7.

Yunus, R., A. Fakhru'l-Razi, T. L. Ooi, S. E. Iyuke and J. M. Perez (2004). "Lubrication properties of trimethylolpropane esters based on palm oil and palm kernel oils." European journal of lipid science and technology **106**(1): 52-60.

Zafari, F., M. Rahi, N. Moshtagh and H. Nazockdast (2014). "The improvement of bitumen properties by adding nanosilica." Study of Civil Engineering and Architecture **3**(1): 62-69.

Zakaria, N. M. (2020). Characterisation of bitumen and asphalt mixture with recycled waste plastic (RWP) modified binder, University of Nottingham.

Zhang, R., J. S. Daniel and E. V. Dave (2018a). Evaluation of viscoelastic properties and cracking behaviour of asphalt mixtures with laboratory aging. RILEM 252-CMB-Symposium on chemo mechanical characterization of bituminous materials, Springer.

Zhang, Y., B. Birgisson and R. L. Lytton (2016). "Weak form equation–based finite-element modeling of viscoelastic asphalt mixtures." Journal of Materials in Civil Engineering **28**(2): 04015115.

Zhang, Y. and Y. Gao (2021). "Predicting crack growth in viscoelastic bitumen under a rotational shear fatigue load." Road Materials and Pavement Design **22**(3): 603-622.

Zhang, Y., F. Gu, X. Luo, B. Birgisson and R. L. Lytton (2018b). "Modeling stress-dependent anisotropic elastoplastic unbound granular base in flexible pavements." Transportation Research Record **2672**(52): 46-56.

Zhang, Y., X. Luo, R. Luo and R. L. Lytton (2014). "Crack initiation in asphalt mixtures under external compressive loads." Construction and Building Materials **72**: 94-103.

Zhang, Y., T. Ma, X. Ding, T. Chen, X. Huang and G. Xu (2018c). "Impacts of air-void structures on the rutting tests of asphalt concrete based on discretized emulation." Construction and Building Materials **166**: 334-344.

Zhang, Y., T. Ma, X. Luo, X. Huang and R. L. Lytton (2019). "Prediction of dynamic shear modulus of fine aggregate matrix using discrete element method and modified Hirsch model." Mechanics of Materials **138**: 103148.

Zhao, Y., F. Gu, J. Xu and J. Jin (2010). "Analysis of aging mechanism of SBS polymer modified asphalt based on Fourier transform infrared spectrum." Journal of Wuhan University of Technology-Mater. Sci. Ed. **25**(6): 1047-1052.

Zhao, Y., L. Tong and Y. Zhu (2019). "Investigation on the Properties and Distribution of Air Voids in Porous Asphalt with Relevance to the Pb (II) Removal Performance." Advances in Materials Science and Engineering **2019**.

Appendices

Appendix A

Publications originating from this study

The doctoral thesis is based on the following appended publications:

1. Omairey, E.L., Gu, F. and Zhang, Y., 2020. An equation-based Multiphysics modelling framework for oxidative ageing of asphalt pavements. *Journal of Cleaner Production*. https://doi.org/10.1016/j.jclepro.2020.124401
2. Omairey, E.L., Zhang, Y., Gu, F., Ma, T., Hu, P. and Luo, R., 2020. Rheological and fatigue characterisation of bitumen modified by antiageing compounds. *Construction and Building Materials*, 265, p.120307. https://doi.org/10.1016/j.conbuildmat.2020.120307
3. Omairey, E.L., Zhang, Y., Al-Malaika, S., Sheena, H. and Gu, F., 2019. Impact of antiageing compounds on oxidation ageing kinetics of bitumen by infrared spectroscopy analysis.*Construction and Building Materials*, 223, pp.755-764. https://doi.org/10.1016/j.conbuildmat.2019.07.021
4. Omairey, E.L., Zhang, Y., Soenen, H., and Carbonneau, X. Parametric Analysis and Field Validations of Oxidative Ageing in Asphalt Pavements using Multiphysics Modelling Approaches [under review for an international journal].

Other relevant publications:

The author also contributed to the following publications, which are related to the research project:

1. Yang, Y., Zhang, Y., Omairey, E., Cai, J., Gu, F. and Bridgwater, A.V., 2018. Intermediate pyrolysis of organic fraction of municipal solid waste and rheological study

of the pyrolysis oil for potential use as bio-bitumen. *Journal of Cleaner Production*, 187, pp.390-399. https://doi.org/10.1016/j.jclepro.2018.03.205

2. Omairey, E.L., Zhang, Y., Artamendi, I. and Allen, B., 2021. Deriving and characterising alternative bitumen from waste plastics. *Proceeding of the 7th E&E Congress* [Accepted for publication on 16 October 2019].

The work in this study was presented in the following conferences:

1. RILEM International Symposium on Bituminous Materials. Virtual event, Lyon, France (14-16 December 2020). The research poster was awarded the best poster award title (the poster is shown in **Appendix B**). Award nomination: https://isbmlyon2020.sciencesconf.org/resource/page/id/23
2. 98th Annual Transportation Research Board (TRB) Meeting. Washington D.C., USA (13-17 January 2019).
3. 8th International Transportation PhD Student Symposium. RWTH Aachen University, Aachen, Germany (12-13 September 2019).
4. Comsol Conference. Cambridge, UK (24-26 September 2019).
5. Aston Postgraduate Research Conference. Aston University, Birmingham, UK (19 April 2018).
6. 7th Eurasphalt and Eurobitume (E&E) Congress. virtual event, Madrid, Spain (upcoming event, 15-17 June 2021).
7. International Symposium on Frontiers of Road and Airport Engineering, Delft, NL (upcoming event, 12-14 July 2021).

Appendix B

The research poster presented in RILEM International Symposium on Bituminous Materials:

RILEM International Symposium on Bituminous Materials

December 14th-16th 2020 – Lyon, France

Multiphysics Simulation and Validation of Field Ageing of Asphalt Pavements

Eman Omairey & Yuqing Zhang

Aston University, Birmingham, UK

Long-term field ageing of asphalt pavement plays a vital role in limiting the service life of pavements.

Models were established to represent the multiple physics that contribute to the ageing of asphalt pavements (Glover et al. (1998-2014))

These four ageing-related physics were mathematically modelled individually in the literature ...

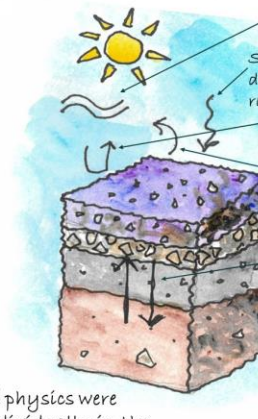

These models include:
(1) heat transfer to determine pavement temperature profile,

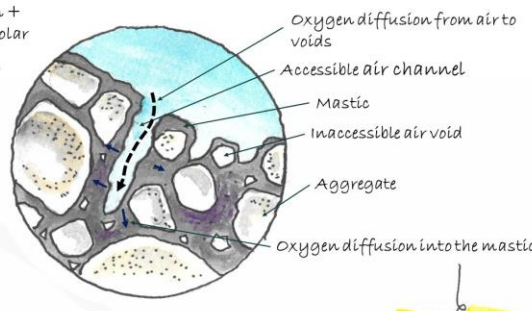

(2) diffusion of oxygen from air into the interconnected air voids of asphalt pavement,
(3) diffusion of oxygen from the air void channels into the asphalt mastic coating films

... and (4) growth of oxidation products in asphalt binders.

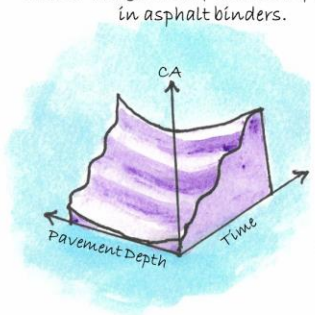

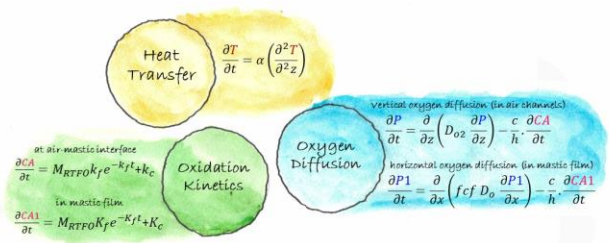

HOWEVER, they were not effectively integrated into a comprehensive model....

WHY

There are few challenges when modelling these mathematical equations, they are:

- Circularly dependent
- Time dependent
- Highly non-linear
- Need non user-friendly interfaces

The weak-form PDE-based FE modelling is a tool that can achieve the objective.

COMSOL software provides an efficient computational platform to solve the weak-form PDEs and address the coupling effects of different physics. Thus, an integrated FE model will be used to compute the change of each physics during the oxidative ageing process.

Physics	Strong Form	Weak Form
Heat Transfer	$\frac{\partial T}{\partial t} = \alpha\left(\frac{\partial^2 T}{\partial^2 z}\right)$	-Tt*test(T)*material.rho*material.Cp*1[m]-material.k_iso*Tx*test(Tx)*1[m]-material.k_iso*Ty*test(Ty)*1[m]
Vertical Diffusion of Oxygen in Interconnected Air Channels	$\frac{\partial P}{\partial t} = \frac{\partial}{\partial z}\left(D_{o2}\frac{\partial P}{\partial z}\right) - \frac{c}{h}\cdot\frac{\partial CA}{\partial t}$	Pair*test(Pair)+(if(Pair<0.0001[atm],0,c0*T*R/h*d(CAi,TIME)))*test(Pair)+Pairx*test(Pairx)*Do2+Do2*Pairy*test(Pairy)
Horizontal Diffusion of Oxygen in Mastic Coating Film	$\frac{\partial P1}{\partial t} = \frac{\partial}{\partial x}\left(fcf\, D_o \frac{\partial P1}{\partial x}\right) - \frac{c}{h}\cdot\frac{\partial CA1}{\partial t}$	Pbt*test(Pb)+(if(Pb<0.0001[atm],0,c0*T*R/h*d(CAb,TIME)))*test(Pb)+Pbx*test(Pbx)*D*fcf+D*fcf*Pby*test(Pby)
CA Growth on the Air-mastic Interface	$\frac{\partial CA}{\partial t} = M_{RTFO} k_f e^{-k_f t} + k_c$	CAit*test(CAi)-(if(Pair<0.0001[atm],0,M*Kf*exp(-Kf*t)+Kc)) *test(CAi)
CA Growth in the Asphalt Mastic Film	$\frac{\partial CA1}{\partial t} = M_{RTFO} K_f e^{-K_f t} + K_c$	CAbt*test(CAb)-(if(Pb<0.0001[atm],0,M*kf*exp(-kf*t)+kc)) *test(CAb)

Proposed Model Geometry

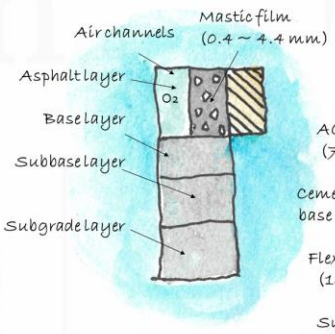

A two-dimensional geometry was built to represent the pavement structure..

The dimensions of the geometry are customised according to the pavement structure and mixture's volumetric properties

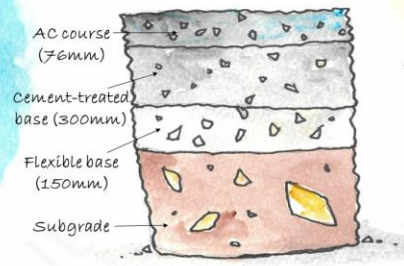

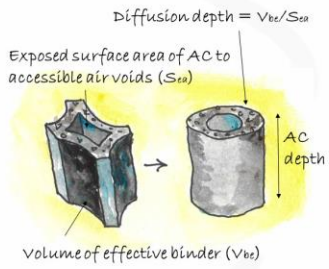

For example, thickness of mastic coating film in the 2D geometry is defined as the diffusion depth (d_D) which is the mastic film thickness that surrounds the interconnected air channels

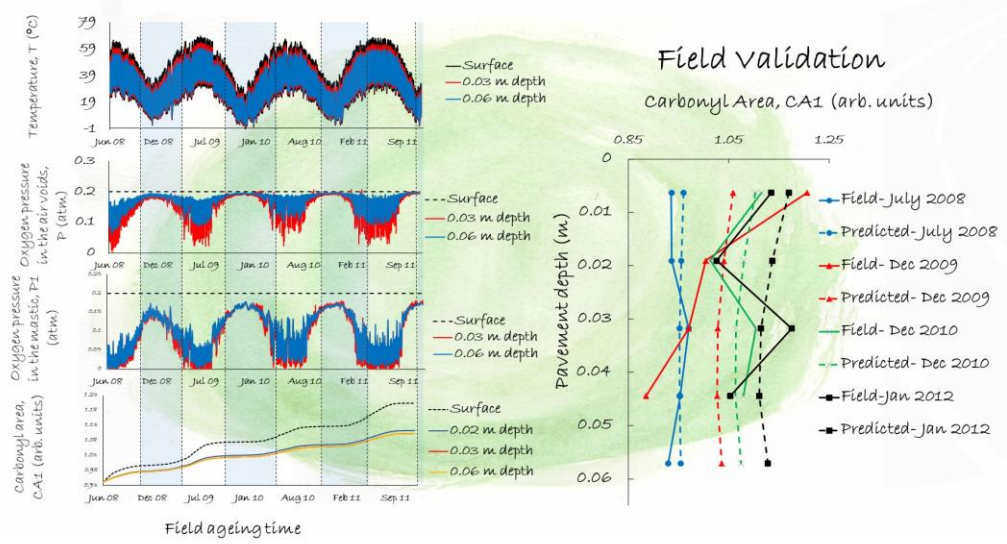

Results

Field Validation

Conclusions

- The model can effectively address the circular dependency between the ageing-related multi-physics.
- Weak-form PDE based FEM can effectively solve the circular dependence and can reliably predict the annual hourly profiles of temperatures, oxygen pressures and oxidation products along pavement depth at different climate zones.
- Oxidative ageing product (Carbonyl) decreases with asphalt layer depth in general (depending on boundary conditions), e.g., C shape if unbounded base, and r shape if treated base. Additionally, carbonyl grows much quicker in summer while remains almost unchanged in winter.
- Next step work is to predict the stiffness gradient and damages caused by temperature and ageing gradients under loading applications

Get in Touch!

Eman Omairey
PhD Candidate MSc BSc PGCert FHEA GMICE
omaireye@aston.ac.uk
Aston University
BIRMINGHAM
eman-lafta
Eman Lafta Omairey

Financial Support:
SchlumbergerFoundation Faculty for the Future